Doctor of Philosophy

at the University of Leicester

by

Chee Pin Tan B. Eng., Leicester
Control and Instrumentation Research Group
Engineering Department
University of Leicester

May 2, 2002

Sliding mode observers for fault detection and isolation

Chee Pin Tan

Abstract

This thesis describes the use of a class of sliding mode observers for fault detection and isolation purposes. Existing work has shown that the equivalent output error injection term associated with the sliding mode observer, which represents the average value of the nonlinear switched term (which induces and maintains the sliding motion), if properly scaled, yields accurate reconstructions of actuator faults. Existing observer design methods generate a certain class of observer gains, but do not utilise all degrees of freedom. In this thesis, a new method, exploiting this freedom is presented. The method uses Linear Matrix Inequalities and is easily implementable using standard software packages. New methods for accurately reconstructing sensor faults are also presented where appropriate filtering of certain measurable signals yields a fictitious system in which the original sensor faults are treated as actuator faults. Using the principles of actuator fault reconstruction in the existing work, sliding mode observers can be designed for the fictitious system to accurately reconstruct the sensor faults. This improves on the previous work where effectively only the steady state components of the sensor faults could be reconstructed. A new method using Linear Matrix Inequalities is presented, to synthesise observers which can robustly reconstruct faults in the presence of a class system of uncertainty, minimising the effect of the uncertainty on the fault reconstruction in an $\mathcal{L}_2$ sense. The robust fault reconstruction scheme is demonstrated by means of a case study, which is a nonlinear model of an aero-engine. System identification is used to obtain a linear model of the engine. An uncertainty representation is also obtained about which the observer is designed. The results from the case study show that the robust fault reconstruction scheme works and is effective.

Acknowledgements

I would like to thank the following for being instrumental in the writing of this thesis, in one way or another

1. My Lord and Saviour, Jesus Christ, giver of life, and source of my inspiration, without whom, all this would have been impossible.

2. My supervisor Dr. Christopher Edwards, for his tremendous support, encouragement, reliability and friendship, having been there and available at all times when needed. Without him, all this would have been virtually impossible.

3. My parents Mr. and Mrs. Tan Fu Tee, for providing for me for so many years, always ensuring that my only concern was my studies, and being unpossesive in releasing me to do what was good for me.

4. My siblings (and their spouses) Chee Kiat (and Elaine) and Joyce (and David), for their continuing support in whatever I do, always being there for me.

5. Members of the Control Research Group, past and present, in particular Dr. Matthew Turner and Dr. Yi Cao, for helping me at general Control theory and also LaTeX, Dr. Guido Hermann, for helping me in sliding mode theory when I first started, Dr. Emmanuel Prempain for helping me start with Linear Matrix Inequalities, and Dr. Sarah Gatley who has so kindly assisted me with her expertise in aero-engines.

6. Other members of the Control Research Group, for support, friendship, and times of fun and laughter, in particular Ercument Turgkolu , Roderick Hebden, Nai One Lai and Turhan Ozen.

7. Dr Jeremy Gribble, of QinetiQ Ltd., for his helpfulness and support in the aero-engine work, especially during those times when he went out of his way to patiently explain the aero-engine to me.

8. Friends at the Leicester Chinese Christian Church (and also the Young Adults' Fellowship) for their support and friendship, as well as their reminding me to rest(!) particularly Stephen Crofts, Eyen Khoo, Constance Lo, Chris Poon, Olivia Ho and Victoria Suen. Special thanks also to the adults at the Chinese Church for taking care of me when I was here (especially in the area of food and spiritual growth), in particular Nelson and Mei Yi Tang, Esther Ho, Stephen and Belina Tsao, and Eric and Lih Fang Khoo.

9. Friends at the Wesley Methodist Church in Seremban, Malaysia for their friendship, support and blessing in pursuing my further studies, in particular Andrew, Jason, Jasinta, Su Yin, Su Lin, Su May, Hui Shan, Huei Weun and Mei I. Special mention should also go to Eric and Justine Ting, and also Pastor Paul George Ponniah.

10. Last, and *definitely not least*, Priscilla, my fiancee and dearest friend, whom I am looking forward to being united as one with, for her love, affection, support, patience and understanding, especially during those times when this work has caused me to be unable to devote as much time to her as I would have liked to.

Chee Pin Tan

May 2, 2002

Contents

Chapter 1

Introduction and overview of thesis

1.1 Introduction

In the present day, there is an increase in the use of control systems which are becoming more complex and sophisticated. Even though they may be costly and expensive, the benefits of these control systems far outweigh the costs, when productivity can be increased, efficiency enhanced, and the dependence on manual (and error prone) human effort can be cut down. For example, a robotic arm can be used to handle dangerous substances, eliminating hazardous risks to human operators, or a simple thermostat can automatically keep the temperature of a room at a pre-set level despite external temperature fluctuations. These applications reduce the consumption of energy, money, human effort and also any effects caused by human error.

However, these control systems, made by fallible man, are also fallible just like their creators. They are not perfect, and hence are also prone to malfunctions and errors. The causes of these phenomenons are many and diverse, where they could be external circumstances (such as damage to components due to wind gusts or extreme changes in temperature causing a component to fail) or just normal wear and tear of components (such as a measurement sensor giving inaccurate readings due to frequent use and the fact that it has not been calibrated for a long time). Whatever the cause, when these systems start to possess abnormalities, or behave in a way that they are not supposed to, a *fault* is deemed to have occurred [5].

System faults, if allowed to be present for a long period of time without being detected, can cause catastrophic effects, such as loss of human life, environmental pollution, or economic losses. For cases in which the consequences of a fault are not so severe, the early detection of a fault can help improve efficiency, productivity, reliability, and generate financial savings. There is therefore, a need for effective *fault detection and isolation* (FDI). The fundamental

Doctor of Philosophy

at the University of Leicester

by

Chee Pin Tan B. Eng., Leicester
Control and Instrumentation Research Group
Engineering Department
University of Leicester

May 2, 2002

Sliding mode observers for fault detection and isolation

Chee Pin Tan

Abstract

This thesis describes the use of a class of sliding mode observers for fault detection and isolation purposes. Existing work has shown that the equivalent output error injection term associated with the sliding mode observer, which represents the average value of the nonlinear switched term (which induces and maintains the sliding motion), if properly scaled, yields accurate reconstructions of actuator faults. Existing observer design methods generate a certain class of observer gains, but do not utilise all degrees of freedom. In this thesis, a new method, exploiting this freedom is presented. The method uses Linear Matrix Inequalities and is easily implementable using standard software packages. New methods for accurately reconstructing sensor faults are also presented where appropriate filtering of certain measurable signals yields a fictitious system in which the original sensor faults are treated as actuator faults. Using the principles of actuator fault reconstruction in the existing work, sliding mode observers can be designed for the fictitious system to accurately reconstruct the sensor faults. This improves on the previous work where effectively only the steady state components of the sensor faults could be reconstructed. A new method using Linear Matrix Inequalities is presented, to synthesise observers which can robustly reconstruct faults in the presence of a class system of uncertainty, minimising the effect of the uncertainty on the fault reconstruction in an $\mathcal{L}_2$ sense. The robust fault reconstruction scheme is demonstrated by means of a case study, which is a nonlinear model of an aero-engine. System identification is used to obtain a linear model of the engine. An uncertainty representation is also obtained about which the observer is designed. The results from the case study show that the robust fault reconstruction scheme works and is effective.

Acknowledgements

I would like to thank the following for being instrumental in the writing of this thesis, in one way or another

1. My Lord and Saviour, Jesus Christ, giver of life, and source of my inspiration, without whom, all this would have been impossible.

2. My supervisor Dr. Christopher Edwards, for his tremendous support, encouragement, reliability and friendship, having been there and available at all times when needed. Without him, all this would have been virtually impossible.

3. My parents Mr. and Mrs. Tan Fu Tee, for providing for me for so many years, always ensuring that my only concern was my studies, and being unpossesive in releasing me to do what was good for me.

4. My siblings (and their spouses) Chee Kiat (and Elaine) and Joyce (and David), for their continuing support in whatever I do, always being there for me.

5. Members of the Control Research Group, past and present, in particular Dr. Matthew Turner and Dr. Yi Cao, for helping me at general Control theory and also LaTeX, Dr. Guido Hermann, for helping me in sliding mode theory when I first started, Dr. Emmanuel Prempain for helping me start with Linear Matrix Inequalities, and Dr. Sarah Gatley who has so kindly assisted me with her expertise in aero-engines.

6. Other members of the Control Research Group, for support, friendship, and times of fun and laughter, in particular Ercument Turgkolu , Roderick Hebden, Nai One Lai and Turhan Ozen.

7. Dr Jeremy Gribble, of QinetiQ Ltd., for his helpfulness and support in the aero-engine work, especially during those times when he went out of his way to patiently explain the aero-engine to me.

8. Friends at the Leicester Chinese Christian Church (and also the Young Adults' Fellowship) for their support and friendship, as well as their reminding me to rest(!) particularly Stephen Crofts, Eyen Khoo, Constance Lo, Chris Poon, Olivia Ho and Victoria Suen. Special thanks also to the adults at the Chinese Church for taking care of me when I was here (especially in the area of food and spiritual growth), in particular Nelson and Mei Yi Tang, Esther Ho, Stephen and Belina Tsao, and Eric and Lih Fang Khoo.

9. Friends at the Wesley Methodist Church in Seremban, Malaysia for their friendship, support and blessing in pursuing my further studies, in particular Andrew, Jason, Jasinta, Su Yin, Su Lin, Su May, Hui Shan, Huei Weun and Mei I. Special mention should also go to Eric and Justine Ting, and also Pastor Paul George Ponniah.

10. Last, and *definitely not least*, Priscilla, my fiancee and dearest friend, whom I am looking forward to being united as one with, for her love, affection, support, patience and understanding, especially during those times when this work has caused me to be unable to devote as much time to her as I would have liked to.

Chee Pin Tan

May 2, 2002

Contents

Chapter 1

Introduction and overview of thesis

1.1 Introduction

In the present day, there is an increase in the use of control systems which are becoming more complex and sophisticated. Even though they may be costly and expensive, the benefits of these control systems far outweigh the costs, when productivity can be increased, efficiency enhanced, and the dependence on manual (and error prone) human effort can be cut down. For example, a robotic arm can be used to handle dangerous substances, eliminating hazardous risks to human operators, or a simple thermostat can automatically keep the temperature of a room at a pre-set level despite external temperature fluctuations. These applications reduce the consumption of energy, money, human effort and also any effects caused by human error.

However, these control systems, made by fallible man, are also fallible just like their creators. They are not perfect, and hence are also prone to malfunctions and errors. The causes of these phenomenons are many and diverse, where they could be external circumstances (such as damage to components due to wind gusts or extreme changes in temperature causing a component to fail) or just normal wear and tear of components (such as a measurement sensor giving inaccurate readings due to frequent use and the fact that it has not been calibrated for a long time). Whatever the cause, when these systems start to possess abnormalities, or behave in a way that they are not supposed to, a *fault* is deemed to have occurred [5].

System faults, if allowed to be present for a long period of time without being detected, can cause catastrophic effects, such as loss of human life, environmental pollution, or economic losses. For cases in which the consequences of a fault are not so severe, the early detection of a fault can help improve efficiency, productivity, reliability, and generate financial savings. There is therefore, a need for effective *fault detection and isolation* (FDI). The fundamental purpose of an FDI scheme is to generate an alarm when a fault occurs (detection), and then to determine the location of the fault (isolation), so that corrective action or preventive measures can be taken to eliminate or minimise the effect of the fault.

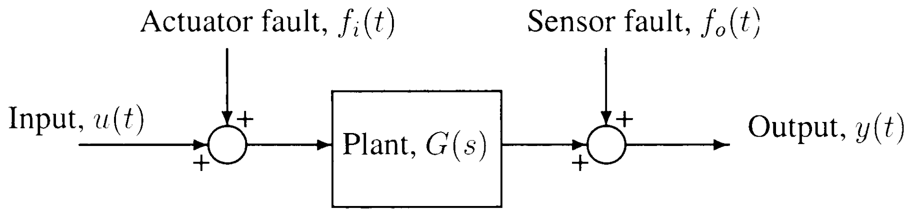

Figure 1.1: Schematic of actuator and sensor faults acting additively on a system

In this thesis, the fault scenarios under consideration are *additive faults*. These additive faults can occur in two places: at the actuators (input) and sensors (output) as shown in Figure 1.1. Actuator faults are faults that act on the system, resulting in the deviation of the process variables. From Figure 1.1 the actual input into the system is $u(t) + f_i(t)$. An example of actuator faults might be damage to a control surface on an aircraft, resulting in the rudder being inoperable. The result is the command (control) signal sent to this device has no effect, and $f_i(t) = -u(t)$. Sensor faults are faults that act on the sensors that measure the system variables, and do not directly affect the process. The source of these faults could be wear and tear of the sensor leading to inaccurate readings, or a total failure of the sensor. These faults will only (indirectly) affect the process if the output measurements are used to generate the input control signal.

A fault can be classified into two main categories: abrupt (quickly varying) and incipient (slowly varying). The effect of abrupt faults are usually obvious; the system will exhibit a sudden unexpected change (and could cause the entire system to fail). In the case of sensor faults, an example would be when the sensor experiences a total failure, yielding a measurement reading of zero. Incipient faults are more subtle, and the effects are not so obvious, sometimes even negligible. This situation results usually from wear and tear on the components, possibly due to frequent use without calibration. In the short term, at worst they cause the efficiency of the system to be degraded. However, if left undetected for a long time, these faults could prove catastrophic and disastrous. It is therefore in the best interest of all to detect these incipient faults as soon as possible.

FDI schemes have been studied and developed for many years, and there is a vast body of literature on this area. Surveys and overviews in this area of FDI have been conducted by

Patton & Chen [5, 85], Frank [34, 36, 35, 88], Frank & Ding [37] and Willsky [117].

This thesis presents work related to the application of sliding mode observers to the problem of fault detection and isolation. The remainder of this chapter presents an overview of this thesis, as well as its contribution to this field of research.

1.2 Structure of thesis

Chapter 2 - This chapter presents an introduction to *fault detection and isolation* (FDI). It gives the reader an overview of the field and the work that has previously been done in this area. It also introduces the notion of *robust* FDI schemes, i.e. - schemes which are able to discriminate between the effect of a fault, and the effect of disturbances/uncertainty in the system.

Chapter 3 - This chapter presents the concepts of sliding mode as well as the sliding mode observer that is used as the basis for the FDI schemes in the later chapters of the thesis. An overview of the developments in sliding mode observers that have led to the one used in this thesis is given. Also, the main characteristics of a sliding mode observer, which are disturbance rejection and order reduction, are also presented.

Chapter 4 - In this chapter a new method for designing a class of sliding mode observers using Linear Matrix Inequalities (LMIs) is presented. The previous design method for this observer did not exploit all available degrees of freedom. The design method presented in the chapter exploits that freedom, and the resulting observer resembles a sub-optimal Linear Quadratic Gaussian (LQG) observer. Additional constraints can also be incorporated to tune the sliding motion, forcing the eigenvalues of the reduced order motion to lie in certain regions of the complex plane. Finally, a more general solution for the observer is presented, in which the closed-loop poles of the linear part can be tuned; however, the sub-optimal solution has to be compromised. The design methods introduced in this chapter underpin the FDI schemes developed in later chapters. The work described in this chapter has been published as a conference paper [104] and a journal paper [105].

Chapter 5 - This chapter presents new ideas which improve on previous sensor fault reconstruction methods (using sliding mode observers). In the previous work, actuator faults can essentially be reconstructed perfectly, but only low frequency (steady-state) details of sensor faults could be obtained. In each of the new methods described in this chapter, certain available signals are filtered to yield 'fictitious systems' in which the sensor fault appears as an 'actuator fault'. Consequently the actuator fault reconstruction ideas using sliding mode observers can be applied to the fictitious system to reconstruct the sensor fault. The methods presented in this chapter can be divided into three classes:

- Complete reconstruction, in which all sensors are assumed to be potentially faulty. A requirement for this situation is that the system must be open loop stable.
- Complete reconstruction, in which only certain sensors are assumed to be faulty. In this case only certain modes (maybe none) of the open loop plant are required to be stable, depending on which sensors are assumed to be potentially faulty.
- Reconstruction with faults dynamics neglected, and all sensors are assumed to be faulty. The requirement is that the open loop system must not posses any integral action.

The work in this chapter has been published as a conference paper [106].

Chapter 6 - This chapter presents a method for designing sliding mode observers which can reconstruct faults and yet be robust to disturbances/uncertainty which may corrupt the quality of the reconstruction resulting from mismatches between the model about which the observer is designed and the real system. Initially, the design method is formulated for the case of actuator faults. The observer is designed using LMIs, so that the upper bound of the $\mathcal{L}_2$ gain from the disturbance/uncertainty to the fault reconstruction is minimised. The method can then be extended to the case of sensor faults, using the ideas of Chapter 5; filtering certain signals to obtain fictitious systems that treat the sensor fault as an 'actuator fault'. The work described in this chapter has been published as a book chapter [107] and as a conference paper [109].

Chapter 7 - An aero-engine case study is presented in this chapter. The engine is a Rolls-Royce 2-spool Spey engine that is used to power modern military aircraft. System identification has been used to obtain a linear model of the engine, at a certain operating condition. An uncertainty distribution matrix is obtained for the linear model which attempts to encapsulate the difference between the linear and nonlinear models. The uncertainty distribution matrix is essential to the design of the robust fault reconstruction scheme in Chapter 6. A robust sensor fault reconstruction scheme is implemented to test the validity of the uncertainty distribution matrix. Finally, a multiple observer robust sensor fault reconstruction scheme is designed based on the assumption that only one sensor can be faulty at any given time. Part of the work in this chapter will be published as a conference paper [108].

Chapter 8 - In this chapter, conclusions are drawn, and future research ideas are outlined.

Appendix A - Presents some background details about LMIs, which are used extensively in this thesis. In particular, some well known control applications which can be solved using LMIs are described together with some common LMI solvers.

Appendix B - Outlines the basic mathematical notions that are used in this thesis.

Appendix C - Attached to this thesis is a disk containing various *.mat* files generated from Matlab which in turn contain matrices that have been omitted from the thesis text for space considerations. A description of the individual *.mat* files and their contents is given.

Chapter 2

Introduction to Fault Detection and Isolation

2.1 Introduction

In the previous chapter, the importance of fault detection and isolation (FDI) schemes has been outlined. This chapter seeks to briefly describe some of the FDI concepts and methodologies that have been developed over the years.

There are two main methods for FDI; *hardware redundancy* and *analytical redundancy*.

In FDI schemes that use hardware redundancy, additional sensors are added to the system so that more than one sensor will measure a certain variable. In the event of a fault, it is intended that some of these sensors will exhibit results contradicting the others, and the fault can be identified. However, this may not always be physically and financially feasible; additional sensors incur additional costs, take up more space, and cause the system to be heavier. This method will not be discussed in this thesis which concentrates on analytical redundancy.

2.2 Model based FDI

In the case of analytical redundancy, the FDI scheme is designed using knowledge of the input-output relationship of the system in the form of some kind of model. The inputs and outputs of the system are then processed to generate a *residual* [5]. Ideally, the residual should be zero for a fault-free case, and be nonzero if and only if there is a fault in the system. The FDI scheme must be designed properly in order to fulfil this condition.

The advantage of an analytical redundancy scheme is that a minimal number of sensors are needed. However, a good model of the system (describing the input-output relationship) is required, hence analytical redundancy FDI is also known as *model based FDI* [5]. A schematic diagram of a model based residual generator is shown in Figure 2.1.

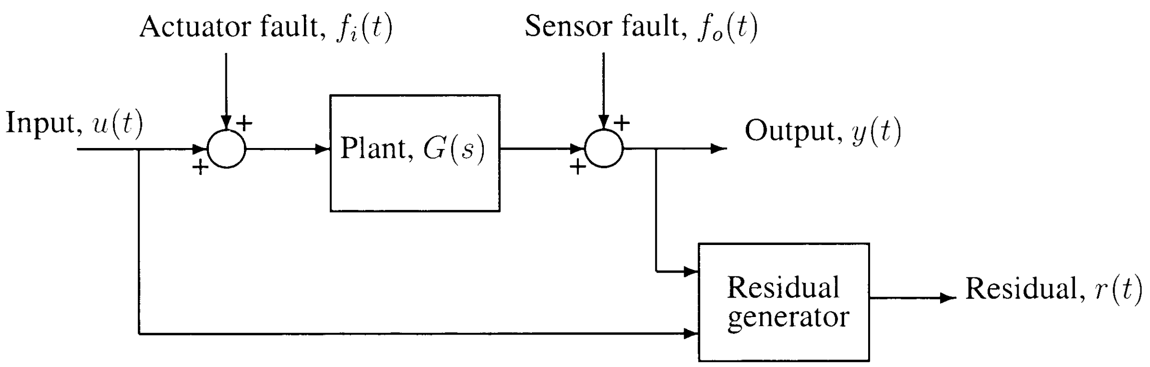

Figure 2.1: Schematic of the model based residual generator

For good fault isolation, the FDI schemes are usually designed so that in the occurrence of certain faults, the residuals will exhibit a fixed direction in the residual space [22, 115]. Hence, when a fault occurs, the direction of the residual indicates the location of the fault.

2.2.1 Fault detection filter

A very popular model based FDI scheme is the *fault detection filter* (FDF) scheme. It is the most general form of model based FDI. Most of the schemes described in this chapter are a subset of the FDF scheme. This methodology was firstly introduced by Beard [2] and Jones [56]. There have been further developments in the FDF scheme, in particular with regard to the issue of fault isolation. Kinneart & Peng [61] designed their FDF scheme assuming that only a single fault occurs at any given time. Chen & Speyer [9], Liu & Si [65], and Massoumnia *et al.* [72] designed FDF schemes that can handle the occurrence of simultaneous faults. Speyer [22, 115] used eigenstructure assignment techniques to enhance the isolation capability of the faults.

2.2.2 Observer based fault detection

A popular subset of the FDF scheme is the *observer based* method. The original purpose of an observer is to estimate the states of the system, which are usually not available in real engineering situations due to infeasibility or impracticality. An observer is essentially a mathematical model of the system. The input is injected into the observer and the observed system. Then the outputs of both the observer and system are compared. The difference between both outputs (termed the *output estimation error*) is fed back linearly into the observer, so that the observer's output can be adjusted to follow the system output. The simplest form of an observer is the linear Luenberger observer [68]. For example, consider a nominal state-space system

$$\dot{x}(t) = Ax(t) + Bu(t) \tag{2.1}$$

$$y(t) = Cx(t) \tag{2.2}$$

where $x \in \mathcal{R}^n$, $y \in \mathcal{R}^p$ and $u \in \mathcal{R}^m$ respectively represent the states, outputs and inputs. A Luenberger observer for $x(t)$ takes the form

$$\dot{\hat{x}}(t) = A\hat{x}(t) + Bu(t) - G_l e_y(t) \tag{2.3}$$

$$\hat{y}(t) = C\hat{x}(t) \tag{2.4}$$

where the hat superscripts indicate the variable estimates and $e_y(t) := \hat{y}(t) - y(t)$ is the output estimation error. The gain $G_l \in \mathcal{R}^{n \times p}$ is a design matrix. Defining the state estimation error as $e(t) := \hat{x}(t) - x(t)$, the following error system can be obtained from (2.1) - (2.4)

$$\dot{e}(t) = (A - G_l C)e(t) \tag{2.5}$$

Hence if the pair (A, C) is *observable* [68], a matrix G_l can be chosen to make $(A - G_l C)$ have stable eigenvalues, and hence the error vector $e(t)$ will decay asymptotically to zero and hence $\hat{x}(t) \rightarrow x(t)$. A schematic diagram of the Luenberger observer appears in Figure 2.2.

In observer based FDI, the signal $e_y(t)$ is used to generate the residual. Hence, for the purposes of FDI, the issue of accurate state estimation is not of primary importance. For example, if a fault occurs, the signal $e_y(t)$ becomes nonzero because of the fault. This would not be ideal in the case of state estimation, but it fulfils the objectives of FDI and indicates an alarm condition when a fault is present. Examples of FDI schemes using Luenberger observers are given in [9, 22, 71, 82, 115]. This body of work describes methodologies for the design of the linear gain G_l and approaches for processing the signal $e_y(t)$ so that the resulting residual is able to isolate the fault.

Clark [16, 14] designed a sensor FDI scheme using multiple Luenberger observers, each designed for one sensor; so that when a fault occurs, one of the observers will produce state estimates contradicting the other observers, and from there, the fault can be isolated. This was subsequently refined in [15] to give a scheme based on only one observer to accomplish the same purpose.

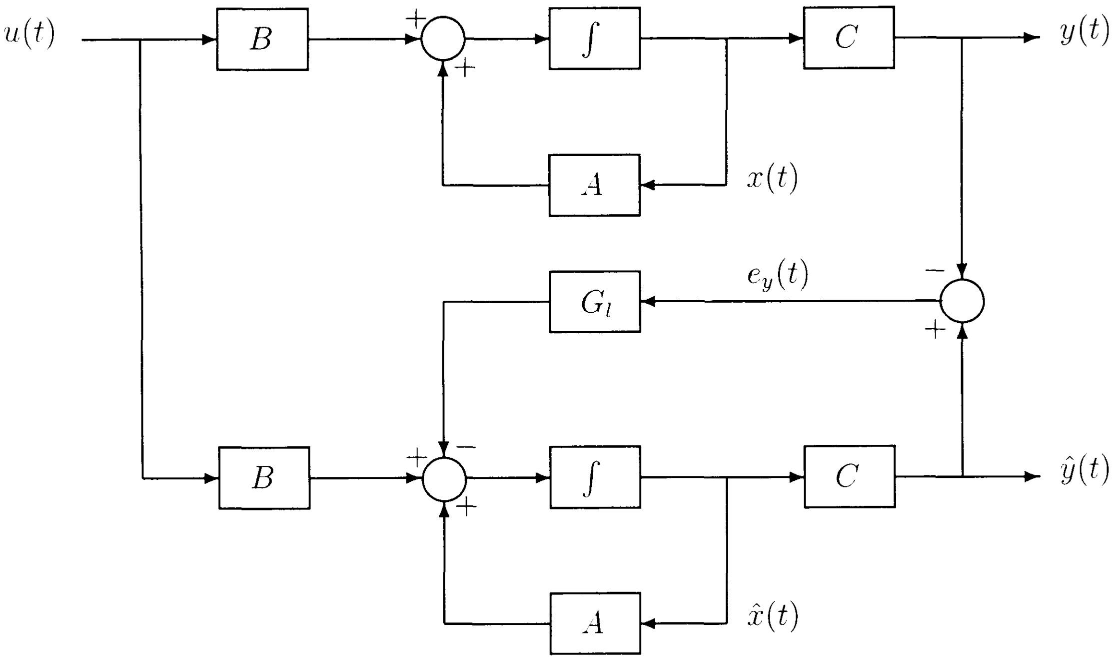

Figure 2.2: Schematic of the Luenberger observer

2.2.3 Parity space approach for FDI

Another class of model based FDI schemes is the *parity space* approach. Examples of such schemes are described by Chow & Willsky [12], Ding *et al.* [20], Lou *et al.* [67], Kinneart [60], Gertler & Kunwer [44], Gertler & Singer [46], Peng *et al.* [92], Deckert *et al.* [19], Gertler & Monajemy [45] and Wu & Wang [119]. In this approach, a number of input-output data points are sampled at a fixed rate, from a certain time instant up to the present time instant. The residual is generated by multiplying a *parity vector* with a function of the sampled data points. This function is dependent on the input-output relationship of the system. The parity vector is designed so that in the absence of faults, the residual will be zero, and when a fault occurs, the residual will be nonzero.

This approach can also be extended to observer based FDI: Wu & Wang [119] presented a scheme where the parity vector is multiplied by the output estimation error from an observer to generate the residual.

2.2.4 Stochastic and statistical FDI

Another method for model based FDI is the class of stochastic and statistical methods. In these methods, the residual is tested for its statistical properties such as zero-meanness, covariance or whiteness. When a fault occurs, these entities of the residual will deviate from their fault-free conditions, making it obvious for an alarm to be sounded. Examples of stochastic and statistical FDI have been demonstrated in [17, 28, 57, 75, 74, 118].

2.3 Robustness in FDI

In analytical redundancy based FDI, a model is required. The model is usually a linear approximation of the actual system about a certain operating point, and therefore, is not a completely accurate representation of the system. In obtaining the model, some of the dynamics could have been neglected, approximations will have been employed and estimates of certain parameters will have been made. This results in a mismatch between the model and the actual system. In modelling terms this discrepancy is accounted for by the introduction of a class of uncertainty.

A result of this mismatch/uncertainty is that the model based FDI schemes will not be accurate when implemented on the actual system. Both faults and uncertainty will cause the residuals to be nonzero, hence the effects of faults and uncertainty cannot be properly distinguished. As a consequence, the residual could potentially be nonzero (due to the system uncertainty) when a fault is absent, resulting in a false alarm, or even worse, the uncertainty could mask the effect of a fault, resulting in the fault not being detected.

It is clear that there is a requirement for FDI schemes that are robust to model uncertainty; producing residuals which are sensitive to faults but insensitive to uncertainty. Many robust FDI schemes have been developed over the years, using ideas that are common in the area of control. These will be briefly described in the sequel.

2.3.1 Robust FDI using eigenstructure assignment

Robust FDI schemes using eigenstructure assignment have been presented in [83, 84, 87, 90, 90, 120]. This method is usually applied to existing FDI schemes (such as the FDF or observer based methods). In designing the FDI scheme, certain eigenvalues/eigenvectors are assigned, to fulfil robustness properties. The robustness usually arises from making the transfer function from the model uncertainty to the residual zero, by using the design freedom available. Patton *et al.* have shown in [83, 84, 87, 90] conditions under which this is possible.

2.3.2 Robust FDI using parity equations

A method for robust FDI using parity equations has been presented by Lou *et al.* [67] and then re-explained in Chapter 7 of [5]. In [67], Lou *et al.* use optimisation techniques to find the 'best' parity vector so that the effect of the uncertainty on the residual is minimised. In the observer based method presented by Wu & Wang [119], the observer gain as well as the parity vector was chosen to minimise the magnitude of the residual during the fault-free operation. Other methods for robust residual generation using parity equations are found in [12, 20, 44, 46, 60].

2.3.3 Robust FDI schemes using the unknown input observer

A specific example of the observer based FDI method is one that uses a so-called *unknown input observer* (UIO) [30, 53, 64, 63, 124]. If certain conditions are satisfied, a UIO is able to provide accurate state estimation that is robust to unknown inputs (usually disturbances or uncertainty), hence the state estimation error (and equivalently the residual for an FDI scheme) will be zero.

For robust FDI using UIOs, Chen & Zhang [7] classified the faults into 'faults of interest' and 'faults of no interest'. They then designed the UIO treating the faults of no interest and also the system uncertainty as the unknown inputs, and therefore the UIO will generate a zero residual when the faults of no interest occur. Then they designed another UIO that treats other faults as faults of no interest. They go on designing more UIOs until every fault will be a fault of interest in at least one UIO. The residuals generated by every UIO are robust to the uncertainty, and a logic sequence is used to isolate the fault. In Chen *et al.* [6], the uncertainty was assumed to be the unknown input when designing the observer, and hence the UIO was able to generate the fixed directional residuals, while being robust and insensitive to the system uncertainty.

Other robust FDI methods using UIOs are available in the literature, in particular Watanabe & Himmelblau [114], Ge & Fang [42, 43], Yu & Shields [129], Wang & Daley [113] and Dassanayake *et al.* [18].

2.3.4 Robust FDI using frequency domain methods

Robust FDI methods have also been designed using frequency domain methods similar to those used for robust control [99, 130]. Typically, frequency domain methods attempt to minimise the effect of the uncertainty on the residual, or maximise the effect of the fault on the residual, or both, using $\mathcal{H}_\infty$ or μ-analysis/synthesis methods. Patton *et al.* [54, 89, 95] designed an observer based FDI scheme that places a lower bound on the ratio of the effect of the fault on the residual to the $\mathcal{H}_\infty$ norm from the uncertainty to the residual. Examples of frequency domain methods are also given in Stoustrup *et al.* [59, 81, 103], Faitakis & Kantor [31], Sauter & Hamelin [48, 97] and Ding & Frank [21].

2.3.5 Robust FDI schemes using threshold selection

In the event that perfect decoupling of residuals from the uncertainty is not possible, the residual will be nonzero even in the absence of a fault. A method that can be used to overcome this is the *threshold selection* method. Here a threshold is selected, such that in the presence of a fault, the residual will exceed the threshold, and an alarm will be generated. This threshold can be fixed or time-varying, and is calculated from the parameters of the system, the properties of any noise, the likely properties of the fault, as well as any known properties of the uncertainty.

Examples of robust FDI methods using threshold selection are [4, 29, 40, 41].

2.4 Fault reconstruction

This section describes *fault reconstruction* ideas, (also known as *fault identification* [5]). Fault reconstruction is different from the majority of FDI methods described previously in the sense that it not only detects and isolates the fault, but provides an estimate of the fault. This approach is very useful for incipient faults and slow drifts, which are difficult to detect. It is also particularly useful when designing a fault tolerant control system. This idea of fault reconstruction is similar to the work of estimating disturbances or unknown parameters by Chui & Chen [13], Mealy & Tang [73], Chen & Fukuda [10], Spathopoulos & Grobov [101], Chen [8], Jiang *et al.* [55], Marro *et al.* [70], Haskara & Ozguner [49], Saberi *et al.* [94], Xu & Hashimoto [123] and Floret-Pontet & Lamnabhi-Lagarrigue [33]. Some examples of fault reconstruction are available in [26, 27, 122, 126, 128]. This principle of fault reconstruction is the FDI methodology that will be used in this thesis.

2.5 Conclusion

This chapter has presented an introduction and explained the necessity and importance of FDI schemes, and also also attempted to give an overview of the various FDI schemes in the literature. In addition, the concept of an observer, which is vital to the work in this thesis, has been presented. In actual practice, most of the mentioned FDI schemes have very limited application because they are dependent on the availability and accuracy of linear models, which may vary considerably when operating conditions change. The exceptions are the FDI schemes using the threshold method and the stochastic and statistical method, which are much less dependent on linearised models. This thesis seeks to develop fault reconstruction, because it is of more use than simply fault detection and isolation, for reasons mentioned in §2.4. This is by no means an easy task, as evidenced by the relatively few fault reconstruction papers in the overall FDI literature, and the work in this thesis seeks to contribute to this area of research.

Chapter 3

Development of sliding mode observers

3.1 Introduction

The previous chapter has described various FDI schemes that are available in the literature. So-called sliding mode observers have also been used for FDI [26, 27, 52, 102, 125, 128]. Before discussing these strategies, an introduction to sliding modes in general and sliding mode observers in particular will be presented. The purpose of this chapter is two-fold: firstly to introduce the concept of a sliding mode observer, and secondly to demonstrate the developments in sliding mode observers that are relevant to the new work described in this thesis. In the literature, there have been many sliding mode observer formulations and design methods [1, 23, 50, 62, 98, 100, 110, 111, 112, 121, 127]. However, only the observers that are directly relevant to the developments in this thesis will be described; the ones proposed by Utkin [110], Walcott & Zak [112, 111] and Edwards & Spurgeon [23, 25].

3.2 Sliding mode observers

In the typical Luenberger observer introduced in §2.2.2, the output estimation error is fed back linearly to make the state estimation error asymptotically stable. In a so-called sliding mode observer, the output estimation error is fed back through a *nonlinear discontinuous term*. To illustrate this, consider a linear state-space system described by

$$\dot{x}(t) = Ax(t) + Bu(t) \tag{3.1}$$

$$y(t) = Cx(t) \tag{3.2}$$

where the system matrices are given by

$$A = \begin{bmatrix} 0 & 1 \\ -2 & 0 \end{bmatrix}, \quad B = \begin{bmatrix} 0 \\ 1 \end{bmatrix}, \quad C = \begin{bmatrix} 1 & 1 \end{bmatrix} \tag{3.3}$$

Consider a nonlinear discontinuous observer scheme for (3.1) - (3.2) defined by

$$\dot{\hat{x}}(t) = A\hat{x}(t) + Bu(t) + G_n\nu \tag{3.4}$$

$$\hat{y}(t) = C\hat{x}(t) \tag{3.5}$$

where $(\hat{x}, \hat{y})$ are estimates of (x, y) and G_n is an appropriate fixed gain matrix. Define the state estimation error $e(t) := \hat{x}(t) - x(t)$ and the output estimation error $e_y(t) := \hat{y}(t) - y(t)$. Suppose the discontinuous term ν is defined as

$$\nu = \begin{cases} 1 & \text{if} \;\; e_y > 0 \\ -1 & \text{if} \;\; e_y < 0 \end{cases} \tag{3.6}$$

The error system is governed by

$$\dot{e}(t) = Ae(t) + G_n\nu \tag{3.7}$$

From (3.6), it is clear that ν is discontinuous. Therefore the differential equation describing (3.7) has a discontinuous right hand side. For discussions on the solution for (3.7) for the special case when $e_y = 0$, see Filippov [32] and Ryan [93].

From (3.6) and (3.7) it can be seen that the dynamics associated with the state estimation error is a type of variable structure system [25]: the output error injection term is deliberately changed during the observation process, according to some defined rule (in this case the one in (3.6)) which depends on the trajectory of the output estimation error vector $e_y(t)$. From (3.6), it is clear that the term ν switches discontinuously about the surface $\mathcal{S} = \{e : Ce = 0\}$. The purpose of the discontinuous term ν is to drive the trajectories of the error system onto this surface, and force them to remain there. Notice that in this case, being constrained to $\mathcal{S}$ corresponds to a situation in which the output of the observer is identical to the output of the system.

The following simulation was carried out for the system in (3.1) - (3.2) with the observer scheme (3.4) - (3.5) where the distribution matrix

$$G_n = \begin{bmatrix} 1 \\ -2 \end{bmatrix}$$

The initial condition of the states were assumed to be 0.5 and -0.8 respectively, and the initial conditions of the observer states were set to 0. For simplicity assume $u(t) = 0$. The following simulation results were obtained.

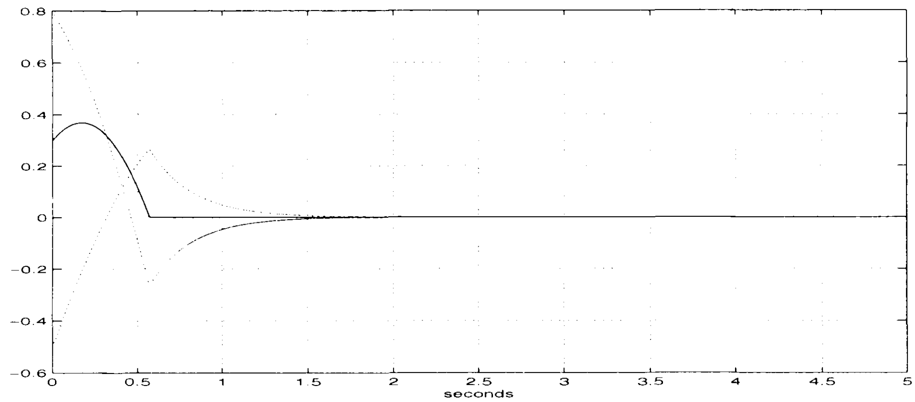

Figure 3.1: *The solid line is the output estimation error $e_y(t)$. The dotted lines are the state estimation error $e(t)$.*

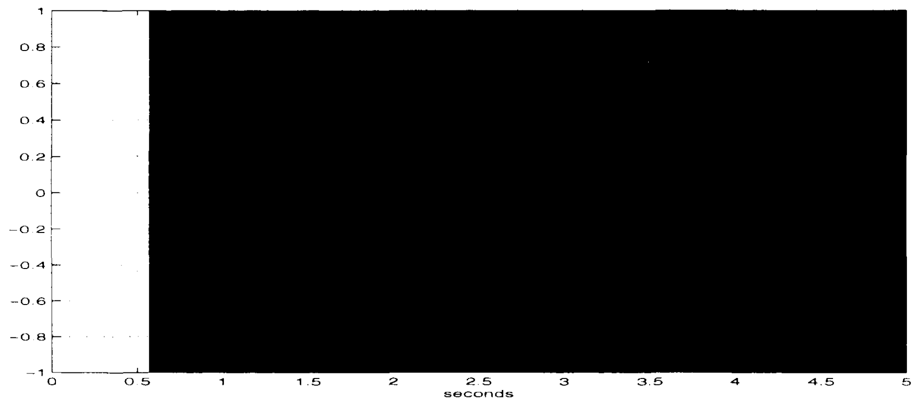

Figure 3.2: *The nonlinear discontinuous term ν.*

Figure 3.1 shows how the output estimation error $e_y(t)$ has been forced to zero in finite time (at about 0.66 seconds) and remains at zero from then on. This finite time convergence arises because of the discontinuous term ν. Figure 3.2 shows the nonlinear discontinuous term ν. When the state estimation error has been forced onto the sliding surface $\mathcal{S}$, the term ν starts to switch at a very high frequency.

When the state estimation error has been forced onto and remains on the surface $\mathcal{S}$, the observer is said to be in a *sliding mode* [110]. In the literature $\mathcal{S}$ is commonly referred to as the sliding surface. During the sliding motion, the error system will experience a *reduced order motion* [110]. It can be seen from Figure 3.1 that although $e_y(t) = Ce(t) = 0$ after 0.66 seconds, the state estimation error $e(t) \neq 0$ but decays exponentially to zero. This is governed by the reduced order motion. This is best observed by introducing a coordinate transformation $x \mapsto T_c x$ where

$$T_c = \begin{bmatrix} 2 & 1 \\ 1 & 1 \end{bmatrix} \tag{3.8}$$

In this new coordinate system, the output distribution matrix becomes

$$C \mapsto CT_c^{-1} = \begin{bmatrix} 0 & 1 \end{bmatrix}$$

and hence the error state space is decomposed into measured (e_y) and unmeasured (e_1) states

$$e \mapsto T_c e = \begin{bmatrix} e_1 \\ e_y \end{bmatrix}$$

After applying the coordinate transformation from (3.8), $A \mapsto T_c A T_c^{-1}, G_n \mapsto T_c G_n$ and the error system in (3.7) can be re-written as

$$\dot{e}_1(t) = -4e_1(t) + 6e_y(t) \tag{3.9}$$

$$\dot{e}_y(t) = -3e_1(t) - 4e_y(t) - \nu \tag{3.10}$$

During the sliding motion, $e_y(t) = 0$ and hence equation (3.9) becomes

$$\dot{e}_1(t) = -4e_1(t) \tag{3.11}$$

which is the reduced order motion, where the number -4 is its eigenvalue.

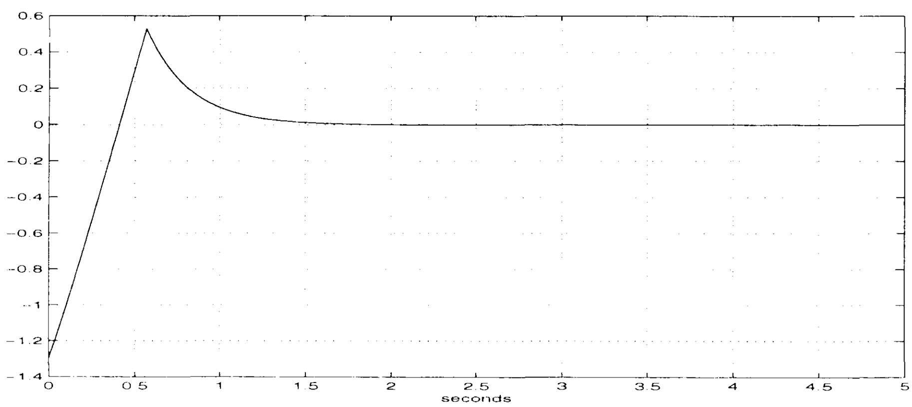

Figure 3.3: *The non-output error vector $e_1(t)$.*

Figure 3.3 shows the reduced order motion associated with $e_1(t)$ for the previous simulation. Of course this is valid only after sliding motion has taken place, at 0.66 seconds. Notice that $e_1(t)$ behaves as a first order decay as predicted in (3.11).

For a sliding mode observer, two things need to be designed: the nonlinear discontinuous term and its distribution matrix (ν and G_n respectively in this example). These must be designed so that the output estimation error is driven to zero in finite time, and to ensure the reduced order sliding motion is stable.

The rest of this chapter will describe the Utkin [110], Walcott - Zak [111] and the Edwards - Spurgeon [23] observers.

3.3 The Utkin observer

The observer described in the previous section may be termed an Utkin observer [110]. Here, the concepts described in the previous section will be explained for a more general system. Consider the linear system described by

$$\dot{x}(t) = Ax(t) + Bu(t) \tag{3.12}$$

$$y(t) = Cx(t) \tag{3.13}$$

where $A \in \mathcal{R}^{n\times n}, B \in \mathcal{R}^{n\times m}, C \in \mathcal{R}^{p\times n}$ and the pair (A, C) is observable. Introduce a linear nonsingular change of coordinates associated with the matrix

$$T_c = \begin{bmatrix} N_c^T \\ C \end{bmatrix} \tag{3.14}$$

where the columns of N_c span the null space of C. Applying the change of coordinates so that $x \mapsto T_c x$, then the triple (A, B, C) will become

$$T_c A T_c^{-1} = \begin{bmatrix} A_{11} & A_{12} \\ A_{21} & A_{22} \end{bmatrix}, \quad T_c B = \begin{bmatrix} B_1 \\ B_2 \end{bmatrix}, \quad C T_c^{-1} = \begin{bmatrix} 0 & I_p \end{bmatrix} \tag{3.15}$$

where $A_{11} \in \mathcal{R}^{(n-p)\times(n-p)}$ and $B_1 \in \mathcal{R}^{(n-p)\times m}$.

Utkin [110] proposed an observer of the form

$$\dot{\hat{x}}(t) = A\hat{x}(t) + Bu(t) + G_n\nu \tag{3.16}$$

$$\hat{y}(t) = C\hat{x}(t) \tag{3.17}$$

where $(\hat{x}, \hat{y})$ are the estimates of (x, y), and ν is a nonlinear discontinuous term. Define $e(t) := \hat{x}(t) - x(t)$ and $e_y(t) := \hat{y}(t) - y(t)$ as the state estimation and output estimation errors respectively. The term ν is defined component-wise as

$$\nu_i = \rho\, sgn(\hat{y}_i - y_i), \quad i = 1, 2, ..., p \tag{3.18}$$

where sgn is the $signum$ function, and ρ is a positive real scalar.

From (3.18), the term ν has been designed to switch discontinuously about the sliding surface $\mathcal{S} = \{e : Ce = 0\}$ and to drive the trajectories of $e(t)$ to $\mathcal{S}$. Assume (in the coordinate system of (3.15)) the gain G_n has the structure

$$G_n = \begin{bmatrix} G_{n,1} \\ -I_p \end{bmatrix} \tag{3.19}$$

where $G_{n,1} \in \mathcal{R}^{(n-p)\times p}$. The matrix $G_{n,1}$ represents the design freedom in the observer. Using the definition for $e(t)$, the following error system is obtained from equations (3.12) - (3.13) and (3.16) - (3.17)

$$\dot{e}(t) = Ae(t) + G_n\nu \tag{3.20}$$

Partitioning the error system (3.20) conformably with the coordinate system in (3.15) yields

$$\dot{e}_1(t) = A_{11}e_1(t) + A_{12}e_y(t) + G_{n,1}\nu \tag{3.21}$$

$$\dot{e}_y(t) = A_{21}e_1(t) + A_{22}e_y(t) - \nu \tag{3.22}$$

where $e_1 \in \mathcal{R}^{n-p}$. From the definition of ν, equation (3.22) becomes (component-wise)

$$\dot{e}_{y,i}(t) = A_{21,i}e_1(t) + A_{22,i}e_y(t) - \rho\, sgn(e_{y,i}) \tag{3.23}$$

where $A_{21,i}$ and $A_{22,i}$ represent the i-th rows of A_{21} and A_{22} respectively.

From (3.23), it is straightforward to show that

$$\begin{aligned} e_{y,i}\dot{e}_{y,i} &= e_{y,i}(A_{21,i}e_1 + A_{22,i}e_y) - \rho|e_{y,i}| \\ &< -|e_{y,i}|(\rho - |(A_{21,i}e_1 + A_{22,i}e_y)|) \end{aligned}$$

If the scalar ρ is large enough such that it satisfies $\rho > |A_{21,i}e_1 + A_{22,i}e_y| + \eta$, for some $\eta > 0$, then it can be shown that

$$e_{y,i}\dot{e}_{y,i} < -\eta|e_{y,i}| \tag{3.24}$$

The differential inequality (3.24) is called the *reachability condition* [25]. When this reachability condition is satisfied, that particular component of the output estimation error $e_y(t)$ will be forced to zero in finite time and subsequently remains at zero. When every component of $e_y(t)$ has been forced to zero, sliding motion takes place.

The properties of the sliding motion will be investigated in the following subsections: in particular, the effect of the choice of $G_{n,1}$ will be described.

3.3.1 The concept of equivalent output error injection

Before analysing the properties of the sliding motion, an interpretation of the nonlinear discontinuous term ν will be given in terms of its 'average' or low-frequency behaviour. When sliding motion has been achieved, $e_y(t) = \dot{e}_y(t) = 0$, and hence the error system defined by (3.21) - (3.22) can be written as

$$\dot{e}_1(t) = A_{11}e_1(t) + G_{n,1}\nu_{eq} \tag{3.25}$$

$$0 = A_{21}e_1(t) - \nu_{eq} \tag{3.26}$$

where ν_{eq} is the so-called *equivalent output error injection* that is required to maintain the sliding motion. This is not the term ν that is applied to the system, but rather, the *averaged* injection applied to maintain sliding motion ($e_y(t) = \dot{e}_y(t) = 0$). Note that this concept of equivalent output error injection is valid only during the sliding motion, and hence (3.25) - (3.26) are valid only when sliding takes place on the surface $\mathcal{S}$.

From [110] an appropriate way to extract the term ν_{eq} is to pass the components of the discontinuous switched term ν through a low pass filter, of time constant τ, satisfying the following differential equation

$$\tau\dot{\nu}_{eq,i} + \nu_{eq,i} = \nu_i \tag{3.27}$$

3.3.2 Properties of the sliding motion

This subsection will analyse the behaviour of the system during the sliding motion. Eliminating the term ν_{eq} from (3.25) - (3.26) yields the following expression

$$\dot{e}_1(t) = (A_{11} + G_{n,1}A_{21})e_1(t) \tag{3.28}$$

This represents the reduced order motion (of order $n - p$) that will be experienced by the system during the sliding motion. This order reduction is a typical feature of sliding mode systems [110, 25].

From the Popov-Belevitch-Hautus (PBH) rank test [25], if the pair (A, C) is fully observable, then the following matrix

$$\begin{bmatrix} sI_n - A \\ C \end{bmatrix} \tag{3.29}$$

will have full column rank for all values of s. Partitioned into the coordinates of (3.15), the expression in (3.29) becomes

$$\begin{bmatrix} sI_{n-p} - A_{11} & -A_{12} \\ -A_{21} & sI_p - A_{22} \\ 0 & I_p \end{bmatrix} \tag{3.30}$$

For (3.30) to have full column rank, the following matrix pencil must have full column rank

$$\begin{bmatrix} sI_{n-p} - A_{11} \\ -A_{21} \end{bmatrix} \tag{3.31}$$

for all values of s. From the PBH rank test this is equivalent to the pair (A_{11}, A_{21}) being fully observable.

Therefore if (A, C) is observable, then (A_{11}, A_{21}) will also be observable, hence an appropriate matrix $G_{n,1}$ can always be chosen to ensure that the reduced order motion in (3.28) is stable.

The next subsection discusses the example from §3.1 in the context of the ideas presented above.

3.3.3 An example

Consider a second order state-space system described by (3.12) and (3.13) where

$$A = \begin{bmatrix} 0 & 1 \\ -2 & 0 \end{bmatrix}, \quad B = \begin{bmatrix} 0 \\ 1 \end{bmatrix}, \quad C = \begin{bmatrix} 1 & 1 \end{bmatrix} \tag{3.32}$$

which represents a simple harmonic oscillator. For simplicity assume $u(t) = 0$. Define a nonsingular matrix T_c from (3.14)

$$T_c = \begin{bmatrix} 1 & -1 \\ 1 & 1 \end{bmatrix} \tag{3.33}$$

so that $x \mapsto T_c x$. The system triple (A, B, C) becomes

$$T_c A T_c^{-1} = \begin{bmatrix} 0.5 & 1.5 \\ -1.5 & -0.5 \end{bmatrix}, \quad T_c B = \begin{bmatrix} -1 \\ 1 \end{bmatrix}, \quad C T_c^{-1} = \begin{bmatrix} 0 & 1 \end{bmatrix} \tag{3.34}$$

In the coordinates of (3.34), suppose the nonlinear gain from (3.19) $G_{n,1} = 3$. In this case the sliding motion will be governed by $A_{11} + G_{n,1}A_{21} = -4$, which is stable. In the original coordinates of (3.32), the nonlinear gain can be calculated as

$$G_n = T_c^{-1} \begin{bmatrix} G_{n,1} \\ -I_p \end{bmatrix} = \begin{bmatrix} 0.5 & 0.5 \\ -0.5 & 0.5 \end{bmatrix} \begin{bmatrix} 3 \\ -1 \end{bmatrix} = \begin{bmatrix} 1 \\ -2 \end{bmatrix} \tag{3.35}$$

This choice of $G_{n,1} = 3$ has resulted in the observer design described in §3.1 where $\rho = 1$. The following figures are associated with the simulation described in §3.2.

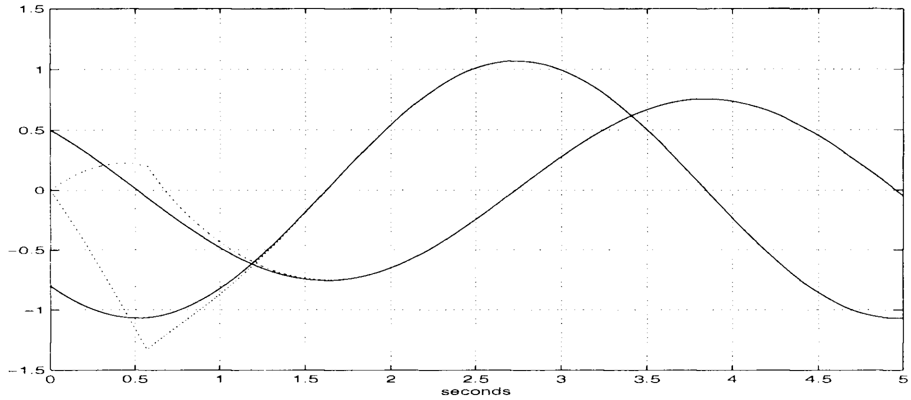

Figure 3.4: *System states $x(t)$ and the observer estimates $\hat{x}(t)$. The dotted lines represent the estimated states.*

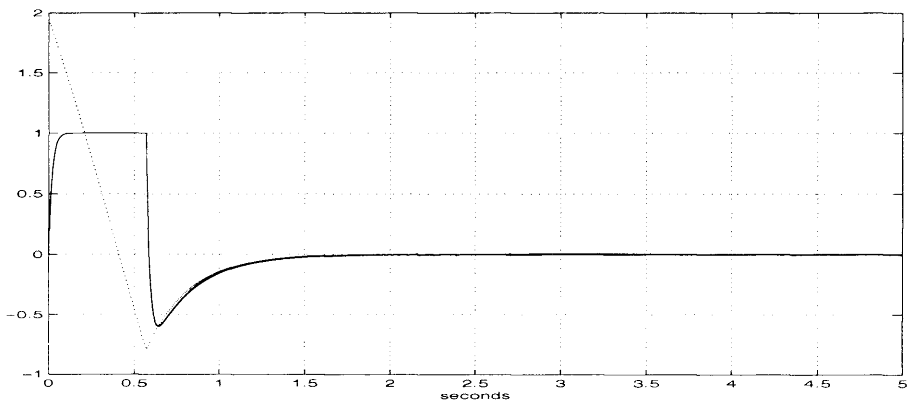

Figure 3.5: *The equivalent output error injection, ν_{eq}. The dotted line is $A_{21}e_1(t)$. Note that as sliding motion is achieved, both the lines converge, as predicted in (3.26).*

Figure 3.4 shows the system states and the observer estimates, where it can be seen that at approximately 1.5 seconds, perfect tracking of the states takes place. Figure 3.5 shows the equivalent output error injection signal ν_{eq} obtained from passing the term ν from Figure 3.2 through a low pass filter of time constant $\tau = 0.02$ seconds. Notice that the term ν_{eq} conforms to equation (3.26) after the sliding motion has taken place at approximately 0.66 seconds.

In the following simulations the same observer is used but the initial conditions of the states have been changed to be 0.5 and -1.5 respectively. The initial conditions of the observer are once again at 0. This situation represents effectively an increase in the initial conditions of $e_1(t)$ and $e_y(t)$.

From Figure 3.6, the output estimation error $e_y(t)$ pierces the surface $\mathcal{S} = \{e : Ce = 0\}$ at approximately 0.87 seconds, but does not remain there. This is due to the fact that the

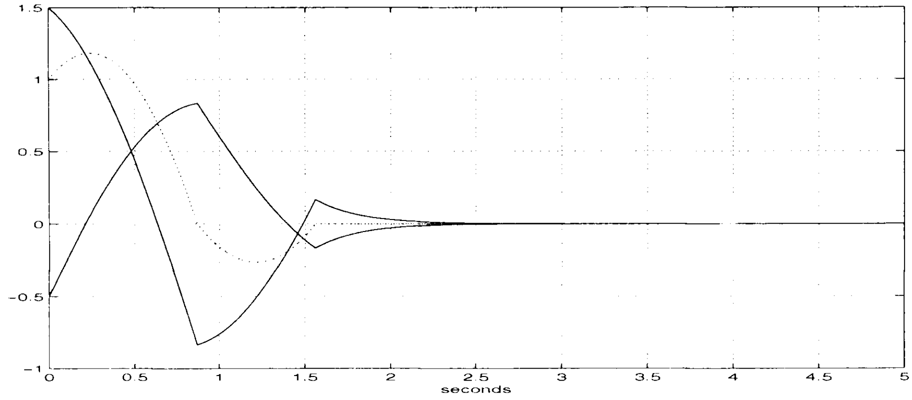

Figure 3.6: *The dotted line is the output estimation error $e_y(t)$. The solid lines are the components of the state estimation error $e(t)$.*

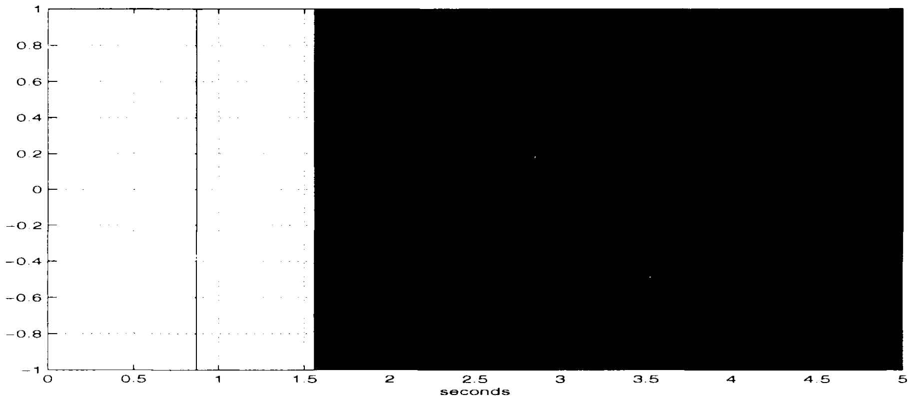

Figure 3.7: *The discontinuous term ν with larger error initial conditions.*

reachability condition has not yet been satisfied, because of the larger state estimation errors at that time instant. However, when $e_y(t)$ reaches 0 again at approximately 1.55 seconds, it remains there, and sliding motion begins. At this point, the error vector $e(t)$ is much smaller than it was at 0.87 seconds, and the reachability condition has been satisfied. Figure 3.7 shows the discontinuous term ν for the case when the initial errors are large.

3.3.4 Disturbance rejection properties

Suppose equation (3.12) is now replaced by

$$\dot{x}(t) = Ax(t) + Bu(t) + M\xi(t, x, u) \tag{3.36}$$

where $\xi \in \mathcal{R}^q$ is a disturbance vector, and $M \in \mathcal{R}^{n \times q}$ is the disturbance distribution matrix.

Suppose the gain G_n is designed such that it is matched to the disturbance matrix i.e. $M = G_n X$ for some $X \in \mathcal{R}^{p \times q}$. Then in the coordinates of (3.15) and (3.19), the following condition will be satisfied

$$M = \begin{bmatrix} G_{n,1}X \\ -X \end{bmatrix} \tag{3.37}$$

and the error system (3.21) - (3.22) becomes

$$\dot{e}_1(t) = A_{11}e_1(t) + A_{12}e_y(t) + G_{n,1}\nu - G_{n,1}X\xi(t,x,u) \tag{3.38}$$

$$\dot{e}_y(t) = A_{21}e_1(t) + A_{22}e_y(t) - \nu + X\xi(t,x,u) \tag{3.39}$$

From (3.39), it is straightforward to show that

$$\begin{aligned} e_{y,i}\dot{e}_{y,i} &= e_{y,i}(A_{21,i}e_1 + A_{22,i}e_y + X_i\xi) - \rho|e_{y,i}| \\ &< -|e_{y,i}|(\rho - |A_{21,i}e_1 + A_{22,i}e_y + X_i\xi|) \end{aligned}$$

If $\rho > |A_{21,i}e_1 + A_{22,i}e_y + X_i\xi| + \eta$ for a scalar $\eta > 0$ then the reachability condition in (3.24) will be satisfied, and an ideal sliding motion takes place in finite time.

When sliding motion has been attained, equations (3.38) - (3.39) become

$$\dot{e}_1(t) = A_{11}e_1(t) + G_{n,1}\nu_{eq} - G_{n,1}X\xi(t,x,u) \tag{3.40}$$

$$0 = A_{21}e_1(t) - \nu_{eq} + X\xi(t,x,u) \tag{3.41}$$

Eliminating ν_{eq} from (3.40) and (3.41) yields

$$\dot{e}_1(t) = (A_{11} + G_{n,1}A_{21})e_1(t) \tag{3.42}$$

which is independent of the disturbance $\xi(t,x,u)$. Notice that for the existence of an ideal sliding motion, the matching condition (3.37) is not required; a large enough ρ is sufficient to induce sliding motion. The matching condition is only required for the reduced order motion to be independent of $\xi(t,x,u)$. From (3.42), $e_1(t) \to 0$, and hence from (3.41), $\nu_{eq} \to X\xi(t,x,u)$. Hence the term ν_{eq} is able to provide information about the disturbance.

Consider the case when

$$M = \begin{bmatrix} 1 \\ -2 \end{bmatrix}$$

and $\xi(t,x,u) = 0.2\,sin\,x_1(t)$. Notice from (3.35) that $G_n = M$ and hence the matching condition from (3.37) is satisfied where $X = 1$. Assuming the same initial conditions as in §3.3.3, the following simulation results were obtained.

From Figures 3.8 and 3.9, sliding motion is achieved after approximately 0.66 seconds and the error vectors experience a first order decay, as before, unaffected by the disturbance. This

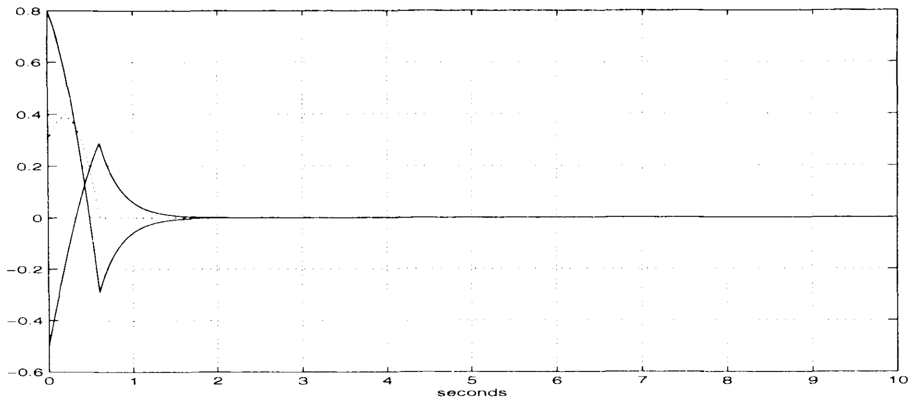

Figure 3.8: *The dotted line is the output estimation error* $e_y(t)$. *The solid lines are the components of the state estimation error* $e(t)$.

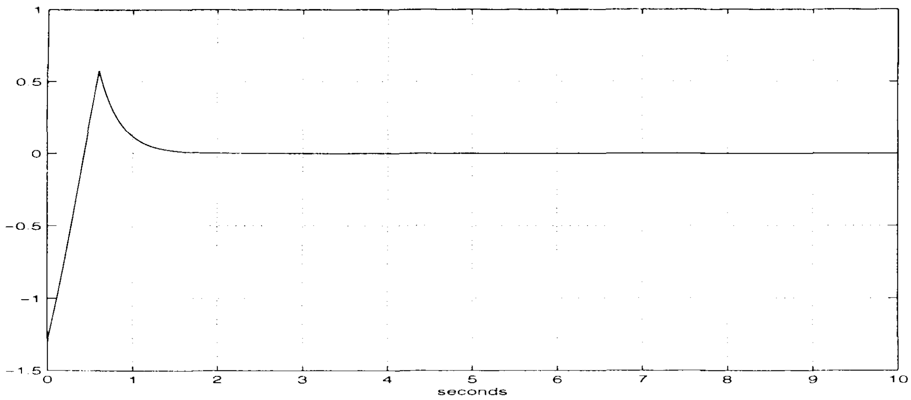

Figure 3.9: *The error vector associated with the sliding motion,* $e_1(t)$

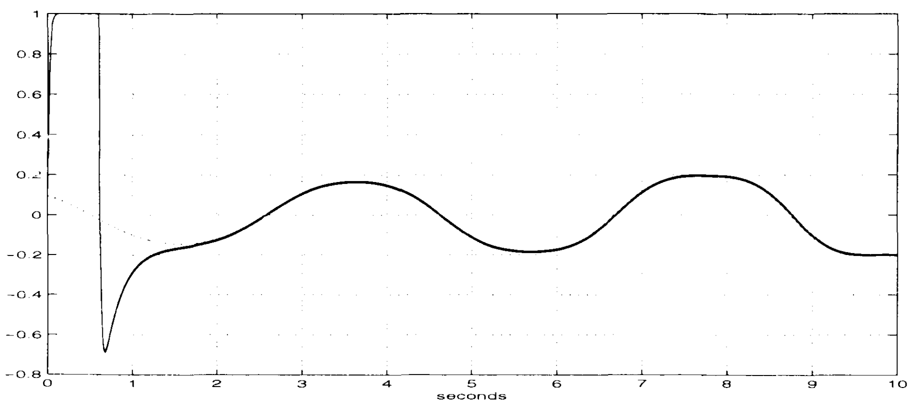

Figure 3.10: *The solid line is the equivalent output error injection* ν_{eq}. *The dotted line is the disturbance* $\xi(t, x, u)$.

disturbance rejection property is a major advantage of sliding mode observers over the nominal Luenberger observer. From Figure 3.10, the effect of the disturbance $\xi(t, x, u)$ can be seen in the signal ν_{eq}. When the reduced order motion $e_1(t)$ has become small (at about 1.5 seconds), the signal ν_{eq} 'reproduces' the disturbance $\xi(t, x, u)$ (with a small delay due to the low-pass filter used to obtain ν_{eq}). Notice that the term ν was not designed with any a-priori knowledge about $\xi(t, x, u)$, except that it is bounded. This feature of 'disturbance tracking' is essential to the work in this thesis.

3.3.5 Pseudo-sliding by smoothing the discontinuous term

From Figure 3.2, the term ν is discontinuous with very high frequency switching. Systems with discontinuities often pose problems for simulation packages and generally cause an increase in the computational burden. It is often useful to 'smooth' the discontinuity. (This is particularly true for sliding mode control systems where high frequency switched control signals would represent an unacceptable input). Recall that ν is defined component-wise by $\nu_i = \rho\, sgn(e_{y,i})$, which can also be expressed as

$$\nu_i = \rho \frac{e_{y,i}}{|e_{y,i}|} \tag{3.43}$$

From [25, 26, 27], a method to smooth ν would be to approximate (3.43) by

$$\nu_i = \rho \frac{e_{y,i}}{|e_{y,i}| + \delta} \tag{3.44}$$

where δ is a small positive scalar. This results in a trade-off between ideal performance and maintaining a smooth output error injection.

Repeating the simulation in §3.3.3, and expressing ν as in (3.44) with $\delta = 0.0001$, the following figures were obtained:

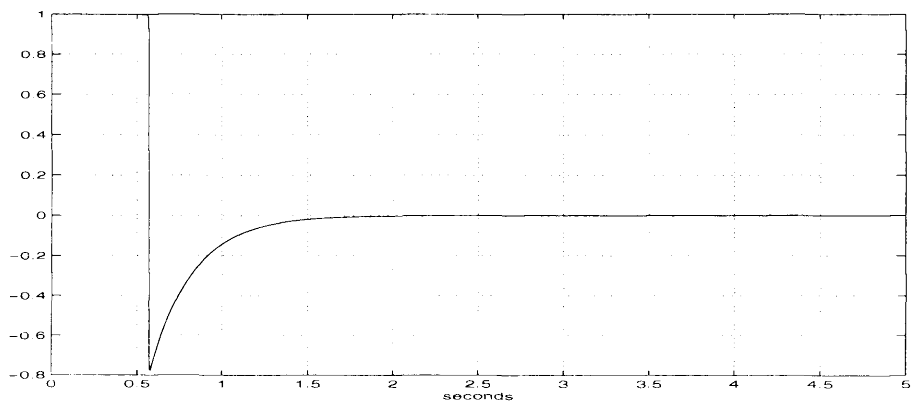

Figure 3.11: *The output error injection term ν after being smoothed*

Figure 3.11 shows the smooth injection term ν from (3.44). Notice that its shape is similar to ν_{eq} from Figure 3.5. From Figure 3.12, it can be seen that the performance of the system is relatively unaffected (in comparison with Figure 3.1). Technically in this situation ideal

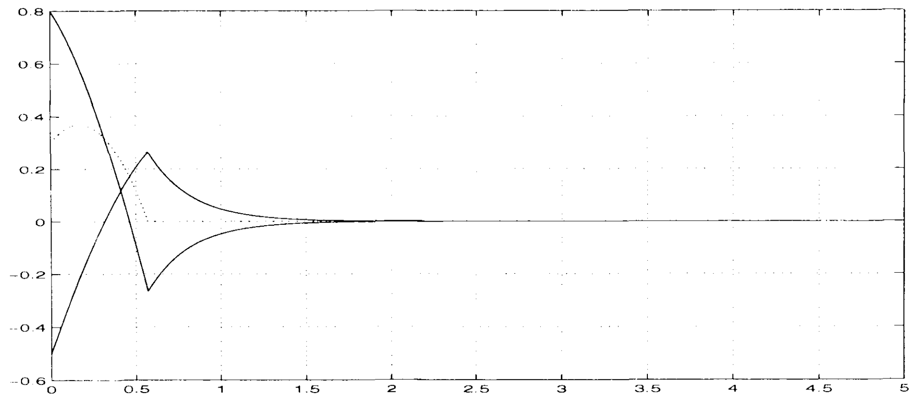

Figure 3.12: *The dotted line is the output estimation error $e_y(t)$. The solid lines are the components of the state estimation error $e(t)$.*

sliding is not taking place. Instead $e_y(t)$ is driven to a small boundary layer around the surface $\mathcal{S}$ [110, 25].

3.3.6 A modification to include a linear term

For the observer that has been discussed, the size of the parameter ρ dictates the size of the domain in which sliding takes place. However, for practical reasons, a very large value of ρ is not desirable and hence there is a trade off.

For motivation purposes consider an unstable state-space system[1]

$$A = \begin{bmatrix} -2 & -3 \\ 1 & 3 \end{bmatrix}, \quad B = \begin{bmatrix} 0 \\ 1 \end{bmatrix}, \quad C = \begin{bmatrix} 0 & 1 \end{bmatrix} \tag{3.45}$$

To design an Utkin observer no change of coordinates is needed because the matrix C is already in the required structure of (3.15). Specifying $G_{n,1} = 0$ will yield a reduced order motion pole of $A_{11} + G_{n,1}A_{21} = -2$. In the following the gain ρ has been specified to be 1.

A series of simulations was carried out for different initial conditions of (e_1, e_y), both components ranging from -3 to $+3$.

In Figure 3.13, the 'shaded' area is the region in which the initial conditions of (e_1, e_y) must lie for sliding motion to occur. Elsewhere the observer fails to provide converging state esti-

[1]In the following simulations full state feedback $u(t) = Kx(t)$ where

$$K = \begin{bmatrix} 1 & -1 \end{bmatrix}$$

has been employed so that $\lambda(A + BK) = \{\pm 1.4142i\}$. The reason for this choice of closed loop eigenvalues is that the states will be oscillatory, and the tracking of the states can be observed if desired.

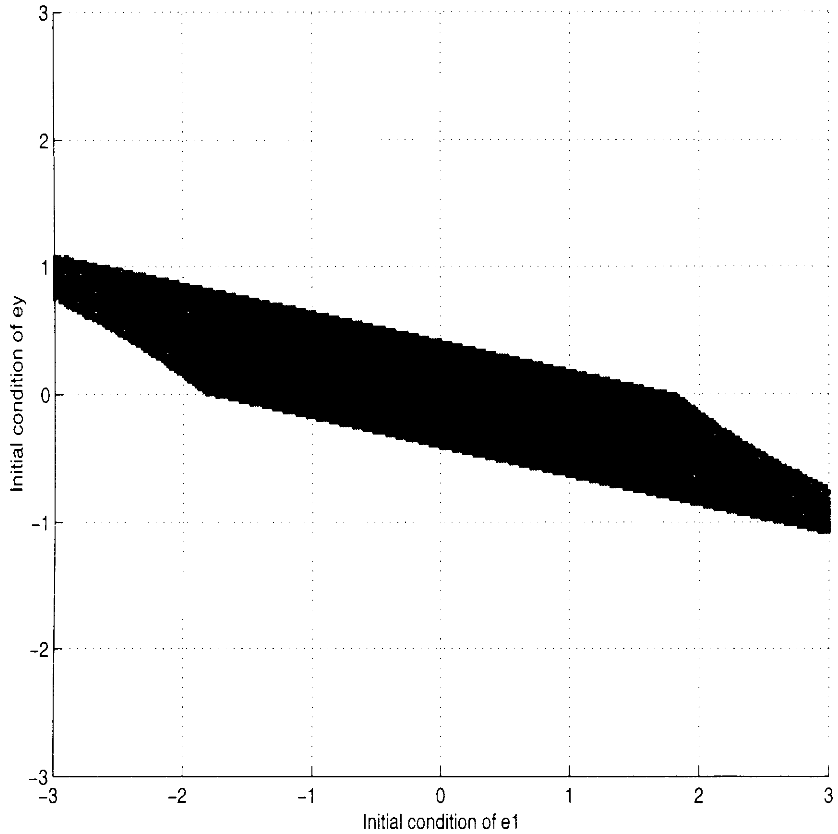

Figure 3.13: *The sliding region*

mations. The shaded region is sometimes referred to as the *sliding patch* [100]. Of course the size of the shaded area can be enlarged by increasing the value of ρ, but for practical reasons, that may be undesirable.

Consider the effect of adding an output error feedback term to the observer. Equation (3.16) can be modified to be

$$\dot{\hat{x}}(t) = A\hat{x}(t) - G_l e_y(t) + Bu(t) + G_n \nu \tag{3.46}$$

where $G_l \in \mathcal{R}^{n \times p}$. Slotine *et al.* [100] argued that an appropriate choice of the gain G_l will enlarge the sliding patch. From equations (3.12), (3.13) and (3.17), this results in the state estimation error system

$$\dot{e}(t) = (A - G_l C)e(t) + G_n \nu \tag{3.47}$$

The error system in (3.47) can be analysed with respect to quadratic stability[2] by using a positive definite quadratic function

$$\mathcal{V} = e^T P e \tag{3.48}$$

where $P \in \mathcal{R}^{n \times n}$ is a symmetric positive definite matrix.

[2]For details on the concept of quadratic stability, see §B.2 in the appendix.

Differentiating (3.48) with respect to time yields

$$\begin{aligned} \dot{\mathcal{V}} &= \dot{e}^T P e + e^T P \dot{e} \\ &= e^T (P(A - G_l C) + (A - G_l C)^T P) e + 2 e^T P G_n \nu \end{aligned} \tag{3.49}$$

If P and G_l can be chosen such that the expression in (3.49) is negative, then the error system in (3.47) is (globally) quadratically stable for all values of ρ.

For the system in (3.45), the linear gain was specified to be

$$G_l = \begin{bmatrix} -3 \\ 6 \end{bmatrix} \tag{3.50}$$

and the resulting closed loop error system in (3.47) can be written as

$$\dot{e}_1(t) = -2e_1(t) \tag{3.51}$$

$$\dot{e}_y(t) = e_1(t) - 3e_y(t) - sgn(e_y) \tag{3.52}$$

Consider a positive definite quadratic function as in (3.48) where the error vector e and matrix P respectively are

$$e = \begin{bmatrix} e_1 \\ e_y \end{bmatrix}, \quad P = \begin{bmatrix} \frac{1}{4} & 0 \\ 0 & 1 \end{bmatrix} \tag{3.53}$$

and hence the quadratic function from (3.48)

$$\mathcal{V} = \frac{1}{4} e_1^2 + e_y^2$$

Differentiating with respect to time yields

$$\begin{aligned} \dot{\mathcal{V}} &= \frac{1}{2} e_1 \dot{e}_1 + 2 e_y \dot{e}_y \\ &= \frac{1}{2} e_1(-2e_1) + 2e_y(e_1 - 3e_y - sgn(e_y)) \\ &= -e_1^2 - 6e_y^2 + 2e_1 e_y - 2|e_y| \\ &= -(e_1 - e_y)^2 - 5e_y^2 - 2|e_y| \end{aligned}$$

which is negative, and hence global stability of this error system has been proven. When the magnitude of the errors become small enough, the reachability condition in (3.24) is satisfied and sliding motion takes place. This example shows that in certain circumstances the introduction of a linear output error injection term can be beneficial.

3.4 The Walcott - Zak observer

This subsection considers the design of a robust sliding mode observer incorporating both linear and nonlinear output error injection terms. Consider the uncertain system

$$\dot{x}(t) = Ax(t) + Bu(t) + d(t, x, u) \tag{3.54}$$

$$y(t) = Cx(t) \tag{3.55}$$

where $A \in \mathcal{R}^{n\times n}, B \in \mathcal{R}^{n\times m}, C \in \mathcal{R}^{p\times n}$ and $p \geq m$. The matrices B and C are assumed to be full rank. The function $d : \mathcal{R}_+ \times \mathcal{R}^n \times \mathcal{R}^m \to \mathcal{R}^n$ is unknown and represents the system uncertainty. Assume that

$$d(t, x, u) = B\xi(t, x, u) \tag{3.56}$$

where the function $\xi : \mathcal{R}_+ \times \mathcal{R}^n \times \mathcal{R}^m \to \mathcal{R}^m$ is unknown but bounded, so that

$$||\xi(t, x, u)|| \leq \alpha(t, y, u) \tag{3.57}$$

where $\alpha : \mathcal{R}_+ \times \mathcal{R}^p \to \mathcal{R}_+$ is a known function. In practice, the function $\alpha(t, y, u)$ is found by carrying out experiments on the system to estimate the magnitude of the uncertainty $\xi(t, x, u)$. Walcott & Zak [112, 111] assume that

- (A, C) is fully observable and hence there exists a matrix $G_l \in \mathcal{R}^{n\times p}$ so that the matrix $A_o := A - G_lC$ is stable
- There exists a pair (P, Q) which satisfies

$$PA_o + A_o^T P = -Q \tag{3.58}$$

and

$$C^T F^T = PB \tag{3.59}$$

for some $F \in \mathcal{R}^{m\times p}$ where P and Q are symmetric positive definite.

The problem considered by Walcott & Zak involves estimating the states $x(t)$ of the uncertain system given in (3.54) so that the error system

$$e(t) = \hat{x}(t) - x(t) \tag{3.60}$$

is quadratically stable despite the presence of uncertainty. Utilising the assumptions above, Walcott & Zak [111] propose an observer of the form

$$\dot{\hat{x}}(t) = A_o\hat{x}(t) + G_l y(t) + Bu(t) + \nu \tag{3.61}$$

$$\hat{y}(t) = C\hat{x}(t) \tag{3.62}$$

where

$$\nu = -\rho(t, y, u)\frac{P^{-1}C^T F^T FCe}{||FCe||}, \quad FCe \neq 0 \tag{3.63}$$

and the scalar function $\rho(.)$ is any function satisfying

$$\rho(t, y, u) \geq \alpha(t, y, u) + \eta_o \tag{3.64}$$

where η_o is some positive scalar.

From (3.54) - (3.55) and (3.61) - (3.62), the following equation is obtained

$$\dot{e}(t) = A_o e(t) - B\xi(t, x, u) + \nu \tag{3.65}$$

To prove that the error system is quadratically stable, consider the quadratic Lyapunov function $\mathcal{V} = e^T Pe$. Taking the derivative along the system trajectory

$$\begin{aligned}
\dot{\mathcal{V}} &= \dot{e}^T Pe + e^T P\dot{e} \\
&= e^T(PA_o + A_o^T P)e - 2e^T PB\xi + 2e^T P\nu \\
&= e^T(PA_o + A_o^T P)e - 2e^T PB\xi - 2\rho\frac{e^T C^T F^T FCe}{||FCe||} \\
&= e^T(PA_o + A_o^T P)e - 2e^T PB\xi - 2\rho||FCe||
\end{aligned}$$

Utilising (3.58) and the structural constraint (3.59),

$$\begin{aligned}
\dot{\mathcal{V}} &= -e^T Qe - 2e^T C^T F^T \xi - 2\rho||FCe|| \\
&\leq -e^T Qe + 2||FCe||||\xi|| - 2\rho||FCe|| \\
&\leq -e^T Qe - 2||FCe||(\rho - ||\xi||) \\
&\leq -e^T Qe - 2\eta_o||FCe||
\end{aligned}$$

and hence $\dot{\mathcal{V}} < 0$ and the error system (3.65) is quadratically stable. Walcott & Zak [112, 111] propose an algorithm for designing the observer which can be summarised as follows :

Step 1 : Choose the spectrum of A_o and compute G_l accordingly.

Step 2 : In order to solve $PB = C^T F^T$, express the elements of P symbolically in terms of the elements of F. Name the expression for P as P_F.

Step 3 : Form the matrix equality $PA_o + A_o^T P = -Q$. Obtain an expression for Q in terms of the elements of F and P_F. Call this expression $Q(F, P_F)$

Step 4 : Choose the elements of $Q(F, P_F)$ so that it is positive definite. This can be done by ensuring that $\triangle_i [Q(F, P_F)] > 0, i = 1, ..., n$ where $\triangle_i$ indicates the determinant of the i-th principle submatrix. From here, the elements of F can be obtained.

Step 5 : Equate $P = P_F$, and from there calculate the elements of P.

Though this approach and algorithm seem quite appealing, it will be tedious to perform the necessary calculations for large systems, and therefore may require a symbolic manipulation package. More importantly there is no indication of the type of system which will produce a successful design.

3.5 The Edwards - Spurgeon observer

This section will present the observer proposed by Edwards & Spurgeon [23]. Their observer has a similar structure to the Walcott-Zak observer, but the design method is different. Consider the dynamic system:

$$\dot{x}(t) = Ax(t) + Bu(t) + M\xi(t, x, u) \tag{3.66}$$

$$y(t) = Cx(t) \tag{3.67}$$

where $A \in \mathcal{R}^{n\times n}, B \in \mathcal{R}^{n\times m}, C \in \mathcal{R}^{p\times n}$ and $M \in \mathcal{R}^{n\times q}$ where $p \geq q$. Assume that the matrices C and M are full rank and the function $\xi : \mathcal{R}_+ \times \mathcal{R}^n \times \mathcal{R}^m \to \mathcal{R}^q$ is unknown but bounded so that

$$||\xi(t, x, u)|| \leq \alpha(t, y, u) \tag{3.68}$$

where $\alpha : \mathcal{R}_+ \times \mathcal{R}^p \to \mathcal{R}_+$ is a known function. In the case when $M = B$ this set up is identical to that described in §3.4 for the Walcott-Zak observer.

3.5.1 Coordinate transformations

It has been proven in [23, 25] that if $rank\ (CM) = q$ then there exists a change of coordinates T_o such that the triple (A, M, C) can be written in the form

$$A = \left[\begin{array}{c|c} A_{11} & A_{12} \\ \hline A_{211} & \\ & A_{22} \\ A_{212} & \end{array}\right], \quad M = \begin{bmatrix} 0 \\ M_2 \end{bmatrix}, \quad C = \begin{bmatrix} 0 & T \end{bmatrix} \tag{3.69}$$

where $T \in \mathcal{R}^{p\times p}$ and is orthogonal. The matrices $A_{11} \in \mathcal{R}^{(n-p)\times(n-p)}$, $A_{211} \in \mathcal{R}^{(p-q)\times(n-p)}$ and when partitioned have the structure

$$A_{11} = \begin{bmatrix} A_{11}^o & A_{12}^o \\ 0 & A_{22}^o \end{bmatrix} \quad \text{and} \quad A_{211} = \begin{bmatrix} 0 & A_{21}^o \end{bmatrix} \tag{3.70}$$

where $A_{11}^o \in \mathcal{R}^{r\times r}$ and $A_{21}^o \in \mathcal{R}^{(p-q)\times(n-p-r)}$ for some $r \geq 0$ and the pair (A_{22}^o, A_{21}^o) is completely observable. Furthermore, the eigenvalues of A_{11}^o are the invariant zeros of (A, M, C). Assume that A_{11}^o is stable, then from the observability of (A_{22}^o, A_{21}^o), it can be said that (A_{11}, A_{211}) is detectable. The matrix $M_2 \in \mathcal{R}^{p\times q}$ has the structure

$$M_2 = \begin{bmatrix} 0 \\ M_o \end{bmatrix} \tag{3.71}$$

where $M_o \in \mathcal{R}^{q\times q}$ is nonsingular.

Introduce a new change of coordinates

$$T_L = \begin{bmatrix} I_{n-p} & L \\ 0 & T \end{bmatrix} \tag{3.72}$$

where

$$L = \begin{bmatrix} L^o & 0 \end{bmatrix} \tag{3.73}$$

and $L^o \in \mathcal{R}^{(n-p)\times(p-q)}$ is a design matrix. Applying the change of coordinates induced by T_L, the triple (A, M, C) in (3.69) can be transformed to be

$$\mathcal{A} = \begin{bmatrix} \mathcal{A}_{11} & \mathcal{A}_{12} \\ \mathcal{A}_{21} & \mathcal{A}_{22} \end{bmatrix}, \quad \mathcal{M} = \begin{bmatrix} 0 \\ \mathcal{M}_2 \end{bmatrix}, \quad \mathcal{C} = \begin{bmatrix} 0 & I_p \end{bmatrix} \tag{3.74}$$

where $\mathcal{A}_{11} = A_{11} + L^o A_{211}$ and $\mathcal{M}_2 \in \mathcal{R}^{p\times q}$. Since (A_{11}, A_{211}) is detectable, L^o can be chosen so that $\mathcal{A}_{11}$ is stable.

3.5.2 Observer formulation

Edwards & Spurgeon [23, 25] propose a state observer of the form

$$\dot{\hat{x}}(t) = A\hat{x}(t) + Bu(t) - G_l e_y(t) + G_n \nu \tag{3.75}$$

$$\hat{y}(t) = C\hat{x}(t) \tag{3.76}$$

where $G_l \in \mathcal{R}^{n\times p}$ and $G_n \in \mathcal{R}^{n\times p}$ and $e_y(t) := \hat{y}(t) - y(t)$ is the output estimation error. The discontinuous vector ν is defined by

$$\nu = -\rho(t, y, u)\frac{e_y}{||e_y||}, \quad e_y \neq 0 \tag{3.77}$$

where $\rho(t, y, u)$ is a positive scalar function dependent on the magnitude of the uncertainty.

Defining the state estimation error as $e(t) := \hat{x}(t) - x(t)$, from (3.66) and (3.75), (3.67) and (3.76), the following error system can be obtained

$$\dot{e}(t) = A_o e(t) + G_n \nu - M\xi(t, x, u) \tag{3.78}$$

where $A_o = A - G_l C$.

Applying the change of coordinates $T_{cal} = T_L T_o$ such that $e \mapsto T_{cal} e = e_L$, then (3.78) will become

$$\dot{e}_L(t) = \mathcal{A}_o e_L(t) + \mathcal{G}_n \nu - \mathcal{M}\xi(t, x, u) \tag{3.79}$$

where $\mathcal{G}_l = T_{cal} G_l, \mathcal{G}_n = T_{cal} G_n$ and $\mathcal{A}_o = \mathcal{A} - \mathcal{G}_l \mathcal{C}$.

Edwards & Spurgeon [23, 25] chose $\mathcal{G}_l$ and $\mathcal{G}_n$ to be

$$\mathcal{G}_l = \begin{bmatrix} \mathcal{A}_{12} \\ \mathcal{A}_{22} - \mathcal{A}_{22}^s \end{bmatrix} \quad \text{and} \quad \mathcal{G}_n = \begin{bmatrix} 0 \\ P_o^{-1} \end{bmatrix} \tag{3.80}$$

where $\mathcal{A}_{22}^s \in \mathcal{R}^{p \times p}$ is a stable design matrix and P_o is a Lyapunov matrix for $\mathcal{A}_{22}^s$. A convenient choice of the scalar function $\rho : \mathcal{R}_+ \times \mathcal{R}^p \times \mathcal{R}^m \to \mathcal{R}_+$ is

$$\rho(t, y, u) \geq \|P_o C M\| \alpha(t, y, u) + \eta_o \tag{3.81}$$

where η_o is a positive scalar. Using the definitions of $\mathcal{C}$ and $\mathcal{M}$ given in (3.74), and partitioning $e_L = \begin{bmatrix} e_1^T & e_y^T \end{bmatrix}^T$, it is straightforward to show that the error equation (3.79) can be partitioned as

$$\dot{e}_1(t) = \mathcal{A}_{11} e_1(t) \tag{3.82}$$

$$\dot{e}_y(t) = \mathcal{A}_{21} e_1(t) + \mathcal{A}_{22}^s e_y(t) + P_o^{-1} \nu - \mathcal{M}_2 \xi(t, x, u) \tag{3.83}$$

The linear closed-loop system matrix

$$\mathcal{A}_o = \begin{bmatrix} \mathcal{A}_{11} & 0 \\ \mathcal{A}_{21} & \mathcal{A}_{22}^s \end{bmatrix} \tag{3.84}$$

which is stable.

Edwards & Spurgeon have proven in Proposition 6.1 of [25] that if there exists a Lyapunov matrix $\mathcal{P}$ of the structure

$$\mathcal{P} = \begin{bmatrix} P_1 & 0 \\ 0 & P_o \end{bmatrix} \tag{3.85}$$

where $P_1 \in \mathcal{R}^{(n-p)\times(n-p)}$ and $P_o \in \mathcal{R}^{p\times p}$ that satisfies

$$\mathcal{P}\mathcal{A}_o + \mathcal{A}_o^T\mathcal{P} < 0 \tag{3.86}$$

then the sliding mode observer is quadratically stable.

In Corollary 6.1 of [25], it is proved that sliding motion takes place on $\mathcal{S} = \{e : Ce = 0\}$ in finite time, by using a positive Lyapunov function $\mathcal{V}_s = e_y^T P_o e_y$.

3.5.3 Existence conditions for the sliding mode observer

Edwards & Spurgeon have proven in Proposition 6.2 of [25] that the necessary and sufficient conditions for the existence of a sliding mode observer of the form (3.75) - (3.76) that can reject the disturbance described by (3.66) and (3.68), are

- $rank(CM) = q$ (this implies that $p \geq q$)
- the invariant zeros (if any) of the triple (A, M, C) must be stable

The first condition is related to the disturbance rejection features of the observer, while the second condition is related to the stability of the sliding motion.

Remark : In the case of square systems ($p = q$), it can be seen that the matrix L^o does not exist. In this scenario, the sliding motion will be governed by the $n - p$ invariant zeros of the triple (A, M, C), and there will be no freedom associated with tuning the sliding motion [23].

A design method for the Edwards & Spurgeon observer can be summarised as follows

Step 1 : Check that $rank(CM) = q$ and that the invariant zeros of (A, M, C) lie in the negative left half plane. If not, then this observer cannot be designed.

Step 2 : Compute the transformation T_o and transform the triple (A, M, C) to the canonical form in (3.69).

Step 3 : Compute L^o so that $\mathcal{A}_{11}$ is stable.

Step 4 : From the value of L^o obtained, calculate T_L, and transform the system triple to the coordinate system in (3.74).

Step 5 : Choose a stable matrix $\mathcal{A}_{22}^s$.

Step 6 : Compute P_o to ensure $P_o\mathcal{A}_{22}^s + (P_o\mathcal{A}_{22}^s)^T < 0$.

Step 7 : Calculate $\mathcal{G}_l$ and $\mathcal{G}_n$ using (3.80). Then calculate the gains in the original coordinates by using the equations

$$G_l = T_{cal}^{-1}\mathcal{G}_l \qquad G_n = T_{cal}^{-1}\mathcal{G}_n$$

Step 8 : Estimate the magnitude of the uncertainty $\xi(t,x,u)$ (by means of experiment etc.) and estimate its bounding function $\alpha(t,y,u)$. Calculate the nonlinear gain $\rho(t,y,u)$ by using the inequality

$$\rho(t,y,u) \geq \|P_oCM\|\alpha(t,y,u) + \eta_o$$

This design method is straight-forward and no symbolic manipulations are needed. It is also easily implementable using available Matlab commands. A design example for this observer is available on page 146 of [25].

3.6 Conclusion

This chapter has shown how sliding mode observers have been developed over the years, and also demonstrated some of the sliding mode concepts that will be used in this thesis. Utkin designed an observer with a simple switched term. Via the Utkin observer, the concepts of reduced order motion, equivalent output error injection, disturbance rejection and smoothing approximations were demonstrated. Walcott & Zak included a linear gain into their observer structure, and used a Lyapunov approach to prove stability. In their design method, symbolic manipulation was used, which could be difficult for high order systems. Edwards & Spurgeon designed an observer similar in structure to the one by Walcott & Zak, and stated the conditions that need to be satisfied for the observer to exist. They also proposed a design method, which is straightforward. The Edwards & Spurgeon observer will be used in the work in this thesis.

Chapter 4

An LMI method for designing sliding mode observers

4.1 Introduction

This chapter will present a new design method for the sliding mode observer of Edwards & Spurgeon [23, 25]. In the method described in [23, 25] (and summarised in §3.5.3), certain degrees of freedom were not fully exploited; when the observer gains were selected, the sliding motion was already assumed to have been selected. The new design method proposed in this chapter seeks to exploit that freedom, so that the design of the sliding motion is incorporated into the design of the observer gains.

In this chapter, the sliding mode observer will be designed using Linear Matrix Inequalities (LMIs) [3]. A Riccati inequality will be solved, to obtain a sub-optimal Linear Quadratic Gaussian (LQG) solution. The sub-optimality arises from the fact that the solution is constrained to have a specific structure [23, 25]. As in classical LQG theory [69], there are two weighting matrices that influence the solution, which are the performance weighting matrix, and a noise amplification matrix.

All the ideas in this chapter will be demonstrated with a 7-th order aircraft model taken from [51].

4.2 Using LMIs to design a sliding mode observer: a simple illustration

This section will illustrate how an Edwards - Spurgeon observer described in §3.5 can be designed using LMIs. This seeks to motivate the method which will be described later.

Consider the second order system in §3.3.6 described by the triple (A, B, C) in (3.45). The system triple is already in the form of (3.74), and hence no coordinate transformations are needed. The problem now is to find a Lyapunov matrix of the structure (3.85) i.e.

$$P = \begin{bmatrix} p_1 & 0 \\ 0 & p_o \end{bmatrix} \tag{4.1}$$

where $p_1, p_o \in \mathcal{R}$ and a gain matrix

$$G_l = \begin{bmatrix} g_1 \\ g_2 \end{bmatrix} \tag{4.2}$$

where $g_1, g_2 \in \mathcal{R}$ to satisfy the inequality

$$P(A - G_lC) + (A - G_lC)^T P < 0 \tag{4.3}$$

Substituting from (3.45), (4.1) and (4.2) into (4.3),

$$\begin{aligned}
& \begin{bmatrix} p_1 & 0 \\ 0 & p_o \end{bmatrix} \begin{bmatrix} -2 & -3-g_1 \\ 1 & 3-g_2 \end{bmatrix} + \begin{bmatrix} -2 & 1 \\ -3-g_1 & 3-g_2 \end{bmatrix} \begin{bmatrix} p_1 & 0 \\ 0 & p_o \end{bmatrix} < 0 \\
\Leftrightarrow & \begin{bmatrix} -4p_1 & -3p_1 + p_o - p_1g_1 \\ -3p_1 + p_o - p_1g_1 & 6p_o - 2p_og_2 \end{bmatrix} < 0 \\
\Leftrightarrow \quad & p_1 \begin{bmatrix} -4 & -3 \\ -3 & 0 \end{bmatrix} + p_o \begin{bmatrix} 0 & 1 \\ 1 & 6 \end{bmatrix} + p_1g_1 \begin{bmatrix} 0 & -1 \\ -1 & 0 \end{bmatrix} + p_og_2 \begin{bmatrix} 0 & 0 \\ 0 & -2 \end{bmatrix} < 0
\end{aligned} \tag{4.4}$$

The inequality (4.4) can be re-written as an LMI in the form of (A.1) in Appendix A where the 'fixed matrices' are

$$F_0 = 0_{2\times 2}, F_1 = \begin{bmatrix} 4 & 3 \\ 3 & 0 \end{bmatrix}, F_2 = \begin{bmatrix} 0 & -1 \\ -1 & -6 \end{bmatrix}, F_3 = \begin{bmatrix} 0 & 1 \\ 1 & 0 \end{bmatrix}, F_4 = \begin{bmatrix} 0 & 0 \\ 0 & 2 \end{bmatrix}$$

and the LMI variables are

$$x_1 = p_1, \; x_2 = p_o, \; x_3 = p_1g_1, \; x_4 = p_og_2$$

Given x_1, x_2, x_3, x_4, the variables p_1, p_o, g_1 and g_2 can be determined uniquely. The LMI problem in (4.4) can be solved utilising software described by [39]. The LMI toolbox routine $feasp$ (which calculates a feasible solution for inequality (4.4)), yields the following results

$$x_1 = p_1 = 2.130, \; x_2 = p_o = 1.633, \; x_3 = -5.1268, \; x_4 = 8.1582$$

From the definitions of x_3 and x_4, the gain $\mathcal{G}_l$ can be back-calculated as

$$\mathcal{G}_l = \begin{bmatrix} -2.4069 \\ 6.4580 \end{bmatrix}$$

This example is meant only as an illustration. As in [23, 25], this approach assumed that the sliding motion is fixed. A more general problem is posed in the next section.

4.3 Preliminaries and problem statement

The purpose of this section is to lay the foundation for the work presented in this chapter. As in §3.5 consider the uncertain system

$$\dot{x}(t) = Ax(t) + Bu(t) + M\xi(t, x, u) \tag{4.5}$$

$$y(t) = Cx(t) \tag{4.6}$$

where $A \in \mathcal{R}^{n\times n}, B \in \mathcal{R}^{n\times m}, C \in \mathcal{R}^{p\times n}$ and $M \in \mathcal{R}^{n\times q}$ where $p \geq q$. Assume that the matrices C and M are full rank and the function $\xi : \mathcal{R}_+ \times \mathcal{R}^n \times \mathcal{R}^m \rightarrow \mathcal{R}^q$ is unknown but bounded so that

$$\|\xi(t, x, u)\| \leq \alpha(t, y, u) \tag{4.7}$$

where $\alpha : \mathcal{R}_+ \times \mathcal{R}^p \rightarrow \mathcal{R}_+$ is a known function.

Assume

A1 CM has full column rank

A2 the invariant zeros (if any) of (A, M, C) are stable

As in §3.5.2, the objective is to design an observer of the form

$$\dot{\hat{x}}(t) = A\hat{x}(t) + Bu(t) - G_l e_y(t) + G_n\nu \tag{4.8}$$

$$\hat{y}(t) = C\hat{x}(t) \tag{4.9}$$

where $G_l \in \mathcal{R}^{n\times p}$ and $G_n \in \mathcal{R}^{n\times p}$ and $e_y(t) := \hat{y}(t) - y(t)$ is the output estimation error. The discontinuous vector ν is defined by

$$\nu = -\rho(t, y, u)\frac{e_y}{\|e_y\|}, \quad e_y \neq 0 \tag{4.10}$$

where $\rho(t, y, u)$ is a positive scalar function dependent on the magnitude of the uncertainty.

In §3.5, this observer was designed in the coordinates of (3.74), where the sliding motion (or equivalently L from (3.73)) had already been fixed, the gains were in the coordinates of (3.80) and the Lyapunov matrix had the structure in (3.85). In this chapter, the observer will be designed in the coordinates of (3.69). In this way, the freedom associated with the variable L is included in the design. As in §3.5.1, assume the triple (A, M, C) has the form

$$A = \left[\begin{array}{c|c} A_{11} & A_{12} \\ \hline \begin{array}{c} A_{211} \\ A_{212} \end{array} & A_{22} \end{array}\right], \quad M = \begin{bmatrix} 0 \\ M_o \end{bmatrix}, \quad C = \begin{bmatrix} 0 & T \end{bmatrix} \tag{4.11}$$

where $M_o \in \mathcal{R}^{q\times q}$ is nonsingular and $T \in \mathcal{R}^{p\times p}$ is orthogonal. The pair $A_{11} \in \mathcal{R}^{(n-p)\times(n-p)}$ and $A_{211} \in \mathcal{R}^{(p-q)\times(n-p)}$ is detectable. As in §3.5.1 the unobservable modes of (A_{11}, A_{211}) represent the invariant zeros of (A, M, C). Assumptions A1 and A2 are necessary and sufficient conditions for the existence of the observer [23, 25].

The parameters that need to be designed are the positive scalar $\rho(t, y, u)$, the linear gain G_l, and the nonlinear gain G_n in (4.8). Also a Lyapunov matrix P (of appropriate structure) must exist for the matrix $A - G_lC$. In the design method of Edwards & Spurgeon [23, 25], these matrices have the particular structures of $\mathcal{G}_n$ in (3.80) and $\mathcal{P}$ in (3.85) respectively. For the design method proposed in this chapter, the structures of $\mathcal{G}_n$ and $\mathcal{P}$ will be retained, but they will need to be transformed into the coordinates of (4.11), This can be achieved by applying the inverse of the coordinate transformation T_L in (3.72).

Specifically, in the coordinate system of (4.11), the Lyapunov matrix

$$P = T_L^T \mathcal{P} T_L = \begin{bmatrix} P_1 & P_1 L \\ L^T P_1 & T^T P_o T + L^T P_1 L \end{bmatrix} > 0 \tag{4.12}$$

where $P_1 \in \mathcal{R}^{(n-p)\times(n-p)}$, $P_o \in \mathcal{R}^{p\times p}$ and

$$L = \begin{bmatrix} L^o & 0 \end{bmatrix} \tag{4.13}$$

with $L^o \in \mathcal{R}^{(n-p)\times(p-q)}$. The nonlinear gain matrix

$$G_n = T_L^{-1} \mathcal{G}_n = \begin{bmatrix} -LT^T \\ T^T \end{bmatrix} P_o^{-1} \tag{4.14}$$

Unlike the original design method in [23, 25], the linear gain G_l is not assumed to have any particular structure at this point.

Proposition 4.1 *If a P of the form in (4.12) exists such that*

$$P(A - G_lC) + (A - G_lC)^T P < 0 \tag{4.15}$$

for some $G_l \in \mathcal{R}^{n\times p}$ and $\rho(t, y, u) \geq \|P_oCM\|\alpha(t, y, u) + \eta_o$, $\eta_o > 0$ then the state estimation error $e(t) := \hat{x}(t) - x(t)$ is asymptotically stable.

Proof

From (4.5) - (4.6) and (4.8) - (4.9), the state estimation error is governed by

$$\dot{e}(t) = (A - G_lC)e(t) + G_n\nu - M\xi(t, x, u) \tag{4.16}$$

Assume without a loss of generality that the parameters are in the coordinates of (4.11).

Consider a positive definite Lyapunov function

$$\mathcal{V} = e^T P e$$

Differentiating with respect to time,

$$\begin{aligned} \dot{\mathcal{V}} &= \dot{e}^T P e + e^T P \dot{e} \\ &= e^T (P(A - G_l C) + (A - G_l C)^T P) e + 2e^T P G_n \nu - 2e^T P M \xi \end{aligned}$$

From the definitions of P, G_n and M in (4.12), (4.14) and (4.11) respectively, it is easy to prove that

$$PG_n = C^T, \quad PM = C^T P_o C M \tag{4.17}$$

Using (4.15) and (4.17), $\dot{\mathcal{V}}$ becomes

$$\dot{\mathcal{V}} < 2e^T C^T \nu - 2e^T C^T P_o C M \xi$$

From the definition of ν in (4.10),

$$\begin{aligned} \dot{\mathcal{V}} &< -2\rho \|e_y\| - 2e_y^T P_o C M \xi \\ &\leq -2\|e_y\|(\rho - \|P_o C M\|\alpha) \\ &\leq -2\eta_o \|e_y\| \\ &< 0 \text{ for } e \neq 0 \end{aligned}$$

which proves the quadratic stability of the error system. ■

Applying the change of coordinates T_L in (3.72), the triple (A, M, C) in (4.11) and G_n will be transformed to be

$$\mathcal{A} = \begin{bmatrix} \mathcal{A}_{11} & \mathcal{A}_{12} \\ \mathcal{A}_{21} & \mathcal{A}_{22} \end{bmatrix}, \quad \mathcal{M} = \begin{bmatrix} 0 \\ \mathcal{M}_2 \end{bmatrix}, \quad \mathcal{C} = \begin{bmatrix} 0 & I_p \end{bmatrix}, \quad \mathcal{G}_n = \begin{bmatrix} 0 \\ P_o^{-1} \end{bmatrix} \tag{4.18}$$

where $\mathcal{A}_{11} = A_{11} + L^o A_{211}$ and $\mathcal{M}_2 \in \mathcal{R}^{p \times q}$.

In this coordinate system, the state estimation error system (4.16) can be partitioned to be

$$\dot{e}_1(t) = \mathcal{A}_{11} e_1(t) + (\mathcal{A}_{12} - \mathcal{G}_{l,1}) e_y(t) \tag{4.19}$$

$$\dot{e}_y(t) = \mathcal{A}_{21} e_1(t) + (\mathcal{A}_{22} - \mathcal{G}_{l,2}) e_y(t) + P_o^{-1} \nu - \mathcal{M}_2 \xi(t, x, u) \tag{4.20}$$

where

$$\begin{bmatrix} \mathcal{G}_{l,1} \\ \mathcal{G}_{l,2} \end{bmatrix} = T_L G_l \tag{4.21}$$

Pre-multiplying and post-multiplying (4.15) by $(T_L^{-1})^T$ and T_L^{-1} respectively and then partitioning conformably with (4.18) yields

$$\begin{bmatrix} P_1\mathcal{A}_{11} + \mathcal{A}_{11}^T P_1 & P_1(\mathcal{A}_{12} - \mathcal{G}_{l,1}) + \mathcal{A}_{21}^T P_o \\ (\mathcal{A}_{12} - \mathcal{G}_{l,1})^T P_1 + P_o\mathcal{A}_{21} & P_o(\mathcal{A}_{22} - \mathcal{G}_{l,2}) + (\mathcal{A}_{22} - \mathcal{G}_{l,2})^T P_o \end{bmatrix} < 0 \tag{4.22}$$

This implies that both diagonal blocks of (4.22) are negative definite which in turn implies that $\mathcal{A}_{11}$ and $(\mathcal{A}_{22} - \mathcal{G}_{l,2})$ are stable since P_1 and P_o are symmetric positive definite.

Corollary 4.1 *A stable sliding motion takes place on the surface*

$$\mathcal{S} = \{e : Ce = 0\} \tag{4.23}$$

in finite time and the sliding motion is governed by $\mathcal{A}_{11} = A_{11} + LA_{21}$.

Proof

Introduce a Lyapunov function

$$\mathcal{V}_s = e_y^T P_o e_y$$

Differentiating $\mathcal{V}_s$ with respect to time and using (4.20),

$$\dot{\mathcal{V}}_s = e_y^T(P_o(\mathcal{A}_{22} - \mathcal{G}_{l,2}) + (\mathcal{A}_{22} - \mathcal{G}_{l,2})^T P_o)e_y + 2e_y^T P_o\mathcal{A}_{21}e_1 + 2e_y^T\nu - 2e_y^T P_o\mathcal{M}_2\xi$$

From (4.22), $P_o(\mathcal{A}_{22} - \mathcal{G}_{l,2}) + (\mathcal{A}_{22} - \mathcal{G}_{l,2})^T P_o < 0$ and therefore

$$\begin{aligned} \dot{\mathcal{V}}_s &< 2e_y^T P_o\mathcal{A}_{21}e_1 + 2e_y^T\nu - 2e_y^T P_o\mathcal{M}_2\xi \\ &\leq 2\|e_y\|\|P_o\mathcal{A}_{21}e_1\| - 2\eta_o\|e_y\| \\ &= 2\|e_y\|(\|P_o\mathcal{A}_{21}e_1\| - \eta_o) \end{aligned} \tag{4.24}$$

Notice that

$$\|e_y\|^2 = (\sqrt{P_o}e_y)^T P_o^{-1}(\sqrt{P_o}e_y) \geq \lambda_{min}(P_o^{-1})\|\sqrt{P_o}e_y\|^2 = \lambda_{min}(P_o^{-1})\mathcal{V}_s \tag{4.25}$$

Define η as a scalar satisfying $0 < \eta < \eta_o$. Since from Proposition 4.1 the state estimation is quadratically stable, in finite time $e_1(t)$ enters the domain $\Omega_\eta = \{e_1 : \|P_o\mathcal{A}_{21}e_1\| < \eta_o - \eta\}$ and remains there. Inside the domain Ω_η inequality (4.24) becomes

$$\frac{d\mathcal{V}_s}{dt} < -2\eta\|e_y\| < -2\eta\sqrt{\lambda_{min}(P_o^{-1})}\sqrt{\mathcal{V}_s}$$

Integrating from the time when $e_1(t)$ enters Ω_η until the time when sliding motion takes place,

$$\int_{\mathcal{V}_s(t_\Omega)}^{0} \frac{1}{\sqrt{\mathcal{V}_s}} d\mathcal{V}_s < -2\eta\sqrt{\lambda_{min}(P_o^{-1})} \int_{t_\Omega}^{t_s} dt$$

where $\mathcal{V}_s(t_\Omega)$ is the initial condition of $\mathcal{V}_s$ at $t = t_\Omega$, the time at which $e_1(t)$ enters Ω_η, and t_s is the time at which the sliding motion begins. It can be shown that the time taken to attain sliding motion t_s is given by

$$t_s < \eta^{-1}\sqrt{\frac{\mathcal{V}_s(t_\Omega)}{\lambda_{min}(P_o^{-1})}} + t_\Omega$$

This proves that sliding motion takes place on $\mathcal{S}$ in finite time.

When sliding motion has been achieved, $e_y(t) = \dot{e}_y(t) = 0$ and from (4.19) - (4.20), the remaining dynamics $e_1(t)$ are governed by $\mathcal{A}_{11} = A_{11} + LA_{21}$ which is stable. ■

Based on the results of Proposition 4.1 and Corollary 4.1, the new observer design method can be stated as:

Find matrices L^o, G_l, P_1 and P_o that satisfy the Lyapunov inequality $$P(A - G_lC) + (A - G_lC)^T P < 0$$ where $P > 0$ has the structure in (4.12).

4.4 Synthesis procedure for designing the sliding mode observer

In this chapter, P and G_l will be chosen so that the matrix inequality

$$P(A - G_lC) + (A - G_lC)^T P < -PWP - PG_lVG_l^T P \tag{4.26}$$

is satisfied, where the design weighting matrices $W \in \mathcal{R}^{n\times n}$ and $V \in \mathcal{R}^{p\times p}$ are assumed to be symmetric positive definite. The rationale for the matrix inequality (4.26) will be given later. Inequality (4.26) can be written as:

$$PA + A^T P - YC - (YC)^T + PWP + YVY^T < 0 \tag{4.27}$$

where $Y := PG_l$. Using standard matrix manipulations, inequality (4.27) is identical to

$$PA + A^T P + (Y^T - V^{-1}C)^T V(Y^T - V^{-1}C) - C^T V^{-1} C + PWP < 0 \tag{4.28}$$

For a choice of

$$Y^T = V^{-1}C \tag{4.29}$$

the necessary and sufficient condition for (4.28) (and hence also (4.27)) to hold is that the matrix P satisfies

$$PA + A^T P - C^T V^{-1} C + PWP < 0 \tag{4.30}$$

since (4.29) results in the third term in (4.28) being eliminated.

The problem considered here is one of minimising $trace(P^{-1})$ subject to P satisfying inequality (4.30).

From the solution for P that is obtained, the observer gain G_l can then be directly calculated as

$$G_l = P^{-1} C^T V^{-1} \tag{4.31}$$

which follows from equation (4.29) and the definition of Y.

Remark : Applying the linear change of coordinates T_L in (3.72), the linear gain $\mathcal{G}_l$ in the (e_1, e_y) coordinates (4.18) can be calculated from (4.31) as $\mathcal{G}_l = \mathcal{P}^{-1}\mathcal{C}^T V^{-1}$ and hence can be shown to be

$$\mathcal{G}_l = \begin{bmatrix} 0 \\ P_o^{-1} V^{-1} \end{bmatrix} \tag{4.32}$$

This structure shows that the output estimation error $e_y(t)$ will not be fed back to $e_1(t)$, the error states associated with the sliding motion.

4.4.1 The connection with the Algebraic Riccati Equation

The motivation for the choice of the inequality posed in (4.26), and for minimising $trace(P^{-1})$ subject to (4.30) and (4.12), will be discussed here. In the absence of the uncertainty $\xi(t, x, u)$ and as $\rho \to 0$, the observer tends to a linear formulation. Defining $Q := P^{-1}$, then pre and post multiplying inequality (4.30) by Q, the following inequality can be obtained:

$$AQ + QA^T - QC^T V^{-1} CQ + W < 0 \tag{4.33}$$

The linear gain can now be calculated as $G_l = QC^T V^{-1}$. The objective is thus to minimise $trace(Q)$ subject to (4.33).

The standard LQG optimal observer design method as described in [69] uses the stabilising solution Q_{are} to the Algebraic Riccati Equation (ARE)

$$AQ_{are} + Q_{are}A^T - Q_{are}C^T V^{-1} CQ_{are} + W = 0 \tag{4.34}$$

to calculate optimal observer gain $G_{l,are} := Q_{are}C^T V^{-1}$. The associated optimal cost is given by $trace(Q_{are})$.

Lemma 4.1 *Let Q be any symmetric positive definite matrix satisfying (4.33), and let Q_{are} be the stabilising solution to the ARE (4.34). Then $Q > Q_{are}$ and hence $trace(Q) > trace(Q_{are})$.*

Proof

Inequality (4.33) can be expressed as

$$AQ + QA^T - QC^T V^{-1} CQ + W + \triangle = 0 \tag{4.35}$$

for some symmetric positive definite matrix $\triangle$. Subtracting (4.34) from (4.35) and defining $\tilde{Q} = Q - Q_{are}$, implies

$$A\tilde{Q} + \tilde{Q}A^T - QC^T V^{-1} CQ + Q_{are} C^T V^{-1} C Q_{are} + \triangle = 0 \tag{4.36}$$

Then substituting $Q_{are} = Q - \tilde{Q}$ into inequality (4.36) yields

$$(A - QC^T V^{-1} C)\tilde{Q} + \tilde{Q}(A - QC^T V^{-1} C)^T + \triangle + \tilde{Q}C^T V^{-1} C\tilde{Q} = 0 \tag{4.37}$$

Since inequality (4.33) can be re-written as

$$(A - QC^T V^{-1} C)Q + Q(A - QC^T V^{-1} C)^T + QC^T V^{-1} CQ + W < 0 \tag{4.38}$$

and $Q > 0$, it follows that $(A - QC^T V^{-1} C)$ is stable. Therefore, as argued in Lemma 3 in [116], equation (4.37) implies $\tilde{Q} > 0$ and hence $Q > Q_{are}$ as claimed. The fact that $trace(Q) > trace(Q_{are})$ follows from the properties of the $trace$ operator. ■

From Lemma 4.1, the requirement of minimising $trace(Q)$ follows from the desire to approach the true minimal cost given by $trace(Q_{are})$. Of course a particular sub-optimal cost is enforced here by the requirement that $P := Q^{-1}$ has the structure of (4.12).

In inequality (4.33), W is the performance weighting matrix for the observer, and V is the co-variance matrix of the system's sensor noise. As in classical LQG theory the choice of W and V can be used to trade off performance and noise amplification.

4.5 Practical implementation

By using the Schur complement [3], the matrix inequality in (4.30) is equivalent to

$$\begin{bmatrix} PA + A^T P - C^T V^{-1} C & P \\ P & -W^{-1} \end{bmatrix} < 0 \tag{4.39}$$

If $X \in \mathcal{R}^{n \times n}$ is symmetric positive definite, then (again using the Schur complement) the following inequality

$$\begin{bmatrix} -P & I_n \\ I_n & -X \end{bmatrix} < 0 \tag{4.40}$$

is equivalent to $X > P^{-1}$. Thus minimising $trace(P^{-1})$ subject to (4.30) can be implemented by minimising $trace(X)$ subject to the LMIs (4.39) and (4.40). Writing P from (4.12) in terms of LMI variables

$$P = \begin{bmatrix} P_{11} & P_{12} \\ P_{12}^T & P_{22} \end{bmatrix} > 0 \tag{4.41}$$

where $P_{11} \in \mathcal{R}^{(n-p)\times(n-p)}$, $P_{22} \in \mathcal{R}^{p \times p}$ and $P_{12} := \begin{bmatrix} P_{121} & 0 \end{bmatrix}$ with $P_{121} \in \mathcal{R}^{(n-p)\times(p-q)}$ (due to the structure of L), then the elements of P in (4.12) can be calculated in terms of the LMI variables P_{11}, P_{121}, P_{22} by the following equations

$$P_1 = P_{11} \tag{4.42}$$

$$L^o = P_{11}^{-1} P_{121} \tag{4.43}$$

$$P_o = T(P_{22} - P_{12}^T P_{11}^{-1} P_{12}) T^T \tag{4.44}$$

It follows that the constrained minimisation problem represents a convex optimisation problem with regard to P_{11}, P_{121}, P_{22} and X. The approach can be formally stated as:

Minimise $trace(X)$ with respect to the variables P_{11}, P_{121}, P_{22} and X subject to the LMIs given in (4.39) and (4.40).

Standard LMI software, such as [39] can be used to synthesise numerically P and X, which will return values for P_{11}, P_{121}, P_{22} and X. From there, the observer parameters can be obtained: L^o from (4.43), P_o from (4.44), G_l from (4.31) and G_n from (4.14).

4.6 Design of the sliding motion system matrix

A consequence of the design procedure proposed in §4.4 is that the dynamics of the sliding motion, although guaranteed to be stable, are designed somewhat implicitly. This section considers the sliding motion design problem and shows how additional LMI constraints can be augmented with (4.39) and (4.40) to tune the sliding mode performance. Pre-multiplying by $(T_L^{-1})^T$ and post-multiplying by T_L^{-1}, the matrix inequality (4.30) becomes

$$\mathcal{P}\mathcal{A} + \mathcal{A}^T\mathcal{P} - \mathcal{C}^T V^{-1} \mathcal{C} + \mathcal{P}\mathcal{W}\mathcal{P} < 0 \tag{4.45}$$

where $\mathcal{W} := T_L W {T_L}^T$. The top left $(n-p) \times (n-p)$ block of (4.45) is given by

$$P_1 \mathcal{A}_{11} + \mathcal{A}_{11}^T P_1 + P_1 \mathcal{W}_1 P_1 < 0 \tag{4.46}$$

where $\mathcal{W}_1 \in \mathcal{R}^{(n-p)\times(n-p)} > 0$ is the top left sub-block of $\mathcal{W}$ and $\mathcal{A}_{11} = A_{11} + L^o A_{211}$ is the sliding motion system matrix. If the matrix W is partitioned as

$$W = \begin{bmatrix} W_{11} & W_{12} & W_{13} \\ W_{12}^T & W_{22} & W_{23} \\ W_{13}^T & W_{23}^T & W_{33} \end{bmatrix} \tag{4.47}$$

where $W_{11} \in \mathcal{R}^{(n-p)\times(n-p)}$ and $W_{22} \in \mathcal{R}^{(p-q)\times(p-q)}$ then from the definition of T_L and exploiting the special structure of L,

$$\mathcal{W}_1 = W_{11} + L^o W_{12}^T + W_{12}(L^o)^T + L^o W_{22}(L^o)^T \tag{4.48}$$

and hence inequality (4.46) can be written as

$$P_1\mathcal{A}_{11} + \mathcal{A}_{11}^T P_1 + P_1 W_{11} P_1 + P_1 L^o W_{12}^T P_1 + (P_1 L^o W_{12}^T P_1)^T + P_1 L^o W_{22}(L^o)^T P_1 < 0 \tag{4.49}$$

In the special case where $W_{12} = 0$ then

$$P_1 \mathcal{A}_{11} + \mathcal{A}_{11}^T P_1 + P_1 W_{11} P_1 + P_1 L^o W_{22}(L^o)^T P_1 < 0 \tag{4.50}$$

Using the definition of $\mathcal{A}_{11}$, inequality (4.50) can be re-written as

$$P_1(A_{11} + L^o A_{211}) + (A_{11} + L^o A_{211})^T P_1 + P_1 W_{11} P_1 + P_1 L^o W_{22}(L^o)^T P_1 < 0 \tag{4.51}$$

This is identical in structure to inequality (4.26) and hence W_{11} and W_{22} may be interpreted as playing the roles of performance and noise attenuation matrices in an LQG sense for the observer problem associated with the pair (A_{11}, A_{211}). Technically of course for this to represent an LQG problem the variable P_1 would need to be chosen to minimise the $trace(P_1^{-1})$. However since

$$trace(P^{-1}) = trace(P_1^{-1}) + trace(LT^T P_o^{-1} T L^T) + trace(T^T P_o^{-1} T) \tag{4.52}$$

and $trace(P^{-1})$ is minimised as part of the optimisation, some form of implicit minimisation of $trace(P_1^{-1})$ takes place. Thus the choice of W_{11} and W_{22} can be used to tune the sliding motion.

4.6.1 Tuning the sliding motion by pole placement

Furthermore, from the definitions of $\mathcal{A}_{11}$ and P_{121},

$$P_1\mathcal{A}_{11} = P_{11}A_{11} + P_{121}A_{211} \tag{4.53}$$

which is linear with respect to the LMI optimisation variables P_{11} and P_{121}. Additional LMIs can be employed together with (4.39) and (4.40) to achieve pole placement of $\mathcal{A}_{11}$ in regions of the complex plane. One approach is to use root-clustering methods presented by Gutman & Jury [47] . Typically the poles may be required to lie in

- a conic sector centered at (0,0) with inner angle θ_a
- a disc of radius r_a and centre $(q_a, 0)$
- a vertical strip $a_a < x < b_a$

If s represents a point on the complex plane, and s^* represents its complex conjugate, then the following inequalities will describe the respective regions [39]

$$\begin{bmatrix} (s+s^*)\sin\frac{1}{2}\theta_a & -(s-s^*)\cos\frac{1}{2}\theta_a \\ (s-s^*)\cos\frac{1}{2}\theta_a & (s+s^*)\sin\frac{1}{2}\theta_a \end{bmatrix} < 0 \tag{4.54}$$

$$\begin{bmatrix} -r_a & s-q_a \\ s^*-q_a & -r_a \end{bmatrix} < 0 \tag{4.55}$$

$$\begin{bmatrix} s+s^*-2b_a & 0 \\ 0 & -(s+s^*)+2a_a \end{bmatrix} < 0 \tag{4.56}$$

To transform the scalar case in (4.54) - (4.56) to the matrix case, Chilali & Gahinet [11] substituted $(1, s, s^*)$ with $(P_1, P_1\mathcal{A}_{11}, \mathcal{A}_{11}^T P_1)$ and hence, the following LMIs will describe those regions

$$\begin{bmatrix} (P_1\mathcal{A}_{11}+\mathcal{A}_{11}^T P_1)\sin\frac{1}{2}\theta_a & -(P_1\mathcal{A}_{11}-\mathcal{A}_{11}^T P_1)\cos\frac{1}{2}\theta_a \\ (P_1\mathcal{A}_{11}-\mathcal{A}_{11}^T P_1)\cos\frac{1}{2}\theta_a & (P_1\mathcal{A}_{11}+\mathcal{A}_{11}^T P_1)\sin\frac{1}{2}\theta_a \end{bmatrix} < 0 \tag{4.57}$$

$$\begin{bmatrix} -r_a P_1 & P_1\mathcal{A}_{11}-q_a P_1 \\ \mathcal{A}_{11}^T P_1 - q_a P_1 & -r_a P_1 \end{bmatrix} < 0 \tag{4.58}$$

$$\begin{bmatrix} P_1\mathcal{A}_{11} + \mathcal{A}_{11}^T P_1 - 2b_a P_1 & 0 \\ 0 & -(P_1\mathcal{A}_{11} + \mathcal{A}_{11}^T P_1) + 2a_a P_1 \end{bmatrix} < 0 \qquad (4.59)$$

In order to obtain a convex optimisation problem, write $P_1\mathcal{A}_{11} = P_{11}A_{11} + P_{121}A_{211}$ and substitute into (4.57) - (4.59). This results in a well-posed convex problem as the inequalities (4.57) - (4.59) are affine in P_{11} and P_{121}.

The optimisation problem can be formally stated as:

Minimise $trace(X)$ with respect to the variables P_{11}, P_{121}, P_{22} and X subject to the LMIs given in (4.39) and (4.40) and any subset of (4.57) - (4.59).

4.7 Design algorithm summary

The results of §4.4 and §4.6 can be summarised in the form of a design algorithm:

Step 1 : Check that $rank(CM) = q$. If not, the approach is not applicable. Then obtain the canonical form of Edwards & Spurgeon [25] as given in equation (4.11). Check that the eigenvalues of A_{11}^o have negative real parts. If not, the approach is not applicable.

Step 2 : Define the matrix variables $P \in \mathcal{R}^{n\times n}$ as in (4.41), and $X \in \mathcal{R}^{n\times n}$.

Step 3 : Specify the weighting matrices $W \in \mathcal{R}^{n\times n}$ and $V \in \mathcal{R}^{p\times p}$.

Step 4 : Form the LMIs (4.39) and (4.40) where A and C are in the coordinates of (4.11).

Step 5 : If the eigenvalues of the sliding motion governed by $\mathcal{A}_{11}$ are required to lie in any particular region, form the relevant LMIs as a subset of (4.57) - (4.59).

Step 6 : Minimise $trace(X)$ subject to the LMIs formed in steps 4 and 5.

Step 7 : Partition the resulting matrix P to obtain P_{11}, P_{121} and P_{22} as defined in (4.41). Compute $L^o = P_{11}^{-1}P_{121}$ from (4.43) and $P_o = T(P_{22} - P_{12}^T P_{11}^{-1}P_{12})T^T$ from (4.44) where T is the orthogonal matrix from (4.11).

Step 8 : The observer gains can be computed (in the coordinates of (4.11)) as

$$G_l = P^{-1}C^T V^{-1} \quad \text{and} \quad G_n = \begin{bmatrix} -LT^T \\ T^T \end{bmatrix} P_o^{-1}$$

Step 9 : In the original coordinates, the gains are

$$G_l \to T_o^{-1} G_l \quad \text{and} \quad G_n \to T_o^{-1} G_n$$

where T_o is the coordinate transformation which induces the coordinates of (4.11). □

4.8 A modification

This section presents a more general solution than the design method in §4.4, where the variable Y was constrained as $Y = C^T V^{-1}$. In this section, Y is left as a free variable.

The matrix inequality in (4.27) is equivalent to

$$\begin{bmatrix} PA + A^T P - YC - (YC)^T & P & Y \\ P & -W^{-1} & 0 \\ Y^T & 0 & -V^{-1} \end{bmatrix} < 0 \tag{4.60}$$

by using the Schur complement. It follows that using the description of P in (4.41), the inequality (4.60) is affine in the variables P_{11}, P_{121}, P_{22} and Y. Thus the problem of minimising $trace(X)$ subject to (4.60) and (4.40) is a well posed LMI problem in $P_{11}, P_{121}, P_{22}, Y$ and X, and can be solved using standard software routines. The observer gain G_l can be directly calculated as

$$G_l = P^{-1} Y \tag{4.61}$$

which follows from the definition of Y. This will lead to the same choice of gain G_l that would be obtained from §4.4 namely $G_l = P^{-1} C^T V^{-1}$. In this section additional constraints will be introduced which force the eigenvalues of $(A - G_l C)$ to lie in specified regions of the complex plane whilst minimising $trace(P^{-1})$.

The eigenvalues of $(A - G_l C)$ will be placed in the same type of regions as those described in §4.6, specifically:

- a conic sector centered at (0,0) with inner angle θ_o
- a disc of radius r_o and centre $(q_o, 0)$
- a vertical strip $a_o < x < b_o$

As in §4.6, the following inequalities describe these regions:

$$\begin{bmatrix} (PA_o + A_o^T P)\sin\frac{1}{2}\theta_o & -(PA_o - A_o^T P)\cos\frac{1}{2}\theta_o \\ (PA_o - A_o^T P)\cos\frac{1}{2}\theta_o & (PA_o + A_o^T P)\sin\frac{1}{2}\theta_o \end{bmatrix} < 0 \tag{4.62}$$

$$\begin{bmatrix} -r_o P & PA_o - q_o P \\ A_o^T P - q_o P & -r_o P \end{bmatrix} < 0 \tag{4.63}$$

$$\begin{bmatrix} PA_o + A_o^T P - 2b_o P & 0 \\ 0 & -PA_o + A_o^T P + 2a_o P \end{bmatrix} < 0 \tag{4.64}$$

In order to obtain a convex optimisation problem, write $PA_o = PA - YC$ from the definitions of A_o and Y. This results in a well-posed convex problem as the inequalities (4.62) - (4.64) are affine in the variables P and Y. Thus the new optimisation problem can be stated as:

Minimise $trace(X)$ with respect to the variables $P_{11}, P_{121}, P_{22}, X$ and Y subject to the LMIs (4.40) and (4.60) and any subset of (4.62) - (4.64).

Remark :

- As a result of the additional constraints (4.62) - (4.64), Y can no longer be constrained as in (4.29), as it is now needed for pole-placement of $(A - G_l C)$.
- The value of $trace(X)$ would be expected to be larger than the case when (4.62) - (4.64) are not included. This is because in the absence of the constraints (4.62) - (4.64), the variable Y is free to be $Y = C^T V^{-1}$; this condition causes the left hand side of inequality (4.28) to be at its minimum, and hence has the most freedom for any optimisation objective.

4.8.1 Effect on the sliding motion system matrix design

This subsection will consider the effect on the sliding motion system matrix when Y is not constrained as in (4.29). Applying the linear change of coordinates T_L to (4.27), the top left block will be

$$P_1\mathcal{A}_{11} + \mathcal{A}_{11}^T P_1 + P_1\mathcal{W}_1 P_1 + \mathcal{Y}_1 V \mathcal{Y}_1^T < 0 \tag{4.65}$$

where

$$\begin{bmatrix} \mathcal{Y}_1 \\ \mathcal{Y}_2 \end{bmatrix} = (T_L^{-1})^T Y \tag{4.66}$$

and $\mathcal{Y}_1 \in \mathcal{R}^{(n-p)\times p}$. Substituting for $\mathcal{W}_1$ from (4.48) and for the special case where $W_{12} = 0$,

$$P_1\mathcal{A}_{11} + \mathcal{A}_{11}^T P_1 + P_1 W_{11} P_1 + P_1 L^o W_{22}(L^o)^T P_1 + \mathcal{Y}_1 V \mathcal{Y}_1^T < 0 \tag{4.67}$$

This is different from (4.50) because of the term $\mathcal{Y}_1 V \mathcal{Y}_1^T$ which is positive definite. Although arguments likening (4.67) to an LQG structure for the pair (A_{11}, A_{211}) can still be made, the results will be more conservative because of the term $\mathcal{Y}_1 V \mathcal{Y}_1^T$. Again, the constraints (4.57) - (4.59) can be incorporated to influence the sliding mode poles.

4.8.2 Design algorithm summary

The design algorithm associated with this section is almost identical to that in §4.7:

Step 1 : Identical to step 1 in §4.7.

Step 2 : Define the matrix variables P and X as in §4.7, and also $Y \in \mathcal{R}^{n\times p}$.

Step 3 : Identical to step 3 in §4.7.

Step 4 : Form the LMIs (4.60) and (4.40), where A and C are in the coordinates of (3.69).

Step 5 : Identical to step 5 in §4.7.

Step 6 : If the eigenvalues of $(A - G_l C)$ are required to lie in any specific region, form the relevant LMIs as a subset of inequalities (4.62) - (4.64).

Step 7 : Minimise $trace(X)$ subject to the LMIs formed in steps 4, 5 and 6 and partition the matrix P as in step 7 from §4.7 to obtain L and P_o.

Step 8 : The observer gain matrices (in the coordinates of (3.69)) can then be calculated as

$$G_l = P^{-1}Y \quad \text{and} \quad G_n = \begin{bmatrix} -LT^T \\ T^T \end{bmatrix} P_o^{-1}$$

where T is the orthogonal matrix from (3.69).

Step 9 : Identical to step 9 in §4.7. □

4.9 An example

The new design method proposed in this chapter will now be demonstrated by an example. This example is a 7-th order aircraft model taken from Heck *et al.* [51]. The system matrices are

$$A = \begin{bmatrix} 0 & 0 & 1.0000 & 0 & 0 & 0 & 0 \\ 0 & -0.1540 & -0.0042 & 1.5400 & 0 & -0.7440 & -0.0320 \\ 0 & 0.2490 & -1.0000 & -5.2000 & 0 & 0.3370 & -1.1200 \\ 0.0386 & -0.9960 & -0.0003 & -2.1170 & 0 & 0.0200 & 0 \\ 0 & 0.5000 & 0 & 0 & -4.0000 & 0 & 0 \\ 0 & 0 & 0 & 0 & 0 & -20.0000 & 0 \\ 0 & 0 & 0 & 0 & 0 & 0 & -25.0000 \end{bmatrix}$$

$$B = M = \begin{bmatrix} 0 & 0 \\ 0 & 0 \\ 0 & 0 \\ 0 & 0 \\ 0 & 0 \\ 20 & 0 \\ 0 & 25 \end{bmatrix}$$

$$C = \begin{bmatrix} 0 & -0.1540 & -0.0042 & 1.5400 & 0 & -0.7440 & -0.0320 \\ 0 & 0.2490 & -1.0000 & -5.2000 & 0 & 0.3370 & -1.1200 \\ 1.0000 & 0 & 0 & 0 & 0 & 0 & 0 \\ 0 & 0 & 0 & 0 & 1.0000 & 0 & 0 \end{bmatrix}$$

where the states, inputs and outputs respectively are:

$$x = \begin{bmatrix} \phi \\ r \\ p \\ \delta \\ x_7 \\ \delta_r \\ \delta_a \end{bmatrix} \begin{array}{l} \text{bank angle } (rad) \\ \text{yaw rate } (rad/s) \\ \text{roll rate } (rad/s) \\ \text{sideslip angle } (rad) \\ \text{washout filter state} \\ \text{rudder deflection } (rad) \\ \text{aileron deflection } (rad) \end{array}$$

$$u = \begin{bmatrix} \delta_{rc} \\ \delta_{ac} \end{bmatrix} \begin{array}{l} \text{rudder command}(rad) \\ \text{aileron command}(rad) \end{array}$$

$$y = \begin{bmatrix} r_a \\ p_a \\ \phi \\ x_7 \end{bmatrix} \begin{array}{l} \text{roll acceleration } (rad/s^2) \\ \text{yaw acceleration}(rad/s^2) \\ \text{bank angle } (rad) \\ \text{washout filter state} \end{array}$$

The following matrices were obtained for the canonical form described in §4.3: the system matrix

$$A = \begin{bmatrix} -2.0722 & 5.0994 & 1.6893 & 0 & -0.1801 & 0.5527 & -0.6465 \\ 0.0000 & -0.0000 & -0.0000 & 0 & 0.0000 & -0.4607 & -0.8969 \\ 0.0000 & 0.0000 & 0.0000 & 0 & -0.0000 & 0.9884 & -0.4625 \\ -0.0000 & 0.4962 & 0.0226 & -4.0000 & 0 & 0.0000 & 0.0000 \\ 0.0000 & 0.0122 & -0.9159 & 0 & 0 & 0 & 0.0000 \\ -20.1535 & -3.2909 & -6.9001 & 0 & 0.1583 & -25.7219 & 0.6257 \\ 15.4751 & 5.0661 & -1.3973 & 0 & -0.1370 & 2.3305 & -20.4769 \end{bmatrix}$$

and the input and output distribution matrices are

$$B = M = \begin{bmatrix} 0 & 0 \\ 0 & 0 \\ 0 & 0 \\ 0 & 0 \\ 0 & 0 \\ 0.0000 & 25.8356 \\ 16.3353 & -10.8242 \end{bmatrix}$$

$$C = \begin{bmatrix} 0 & 0 & 0 & 0 & 0 & -0.4126 & -0.9109 \\ 0 & 0 & 0 & 0 & 0 & -0.9109 & 0.4126 \\ 0 & 0 & 0 & 0 & 1.0000 & 0 & 0 \\ 0 & 0 & 0 & 1.0000 & 0 & 0 & 0 \end{bmatrix}$$

respectively. From the system matrix A, the following can be isolated

$$A_{11} = \begin{bmatrix} A_{11}^o & A_{12}^o \\ 0 & A_{22}^o \end{bmatrix} = \left[\begin{array}{c|cc} -2.0722 & 5.0994 & 1.6893 \\ \hline 0.0000 & 0.0000 & 0.0000 \\ 0.0000 & 0.0000 & 0.0000 \end{array}\right]$$

and

$$A_{211} = \begin{bmatrix} 0 & A_{21}^o \end{bmatrix} = \left[\begin{array}{c|cc} 0.0000 & 0.4962 & 0.0226 \\ 0.0000 & 0.0122 & -0.9159 \end{array}\right]$$

Also from the output distribution matrix C, the orthogonal matrix

$$T = \begin{bmatrix} 0 & 0 & -0.4126 & -0.9109 \\ 0 & 0 & -0.9109 & 0.4126 \\ 0 & 1.0000 & 0 & 0 \\ 1.0000 & 0 & 0 & 0 \end{bmatrix}$$

can be identified. Notice from A_{11} that the system has an invariant zero at -2.0722.

4.9.1 The optimal solution

Specifying the weights W and V from inequality (4.39) to be

$$W = \begin{bmatrix} W_{11} & W_{12} & W_{13} \\ W_{12}^T & W_{22} & W_{23} \\ W_{13}^T & W_{23}^T & W_{33} \end{bmatrix} = \begin{bmatrix} 0.08I_3 & 0 & 0 \\ 0 & 0.08I_2 & 0 \\ 0 & 0 & 0.05I_2 \end{bmatrix} \tag{4.68}$$

$$V = 0.2I_4 \tag{4.69}$$

and implementing the synthesis procedure in §4.4, i.e. minimising $trace(P^{-1})$ subject to (4.39) and (4.40), yields the following results:

$$L^o = \begin{bmatrix} -3.5281 & -0.1519 \\ -1.6176 & -0.2722 \\ 0.5550 & 0.8274 \end{bmatrix}$$

$$P_o = \begin{bmatrix} 1.8468 & 0.4484 & 0.2924 & 3.3825 \\ 0.4484 & 0.2267 & 0.0900 & 0.4750 \\ 0.2924 & 0.0900 & 2.9842 & -1.3817 \\ 3.3825 & 0.4750 & -1.3817 & 84.7829 \end{bmatrix}$$

From the value of L^o obtained, it follows that the sliding motion system matrix

$$\mathcal{A}_{11} = A_{11} + L^o A_{211} = \begin{bmatrix} -2.0722 & 3.3470 & 1.7488 \\ 0.0000 & -0.8059 & 0.2128 \\ 0.0000 & 0.2855 & -0.7453 \end{bmatrix} \tag{4.70}$$

The linear gain matrix (in the coordinates of (4.11))

$$G_l = P^{-1}C^TV^{-1} = \begin{bmatrix} -0.6525 & 0.6311 & 0.4093 & 0.2372 \\ -0.3623 & 0.2575 & 0.5380 & 0.1172 \\ 0.3532 & 0.0269 & -1.4545 & -0.0707 \\ -0.1715 & 0.1856 & 0.0415 & 0.0655 \\ -0.3119 & -0.1570 & 1.7300 & 0.0415 \\ 7.4533 & -34.7365 & 0.2717 & -0.0983 \\ -9.6141 & 27.5423 & 0.2193 & 0.2328 \end{bmatrix} \tag{4.71}$$

and the gain associated with the nonlinear output error injection

$$G_n = \begin{bmatrix} -LT^T \\ T^T \end{bmatrix} P_o^{-1} = \begin{bmatrix} -0.1305 & 0.1262 & 0.0819 & 0.0474 \\ -0.0725 & 0.0515 & 0.1076 & 0.0234 \\ 0.0706 & 0.0054 & -0.2909 & -0.0141 \\ -0.0343 & 0.0371 & 0.0083 & 0.0131 \\ -0.0624 & -0.0314 & 0.3460 & 0.0083 \\ 1.4907 & -6.9473 & 0.0543 & -0.0197 \\ -1.9228 & 5.5085 & 0.0439 & 0.0466 \end{bmatrix} \tag{4.72}$$

It can be shown that:

$$\lambda(A - G_lC) = \{-70.3606, -23.6149, -4.0551, -0.7589 \pm 0.9881i, -1.9096, -1.2967\}$$

and the sliding motion is governed by $\lambda(\mathcal{A}_{11}) = \{-2.0722, -0.5273, -1.0239\}$. Notice the invariant zero appears in the dynamics of the sliding motion. This design will be used as a benchmark. The effect of varying the weighting matrices W and V and the inclusion of additional LMI constraints will be explored in the following subsections.

4.9.2 Simulation results

The following simulation uses the matrices and parameters obtained from the synthesis in §4.9.1. In the aircraft system, initial perturbations of $-0.1\ rad$, $0.0843\ rad$ and 0.1 to the bank angle, sideslip angle and washout filter state respectively were assumed. The remaining initial conditions of the plant were set to zero. The initial conditions of the observer were all set to zero. In this simulation $\rho(t, y, u) = 0.5$ was chosen [1] and the discontinuous injection vector

[1]Throughout this thesis, the parameter $\rho(t, y, u)$ will be chosen as a constant scalar. It can in fact be chosen as a time-varying function, but the time-varying properties of the disturbance signal $\xi(t, x, u)$ will need to be known.

from (4.10) has been smoothed by approximating

$$\nu = -\rho(t, y, u)\frac{e_y}{\|e_y\| + \delta} \tag{4.73}$$

with $\delta = 1 \times 10^{-5}$ [27, 25, 26].

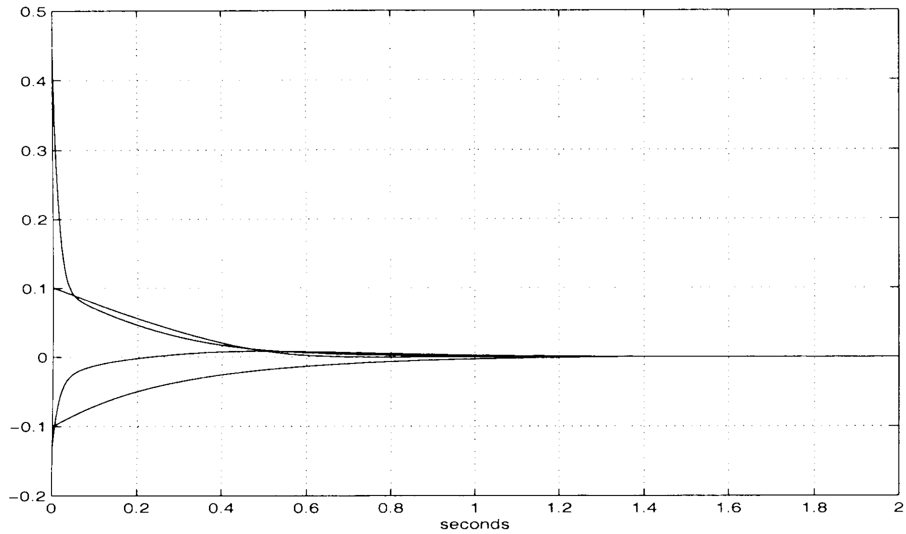

Figure 4.1: *Output estimation error $e_y(t)$: this shows that sliding motion takes place in finite time.*

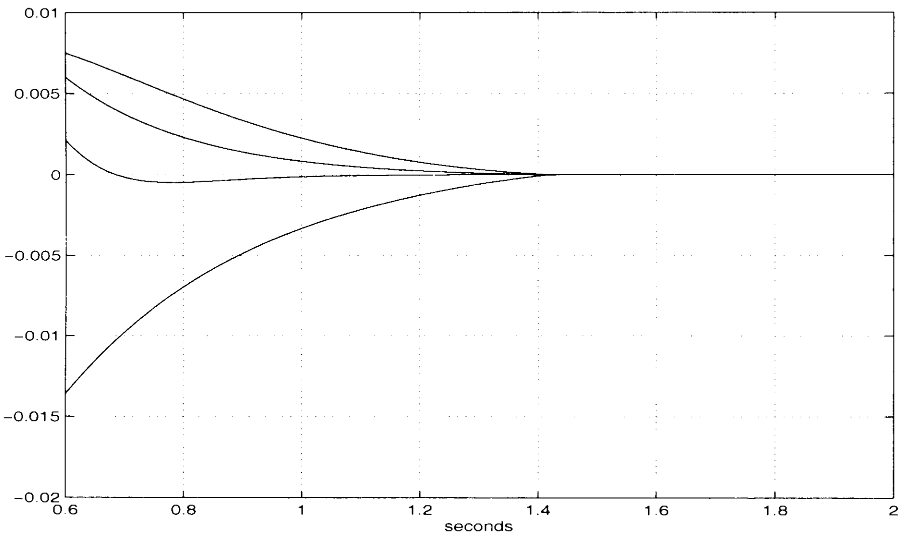

Figure 4.2: *Output estimation error $e_y(t)$ (at a much smaller scale)*

Figure 4.1 shows the evolution of the four output estimation error signals that comprise $e_y(t)$. It can be seen from Figure 4.2 (which is a 'blown up' version of Figure 4.1) that the vector $e_y(t)$ reaches the sliding surface and that sliding takes place after 1.4 seconds approximately. Figure 4.3 shows the evolution of the state estimation errors (over a different time scale).

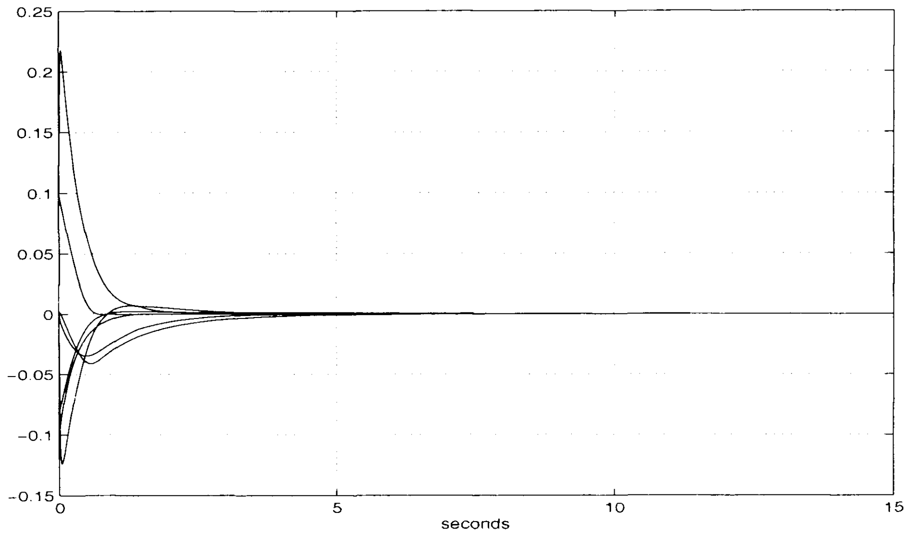

Figure 4.3: *State estimation error of the system*

4.9.3 The effect of increasing W_{11}

Increasing W_{11} by a factor of 10, the new weighting matrices become

$$W = \begin{bmatrix} 0.8I_3 & 0 & 0 \\ 0 & 0.08I_2 & 0 \\ 0 & 0 & 0.05I_2 \end{bmatrix}$$
$$V = 0.2I_4$$

Repeating the synthesis procedure in §4.4, the following results were obtained:

$$\lambda(A - G_l C) = \{-89.5964, -24.8035, -4.0452, -1.5789 \pm 0.7111i, -1.2569 \pm 1.0604i\}$$

and the eigenvalues of the sliding motion system matrix

$$\lambda(\mathcal{A}_{11}) = \{-2.0722, -0.9975, -1.8643\}$$

Notice, as argued in §4.6, the differential weighting of W_{11} and W_{22} in favour of W_{11} has made the sliding mode dynamics faster (except for the eigenvalue at -2.0722 associated with the invariant zero, which will always appear as a sliding mode pole).

4.9.4 The effect of increasing W_{22}

Increasing W_{22} by a factor of 10, the weighting matrices become

$$W = \begin{bmatrix} 0.08I_3 & 0 & 0 \\ 0 & 0.8I_2 & 0 \\ 0 & 0 & 0.05I_2 \end{bmatrix}$$

$$V = 0.2I_4$$

Repeating the synthesis procedure in §4.4, the following results were obtained

$$\lambda(A - G_lC) = \{-190.4475, -30.1623, -4.4815, -0.6816 \pm 0.3835i, -1.9643 \pm 0.0463i\}$$

and the eigenvalues of the sliding motion system matrix

$$\lambda(\mathcal{A}_{11}) = \{-2.0722, -0.7535, -0.2086\}$$

Notice that the differential weighting of W_{22} compared to W_{11} has made the sliding motion dynamics slower. As discussed in §4.6, the matrices W_{11} and W_{22} play the roles of performance and noise attenuation matrices respectively in an LQG sense. This is demonstrated in §4.9.3 and §4.9.4. Increasing the size of the matrix W_{11} caused $\lambda(\mathcal{A}_{11})$ to go further into the left half plane, whilst increasing the size of the matrix W_{22} had the opposite effect on $\lambda(\mathcal{A}_{11})$. In both cases, the eigenvalues of $A - G_lC$ have generally increased, as both situations involve an increase in magnitude of the matrix W relative to V.

4.9.5 Placing the eigenvalues of the sliding motion system matrix

In this subsection, several LMIs will be added as described in §4.6 to force the eigenvalues of $\mathcal{A}_{11}$ to lie in a specified region. The region is an intersection of the following constraints:

- a circle with centre $(-2, 0)$ and radius 1
- an upper bound vertical strip intersecting the real axis at -2

Applying the synthesis procedure from §4.6 with the weighting matrices from §4.9.1, the following results were obtained:

$$\lambda(A - G_lC) = \{-89.4654, -22.8376, -4.0606, -2.5796 \pm 0.9593i, -1.8314 \pm 0.3551i\}$$

and the eigenvalues of the sliding motion system matrix

$$\lambda(\mathcal{A}_{11}) = \{-2.0722, -2.0027 \pm 0.0949i\}$$

It can be clearly seen that the eigenvalues of $\mathcal{A}_{11}$ have been successfully forced into the specified region.

4.9.6 Placing the eigenvalues of the linear part of the observer (the modification)

In §4.9.1, the optimal solution yielded an eigenvalue very far in the left half plane at -70.6303. Furthermore, there were two relatively undamped poles at $-0.7589 \pm 0.9881i$. In this subsection, several constraints will be added to the LMI optimisation so that the poles can be forced into a specified region, whilst still minimising $trace(P^{-1})$.

Using the original weighting matrices in §4.9.1, and applying the synthesis procedure in §4.8, i.e. minimising $trace(P^{-1})$ subject to (4.27) and (4.40), and at the same time applying the following constraints on the observer - the eigenvalues of $A - G_lC$ must lie in

- an upper bound vertical strip intersecting the real axis at -2
- a lower bound vertical strip intersecting the real axis at -30
- a conic sector of half inner angle 45^o

the following results were obtained :

$$\lambda(A - G_lC) = \{-27.4056, -19.4923, -5.0702, -4.1022, -2.4683, -2.1552, -3.3334\}$$

and the eigenvalues of the sliding motion system matrix

$$\lambda(\mathcal{A}_{11}) = \{-2.0722, -2.1582 \pm 0.0749i\}$$

It can be seen that the poles are now more in a preferable region, however, the sub-optimality has been lost. This is a trade-off that needs to be made by the designer.

4.10 Conclusion

This chapter has demonstrated how Linear Matrix Inequalities (LMIs) can be used to synthesise the gains of a sliding mode observer. A formulation has been presented in which the linear component of the observer resembles a sub-optimal version of the classical LQG observer and two design weighting matrices allow a trade-off between performance and sensor noise.

In this approach, the system matrix that governs the sliding motion can be indirectly designed using notions from LQG theory. Certain partitions of the state weighting matrix play the roles of the 'performance weighting' and 'noise amplification' matrices for the sliding motion. It has also been shown how additional LMIs can be added to force the eigenvalues of the sliding motion matrix to lie in certain regions of the complex plane by using pole-placement and root-clustering methods whilst still maintaining a convex optimisation problem.

Finally, a modification to the design procedure was presented - where a more general solution was obtained in which, by adding additional LMI constraints, the eigenvalues of the linear part of the observer were forced to lie in specified regions.

Chapter 5

Sliding mode observers to reconstruct sensor faults

5.1 Introduction

At the beginning of Chapter 3, it was mentioned that sliding mode observers have been used for FDI schemes. Hermans & Zarrop [52], Yang & Saif [125], and Sreedhar *et al.* [102] have designed sliding mode observers such that in the presence of faults, the observer ceases to slide. This causes the output estimation error to be nonzero, and this signal is used as the residual to indicate the occurrence of a fault. Edwards *et al.* [27, 26] designed a sliding mode FDI scheme which maintained sliding motion in the presence of faults and reconstructed the faults using the equivalent output error injection. Yeu & Kawaji [128] subsequently designed a fault reconstruction scheme for a descriptor system, using a similar approach. Xiong & Saif [122] designed a sliding mode observer for certain components of the system state, and reconstructed the fault using the same equivalent output error injection approach.

In Edwards *et al.* [27, 26], reconstructions of actuator faults could be accurately obtained. However, in the case of sensor faults, only the steady-state component of the sensor faults could be reconstructed. The work described in this chapter seeks to improve on the sensor fault reconstruction method by Edwards *et al.* [27, 26].

The underlying principle in each method is that certain signals associated with the system are filtered. The filtered signal appears to be the output of a fictitious system that treats the sensor fault as an 'actuator fault'. As the filtered signal is available online, a sliding mode observer can be designed for the fictitious system, to reconstruct the sensor fault using the actuator fault reconstruction method by Edwards *et al.* [27, 26].

All the methods presented in this chapter will be demonstrated with examples.

5.2 Using sliding mode observers to reconstruct actuator faults

The purpose of this section is to present the background work necessary for this chapter, and basically describes the actuator fault reconstruction method of Edwards *et al.* [27, 26]. Consider a nominal state-space system that is subject to an actuator fault

$$\dot{x}(t) = Ax(t) + Bu(t) + Mf_i(t) \tag{5.1}$$

$$y(t) = Cx(t) \tag{5.2}$$

where $A \in \mathcal{R}^{n\times n}, B \in \mathcal{R}^{n\times m}, C \in \mathcal{R}^{p\times n}$ and $f_i \in \mathcal{R}^q$ represents an actuator fault which is bounded by

$$\|f_i(t)\| \leq \alpha(t, y, u)$$

where α is a known function. The matrix M is the fault distribution matrix.

From §3.5, an Edwards - Spurgeon observer [23, 25] for the system (5.1) - (5.2) is

$$\dot{\hat{x}}(t) = A\hat{x}(t) + Bu(t) - G_l e_y(t) + G_n\nu \tag{5.3}$$

$$\hat{y}(t) = C\hat{x}(t) \tag{5.4}$$

where

$$\nu = -\rho(t, y, u)\frac{e_y}{\|e_y\|}, \quad e_y \neq 0 \tag{5.5}$$

and $e_y(t) := \hat{y}(t) - y(t)$ is the output estimation error.

Defining $e(t) := \hat{x}(t) - x(t)$ as the state estimation error, the following error system can be obtained from (5.1) - (5.2) and (5.3) - (5.4)

$$\dot{e}(t) = (A - G_l C)e(t) + G_n\nu - Mf_i(t) \tag{5.6}$$

Assuming that the following conditions are satisfied

A1 CM has full column rank

A2 all invariant zeros of (A, M, C) (if any) are stable

then there exists a change of coordinates such that the triple (A, M, C) can be written in the form

$$A = \left[\begin{array}{c|c} A_{11} & A_{12} \\ \hline A_{211} & \\ & A_{22} \\ A_{212} & \end{array}\right], \quad M = \begin{bmatrix} 0 \\ M_o \end{bmatrix}, \quad C = \begin{bmatrix} 0 & T \end{bmatrix} \tag{5.7}$$

where $M_o \in \mathcal{R}^{q\times q}$ is nonsingular, $T \in \mathcal{R}^{p\times p}$ is orthogonal and the pair $A_{11} \in \mathcal{R}^{(n-p)\times(n-p)}$ and $A_{211} \in \mathcal{R}^{(p-q)\times(n-p)}$ is detectable. As in §3.5.1 the unobservable modes of (A_{11}, A_{211}) represent the invariant zeros of (A, M, C). In this coordinate system, G_n has the structure

$$G_n = \begin{bmatrix} -LT^T \\ T^T \end{bmatrix} P_o^{-1} \tag{5.8}$$

where $P_o \in \mathcal{R}^{p\times p}$ is symmetric positive definite and

$$L = \begin{bmatrix} L^o & 0 \end{bmatrix} \tag{5.9}$$

where $L^o \in \mathcal{R}^{(n-p)\times(p-q)}$ is a design matrix.

If there exists a symmetric positive definite matrix P of the structure

$$P = \begin{bmatrix} P_1 & P_1 L \\ L^T P_1 & T^T P_o T + L^T P_1 L \end{bmatrix} > 0 \tag{5.10}$$

where $P_1 \in \mathcal{R}^{(n-p)\times(n-p)}$, that satisfies $P(A - G_l C) + (A - G_l C)^T P < 0$, and if the scalar function $\rho(.)$ in (5.5) satisfies $\rho(t, y, u) \geq \|P_o C M\|\alpha(t, y, u) + \eta_o$ where η_o is a positive scalar, then from Proposition 4.1 and Corollary 4.1, sliding motion is attainable in finite time on the surface $\mathcal{S} = \{e : Ce = 0\}$.

As in §4.3, to analyse the sliding motion, it is convenient to change coordinates. Introduce a new change of coordinates $e \mapsto T_L e$ where

$$T_L = \begin{bmatrix} I_{n-p} & L \\ 0 & T \end{bmatrix} \tag{5.11}$$

Applying the change of coordinates induced by T_L to the triple in (5.7) yields

$$\mathcal{A} = \begin{bmatrix} \mathcal{A}_{11} & \mathcal{A}_{12} \\ \mathcal{A}_{21} & \mathcal{A}_{22} \end{bmatrix}, \quad \mathcal{M} = \begin{bmatrix} 0 \\ \mathcal{M}_2 \end{bmatrix}, \quad \mathcal{C} = \begin{bmatrix} 0 & I_p \end{bmatrix} \tag{5.12}$$

where $\mathcal{A}_{11} = A_{11} + L^o A_{211}$ and $\mathcal{M}_2 \in \mathcal{R}^{p\times q}$. Since (A_{11}, A_{211}) is detectable, L^o can be chosen so that $\mathcal{A}_{11}$ is stable. In this coordinate system, the gain $\mathcal{G}_n$ has a special structure and $\mathcal{G}_l$ has a general structure given by

$$\mathcal{G}_l = \begin{bmatrix} \mathcal{G}_{l,1} \\ \mathcal{G}_{l,2} \end{bmatrix}, \quad \mathcal{G}_n = \begin{bmatrix} 0 \\ P_o^{-1} \end{bmatrix} \tag{5.13}$$

where $\mathcal{G}_{l,1} \in \mathcal{R}^{(n-p)\times p}$.

Transforming the error system (5.6) to the coordinates of (5.12) and partitioning conformably

$$\dot{e}_1(t) = \mathcal{A}_{11}e_1(t) + (\mathcal{A}_{12} - \mathcal{G}_{l,1})e_y(t) \tag{5.14}$$

$$\dot{e}_y(t) = \mathcal{A}_{21}e_1(t) + (\mathcal{A}_{22} - \mathcal{G}_{l,2})e_y(t) + P_o^{-1}\nu - \mathcal{M}_2 f_i(t) \tag{5.15}$$

During the sliding motion, $e_y(t) = \dot{e}_y(t) = 0$ and hence (5.14) - (5.15) become

$$\dot{e}_1(t) = \mathcal{A}_{11}e_1(t) \tag{5.16}$$

$$0 = \mathcal{A}_{21}e_1(t) + P_o^{-1}\nu_{eq} - \mathcal{M}_2 f_i(t) \tag{5.17}$$

where ν_{eq} is the equivalent output error injection required to maintain sliding motion as described in §3.3.1. Edwards *et al.* [27, 26] argue that since $\mathcal{M}_2$ has full column rank, a reconstruction for $f_i(t)$ can be defined as

$$\hat{f}_i(t) := (\mathcal{M}_2^T\mathcal{M}_2)^{-1}\mathcal{M}_2^T P_o^{-1}\nu_{eq} \tag{5.18}$$

From [27, 26], since $\mathcal{A}_{11}$ is stable, $e_1(t) \to 0$ and hence from (5.16) - (5.18)

$$\hat{f}_i(t) \to f_i(t) \tag{5.19}$$

The reconstruction signal $\hat{f}_i(t)$ is computable online, since ν_{eq} is computable online by replacing (5.5) with

$$\nu_\delta = -\rho(t, y, u)\frac{e_y}{\|e_y\| + \delta} \tag{5.20}$$

where δ is a small positive constant which governs the accuracy to which the equivalent injection is approximated. For further details see [27, 25].

This section can be summarised as

For the system in (5.1) - (5.2) subject to an actuator fault $f_i(t)$; if conditions A1 and A2 are satisfied, then an Edwards - Spurgeon observer can be designed to reconstruct the fault $f_i(t)$.

5.2.1 A system subject to sensor faults

Consider the nominal system (5.1) - (5.2) subject to sensor faults. In this scenario, $f_i(t) = 0$ and the system equations become

$$\dot{x}(t) = Ax(t) + Bu(t) \tag{5.21}$$

$$y(t) = Cx(t) + f_o(t) \tag{5.22}$$

where $f_o \in \mathcal{R}^p$ is the sensor fault vector. Assuming the sliding mode observer described by (5.3) - (5.5) has been designed for the system, the error system would then satisfy

$$\dot{e}(t) = Ae(t) - G_l e_y(t) + G_n \nu \tag{5.23}$$

$$e_y(t) = Ce(t) - f_o(t) \tag{5.24}$$

Applying the change of coordinates T_L from (5.11), then partitioning (5.23) conformably with (5.12),

$$\dot{e}_1(t) = \mathcal{A}_{11}e_1(t) + \mathcal{A}_{12}(e_y(t) + f_o(t)) - \mathcal{G}_{l,1}e_y(t) \tag{5.25}$$

$$\dot{e}_y(t) + \dot{f}_o(t) = \mathcal{A}_{21}e_1(t) + \mathcal{A}_{22}(e_y(t) + f_o(t)) - \mathcal{G}_{l,2}e_y(t) + P_o^{-1}\nu \tag{5.26}$$

Assuming sliding motion has been attained (and hence $e_y(t) = \dot{e}_y(t) = 0$), the error system (5.25) - (5.26) satisfies

$$\dot{e}_1(t) = \mathcal{A}_{11}e_1(t) + \mathcal{A}_{12}f_o(t) \tag{5.27}$$

$$\dot{f}_o(t) = \mathcal{A}_{21}e_1(t) + \mathcal{A}_{22}f_o(t) + P_o^{-1}\nu_{eq} \tag{5.28}$$

5.2.2 The sensor fault reconstruction method by Edwards *et al.*

In [27, 26], assuming that A is full rank, Edwards *et al.* defined a reconstruction for $f_o(t)$ as

$$\hat{f}_o(t) := (\mathcal{A}_{21}\mathcal{A}_{11}^{-1}\mathcal{A}_{12} - \mathcal{A}_{22})^{-1}P_o^{-1}\nu_{eq} \tag{5.29}$$

At pseudo steady-state $\dot{e}_1(t) \approx 0$, and assuming the sensor fault is a slowly varying drift such that $\dot{f}_o(t) \approx 0$, it follows from (5.27) - (5.29) that

$$\hat{f}_o(t) \rightarrow f_o(t) \tag{5.30}$$

By combining (5.27) - (5.28), it can be seen that

$$P_o^{-1}\nu_{eq} = \dot{f}_o(t) - \mathcal{A}_{21}\mathcal{A}_{11}^{-1}\dot{e}_1(t) + (\mathcal{A}_{21}\mathcal{A}_{11}^{-1}\mathcal{A}_{12} - \mathcal{A}_{22})f_o(t) \tag{5.31}$$

Substituting (5.31) into (5.29), it is straightforward to show that

$$\hat{f}_o(t) = f_o(t) + (\mathcal{A}_{21}\mathcal{A}_{11}^{-1}\mathcal{A}_{12} - \mathcal{A}_{22})^{-1}\dot{f}_o(t) - (\mathcal{A}_{21}\mathcal{A}_{11}^{-1}\mathcal{A}_{12} - \mathcal{A}_{22})^{-1}\mathcal{A}_{21}\mathcal{A}_{11}^{-1}\dot{e}_1(t) \tag{5.32}$$

which demonstrates how the sensor fault reconstruction in (5.29) is corrupted by $\dot{f}_o(t)$ and $\dot{e}_1(t)$ which have been neglected in the analysis. The following parts of this chapter provide improvements to this method of sensor fault reconstruction.

5.3 Two methods to perfectly reconstruct the sensor fault

5.3.1 Secondary observer method

Assume a sliding mode observer has been designed for the system (5.21) - (5.22), and that sliding motion has been attained. The error system will then be governed by (5.27) - (5.28). Equation (5.28) can be re-expressed as

$$P_o^{-1}\nu_{eq} = -\mathcal{A}_{21}e_1(t) - \mathcal{A}_{22}f_o(t) + \dot{f}_o(t) \tag{5.33}$$

Consider a new state $z_1 \in \mathcal{R}^p$ that is a filtered version of $P_o^{-1}\nu_{eq}$ satisfying

$$\dot{z}_1(t) = -A_{f,1}z_1(t) + A_{f,1}P_o^{-1}\nu_{eq} \tag{5.34}$$

where $-A_{f,1} \in \mathcal{R}^{p\times p}$ is a stable filter matrix. Substituting from (5.33) into equation (5.34)

$$\dot{z}_1(t) = -A_{f,1}z_1(t) - A_{f,1}\mathcal{A}_{21}e_1(t) - A_{f,1}\mathcal{A}_{22}f_o(t) + A_{f,1}\dot{f}_o(t) \tag{5.35}$$

Define a new state $w \in \mathcal{R}^p$ as

$$w(t) = z_1(t) - A_{f,1}f_o(t) \tag{5.36}$$

Differentiating (5.36) and substituting into (5.35) for $z_1(t)$ and $\dot{z}_1(t)$ yields

$$\dot{w}(t) = -A_{f,1}\mathcal{A}_{21}e_1(t) - A_{f,1}w(t) + (-A_{f,1}^2 - A_{f,1}\mathcal{A}_{22})f_o(t) \tag{5.37}$$

Consider a new state $z_2 \in \mathcal{R}^p$ that is a filtered version of $z_1(t)$

$$\dot{z}_2(t) = -A_{f,2}z_2(t) + A_{f,2}z_1(t) \tag{5.38}$$

where $-A_{f,2} \in \mathcal{R}^{p\times p}$ is a stable filter matrix.

Substituting from equation (5.36), equation (5.38) becomes

$$\dot{z}_2(t) = -A_{f,2}z_2(t) + A_{f,2}w(t) + A_{f,2}A_{f,1}f_o(t) \tag{5.39}$$

Equations (5.27), (5.37) and (5.39) can be combined to form an augmented state-space system of order $n+p$ represented by

$$\begin{bmatrix} \dot{e}_1(t) \\ \dot{w}(t) \\ \dot{z}_2(t) \end{bmatrix} = \underbrace{\begin{bmatrix} \mathcal{A}_{11} & 0 & 0 \\ -A_{f,1}\mathcal{A}_{21} & -A_{f,1} & 0 \\ 0 & A_{f,2} & -A_{f,2} \end{bmatrix}}_{A_a} \begin{bmatrix} e_1(t) \\ w(t) \\ z_2(t) \end{bmatrix} + \underbrace{\begin{bmatrix} \mathcal{A}_{12} \\ -A_{f,1}^2 - A_{f,1}\mathcal{A}_{22} \\ A_{f,2}A_{f,1} \end{bmatrix}}_{M_a} f_o(t) \tag{5.40}$$

$$z_2(t) = \underbrace{\begin{bmatrix} 0 & 0 & I_p \end{bmatrix}}_{C_a} \begin{bmatrix} e_1(t) \\ w(t) \\ z_2(t) \end{bmatrix} \tag{5.41}$$

Equations (5.40) and (5.41) are now in the form of equations (5.1) and (5.2) and *represent a system with an actuator fault* $f_o(t)$. Note that the system (5.40) - (5.41) is a fictitious system, but its output $z_2(t)$ is easily available by twice filtering the signal $P_o^{-1}\nu_{eq}$. Hence a sliding mode observer can be designed for the system since its state-space matrices (A_a, M_a, C_a) are known, and the sensor fault $f_o(t)$ can be reconstructed using the method by Edwards *et al.* [27, 26] described in §5.2. The observer designed for the system (5.40) - (5.41) will be termed the *secondary observer.*

Define $\nu_{eq,a}$ as the equivalent output error injection associated with the secondary observer, and $G_{n,a}$ as its nonlinear gain. Further, define $P_{o,a} \in \mathcal{R}^{p\times p}$ as the symmetric positive definite matrix that scales $G_{n,a}$ (the same way P_o scales G_n in (5.8)). From the structure of M_a in the observer canonical form of (5.45) (in a similar way to (5.18)), defining the reconstruction for $f_o(t)$ as

$$\hat{f}_o(t) := A_{f,1}^{-1}A_{f,2}^{-1}P_{o,a}^{-1}\nu_{eq,a} \tag{5.42}$$

will result in

$$\hat{f}_o(t) \rightarrow f_o(t) \tag{5.43}$$

as $t \rightarrow \infty$ if A is stable. A schematic diagram of the FDI scheme in this section is shown in Figure 5.1

5.3.2 Existence conditions

The existence conditions for the secondary sliding mode observer will be investigated in this section, based on conditions A1 and A2 in §5.2.

It is easy to see that $C_aM_a = A_{f,2}A_{f,1}$ and since $A_{f,2}$ and $A_{f,1}$ are both stable (and hence full rank), it is clear that condition A1 is satisfied.

The triple (A_a, M_a, C_a) in (5.40) - (5.41) represents a square system, and hence there is no freedom in tuning the sliding motion of the secondary observer [23]. In this case, the observer canonical form in (5.12) can be directly obtained by applying the coordinate transformation

$$T_a = \begin{bmatrix} I_{n-p} & 0 & -\mathcal{A}_{12}A_{f,1}^{-1}A_{f,2}^{-1} \\ 0 & -A_{f,1}^{-1} & -(A_{f,1}+\mathcal{A}_{22})A_{f,1}^{-1}A_{f,2}^{-1} \\ 0 & 0 & I_p \end{bmatrix} \tag{5.44}$$

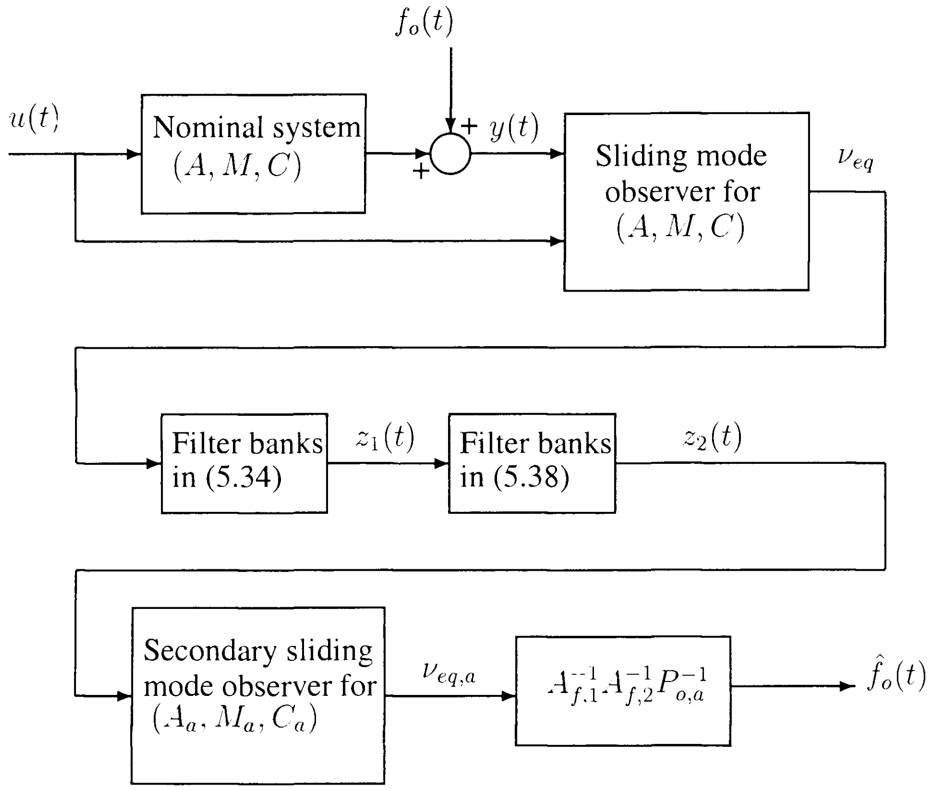

Figure 5.1: Schematic of the FDI scheme using the secondary observer

to the triple (A_a, M_a, C_a) which becomes

$$A_a \to \left[\begin{array}{cc|c} \mathcal{A}_{11} & \mathcal{A}_{12} & * \\ \mathcal{A}_{21} & \mathcal{A}_{22} & * \\ \hline 0 & -A_{f,2}A_{f,1} & * \end{array}\right], M_a \to \left[\begin{array}{c} 0 \\ 0 \\ \hline A_{f,2}A_{f,1} \end{array}\right], C_a \to \left[\begin{array}{cc|c} 0 & 0 & I_p \end{array}\right] \tag{5.45}$$

where the entries '*' play no further part in this analysis of the reduced order motion of the secondary observer. The structure of (A_a, M_a, C_a) in (5.45) shows that the sliding motion is governed by the *eigenvalues of the open loop plant.* This means that this method is applicable only to *open loop stable systems.*

5.3.3 Single observer alternative method

An alternative but related method can be used to reconstruct sensor faults. Consider a new state $z_3 \in \mathcal{R}^p$ that is a filtered version of $y(t)$ from (5.22). Then from (5.22),

$$\dot{z}_3(t) = -A_{f,3}z_3(t) + A_{f,3}Cx(t) + A_{f,3}f_o(t) \tag{5.46}$$

where $-A_{f,3} \in \mathcal{R}^{p\times p}$ is a stable matrix. Equations (5.21) and (5.46) can be combined to form an augmented state space system

$$\begin{bmatrix} \dot{x}(t) \\ \dot{z}_3(t) \end{bmatrix} = \underbrace{\begin{bmatrix} A & 0 \\ A_{f,3}C & -A_{f,3} \end{bmatrix}}_{A_b} \begin{bmatrix} x(t) \\ z_3(t) \end{bmatrix} + \underbrace{\begin{bmatrix} B \\ 0 \end{bmatrix}}_{B_b} u(t) + \underbrace{\begin{bmatrix} 0 \\ A_{f,3} \end{bmatrix}}_{M_b} f_o(t) \quad (5.47)$$

$$z_3(t) = \underbrace{\begin{bmatrix} 0 & I_p \end{bmatrix}}_{C_b} \begin{bmatrix} x(t) \\ z_3(t) \end{bmatrix} \quad (5.48)$$

Equations (5.47) - (5.48) are now in the same form as (5.1) - (5.2) and hence an augmented sliding mode observer of the order $n+p$ can be designed for the system described by (5.47) - (5.48) to reconstruct the fault $f_o(t)$. In the same way as in §5.3.2, the fault reconstruction can be obtained by

$$\hat{f}_o(t) := A_{f,3}^{-1} P_{o,b}^{-1} \nu_{eq,b}$$

where $P_{o,b} \in \mathcal{R}^{p\times p}$ is the symmetric positive definite matrix that scales the nonlinear gain of the augmented observer, and $\nu_{eq,b}$ is the equivalent output error injection of the augmented observer. A schematic diagram of the FDI scheme in this section is shown in Figure 5.2.

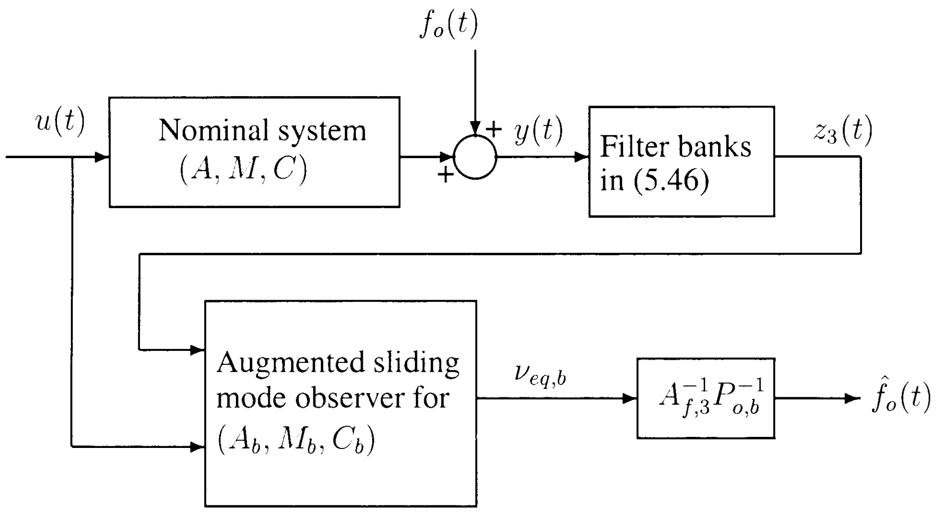

Figure 5.2: Schematic of the FDI scheme using the augmented observer

The triple (A_b, M_b, C_b) represents a square system and the matrices are already in the form of the observer canonical coordinates in (5.12). Hence it is clear that the sliding motion matrix of the augmented observer is given by A, implying that the open loop system needs to be stable. This condition is identical to the requirements for the method in §5.3.1.

5.3.4 Examples

This subsection will demonstrate the methods that have been presented in this section, using the 7-th order aircraft example in §4.9. This system is open loop stable and so the methods described in this section are applicable.

For the secondary observer method presented in §5.3.1, both the primary and secondary observers were designed using the LQG-like design method in §4.4. For the primary observer, the weighting matrices $W = 0.1I_7$ and $V = I_4$. For the secondary observer, the weights $W_a = 0.1I_{11}$ and $V_a = I_4$ and filter matrices were chosen as $A_{f,1} = A_{f,2} = 5I_4$. The synthesised gains of both observers are available in the file *ch5/aircraft/secondaryobs.mat* on the disk attached with this thesis.

In the simulation, the parameters associated with the nonlinear discontinuous term in (5.20) $\rho = \rho_a = 50$, $\delta = 1 \times 10^{-4}$ and $\delta_a = 1 \times 10^{-5}$ were chosen. The subscripts '*a*' indicate that the parameter is associated with the secondary observer.

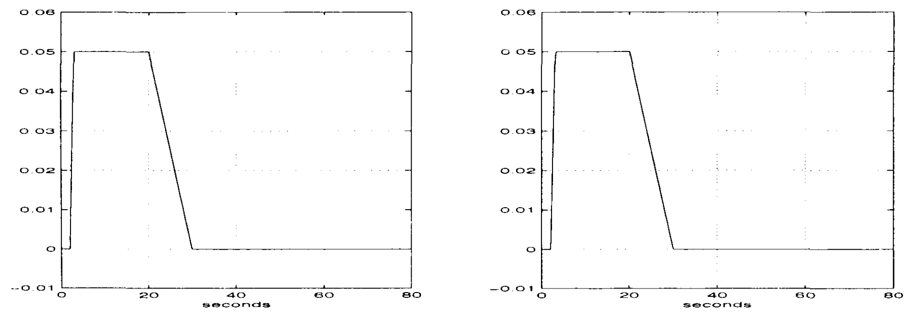

Figure 5.3: *The left subfigure shows a fault on the first sensor. The right subfigure shows its reconstruction using the secondary observer method in §5.3.1.*

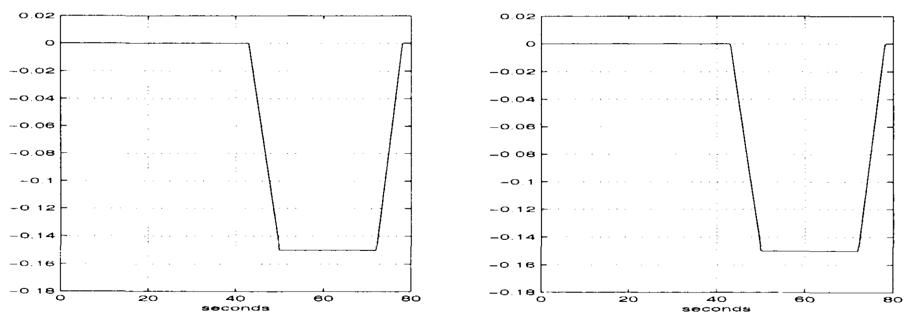

Figure 5.4: *The left subfigure shows the reconstruction of the fault on the second sensor. The right subfigure shows its reconstruction using the secondary observer method in §5.3.1.*

Figures 5.3 and 5.4 show the faults acting on sensors 1 and 2 as well as their reconstructions, using the method in §5.3.1. It can be clearly seen that the reconstruction signals are visually identical to the fault signal.

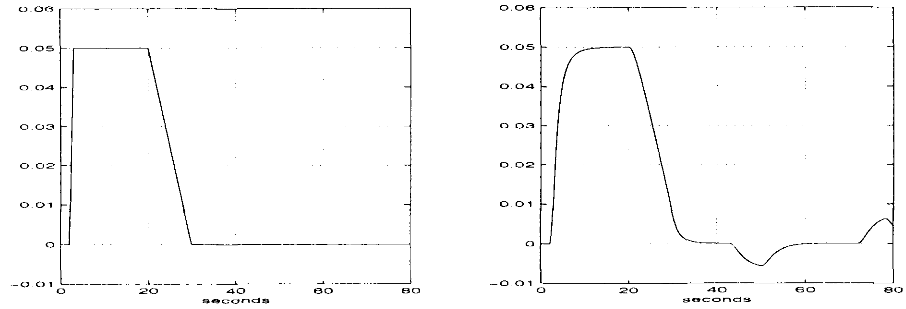

Figure 5.5: *The left subfigure shows the reconstruction of the fault on the first sensor. The right subfigure shows its reconstruction using the method by Edwards et al. from (5.29).*

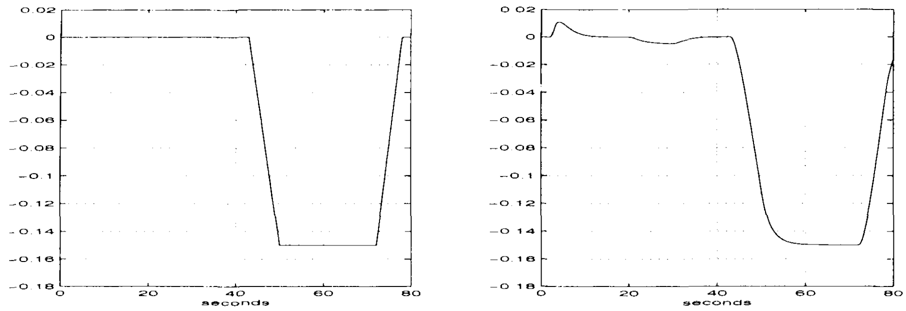

Figure 5.6: *The left subfigure shows the reconstruction of the fault on the second sensor. The right subfigure shows its reconstruction using the method by Edwards et al. from (5.29).*

Figures 5.5 and 5.6 show the fault reconstruction using the method by Edwards *et al.* [27, 26] from equation (5.29), which uses only ν_{eq} from the primary observer. Notice that the fault reconstruction follows the fault for the steady state, but not during the transient. Furthermore, there exists coupling between reconstruction channels during the transients. Therefore, the method in §5.3.1 is an improvement on the method by Edwards *et al.* [27, 26].

For the single observer method in §5.3.3, the augmented observer was also designed using the method in §4.4. The weights $W_b = 0.01I_{11}$ and $V_b = I_4$ and the filtering matrix $A_{f,3} = 10I_4$ were chosen in designing the augmented observer. The resulting gain matrices for the augmented sliding mode observer are available in *ch5/aircraft/singleobs.mat*. The parameters in (5.20) were chosen as $\rho_b = 50$ and $\delta_b = 1 \times 10^{-4}$.

Figures 5.7 and 5.8 show the augmented sliding mode observer faithfully reconstructing both the sensor faults.

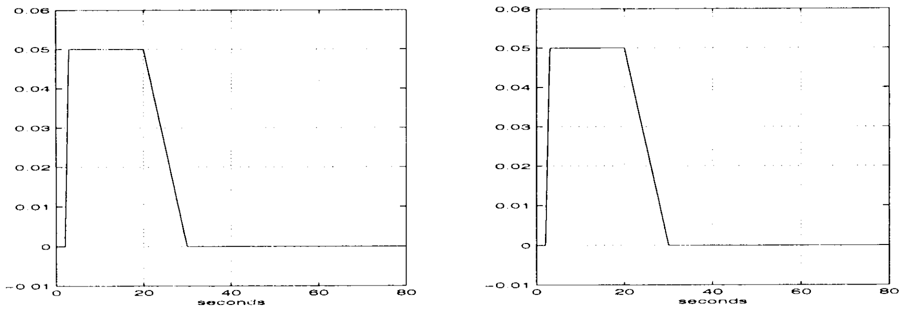

Figure 5.7: *The left subfigure shows a fault on the first sensor. The right subfigure shows its reconstruction using the single augmented observer method in §5.3.3.*

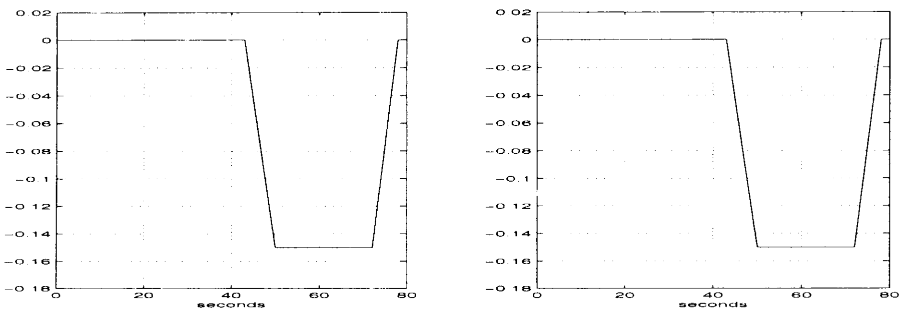

Figure 5.8: *The left subfigure shows the reconstruction of the fault on the second sensor. The right subfigure shows its reconstruction using the single augmented observer method in §5.3.3.*

5.4 Reconstruction of sensor faults assuming some nonfaulty sensors

In §5.3, the methods for sensor fault reconstruction were restricted to systems that are open loop stable. This essentially arises from the fact that the observer design was based on a square system because the number of faulty sensors is equal to the number of outputs (all sensors faulty), allowing no freedom in designing the sliding motion, and causing the sliding motion to be governed by the eigenvalues of the open-loop plant. This section seeks to relax this condition. One way to proceed is to assume that some of the sensors are not prone to be faulty, and hence are perfect. Precedents for this can be found in [96, 120]. This scenario can be mathematically represented by modifying the output equation (5.22) to become

$$y(t) = Cx(t) + Ff_o(t) \tag{5.49}$$

where in this case $f_o \in \mathcal{R}^h$ is the vector of faulty sensors, $F \in \mathcal{R}^{p \times h}$ is the sensor fault distribution matrix, and $rank(F) = h$, where $p > h$.

5.4.1 Secondary observer method

The analysis in §5.3.1 can be repeated by substituting $f_o \in \mathcal{R}^p$ with Ff_o. As a result, the system triple (A_a, M_a, C_a) associated with the augmented secondary observer in (5.40) - (5.41) can be re-written as

$$A_a = \begin{bmatrix} \mathcal{A}_{11} & 0 & 0 \\ -A_{f,1}\mathcal{A}_{21} & -A_{f,1} & 0 \\ 0 & A_{f,2} & -A_{f,2} \end{bmatrix}, M_a = \begin{bmatrix} \mathcal{A}_{12}F \\ -A_{f,1}(A_{f,1} + \mathcal{A}_{22})F \\ A_{f,2}A_{f,1}F \end{bmatrix}, C_a^T = \begin{bmatrix} 0 \\ 0 \\ I_p \end{bmatrix} \tag{5.50}$$

In this scenario, $M_a \in \mathcal{R}^{(n+p)\times h}$ and since $p > h$, there is freedom in tuning the sliding motion of the secondary observer.

5.4.2 Existence conditions

Since $rank(F) = h$ and $C_a M_a = A_{f,1}A_{f,2}F$, condition A1 in §5.2 is satisfied.

Proposition 5.1 *The invariant zeros of (A_a, M_a, C_a) are given by values of s satisfying*

$$rank \begin{bmatrix} sI_{n+p} - \mathcal{A} & 0 \\ \mathcal{C} & F \end{bmatrix} < n + h$$

Furthermore, the invariant zeros of $(A_a, M_a, C_a) \subseteq \lambda(A)$.

Proof

The invariant zeros of (A_a, M_a, C_a) are given by the values of s when

$$P_a(s) := \begin{bmatrix} sI_n - A_a & -M_a \\ C_a & 0 \end{bmatrix}$$

loses rank. Substituting for A_a, M_a and C_a from (5.50),

$$P_a(s) = \begin{bmatrix} sI_{n-p} - \mathcal{A}_{11} & 0 & 0 & -\mathcal{A}_{12}F \\ A_{f,1}\mathcal{A}_{21} & sI_p + A_{f,1} & 0 & A_{f,1}^2 F + A_{f,1}\mathcal{A}_{22}F \\ 0 & -A_{f,2} & sI_p + A_{f,2} & -A_{f,2}A_{f,1}F \\ 0 & 0 & I_p & 0 \end{bmatrix}$$

It is straightforward to show that $P_a(s)$ will lose rank if and only if

$$\tilde{P}_a(s) = \begin{bmatrix} sI_{n-p} - \mathcal{A}_{11} & 0 & -\mathcal{A}_{12}F \\ A_{f,1}\mathcal{A}_{21} & sI_p + A_{f,1} & A_{f,1}^2 F + A_{f,1}\mathcal{A}_{22}F \\ 0 & -A_{f,2} & -A_{f,2}A_{f,1}F \end{bmatrix}$$

loses rank. Pre-multiplying and post-multiplying $\tilde{P}_a(s)$ by

$$\begin{bmatrix} I_{n-p} & 0 & -\mathcal{A}_{12}A_{f,1}^{-1}A_{f,2}^{-1} \\ 0 & -A_{f,1}^{-1} & -(A_{f,1}+\mathcal{A}_{22})A_{f,1}^{-1}A_{f,2}^{-1} \\ 0 & 0 & A_{f,1}^{-1}A_{f,2}^{-1} \end{bmatrix}$$

and

$$\begin{bmatrix} I_p & 0 & 0 \\ 0 & -A_{f,1} & 0 \\ 0 & 0 & -I_p \end{bmatrix}$$

respectively, it follows

$$\begin{aligned} rank\ \tilde{P}_a(s) &= rank \begin{bmatrix} sI_{n-p}-\mathcal{A}_{11} & -\mathcal{A}_{12} & 0 \\ -\mathcal{A}_{21} & sI_p-\mathcal{A}_{22} & 0 \\ 0 & I_p & F \end{bmatrix} \\ &= rank \begin{bmatrix} sI_n-\mathcal{A} & 0 \\ \mathcal{C} & F \end{bmatrix} \end{aligned} \tag{5.51}$$

Hence the invariant zeros of (A_a, M_a, C_a) are given by the values of s when

$$rank \begin{bmatrix} sI_n-\mathcal{A} & 0 \\ \mathcal{C} & F \end{bmatrix} < n+h \tag{5.52}$$

Notice that if s is not an eigenvalue of A, then $det\ (sI_n-\mathcal{A}) \neq 0$ and

$$rank \begin{bmatrix} sI_n-\mathcal{A} & 0 \\ \mathcal{C} & F \end{bmatrix} = n+h$$

Hence the invariant zeros of $(A_a, M_a, C_a) \subseteq \lambda(A)$ as claimed. ■

Remark : If the original system matrix A is stable, then the fact that the invariant zeros of $(A_a, M_a, C_a) \subseteq \lambda(A)$ causes no difficulty. The only implication is that certain modes of the sliding motion are fixed.

5.4.3 Single observer method

As in §5.4.1, by substituting $f_o \in \mathcal{R}^p$ with Ff_o, the triple (A_b, M_b, C_b) from §5.3.3 can be rewritten as

$$A_b = \begin{bmatrix} A & 0 \\ A_{f,3}C & -A_{f,3} \end{bmatrix}, M_b = \begin{bmatrix} 0 \\ A_{f,3}F \end{bmatrix}, C_b = \begin{bmatrix} 0 & I_p \end{bmatrix} \tag{5.53}$$

From (5.53), it can be seen that $C_b M_b = A_{f,3} F$ and it is easy to see that condition A1 is satisfied since $rank\ (F) = h$.

Proposition 5.2 *The invariant zeros of (A_b, M_b, C_b) are given by values of s for which*

$$rank \begin{bmatrix} sI_n - A & 0 \\ C & F \end{bmatrix} < n + h \tag{5.54}$$

Furthermore, the invariant zeros of $(A_b, M_b, C_b) \subseteq \lambda(A)$.

Proof

From (5.53) and (5.54), the invariant zeros of (A_b, M_b, C_b) are given by the values of s for which

$$P_b(s) = \begin{bmatrix} sI_n - A & 0 & 0 \\ -A_{f,3}C & sI_p + A_{f,3} & -A_{f,3}F \\ 0 & I_p & 0 \end{bmatrix}$$

loses normal rank. It is straightforward to show that $P_b(s)$ loses normal rank if and only if

$$rank \begin{bmatrix} sI_n - A & 0 \\ -A_{f,3}C & -A_{f,3}F \end{bmatrix} < n + h$$

Pre-multiplying by the invertible matrix

$$\begin{bmatrix} I_n & 0 \\ 0 & -A_{f,3}^{-1} \end{bmatrix}$$

it is easy to see that the invariant zeros of (A_b, M_b, C_b) are given by the values of s when

$$rank \begin{bmatrix} sI_n - A & 0 \\ C & F \end{bmatrix} < n + h \tag{5.55}$$

Arguing as in proof of Proposition 5.1, the invariant zeros of $(A_b, M_b, C_b) \subseteq \lambda(A)$. ■

Remark : As seen from §5.3 and §5.4, the secondary observer and single observer methods are very similar; both use augmented sliding mode observers of order $n + p$ and have identical existence conditions. However, there are subtle differences. The secondary observer method relies firstly on the existence of a primary observer, which means that the primary triple (A, M, C) needs to be minimum phase, and CM needs to have full column rank. For the single observer method, there is no such requirement, and only one observer needs to be designed. Therefore, for purely sensor fault reconstruction, the single observer method would provide the better option. However, for cases where estimates of the state are required (for example observer based control), then the secondary observer method has the advantage.

5.4.4 Examples

The methods in §5.4 will now be demonstrated on an unstable system. The method in §5.3 is not appropriate for this system. The example is an 8-th order model of a helicopter with 6 outputs and 4 inputs, taken from [24]. The states are given by

$$x = \left[\begin{array}{c|l} \theta & \text{pitch attitude } (rad) \\ \phi & \text{roll attitude } (rad) \\ p & \text{body roll rate } (rad/s) \\ q & \text{body pitch rate } (rad/s) \\ r & \text{body yaw rate } (rad/s) \\ u & \text{forward velocity } (ft/s) \\ v & \text{lateral velocity } (ft/s) \\ w & \text{normal velocity } (ft/s) \end{array}\right.$$

the inputs are

$$u = \left[\begin{array}{c|l} \theta_{0d} & \text{main rotor collective } (deg) \\ \theta_{ls} & \text{longitudinal cyclic } (deg) \\ \theta_{lc} & \text{lateral cyclic } (deg) \\ \theta_{0t} & \text{tail rotor collective } (deg) \end{array}\right.$$

and the measured outputs are

$$y = \left[\begin{array}{c|l} \dot{h} & \text{heave velocity } (ft/s) \\ \theta & \text{pitch attitude } (rad) \\ \phi & \text{roll attitude } (rad) \\ \dot{\psi} & \text{heading rate } (ft/s) \\ q & \text{body pitch rate } (rad/s) \\ p & \text{body roll rate } (rad/s) \end{array}\right.$$

The matrices that define the model are given by

$$A = \begin{bmatrix} 0 & 0 & 0 & 0.9986 & 0.0534 & 0 & 0 & 0 \\ 0 & 0 & 1.0000 & -0.0032 & 0.0595 & 0 & 0 & 0 \\ 0 & 0 & -11.5705 & -2.5446 & -0.0636 & 0.1068 & -0.0949 & 0.0071 \\ 0 & 0 & 0.4394 & -1.9982 & 0 & 0.0167 & 0.0185 & -0.0012 \\ 0 & 0 & -2.0409 & -0.4590 & -0.7350 & 0.0193 & -0.0046 & 0.0021 \\ -32.1036 & 0 & -0.5034 & 2.2979 & 0 & -0.0212 & -0.0212 & 0.0158 \\ 0.1022 & 32.0578 & -2.3472 & -0.5036 & 0.8349 & 0.0212 & -0.0379 & 0.0004 \\ -1.9110 & 1.7138 & -0.0040 & -0.0574 & 0 & 0.0140 & -0.0009 & -0.2905 \end{bmatrix}$$

$$B = M = \begin{bmatrix} 0 & 0 & 0 & 0 \\ 0 & 0 & 0 & 0 \\ 0.1243 & 0.0828 & -2.7525 & -0.0179 \\ -0.0364 & 0.4751 & 0.0143 & 0 \\ 0.3045 & 0.0150 & -0.4965 & -0.2067 \\ 0.2877 & -0.5445 & -0.0164 & 0 \\ -0.0191 & 0.0164 & -0.5445 & 0.2348 \\ -4.8206 & -0.0004 & 0 & 0 \end{bmatrix}$$

$$C = \begin{bmatrix} 0 & 0 & 0 & 0 & 0 & 0.0595 & 0.0533 & -0.9968 \\ 1.0000 & 0 & 0 & 0 & 0 & 0 & 0 & 0 \\ 0 & 1.0000 & 0 & 0 & 0 & 0 & 0 & 0 \\ 0 & 0 & 0 & -0.0535 & 1.0000 & 0 & 0 & 0 \\ 0 & 0 & 1.0000 & 0 & 0 & 0 & 0 & 0 \\ 0 & 0 & 0 & 1.0000 & 0 & 0 & 0 & 0 \end{bmatrix}$$

The open loop poles of the system are

$$\{-11.4968, -2.3036, 0.2342 \pm 0.5513i, -0.1593 \pm 0.5990i, -0.7104, -0.2923\}$$

The system has 2 stable invariant zeros at $\{-0.0014, -0.0054\}$.

In the following it is assumed that all sensors except the second one are potentially faulty.

Therefore the sensor fault distribution matrix F in (5.49) is

$$F = \begin{bmatrix} 1 & 0 & 0 & 0 & 0 \\ 0 & 0 & 0 & 0 & 0 \\ 0 & 1 & 0 & 0 & 0 \\ 0 & 0 & 1 & 0 & 0 \\ 0 & 0 & 0 & 1 & 0 \\ 0 & 0 & 0 & 0 & 1 \end{bmatrix}$$

By using (5.52), it was found that the triple (A_a, M_a, C_a) associated with the augmented secondary observer has no invariant zeros.

All observers were designed using the LQG-like method in §4.4.

For the method in §5.4.1, in designing the primary observer, the weighting matrices were specified to be $W = 0.1I_8$ and $V = I_6$. For the secondary augmented observer, the weighting matrices were specified to be $W_a = 0.1I_{14}$ and $V_a = I_6$ and the filtering matrices $A_{f,1} = A_{f,2} = 10I_6$. The resulting gain matrices are available in *ch5/helicopter/secondaryobs.mat*.

In the simulations that follow, $\rho = \rho_a = 100$, $\delta = \delta_a = 1 \times 10^{-4}$ were chosen.

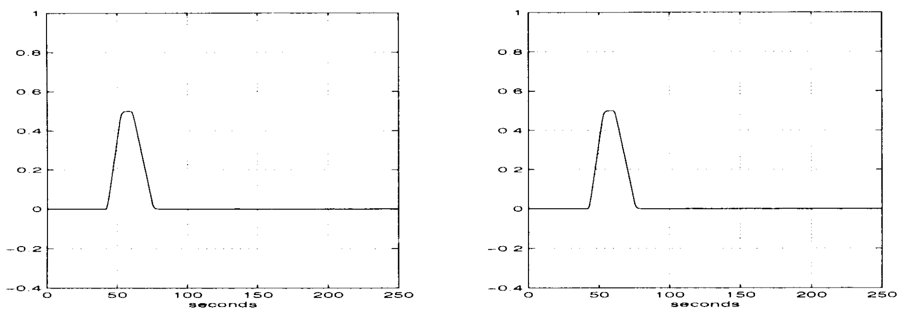

Figure 5.9: *The left subfigure shows a fault on the first sensor. The right subfigure shows its reconstruction using the secondary observer.*

Figures 5.9 - 5.13 show faults acting on sensors 1-5, and also their respective reconstructions. It can be seen that the secondary observer reconstructs the faults almost perfectly.

For the method in §5.4.3, in designing the augmented sliding mode observer, the weighting matrices $W_b = 0.01I_{14}$ and $V_b = I_6$ and the filter matrix $A_{f,3} = 10I_6$ were used. The synthesis results are available in *ch5/helicopter/singleobs.mat*.

During the simulation $\rho_b = 50$ and $\delta_b = 1 \times 10^{-4}$ were used for the parameters associated with the nonlinear term in (5.20).

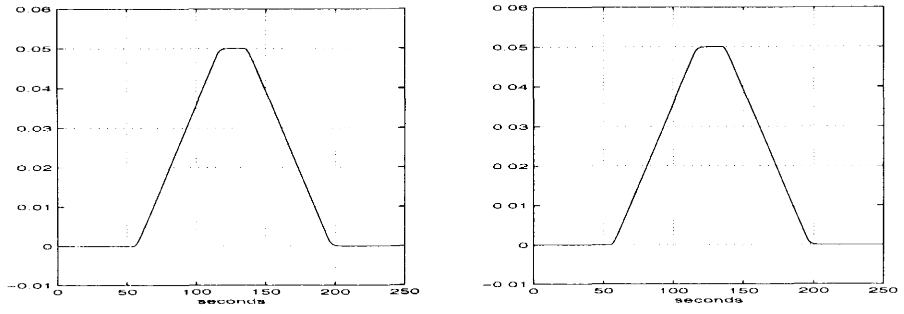

Figure 5.10: *The left subfigure shows a fault on the third sensor. The right subfigure shows its reconstruction using the secondary observer.*

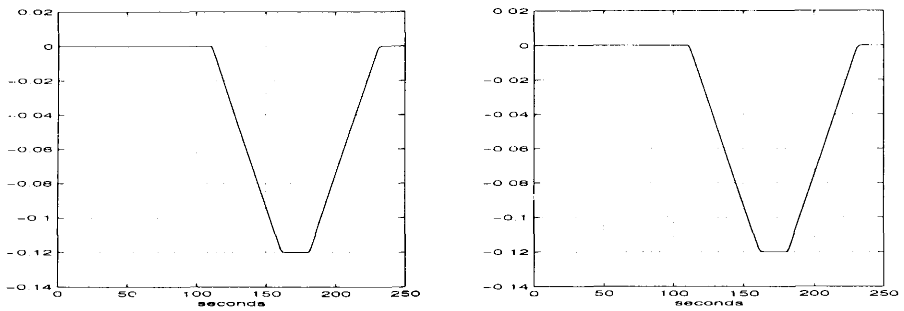

Figure 5.11: *The left subfigure shows a fault on the fourth sensor. The right subfigure shows its reconstruction using the secondary observer.*

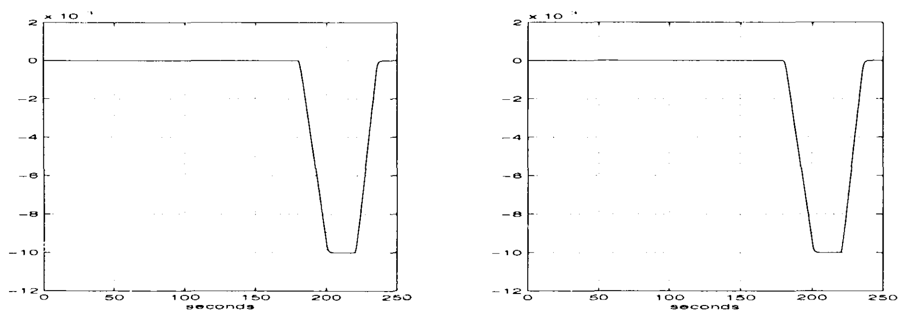

Figure 5.12: *The left subfigure shows a fault on the fifth sensor. The right subfigure shows its reconstruction using the secondary observer.*

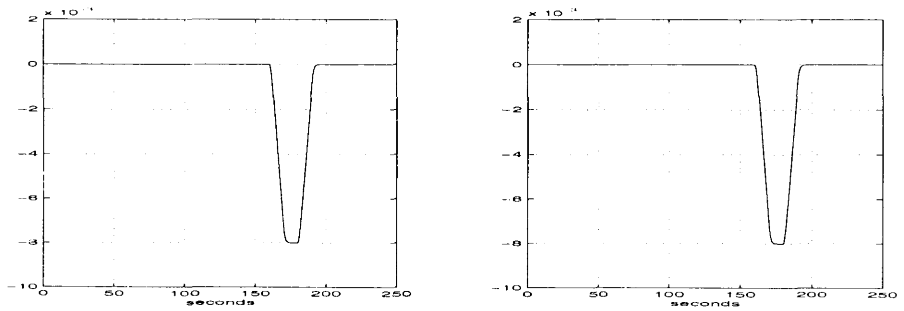

Figure 5.13: *The left subfigure shows a fault on the sixth sensor. The right subfigure shows its reconstruction using the secondary observer.*

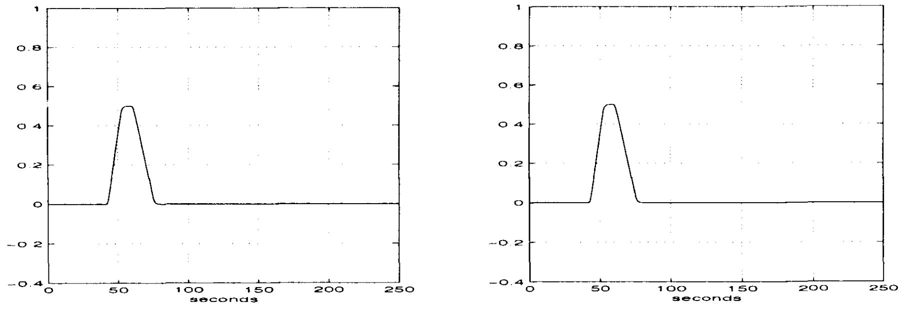

Figure 5.14: *The left subfigure shows a fault on the first sensor. The right subfigure shows its reconstruction using the augmented observer.*

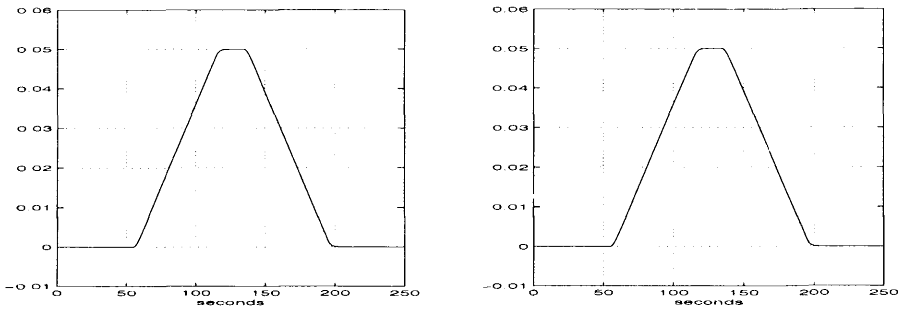

Figure 5.15: *The left subfigure shows a fault on the third sensor. The right subfigure shows its reconstruction using the augmented observer.*

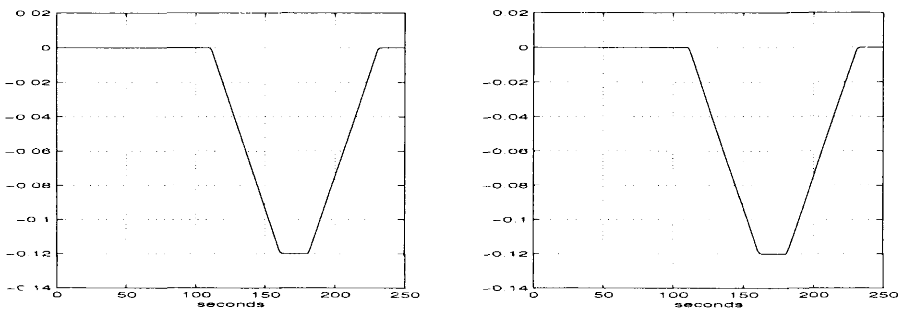

Figure 5.16: *The left subfigure shows a fault on the fourth sensor. The right subfigure shows its reconstruction using the augmented observer.*

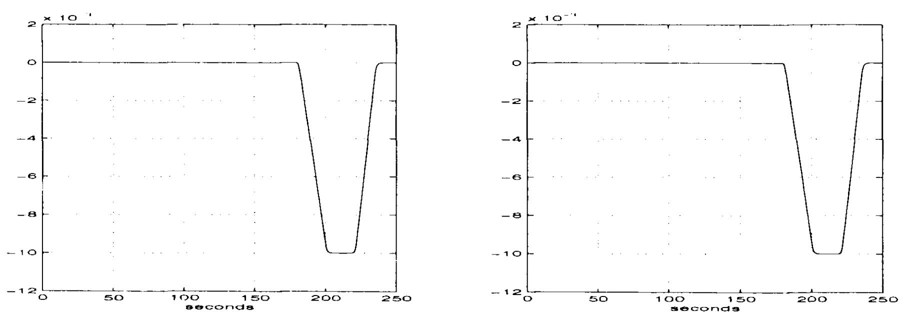

Figure 5.17: *The left subfigure shows a fault on the fifth sensor. The right subfigure shows its reconstruction using the augmented observer.*

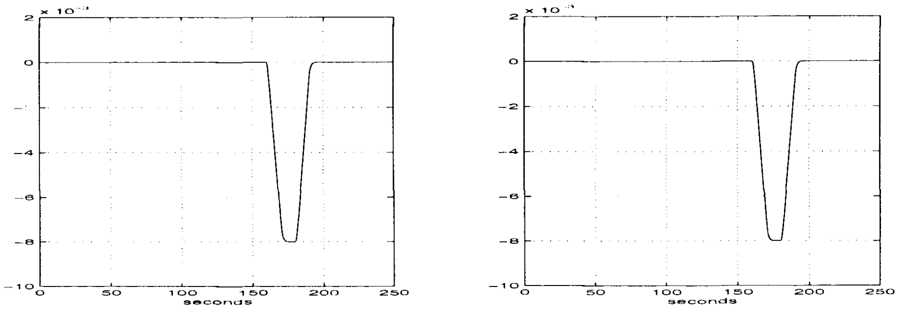

Figure 5.18: *The left subfigure shows a fault on the sixth sensor. The right subfigure shows its reconstruction using the augmented observer.*

Figures 5.14 - 5.18 show the faults acting on the sensors, as well as their reconstructions, and it can be seen that the augmented observer does reconstruct properly the faults.

5.5 Reconstruction of sensor faults for unstable systems where all sensors are assumed faulty

This section presents a method for sensor fault reconstruction, when the conditions in §5.3 cannot be met and the assumptions/conditions in §5.4 are not tenable. The only condition needed in this section is that the system matrix A is full rank, implying that the system should not possess inherently any integral action. The compromise in §5.4 (that only certain sensors are faulty) is not needed. However, in the analysis in this section, the derivative of the sensor fault is neglected ($\dot{f}_o(t) \approx 0$).

Assume a primary observer has been designed for the system (5.21) - (5.22) in §5.2.1 and that sliding motion has been attained. The error system is then be governed by (5.27) - (5.28). Consider a new state $z_4 \in \mathcal{R}^p$ which is a filtered version of $P_o^{-1}\nu_{eq}$

$$\dot{z}_4(t) = -A_{f,4}z_4(t) + A_{f,4}P_o^{-1}\nu_{eq} \tag{5.56}$$

where $-A_{f,4} \in \mathcal{R}^{p\times p}$ is a stable filter matrix. Assume that the sensor fault represents a slow incipient drift $\dot{f}_o(t) \approx 0$. Step sensor failures are relatively easy to detect using sliding mode observers because they usually break the sliding motion which is readily apparent from monitoring $e_y(t)$ [26].

Using the expression for ν_{eq} in (5.28), equation (5.56) becomes

$$\dot{z}_4(t) = -A_{f,4}z_4(t) - A_{f,4}\mathcal{A}_{21}e_1(t) - A_{f,4}\mathcal{A}_{22}f_o(t) \tag{5.57}$$

Combining (5.27) and (5.57), the following state-space representation can be obtained

$$\begin{bmatrix} \dot{e}_1(t) \\ \dot{z}_4(t) \end{bmatrix} = \underbrace{\begin{bmatrix} \mathcal{A}_{11} & 0 \\ -A_{f,4}\mathcal{A}_{21} & -A_{f,4} \end{bmatrix}}_{A_c} \begin{bmatrix} e_1(t) \\ z_4(t) \end{bmatrix} + \underbrace{\begin{bmatrix} \mathcal{A}_{12} \\ -A_{f,4}\mathcal{A}_{22} \end{bmatrix}}_{M_c} f_o(t) \quad (5.58)$$

$$z_4(t) = \underbrace{\begin{bmatrix} 0 & I_p \end{bmatrix}}_{C_c} \begin{bmatrix} e_1(t) \\ z_4(t) \end{bmatrix} \quad (5.59)$$

Equations (5.58) and (5.59) are now in a form similar to equations (5.1) and (5.2). Hence the sliding mode observer in §3.5 can be used to reconstruct the sensor fault $f_o(t)$ using the concepts described in §5.2.

5.5.1 Existence conditions for the sliding mode observer

From (5.58) - (5.59), $C_cM_c = -A_{f,4}\mathcal{A}_{22}$, and hence the necessary and sufficient condition for condition A1 in §5.2 to be satisfied is that $\mathcal{A}_{22}$ is invertible.

The triple (A_c, M_c, C_c) is a square system, and hence, no freedom exists for designing the sliding motion associated with the secondary observer. Assuming $\mathcal{A}_{22}$ is invertible, the observer canonical form in (5.12) can be obtained by applying the change of coordinates

$$T_c = \begin{bmatrix} I_{n-p} & \mathcal{A}_{12}\mathcal{A}_{22}^{-1}A_{f,4}^{-1} \\ 0 & I_p \end{bmatrix} \quad (5.60)$$

to the triple (A_c, M_c, C_c), which would yield

$$A_c \rightarrow \begin{bmatrix} \mathcal{A}_{11} - \mathcal{A}_{12}\mathcal{A}_{22}^{-1}\mathcal{A}_{21} & * \\ -A_{f,4}\mathcal{A}_{21} & * \end{bmatrix}, M_c \rightarrow \begin{bmatrix} 0 \\ -A_{f,4}\mathcal{A}_{22} \end{bmatrix}, C_c \rightarrow \begin{bmatrix} 0 & I_p \end{bmatrix} \quad (5.61)$$

where the entries '*' play no further part in the analysis. It is clear that the sliding motion of the secondary observer is governed by $(\mathcal{A}_{11} - \mathcal{A}_{12}\mathcal{A}_{22}^{-1}\mathcal{A}_{21})$. Therefore the existence conditions for the secondary observer are that $\mathcal{A}_{22}$ must be full rank and $(\mathcal{A}_{11} - \mathcal{A}_{12}\mathcal{A}_{22}^{-1}\mathcal{A}_{21})$ is stable.

Define $\nu_{eq,c}$ as the equivalent output error injection associated with the secondary observer, and $P_{o,c} \in \mathcal{R}^{p\times p}$ as the symmetric positive definite matrix that scales the nonlinear gain of the secondary observer. From (5.61), the reconstruction for $f_o(t)$ is defined as

$$\hat{f}_o(t) := -\mathcal{A}_{22}^{-1}A_{f,4}^{-1}P_{o,c}^{-1}\nu_{eq,c} \quad (5.62)$$

The following section seeks to guarantee the stability of $(\mathcal{A}_{11} - \mathcal{A}_{12}\mathcal{A}_{22}^{-1}\mathcal{A}_{21})$, whilst ensuring that $\mathcal{A}_{22}$ is invertible and $\mathcal{A}_{11}$ is stable.

5.5.2 Using LMIs to guarantee a stable sliding motion for the secondary observer

Assume without a loss of generality, the system triple (A, M, C) from (5.21) - (5.22) is already in the form of (5.7). Applying the linear coordinate transformation (5.11), the system matrix A in the canonical form in (5.12) is

$$\mathcal{A} = \begin{bmatrix} \mathcal{A}_{11} & \mathcal{A}_{12} \\ \mathcal{A}_{21} & \mathcal{A}_{22} \end{bmatrix} = \begin{bmatrix} A_{11} + LA_{21} & (-A_{11}L - LA_{21}L + A_{12} + LA_{22})T^T \\ TA_{21} & T(-A_{21}L + A_{22})T^T \end{bmatrix} \tag{5.63}$$

The problem now is to make $\mathcal{A}_{22}$ invertible and $\mathcal{A}_{11} - \mathcal{A}_{12}\mathcal{A}_{22}^{-1}\mathcal{A}_{21}$ stable by choice of L, which must have the structure given in (5.9), whilst retaining the property that $\mathcal{A}_{11}$ is stable. All these requirements will be incorporated with the design of the primary observer using the LQG-like method in §4.4 which can be summarised as :

Minimise $trace\ (X)$ with respect to the variables X, P_{11}, P_{12} and P_{22} subject to the inequalities

$$\begin{bmatrix} PA + A^TP - C^TV^{-1}C & P \\ P & -W^{-1} \end{bmatrix} < 0 \tag{5.64}$$

$$\begin{bmatrix} -P & I_n \\ I_n & -X \end{bmatrix} < 0 \tag{5.65}$$

where

$$P = \begin{bmatrix} P_{11} & P_{12} \\ P_{12} & P_{22} \end{bmatrix} \tag{5.66}$$

with $P_{11} \in \mathcal{R}^{(n-p)\times(n-p)}$, $P_{22} \in \mathcal{R}^{p\times p}$ and $P_{12} = \begin{bmatrix} P_{121} & 0 \end{bmatrix}$ where $P_{121} \in \mathcal{R}^{(n-p)\times(p-q)}$. The matrices $W \in \mathcal{R}^{n\times n}$ and $V \in \mathcal{R}^{p\times p}$ are symmetric positive definite weights.

It is assumed throughout this section that $det(A) \neq 0$.

The choice of L will be achieved by a two stage process. Suppose L in (5.9) is written as

$$L = L_1 + L_2 \tag{5.67}$$

where L_1 and L_2 *do not necessarily have the same structure as* L. Decompose the canonical transformation in (5.11) as

$$T_L = T_{L,2}T_{L,1} = \begin{bmatrix} I_{n-p} & L_2 \\ 0 & T \end{bmatrix} \begin{bmatrix} I_{n-p} & L_1 \\ 0 & I_p \end{bmatrix} \tag{5.68}$$

Applying the first change of coordinates $T_{L,1}$ to the system matrix A will yield

$$\tilde{A} = \begin{bmatrix} \tilde{A}_{11} & \tilde{A}_{12} \\ \tilde{A}_{21} & \tilde{A}_{22} \end{bmatrix} := \begin{bmatrix} A_{11} + L_1A_{21} & (-A_{11}L_1 - L_1A_{21}L_1 + A_{12} + L_1A_{22}) \\ A_{21} & A_{22} - A_{21}L_1 \end{bmatrix} \tag{5.69}$$

Applying the second change of coordinates $T_{L,2}$, then the $\mathcal{A}$ in (5.63) can be written as

$$\mathcal{A}=\begin{bmatrix} \mathcal{A}_{11} & \mathcal{A}_{12} \\ \mathcal{A}_{21} & \mathcal{A}_{22} \end{bmatrix}=\begin{bmatrix} \tilde{A}_{11}+L_2\tilde{A}_{21} & (-\tilde{A}_{11}L_2-L_2\tilde{A}_{21}L_2+\tilde{A}_{12}+L_2\tilde{A}_{22})T^T \\ T\tilde{A}_{21} & T(\tilde{A}_{22}-\tilde{A}_{21}L_2)T^T \end{bmatrix} \tag{5.70}$$

Based on these definitions the following lemma holds.

Lemma 5.1 *The matrix* $(\mathcal{A}_{11}-\mathcal{A}_{12}\mathcal{A}_{22}^{-1}\mathcal{A}_{21})$ *can be expressed as* KJ^{-1} *where*

$$K = \tilde{A}_{11}-\tilde{A}_{12}\tilde{A}_{22}^{-1}\tilde{A}_{21} \tag{5.71}$$

$$J = I_{n-p}-L_2\tilde{A}_{22}^{-1}A_{21} \tag{5.72}$$

Proof

From the definitions in (5.70),

$$\begin{aligned}
\mathcal{A}_{11} &- \mathcal{A}_{12}\mathcal{A}_{22}^{-1}\mathcal{A}_{21} \\
&= \tilde{A}_{11}+L_2\tilde{A}_{21}-(-\tilde{A}_{11}L_2-L_2\tilde{A}_{21}L_2+\tilde{A}_{12}+L_2\tilde{A}_{22})(\tilde{A}_{22}-\tilde{A}_{21}L_2)^{-1}\tilde{A}_{21} \\
&= \tilde{A}_{11}+L_2\tilde{A}_{21}-(-\tilde{A}_{11}L_2+\tilde{A}_{12}+L_2(\tilde{A}_{22}-\tilde{A}_{21}L_2))(\tilde{A}_{22}-\tilde{A}_{21}L_2)^{-1}\tilde{A}_{21} \\
&= \tilde{A}_{11}+(\tilde{A}_{11}L_2-\tilde{A}_{12})(\tilde{A}_{22}-\tilde{A}_{21}L_2)^{-1}\tilde{A}_{21} \qquad (5.73)
\end{aligned}$$

From the Matrix Inversion Lemma [99],

$$(\tilde{A}_{22}-\tilde{A}_{21}L_2)^{-1}=\tilde{A}_{22}^{-1}+\tilde{A}_{22}^{-1}\tilde{A}_{21}J^{-1}L_2\tilde{A}_{22}^{-1}$$

where J is defined in (5.72) and hence (5.73) becomes

$$\tilde{A}_{11}+(\tilde{A}_{11}L_2-\tilde{A}_{12})\tilde{A}_{22}^{-1}\tilde{A}_{21}+(\tilde{A}_{11}L_2-\tilde{A}_{12})\tilde{A}_{22}^{-1}\tilde{A}_{21}J^{-1}L_2\tilde{A}_{22}^{-1}\tilde{A}_{21} \tag{5.74}$$

By pre-multiplying equation (5.72) with J^{-1} it follows that $J^{-1}L_2\tilde{A}_{22}^{-1}\tilde{A}_{21}=J^{-1}-I_{n-p}$, and $L_2\tilde{A}_{22}^{-1}\tilde{A}_{21}J^{-1}=J^{-1}-I_{n-p}$ follows from post-multiplying (5.72) with J^{-1}. It follows from substituting in (5.74) that

$$\begin{aligned}
\mathcal{A}_{11}-\mathcal{A}_{12}\mathcal{A}_{22}^{-1}\mathcal{A}_{21} &= \tilde{A}_{11}+(\tilde{A}_{11}L_2-\tilde{A}_{12})\tilde{A}_{22}^{-1}\tilde{A}_{21}+(\tilde{A}_{11}L_2-\tilde{A}_{12})\tilde{A}_{22}^{-1}\tilde{A}_{21}(J^{-1}-I_{n-p}) \\
&= \tilde{A}_{11}+(\tilde{A}_{11}L_2-\tilde{A}_{12})\tilde{A}_{22}^{-1}\tilde{A}_{21}J^{-1} \\
&= \tilde{A}_{11}-\tilde{A}_{12}\tilde{A}_{22}^{-1}\tilde{A}_{21}J^{-1}+\tilde{A}_{11}L_2\tilde{A}_{22}^{-1}\tilde{A}_{21}J^{-1} \\
&= \tilde{A}_{11}-\tilde{A}_{12}\tilde{A}_{22}^{-1}\tilde{A}_{21}J^{-1}+\tilde{A}_{11}(J^{-1}-I_{n-p}) \\
&= (\tilde{A}_{11}-\tilde{A}_{12}\tilde{A}_{22}^{-1}\tilde{A}_{21})J^{-1} \\
&= KJ^{-1}
\end{aligned}$$

as claimed. ∎

Lemma 5.2 *If* $det(A) \neq 0$ *then there exists an* L_1 *such that* $\tilde{A}_{22} = (A_{22} - A_{21}L_1)$ *is full rank.*

Proof

Under the assumption that $det(A) \neq 0$ it follows

$$rank \begin{bmatrix} A_{21} & A_{22} \end{bmatrix} = p$$

Thus the matrix pencil

$$\begin{bmatrix} sI_p - A_{22} & A_{21} \end{bmatrix}$$

associated with the PBH controllability test for the fictitious pair (A_{22}, A_{21}) has full rank at $s = 0$. This implies that $s = 0$ is not an uncontrollable mode of (A_{22}, A_{21}). Consequently, L_1 always can be chosen so that

$$\tilde{A}_{22} = A_{22} - A_{21}L_1$$

has nonzero determinant. In other words, if A_{22} is rank deficient, then the pair (A_{22}, A_{21}) is controllable, and an L_1 can be chosen to make $\tilde{A}_{22}$ full rank. ■

Since by assumption $det(A) \neq 0$ it will be assumed for the rest of this section that L_1 has been selected so that $det(\tilde{A}_{22}) \neq 0$.

Lemma 5.3 J *defined in (5.72) is invertible if and only if* $\mathcal{A}_{22}$ *defined in (5.70) is invertible.*

Proof

The matrix J as defined in (5.72) is a Schur complement of

$$J_s := \begin{bmatrix} I_{n-p} & L_2 \\ \tilde{A}_{21} & \tilde{A}_{22} \end{bmatrix} \tag{5.75}$$

since $\tilde{A}_{22}$ is nonsingular. Therefore J is invertible if and only if J_s is invertible. However J_s is invertible if and only if $det(\tilde{A}_{22} - \tilde{A}_{21}L_2) \neq 0$ (which also represents a Schur complement). From the definitions of L, $\tilde{A}_{21}$ and $\tilde{A}_{22}$,

$$det(\tilde{A}_{22} - \tilde{A}_{21}L_2) = det(T^T \mathcal{A}_{22} T) = det(\mathcal{A}_{22})$$

since T is orthogonal. This proves that J is invertible if and only if $\mathcal{A}_{22}$ is invertible. ■

Lemma 5.4 *The matrix* K *defined in (5.71) is invertible if* A *is invertible*

Proof

From (5.63), if A is invertible, $\tilde{A}$ defined in (5.69) is invertible for any choice of L_1. It can be seen from (5.71) that K is a Schur complement for $\tilde{A}$. By design, L_1 is chosen to make $\tilde{A}_{22}$ invertible, and hence K is invertible. ■

The problem is now to force $Re\,\lambda(KJ^{-1}) < 0$ by choice of L_2. However this can also be achieved by forcing the requirement $Re\,\lambda(JK^{-1}) < 0$. (By implication, this would mean that JK^{-1} would have no eigenvalues at the origin, and hence will be invertible. This in turn implies that J will be invertible, and from Lemma 5.3, $\mathcal{A}_{22}$ will be invertible).

The problem of selecting a L_2 so that JK^{-1} is stable is equivalent to finding a symmetric positive definite matrix $\tilde{P} \in \mathcal{R}^{(n-p)\times(n-p)}$ and L_2 satisfying

$$\tilde{P}JK^{-1} + (\tilde{P}JK^{-1})^T < 0 \tag{5.76}$$

From the definition of J in (5.72), inequality (5.76) becomes

$$\tilde{P}K^{-1} + (\tilde{P}K^{-1})^T - \tilde{P}L_2\tilde{A}_{22}^{-1}A_{21}K^{-1} - (\tilde{P}L_2\tilde{A}_{22}^{-1}A_{21}K^{-1})^T < 0 \tag{5.77}$$

Choosing $\tilde{P} = P_1$ from the Lyapunov matrix in (5.10) and recalling that $L = L_1 + L_2$, inequality (5.77) becomes

$$\begin{aligned} P_{11}(K^{-1} + L_1\tilde{A}_{22}^{-1}A_{21}K^{-1}) \;+\; &(P_{11}(K^{-1} + L_1\tilde{A}_{22}^{-1}A_{21}K^{-1}))^T \\ &- P_{11}L\tilde{A}_{22}^{-1}A_{21}K^{-1} - (P_{11}L\tilde{A}_{22}^{-1}A_{21}^{-1}K^{-1})^T < 0 \end{aligned} \tag{5.78}$$

By comparing (5.10) with (5.66) it is easy to see that $P_1 = P_{11}$ and $P_1L = P_{12}$ and hence

$$\begin{aligned} P_{11}(K^{-1} + L_1\tilde{A}_{22}^{-1}A_{21}K^{-1}) \;+\; &(P_{11}(K^{-1} + L_1\tilde{A}_{22}^{-1}A_{21}K^{-1}))^T \\ &- P_{12}\tilde{A}_{22}^{-1}A_{21}K^{-1} - (P_{12}\tilde{A}_{22}^{-1}A_{21}K^{-1})^T < 0 \end{aligned} \tag{5.79}$$

Therefore if inequalities (5.79) and $P_{11} > 0$ have a feasible solution, then the eigenvalues of $\mathcal{A}_{11} - \mathcal{A}_{12}\mathcal{A}_{22}^{-1}\mathcal{A}_{21}$ have negative real parts by choice of L.

Inequality (5.79) can be added to inequalities (5.64) and (5.65) when designing the primary observer. (The requirement $P_{11} > 0$ is satisfied by inequality (5.65) being true). In forcing $\mathcal{A}_{11} - \mathcal{A}_{12}\mathcal{A}_{22}^{-1}\mathcal{A}_{21}$ to be stable, the LMI variables involved here are P_{11} and P_{12}, which are a subset of the variables in the convex optimisation problem in §4.4.

The design problem (incorporating the design method in §4.4) for the primary observer to make both $\mathcal{A}_{11}$ and $\mathcal{A}_{11} - \mathcal{A}_{12}\mathcal{A}_{22}^{-1}\mathcal{A}_{21}$ stable may therefore be summarised as :

Minimise $trace(X)$ with respect to the variables $P_{11}, P_{12}, P_{22}, X$ subject to inequalities (5.79), (5.64) and (5.65).

5.5.3 Forcing the eigenvalues of the sliding motion to lie in a circle

The eigenvalues of $(\mathcal{A}_{11} - \mathcal{A}_{12}\mathcal{A}_{22}^{-1}\mathcal{A}_{21})$ can be forced to lie in a circle centred at $(q_c, 0)$ with a radius r_c rather than just lie in the open LHP. If $q_c < 0$ and $|q_c| > r_c$, then the entire circle lies in the LHP.

Let λ_c represent an eigenvalue of JK^{-1}, and λ_c^* is its complex conjugate. The eigenvalues of KJ^{-1} will lie in the circle centred at $(q_c, 0)$ with a radius r_c if the following inequality is satisfied

$$\begin{bmatrix} -r_c & \frac{1}{\lambda_c} - q_c \\ \frac{1}{\lambda_c^*} - q_c & -r_c \end{bmatrix} < 0 \tag{5.80}$$

From the Schur complement, inequality (5.80) implies

$$\begin{aligned} & -r_c + \frac{1}{r_c}\left(\frac{1}{\lambda_c} - q_c\right)\left(\frac{1}{\lambda_c^*} - q_c\right) < 0 \\ \Rightarrow \quad & -r_c^2 + \frac{1}{\lambda_c\lambda_c^*} - \frac{q_c}{\lambda_c} - \frac{q_c}{\lambda_c^*} + q_c^2 < 0 \end{aligned} \tag{5.81}$$

It is clear that $\lambda_c\lambda_c^* > 0$. Multiplying (5.81) by $\lambda_c\lambda_c^*$ yields

$$(q_c^2 - r_c^2)\lambda_c\lambda_c^* - q_c\lambda_c - q_c\lambda_c^* + 1 < 0 \tag{5.82}$$

If the entire circle lies in the LHP, $q_c^2 - r_c^2 > 0$ and dividing (5.82) by $q_c^2 - r_c^2$ yields

$$(\lambda_c - \tilde{q}_c)(\lambda_c^* - \tilde{q}_c) - \tilde{r}_c^2 < 0 \tag{5.83}$$

where $\tilde{r}_c = \frac{r_c}{q_c^2 - r_c^2}$ and $\tilde{q}_c = \frac{q_c}{q_c^2 - r_c^2}$. Using the Schur complement, inequality (5.83) is equivalent to the inequality

$$\begin{bmatrix} -\tilde{r}_c & \lambda_c - \tilde{q}_c \\ \lambda_c^* - \tilde{q}_c & -\tilde{r}_c \end{bmatrix} < 0 \tag{5.84}$$

From [11], there is a one-to-one mapping $(1, \lambda_c, \lambda_c^*) \rightarrow (\tilde{P}, \tilde{P}JK^{-1}, (\tilde{P}JK^{-1})^T)$, and hence the eigenvalues of KJ^{-1}, which are also the eigenvalues of $\mathcal{A}_{11} - \mathcal{A}_{12}\mathcal{A}_{22}^{-1}\mathcal{A}_{21}$ can be forced to lie in the original circle if the inequality

$$\begin{bmatrix} -\tilde{r}_c\tilde{P} & \tilde{P}JK^{-1} - \tilde{q}_c\tilde{P} \\ (\tilde{P}JK^{-1})^T - \tilde{q}_c\tilde{P} & -\tilde{r}_c\tilde{P} \end{bmatrix} < 0 \tag{5.85}$$

is satisfied. As in §5.5.2, $\tilde{P}$ is chosen to be P_{11} and hence

$$\tilde{P}JK^{-1} = P_{11}K^{-1} - P_{12}\tilde{A}_{22}^{-1}A_{21}K^{-1}$$

which is affine in the LMI variables P_{11} and P_{12}.

Lemma 5.5 *For the method in this section, the reconstruction of the sensor fault will analytically be*

$$\hat{f}_o(t) = f_o(t) + G(s)\dot{f}_o(t)$$

where $G(s) = \mathcal{A}_{22}^{-1}\mathcal{A}_{21}(sI_{n-p} - (\mathcal{A}_{11} - \mathcal{A}_{12}\mathcal{A}_{22}^{-1}\mathcal{A}_{21}))^{-1}\mathcal{A}_{12}\mathcal{A}_{22}^{-1} - \mathcal{A}_{22}^{-1}$

Proof

If $\dot{f}_o(t)$ was not neglected in the analysis, then equation (5.58) will become

$$\begin{bmatrix} \dot{e}_1(t) \\ \dot{z}_4(t) \end{bmatrix} = \begin{bmatrix} \mathcal{A}_{11} & 0 \\ -A_{f,4}\mathcal{A}_{21} & -A_{f,4} \end{bmatrix} \begin{bmatrix} e_1(t) \\ z_4(t) \end{bmatrix} + \begin{bmatrix} \mathcal{A}_{12} \\ -A_{f,4}\mathcal{A}_{22} \end{bmatrix} f_o(t) + \begin{bmatrix} 0 \\ A_{f,4} \end{bmatrix} \dot{f}_o(t) \quad (5.86)$$

Applying the change of coordinates (5.60) to the system in (5.86), and assuming that the secondary sliding mode observer has been designed and sliding motion has been achieved, then the error system associated with the secondary observer (in the observer canonical coordinates of (5.12)) will be

$$\dot{e}_{1,c}(t) = (\mathcal{A}_{11} - \mathcal{A}_{12}\mathcal{A}_{22}^{-1}\mathcal{A}_{21})e_{1,c}(t) - \mathcal{A}_{12}\mathcal{A}_{22}^{-1}\dot{f}_o(t) \quad (5.87)$$

$$0 = -A_{f,4}\mathcal{A}_{21}e_{1,c} + A_{f,4}\mathcal{A}_{22}f_o(t) - A_{f,4}\dot{f}_o(t) + P_{o,c}^{-1}\nu_{eq,c} \quad (5.88)$$

where $e_{1,c}(t)$ is the vector that governs the sliding motion of the secondary observer.

From the definition of $\hat{f}_o(t)$ in (5.62), it is then easy to show from (5.88) that

$$\hat{f}_o(t) = f_o(t) - \mathcal{A}_{22}\dot{f}_o(t) - \mathcal{A}_{22}^{-1}\mathcal{A}_{21}e_{1,c} \quad (5.89)$$

and hence from combining (5.87) and (5.89),

$$\hat{f}_o(t) = f_o(t) + G(s)\dot{f}_o(t) \quad (5.90)$$

where

$$G(s) = \mathcal{A}_{22}^{-1}\mathcal{A}_{21}(sI_{n-p} - (\mathcal{A}_{11} - \mathcal{A}_{12}\mathcal{A}_{22}^{-1}\mathcal{A}_{21}))^{-1}\mathcal{A}_{12}\mathcal{A}_{22}^{-1} - \mathcal{A}_{22}^{-1} \quad (5.91)$$

as claimed. ■

Lemma 5.5 shows how the sensor fault reconstruction in this section is corrupted by the fault derivative, which had been neglected in the analysis. However, this is still an improvement to the method by Edwards *et al.* [27, 26]. From the Matrix Inversion Lemma,

$$(\mathcal{A}_{21}\mathcal{A}_{11}^{-1}\mathcal{A}_{12} - \mathcal{A}_{22})^{-1} = -\mathcal{A}_{22}^{-1} - \mathcal{A}_{22}^{-1}\mathcal{A}_{21}(\mathcal{A}_{11} - \mathcal{A}_{12}\mathcal{A}_{22}^{-1}\mathcal{A}_{21})^{-1}\mathcal{A}_{12}\mathcal{A}_{22}^{-1}$$

and hence the fault reconstruction by Edwards *et al.* [27] in (5.32) can be re-expressed as

$$\hat{f}_o(t) = f_o(t) + G_1 \dot{f}_o(t) + G_2 \dot{e}_1(t) \tag{5.92}$$

where

$$G_1 = -\mathcal{A}_{22}^{-1}\mathcal{A}_{21}(\mathcal{A}_{11} - \mathcal{A}_{12}\mathcal{A}_{22}^{-1}\mathcal{A}_{21})^{-1}\mathcal{A}_{12}\mathcal{A}_{22}^{-1} - \mathcal{A}_{22}^{-1} \tag{5.93}$$

$$G_2 = \mathcal{A}_{22}^{-1}\mathcal{A}_{21}(\mathcal{A}_{11} - \mathcal{A}_{12}\mathcal{A}_{22}^{-1}\mathcal{A}_{21})^{-1} \tag{5.94}$$

This can now be directly compared to the result in Lemma 5.5. In the method presented in this section, the reconstruction $\hat{f}_o(t)$ in (5.90) is not affected at all by $e_1(t)$. The other difference is the way the reconstructions are corrupted by $\dot{f}_o(t)$. It can be seen that G_1 in (5.93) is a steady-state version of $G(s)$ in (5.91). This shows that the reconstruction in (5.90) is corrupted partially by a filtered version of $\dot{f}_o(t)$ and partially by a scaled version of $\dot{f}_o(t)$, whereas the reconstruction in (5.92) is fully corrupted by a scaled version of $\dot{f}_o(t)$, making the corruption more severe.

5.5.4 Examples

In §5.4.4 a method was demonstrated for the unstable case assuming that not all sensors are faulty. If that assumption is not acceptable, then the sensor fault reconstruction method just described in §5.5 can be used, neglecting the dynamics of the fault.

Consider once again the helicopter system from §5.4.4. Note that $\det\ (A) \neq 0$ and so the method described in this section is appropriate.

By transforming the triple (A, M, C) from §5.4.4 to the coordinates of (5.7), the following can be extracted

$$A_{22} = \begin{bmatrix} -0.0000 & -0.0000 & 0.0792 & -0.0127 & 1.0001 & 0.0010 \\ 0.0000 & 0.0000 & 0.1336 & 0.9919 & -0.0006 & -0.0298 \\ -0.0000 & -0.0000 & -0.7244 & 0.0760 & -0.0199 & -0.0279 \\ 0.0000 & 0.0000 & -1.8671 & -10.9450 & 4.3139 & 0.2854 \\ 0.0000 & 0.0000 & 0.1526 & 1.0816 & -2.6711 & -0.0206 \\ 0.0001 & 0.0000 & 0.1074 & 0.5664 & -0.0174 & -0.3060 \end{bmatrix}$$

$$A_{21} = \begin{bmatrix} 0.0000 & 0.0000 \\ -0.0000 & -0.0000 \\ -0.0002 & -0.0114 \\ -0.1044 & -0.0960 \\ 0.0345 & -0.0019 \\ 0.0070 & -0.0102 \end{bmatrix}$$

which shows clearly that A_{22} is rank deficient. The first step is therefore to choose

$$L_1 = \begin{bmatrix} 1 & 1 & 1 & 1 & 1 & 1 \\ 1 & 1 & 1 & 1 & 1 & 1 \end{bmatrix}$$

so that $\tilde{A}_{22} = A_{22} - A_{21}L_1$ from (5.69) is full rank.

The primary observer was designed using the method in §5.5.2 and §5.5.3. The weighting matrices $W = 0.1I_8$ and $V = 0.1I_6$ were used. The spectrum of $\mathcal{A}_{11} - \mathcal{A}_{12}\mathcal{A}_{22}^{-1}\mathcal{A}_{21}$ was required to lie in a circle centred on $(0, -5)$ with a radius of 4.5.

Implementing the synthesis procedures in §5.5.2 yielded the eigenvalues of the sliding motion of the secondary observer

$$\lambda(\mathcal{A}_{11} - \mathcal{A}_{12}\mathcal{A}_{22}^{-1}\mathcal{A}_{21}) = -8.1326 \pm 3.2306i$$

which are stable, and lie in the required circle.

The secondary observer was designed using the LQG-like procedure in §4.4 where the weighting matrices $W_c = I_8$ and $V_c = I_6$ and the filter $A_{f,4} = 10I_6$.

All the observer matrices resulting from the synthesis are available in the disk attached to this thesis in *ch5/helicopter/lastmeth.mat*.

In the simulations that follow, $\rho = \rho_c = 50$, $\delta = 1 \times 10^{-3}$ and $\delta_c = 1 \times 10^{-4}$.

Figures 5.19 - 5.24 show the faults acting on the sensors and their reconstruction signals. Clearly the quality of the reconstruction is not as good as in §5.4.4. Some coupling exists between the reconstruction channels, in particular in Figure 5.23, where the reconstruction of a fault in the fifth sensor is affected by the derivative of a fault in the third sensor, and in Figure 5.24 where the reconstruction of a fault in the sixth sensor is affected by a fault in the second sensor. However, the faults are still reasonably well reconstructed. Importantly, this time, all sensors could be potentially faulty.

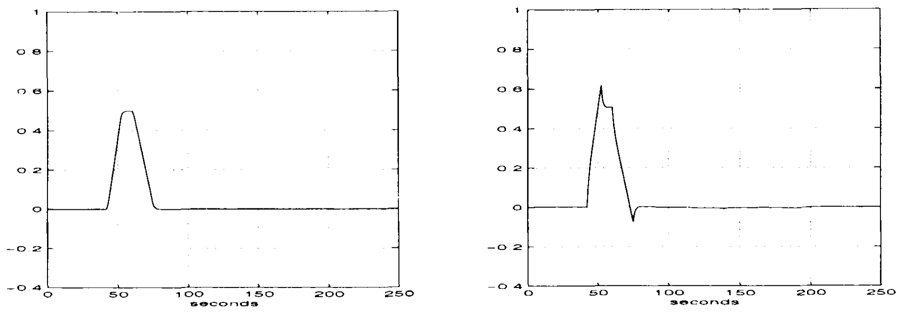

Figure 5.19: *The left subfigure shows a fault on the first sensor. The right subfigure shows its reconstruction using the secondary observer.*

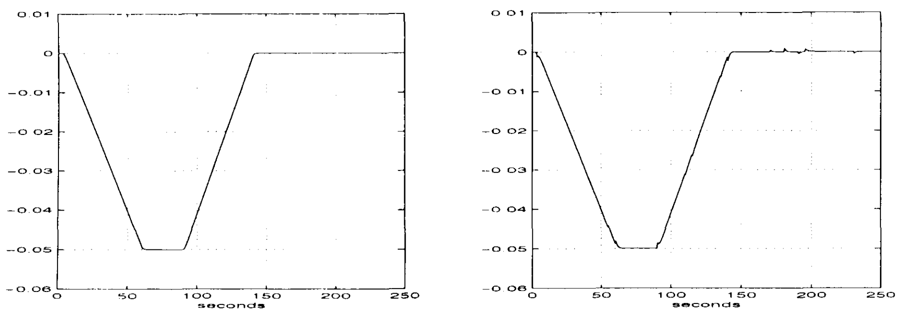

Figure 5.20: *The left subfigure shows a fault on the second sensor. The right subfigure shows its reconstruction using the secondary observer.*

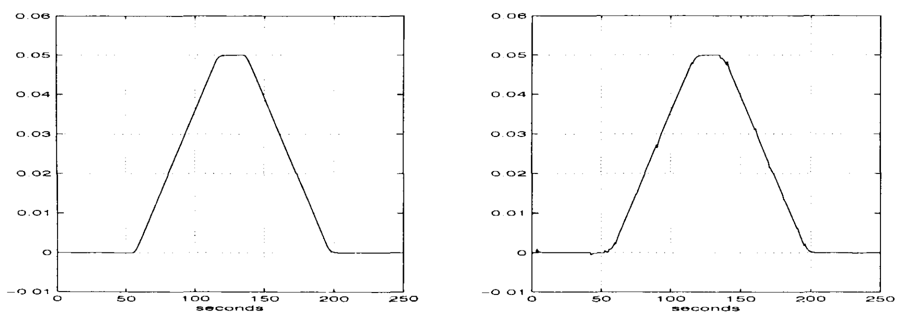

Figure 5.21: *The left subfigure shows a fault on the third sensor. The right subfigure shows its reconstruction using the secondary observer.*

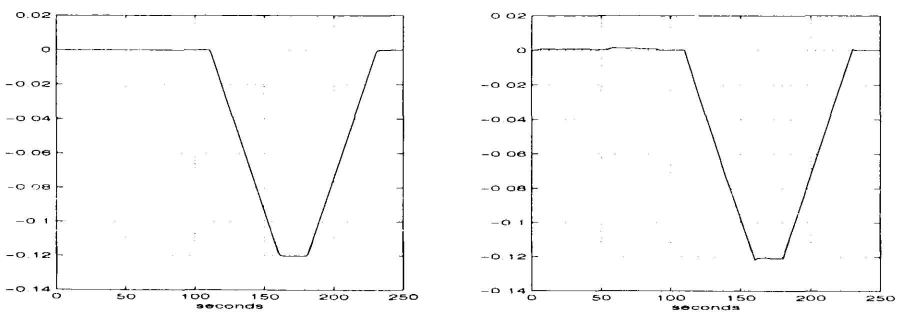

Figure 5.22: *The left subfigure shows a fault on the fourth sensor. The right subfigure shows its reconstruction using the secondary observer.*

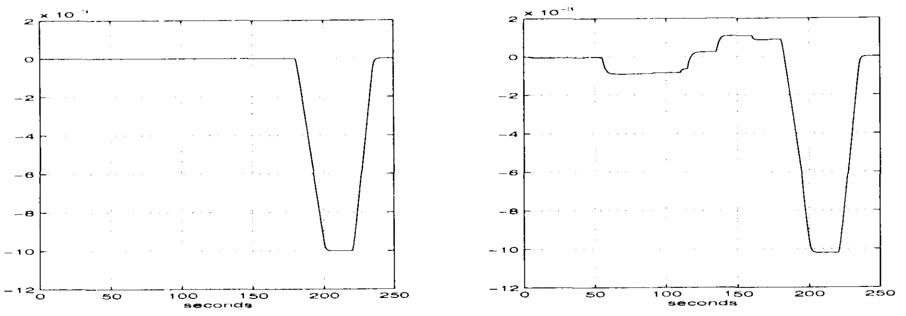

Figure 5.23: *The left subfigure shows a fault on the fifth sensor. The right subfigure shows its reconstruction using the secondary observer.*

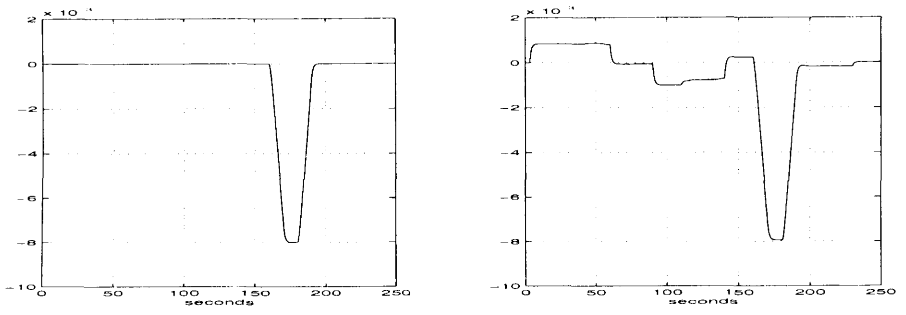

Figure 5.24: *The left subfigure shows a fault on the sixth sensor. The right subfigure shows its reconstruction using the secondary observer.*

5.6 Simulations with noise

In this chapter, all the simulations have been assumed to be noise free. This section seeks to show the effect of sensor noise on the fault reconstruction methods in this chapter. The simulations using the secondary observer method in §5.3.4 are repeated, this time with zero mean Gaussian noise on the sensors. The results are shown in the following figures.

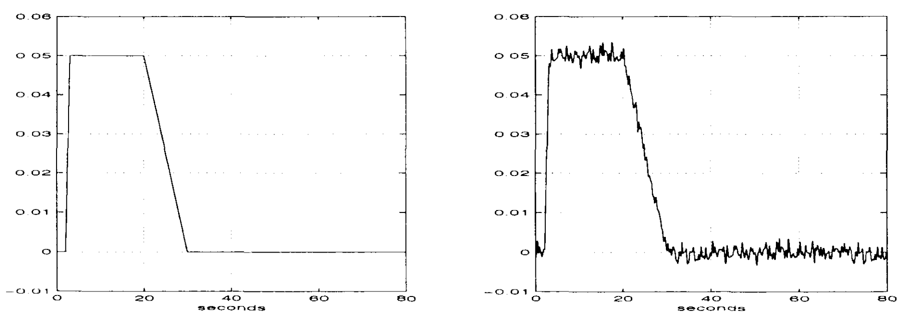

Figure 5.25: *The left subfigure shows a fault on the first sensor. The right subfigure shows its reconstruction using the secondary observer.*

Figures 5.25 and 5.26 show the fault reconstruction in the midst of sensor noise. It can be seen that the reconstructions have become noisy, but they portray the underlying shape of the

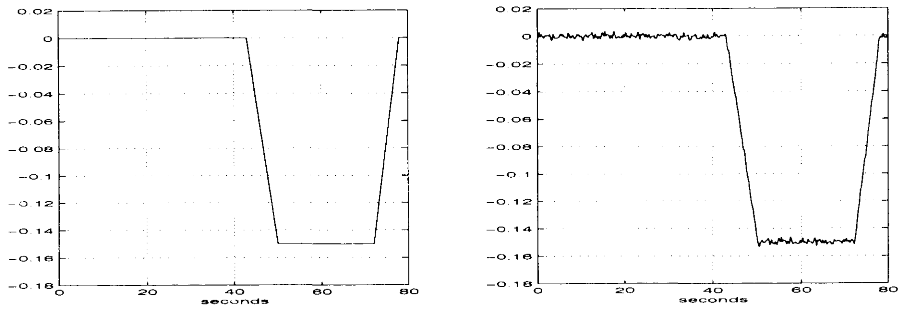

Figure 5.26: *The left subfigure shows the reconstruction of the fault on the second sensor. The right subfigure shows its reconstruction using the secondary observer.*

actual faults, which shows that the sliding mode observer can still reconstruct the faults in the presence of sensor noise. Similar results have been found for the other reconstruction methods.

5.7 Conclusion

This chapter has presented methods for sensor fault reconstruction improving on the work by Edwards *et al.* [27, 26]. In all the methods, certain signals were filtered, resulting in a fictitious system that treat sensor faults as actuator faults. Then the actuator fault reconstruction method by Edwards *et al.* [27, 26] was used to reconstruct the sensor fault. Firstly, in §5.3, two methods for perfect sensor fault reconstruction were presented, where the requirement was that the system was open loop stable. The existence conditions for the two methods are identical. In §5.4, another method for full sensor fault reconstruction was presented, seeking to relax the stability condition, with a compromise that certain sensors were assumed to be not faulty. Finally, in §5.5 another method was presented, that enabled sensor fault reconstruction for unstable systems even though all sensors are faulty, only requiring that the system matrix is full rank. The compromise is that this reconstruction does not capture the fault dynamics.

Chapter 6

Robust actuator and sensor fault reconstruction

6.1 Introduction

In the actuator fault reconstruction method by Edwards *et al.* [27, 25] (which was summarised in §5.2) and the sensor fault reconstruction methods in Chapter 5, there was no consideration of the robustness of the reconstruction methods; i.e. how well the observer reconstructs the faults in the presence of uncertainty/disturbances. In Chapter 2, the importance of robustness in FDI schemes was stated. In the literature, Hermans & Zarrop [52], Yang & Saif [125] and Sreedhar *et al.* [102] used various sliding mode observer formulations for robust FDI. In their methods, the observers were designed such that sliding motion occurs in the presence of uncertainty/disturbances. However, when a fault is present, the sliding motion will be broken, causing the output estimation error to deviate from zero, the nonzero residual indicating the presence of a fault. Xiong & Saif [122] designed the sliding mode observer using an unknown input observer approach such that the uncertainty is considered the unknown input, and the observer error system is robust to it. There was no robustness consideration in the work of Yeu & Kawaji [128].

This chapter presents a method to design the Edwards & Spurgeon observer [23], so that for a system subject to actuator faults, the upper bound on the $\mathcal{L}_2$ gain from the uncertainty/disturbances to the fault reconstruction is minimised. The design method is formulated as an LMI problem, and the minimisation is achieved by using standard LMI routines. Then the method is extended to the case of sensor faults by using the filtering ideas in Chapter 5. All these methods are based on the assumption that sliding motion still takes place in the presence of uncertainty and actuator faults.

The effectiveness of the design methods in this chapter will be demonstrated by two examples;

a VTOL aircraft, and a nonlinear model of a gantry crane.

6.2 A sliding mode observer for a system subject to actuator faults and uncertainty/disturbances

Consider a system that is subject to an actuator fault and also uncertainty/disturbances

$$\dot{x}(t) = Ax(t) + Bu(t) + Mf_i(t) + Q\xi(t,x,u) \tag{6.1}$$

$$y(t) = Cx(t) \tag{6.2}$$

where $A \in \mathcal{R}^{n\times n}, B \in \mathcal{R}^{n\times m}, C \in \mathcal{R}^{p\times n}$, $M \in \mathcal{R}^{n\times q}$ and $Q \in \mathcal{R}^{n\times k}$ where $n > p \geq q$. Assume that the matrices C and M are full rank and the function $f_i : \mathcal{R}_+ \times \mathcal{R}_m \to \mathcal{R}^q$ is unknown but bounded so that

$$||f_i(t)|| \leq \alpha(t,y,u) \tag{6.3}$$

where $\alpha : \mathcal{R}_+ \times \mathcal{R}^m \to \mathcal{R}_+$ is a known function. The signal $\xi : \mathcal{R}_+ \times \mathcal{R}^p \times \mathcal{R}^m \to \mathcal{R}^k$ encapsulates the uncertainty present in the system. It is assumed to be unknown but bounded subject to $||\xi(t,x,u)|| < \beta(t,y,u)$ where the function β is known.

From §3.5, an Edwards - Spurgeon observer [23, 25] for the system (6.1) - (6.2) is

$$\dot{\hat{x}}(t) = A\hat{x}(t) + Bu(t) - G_l e_y(t) + G_n\nu \tag{6.4}$$

$$\hat{y}(t) = C\hat{x}(t) \tag{6.5}$$

where

$$\nu = -\rho(t,y,u)\frac{e_y}{||e_y||}, \quad e_y \neq 0 \tag{6.6}$$

and $e_y(t) := \hat{y}(t) - y(t)$ is the output estimation error.

Defining $e(t) := \hat{x}(t) - x(t)$ as the state estimation error, then from (6.1) - (6.2) and (6.4) - (6.5) the following error system can be obtained

$$\dot{e}(t) = (A - G_lC)e(t) + G_n\nu - Mf_i(t) - Q\xi(t,x,u) \tag{6.7}$$

Assume as in §3.5 that the following conditions have been satisfied

A1 CM has full column rank

A2 all invariant zeros of (A,M,C) (if any) are stable then there exists a change of coordinates such that the triple (A, M, C) can be written in the form

$$A = \left[\begin{array}{c|c} A_{11} & A_{12} \\ \hline A_{211} & \\ & A_{22} \\ A_{212} & \end{array}\right], \quad M = \begin{bmatrix} 0 \\ M_o \end{bmatrix}, \quad C = \begin{bmatrix} 0 & T \end{bmatrix} \tag{6.8}$$

where $M_o \in \mathcal{R}^{q\times q}$ is nonsingular and $T \in \mathcal{R}^{p\times p}$ is orthogonal. The pair $A_{11} \in \mathcal{R}^{(n-p)\times(n-p)}$ and $A_{211} \in \mathcal{R}^{(p-q)\times(n-p)}$ is detectable. As in §3.5.1 the unobservable modes of (A_{11}, A_{211}) represent the invariant zeros of (A, M, C). Define $M_2 \in \mathcal{R}^{p\times q}$ as the bottom p rows of M, which therefore includes the matrix M_o.

In this coordinate system, the nonlinear gain G_n has the structure

$$G_n = \begin{bmatrix} -LT^T \\ T^T \end{bmatrix} P_o^{-1} \tag{6.9}$$

where $P_o \in \mathcal{R}^{p\times p}$ is symmetric positive definite and

$$L = \begin{bmatrix} L^o & 0 \end{bmatrix} \tag{6.10}$$

with $L^o \in \mathcal{R}^{(n-p)\times(p-q)}$. The disturbance distribution matrix has the general structure

$$Q = \begin{bmatrix} Q_1 \\ Q_2 \end{bmatrix} \tag{6.11}$$

where $Q_1 \in \mathcal{R}^{(n-p)\times k}$.

Suppose there exists a symmetric positive definite matrix $P \in \mathcal{R}^{n\times n}$ of the structure

$$P = \begin{bmatrix} P_1 & P_1 L \\ L^T P_1 & T^T P_o T + L^T P_1 L \end{bmatrix} > 0 \tag{6.12}$$

where $P_1 \in \mathcal{R}^{(n-p)\times(n-p)}$ and $P(A - G_l C) + (A - G_l C)^T P < 0$. Define two positive scalars

$$\mu_0 = -\lambda_{max}(P(A - G_l C) + (A - G_l C)^T P), \quad \mu_1 = ||PQ||$$

then the following is true :

Proposition 6.1 *If the positive scalar gain function $\rho(t, y, u)$ in (6.6) satisfies*

$$\rho(t, y, u) \geq ||P_o CM||\alpha(t, y, u) + \eta_o \tag{6.13}$$

where η_o is a small positive scalar, then the state estimation error $e(t)$ in (6.7) is ultimately bounded with respect to the set

$$\Omega_\epsilon = \{e : ||e|| < 2\mu_1\beta/\mu_0 + \epsilon\}$$

where $\epsilon > 0$ is an arbitrarily small positive scalar.

Proof

This proof is adapted from [62]. Define a Lyapunov function $\mathcal{V}(e) = e^T P e$. The derivative along the estimation error state trajectory is :

$$\begin{aligned} \dot{\mathcal{V}} &= e^T(P(A - G_l C) + (A - G_l C)^T P)e - 2e^T PMf_i - 2e^T PQ\xi + 2e^T PG_n\nu \quad (6.14) \\ &\leq -\mu_0 ||e||^2 + 2||e||\mu_1\beta - 2e^T PMf_i + 2e^T PG_n\nu \quad (6.15) \end{aligned}$$

where Rayleigh's inequality has been applied to the first term of (6.14) and the Cauchy-Schwartz inequality has been applied to the third term. From (6.8), (6.12) and (6.9), it can be established that $PM = C^T P_o CM$ and $PG_n = C^T$. Hence (6.15) can be written

$$\begin{aligned} \dot{\mathcal{V}} &\leq -\mu_0||e||^2 + 2||e||\mu_1\beta - 2e^T C^T P_o CMf_i + 2e^T C^T\nu \\ &= -\mu_0||e||^2 + 2||e||\mu_1\beta - 2e_y^T P_o CMf_i + 2e_y^T\nu \end{aligned}$$

From the Cauchy - Schwartz inequality, and the bound on $\rho(t, y, u)$ from (6.13),

$$\begin{aligned} \dot{\mathcal{V}} &\leq -\mu_0||e||^2 + 2||e||\mu_1\beta - 2||e_y||(\rho - ||P_o CM||\alpha) \\ &\leq ||e||(-\mu_0||e|| + 2\mu_1\beta) \quad (6.16) \end{aligned}$$

which proves that the magnitude of $e(t)$ decreases when $||e|| > 2\mu_1\beta/\mu_0$. This implies that in finite time the magnitude of $e(t)$ will be bounded with respect to Ω_ϵ. ■

Proposition 6.1 will now be used to prove the main result of this section, that for an appropriate choice of $\rho(t, y, u)$, sliding motion can be induced on the surface $\mathcal{S} = \{e : Ce = 0\}$.

It is convenient to firstly introduce a new change of coordinates

$$T_L = \begin{bmatrix} I_{n-p} & L \\ 0 & T \end{bmatrix} \quad (6.17)$$

Applying the change of coordinates induced by T_L to the triple in (6.8) yields

$$\mathcal{A} = \begin{bmatrix} \mathcal{A}_{11} & \mathcal{A}_{12} \\ \mathcal{A}_{21} & \mathcal{A}_{22} \end{bmatrix}, \quad \mathcal{M} = \begin{bmatrix} 0 \\ \mathcal{M}_2 \end{bmatrix}, \quad \mathcal{C} = \begin{bmatrix} 0 & I_p \end{bmatrix} \quad (6.18)$$

where $\mathcal{A}_{11} = A_{11} + L^o A_{211}$ and $\mathcal{M}_2 \in \mathcal{R}^{p\times q}$. Since (A_{11}, A_{211}) is detectable, L^o can be chosen so that $\mathcal{A}_{11}$ is stable.

In this coordinate system, the nonlinear gain from (6.9) will have the structure

$$\mathcal{G}_n = \begin{bmatrix} 0 \\ P_o^{-1} \end{bmatrix} \quad (6.19)$$

and the Lyapunov matrix P from (6.12) will have the block diagonal structure

$$\mathcal{P} = \begin{bmatrix} P_1 & 0 \\ 0 & P_o \end{bmatrix} \tag{6.20}$$

The uncertainty/disturbance distribution matrix will have the structure

$$\mathcal{Q} = \begin{bmatrix} \mathcal{Q}_1 \\ \mathcal{Q}_2 \end{bmatrix} = \begin{bmatrix} Q_1 + LQ_2 \\ TQ_2 \end{bmatrix} \tag{6.21}$$

The state estimation error in the new coordinate system is

$$\dot{e}_L(t) = \mathcal{A}_o e_L(t) + \mathcal{G}_n \nu - \mathcal{M} f_i(t) - \mathcal{Q}\xi(t, x, u) \tag{6.22}$$

where $\mathcal{A}_o = \mathcal{A} - \mathcal{G}_l \mathcal{C}$. Partitioning the state estimation error conformably with (6.18) yields

$$\dot{e}_1(t) = \mathcal{A}_{11} e_1(t) + (\mathcal{A}_{12} - \mathcal{G}_{l,1}) e_y(t) - \mathcal{Q}_1 \xi(t, x, u) \tag{6.23}$$

$$\dot{e}_y(t) = \mathcal{A}_{21} e_1(t) + (\mathcal{A}_{22} - \mathcal{G}_{l,2}) e_y(t) + P_o^{-1}\nu - \mathcal{M}_2 f_i(t) - \mathcal{Q}_2 \xi(t, x, u) \tag{6.24}$$

where $\mathcal{G}_{l,1}$ and $\mathcal{G}_{l,2}$ represent appropriate partitions of $\mathcal{G}_l$.

Proposition 6.2 *If the gain function $\rho(.)$ from (6.6) satisfies*

$$\rho(t, y, u) \geq 2\|P_o \mathcal{A}_{21}\| \mu_1 \beta / \mu_0 + \|P_o \mathcal{Q}_2\| \beta + \|P_o \mathcal{M}_2\| \alpha + \eta_o \tag{6.25}$$

where η_o is a positive scalar, then an ideal sliding motion takes place on $\mathcal{S} = \{e : Ce = 0\}$ in finite time.

Proof

Consider a Lyapunov function $\mathcal{V}_s(e_y) = e_y^T P_o e_y$. The derivative along the trajectory is

$$\dot{\mathcal{V}}_s = e_y^T (P_o(\mathcal{A}_{22} - \mathcal{G}_{l,2}) + (\mathcal{A}_{22} - \mathcal{G}_{l,2})^T P_o) e_y + 2 e_y^T P_o (\mathcal{A}_{21} e_1 - \mathcal{M}_2 f_i - \mathcal{Q}_2 \xi + P_o^{-1}\nu)$$

The term $P_o(\mathcal{A}_{22} - \mathcal{G}_{l,2}) + (\mathcal{A}_{22} - \mathcal{G}_{l,2})^T P_o < 0$ because $\mathcal{P}$ from (6.20) is a block diagonal Lyapunov matrix for $(\mathcal{A} - \mathcal{G}_l \mathcal{C})$. Therefore it follows :

$$\begin{aligned} \dot{\mathcal{V}}_s &\leq 2 e_y^T P_o (\mathcal{A}_{21} e_1 - \mathcal{M}_2 f_i - \mathcal{Q}_2 \xi) - 2\rho \|e_y\| \\ &\leq -2\|e_y\| (\rho - \|P_o \mathcal{A}_{21}\| \|e_1\| - \|P_o \mathcal{M}_2\| \alpha - \|P_o \mathcal{Q}_2\| \beta) \end{aligned}$$

From Lemma 6.1, in finite time $e(t) \in \Omega_\epsilon$ which implies $\|e_1\| < 2\mu_1\beta/\mu_0 + \epsilon$. Therefore from the definition of $\rho(t, y, u)$ in (6.25), and using the inequality (4.25), it follows that

$$\dot{\mathcal{V}}_s \leq -2\eta_o \|e_y\| \leq -2\eta_o \eta \sqrt{\mathcal{V}_s} \tag{6.26}$$

where $\eta := \sqrt{\lambda_{min}(P_o^{-1})}$. Using the proof of Corollary 4.1, this proves that the output estimation error $e_y(t)$ will reach zero in finite time, and sliding motion takes place. ■

Remark : Since $\mathcal{M}_2 = CM$, it follows that the definition of $\rho(t, y, u)$ in (6.25) is consistent with the assumption on its size in equation (6.13).

6.3 Robust reconstruction of actuator faults

In this section the sliding mode observer described in (6.4) - (6.6) will be analysed with regard to its ability to robustly reconstruct the fault $f_i(t)$ despite the presence of the uncertainty $\xi(t, x, u)$. The analysis will be performed with the condition that $p > q$. In the case when $p = q$ the sliding motion is completely determined by the invariant zeros of (A, M, C) [23]. The situation when $p > q$ allows some design freedom which can be appropriately exploited. The physical implication of this is that there are more outputs than faults.

Assume that the sliding mode observer described in (6.4) - (6.6) has been designed, and that sliding motion has been achieved, then the output estimation error $e_y(t) = \dot{e}_y(t) = 0$ and equations (6.23) and (6.24) will become

$$\dot{e}_1(t) = \mathcal{A}_{11}e_1(t) - \mathcal{Q}_1\xi(t, x, u) \tag{6.27}$$

$$0 = \mathcal{A}_{21}e_1(t) + P_o^{-1}\nu_{eq} - \mathcal{M}_2 f_i(t) - \mathcal{Q}_2\xi(t, x, u) \tag{6.28}$$

where ν_{eq} is the equivalent output error injection required to maintain sliding motion. It can be calculated by approximating ν in (6.6) as

$$\nu_\delta = -\rho(t, y, u)\frac{e_y}{||e_y|| + \delta} \tag{6.29}$$

where δ is a small positive scalar. In equations (6.27) and (6.28), the vector $\xi(t, x, u)$ will be treated as an unknown exogenous signal. Of course when $\xi(t, x, u) = 0$, this signal has no effect on (6.27) and (6.28).

In the case when $\xi(t, x, u) \neq 0$, the attempted reconstruction of $f_i(t)$ will be corrupted by the exogenous signal $\xi(t, x, u)$. The objective here is to choose a scaling of the equivalent output error injection signal ν_{eq} and the gain L, to minimise the effect of the exogeneous signal on the fault reconstruction. To this end define

$$W_{sc} := \begin{bmatrix} W_1 & M_o^{-1} \end{bmatrix} \tag{6.30}$$

where $W_1 \in \mathcal{R}^{q\times(p-q)}$ and represents design freedom and M_o is given in (6.8). Define a would-be reconstruction signal for $f_i(t)$

$$\hat{f}_i := W_{sc}T^T P_o^{-1}\nu_{eq} \tag{6.31}$$

Rewriting equations (6.27) and (6.28) in terms of the coordinates in (6.8), and re-arranging yields

$$\begin{aligned} \dot{e}_1(t) &= (A_{11}+LA_{21})e_1(t) - (Q_1+LQ_2)\xi(t,x,u) && (6.32)\\ P_o^{-1}\nu_{eq} &= -TA_{21}e_1(t) + TM_2 f_i(t) + TQ_2\xi(t,x,u) && (6.33) \end{aligned}$$

where

$$A_{21} = \begin{bmatrix} A_{211} \\ A_{212} \end{bmatrix}$$

Pre-multiplying (6.33) by $W_{sc}T^T$ implies

$$\hat{f}_i(t) = -W_{sc}A_{21}e_1(t) + f_i(t) + W_{sc}Q_2\xi(t,x,u) \tag{6.34}$$

or in other words $\hat{f}_i(t) = f_i(t) + \hat{G}(s)\xi(t,x,u)$ where the transfer function matrix

$$\hat{G}(s) = W_{sc}A_{21}(sI_{n-p} - (A_{11}+LA_{21}))^{-1}(Q_1+LQ_2) + W_{sc}Q_2 \tag{6.35}$$

The objective now is to minimise the effect of $\xi(t,x,u)$ on the reconstruction $\hat{f}_i(t)$. Using the Bounded Real Lemma [11, 39], the $\mathcal{L}_2$ gain of the transfer function $\hat{G}(s)$ from the exogenous signal $\xi(t,x,u)$ to $\hat{f}_i(t)$ will not exceed γ if the following inequality holds

$$\begin{bmatrix} \hat{P}(A_{11}+LA_{21}) + (A_{11}+LA_{21})^T\hat{P} & -\hat{P}(Q_1+LQ_2) & -(W_{sc}A_{21})^T \\ -(Q_1+LQ_2)^T\hat{P} & -\gamma I_k & (W_{sc}Q_2)^T \\ -W_{sc}A_{21} & W_{sc}Q_2 & -\gamma I_q \end{bmatrix} < 0 \tag{6.36}$$

where γ is a positive scalar and $\hat{P} \in \mathcal{R}^{(n-p)\times(n-p)}$ is symmetric positive definite. The objective is therefore to find $\hat{P}, L$ and W_{sc} to minimise γ subject to the inequality (6.36) and $\hat{P} > 0$. However this must be done in conjunction with satisfying the requirements of obtaining a suitable sliding mode observer as expressed in Proposition 6.2.

Writing P from (6.12) as

$$P = \begin{bmatrix} P_{11} & P_{12} \\ P_{12}^T & P_{22} \end{bmatrix} > 0 \tag{6.37}$$

where $P_{11} \in \mathcal{R}^{(n-p)\times(n-p)}$, $P_{22} \in \mathcal{R}^{p\times p}$ and $P_{12} := \begin{bmatrix} P_{121} & 0 \end{bmatrix}$ with $P_{121} \in \mathcal{R}^{(n-p)\times(p-q)}$, it follows there is a one-to-one correspondence between the variables $(P_{11}, P_{121}, P_{22})$ and (P_1, L^o, P_o) since

$$P_1 = P_{11} \tag{6.38}$$

$$L^o = P_{11}^{-1} P_{121} \tag{6.39}$$

$$P_o = T(P_{22} - P_{12}^T P_{11}^{-1} P_{12})T^T \tag{6.40}$$

Choosing $\hat{P} = P_{11}$ and using the switch of variables in (6.39), inequality (6.36) can be re-written as

$$\begin{bmatrix} P_{11}A_{11} + A_{11}^T P_{11} + P_{12}A_{21} + A_{21}^T P_{12}^T & -(P_{11}Q_1 + P_{12}Q_2) & -(W_{sc}A_{21})^T \\ -(P_{11}Q_1 + P_{12}Q_2)^T & -\gamma I_k & (W_{sc}Q_2)^T \\ -W_{sc}A_{21} & W_{sc}Q_2 & -\gamma I_q \end{bmatrix} < 0 \tag{6.41}$$

Note this is affine with respect to the variables P_{11}, P_{12}, W_1 and γ.

Remark :

- For square systems (when $p = q$), it can be seen that L^o from (6.10) and W_1 from (6.30) do not exist. Hence there is no freedom associated with the design of the sliding motion and the scaling of the equivalent output error injection ν_{eq}.

- In the case when the matrices M and Q are matched to each other, i.e. $Q = MX$ for some $X \in \mathcal{R}^{q\times k}$, then successful decoupling between the fault $f_i(t)$ and disturbance $\xi(t, x, u)$ on the reconstruction $\hat{f}_i(t)$ cannot be attained. The transfer function matrix $\hat{G}(s)$ from (6.35) would become $\hat{G}(s) = X$, and the reconstruction signal would be $\hat{f}_i(t) = f_i(t) + X\xi(t, x, u)$.

6.4 Designing the sliding mode observer

This section will present a method to design the sliding mode observer's linear gain G_l to 'induce' the inequality (6.41). Specifically in this section it is proposed that the linear gain G_l be chosen to satisfy

$$\begin{bmatrix} P(A - G_lC) + (A - G_lC)^T P & P(G_lD_d - B_d) & E^T \\ (G_lD_d - B_d)^T P & -\gamma_o I_{p+k} & H^T \\ E & H & -\gamma_o I_q \end{bmatrix} < 0 \tag{6.42}$$

where P has the structure given in (6.12). The matrices $B_d \in \mathcal{R}^{n\times(p+k)}$, $D_d \in \mathcal{R}^{p\times(p+k)}$, $H \in \mathcal{R}^{q\times(p+k)}$ and $E \in \mathcal{R}^{q\times n}$ are effectively design matrices and their formal interpretations will be given below. The matrix B_d will depend on the structure of the uncertainty, whilst D_d will be an a-priori user defined constant matrix used to tune the performance of the observer. The matrices E and H will depend on the LMI variable W_1 from (6.30), whilst the term γ_o represents a strictly positive scalar.

If a feasible solution to the LMIs (6.37) and (6.42) exists then the requirements of Proposition 6.2 will be fulfilled (since (6.42) implies $P(A-G_lC)+(A-G_lC)^TP < 0$) and hence the choice of G_l, the gain matrix L from (6.39) which follows once P is specified, and G_n from (6.9) and P_o from (6.40) constitute a sliding mode observer design.

In this section the following assumptions will be made on the nonsystem elements in (6.42). Specifically assume :

- The matrix

$$B_d = \begin{bmatrix} 0 & Q \end{bmatrix} \tag{6.43}$$

  where Q is the uncertainty distribution matrix defined in (6.1).

- The matrix

$$D_d = \begin{bmatrix} D_1 & 0 \end{bmatrix} \tag{6.44}$$

  where $D_1 \in \mathcal{R}^{p\times p}$ is nonsingular. This is regarded as a user design parameter to tune the performance of the linear part of the observer.

- The matrix

$$H = \begin{bmatrix} 0 & H_2 \end{bmatrix} \tag{6.45}$$

  where $H_2 \in \mathcal{R}^{q\times k}$ which itself will be chosen to depend on W_1.

Proposition 6.3 *Under assumptions (6.43) - (6.45), inequality (6.42) is feasible if and only if*

$$\begin{bmatrix} PA+A^TP-\gamma_o C^T(D_dD_d^T)^{-1}C & -PB_d & E^T \\ -B_d^TP & -\gamma_o I_{p+k} & H^T \\ E & H & -\gamma_o I_q \end{bmatrix} < 0 \tag{6.46}$$

in which case

$$G_l = \gamma_o P^{-1}C^T(D_dD_d^T)^{-1} \tag{6.47}$$

is an appropriate choice of G_l in (6.42).

Proof

Defining $Y := PG_l$, inequality (6.42) can be re-written as

$$\begin{bmatrix} PA + A^T P - YC - (YC)^T & E^T & YD_d - PB_d \\ E & -\gamma_o I_q & H \\ (YD_d - PB_d)^T & H^T & -\gamma_o I_{p+k} \end{bmatrix} < 0 \tag{6.48}$$

Taking the Schur complement implies that, for $\gamma_o > 0$, inequality (6.48) is equivalent to

$$\begin{bmatrix} PA + A^T P - YC - (YC)^T + \frac{1}{\gamma_o} Y_d Y_d^T & E^T + \frac{1}{\gamma_o} Y_d H^T \\ E + \frac{1}{\gamma_o} H Y_d^T & -\gamma_o I_q + \frac{1}{\gamma_o} H H^T \end{bmatrix} < 0 \tag{6.49}$$

where $Y_d = YD_d - PB_d$.

From the assumptions on the structure of D_d and H in (6.44) and (6.45), $D_d H^T = 0$ and hence (6.49) simplifies to become

$$\begin{bmatrix} PA + A^T P - YC - (YC)^T + \frac{1}{\gamma_o} Y_d Y_d^T & E^T - \frac{1}{\gamma_o} PB_d H^T \\ E - \frac{1}{\gamma_o} H B_d^T P & -\gamma_o I_q + \frac{1}{\gamma_o} H H^T \end{bmatrix} < 0 \tag{6.50}$$

From the assumptions on the structure of D_d and B_d in (6.44) and (6.43), $D_d B_d^T = 0$, and the term

$$\frac{1}{\gamma_o} Y_d Y_d^T = \frac{1}{\gamma_o} Y D_d D_d^T Y^T + \frac{1}{\gamma_o} P B_d B_d^T P$$

A 'completing the square' argument yields :

$$-YC - (YC)^T + \frac{1}{\gamma_o} Y_d Y_d^T = -\gamma_o C^T (D_d D_d^T)^{-1} C + \frac{1}{\gamma_o} P B_d B_d^T P + \triangle_Y$$

where

$$\triangle_Y := \frac{1}{\gamma_o} (Y D_d D_d^T - \gamma_o C^T)(D_d D_d^T)^{-1} (Y D_d D_d^T - \gamma_o C^T)^T \tag{6.51}$$

Thus inequality (6.50) is equivalent to

$$\begin{bmatrix} PA + A^T P - \gamma_o C^T (D_d D_d^T)^{-1} C + \frac{1}{\gamma_o} P B_d B_d^T P + \triangle_Y & E^T - \frac{1}{\gamma_o} PB_d H^T \\ E - \frac{1}{\gamma_o} H B_d^T P & -\gamma_o I_q + \frac{1}{\gamma_o} H H^T \end{bmatrix} < 0 \tag{6.52}$$

A necessary and sufficient condition for (6.52) to hold is that

$$\begin{bmatrix} PA + A^T P - \gamma_o C^T (D_d D_d^T)^{-1} C + \frac{1}{\gamma_o} P B_d B_d^T P & E^T - \frac{1}{\gamma_o} PB_d H^T \\ E - \frac{1}{\gamma_o} H B_d^T P & -\gamma_o I_q + \frac{1}{\gamma_o} H H^T \end{bmatrix} < 0 \tag{6.53}$$

(the sufficiency follows from the choice $Y = \gamma_o C^T (D_d D_d^T)^{-1}$ which makes $\triangle_Y$ from (6.51) identically zero).

Using the Schur complement once again, a necessary and sufficient condition for inequality (6.53) to hold is for the following inequality to hold

$$\begin{bmatrix} PA + A^TP - \gamma_o C^T(D_dD_d^T)^{-1}C & -PB_d & E^T \\ -B_d^TP & -\gamma_o I_{p+k} & H^T \\ E & H & -\gamma_o I_q \end{bmatrix} < 0 \tag{6.54}$$

For the choice of Y, it follows that the linear gain $G_l = \gamma_o P^{-1}C^T(D_dD_d^T)^{-1}$ and the claim is proven. ■

The idea is now to relate inequality (6.46) to the inequality associated with the corruption of the fault estimation signal in (6.41). Defining

$$PA + A^TP = \begin{bmatrix} X_{11} & X_{12} \\ X_{12}^T & X_{22} \end{bmatrix}$$

where $X_{11} \in \mathcal{R}^{(n-p)\times(n-p)}$, inequality (6.46) can be written as

$$\begin{bmatrix} X_{11} & X_{12} & 0 & -(P_{11}Q_1 + P_{12}Q_2) & E_1^T \\ X_{12}^T & X_{22} - \gamma_o T^T(D_1D_1^T)^{-1}T & 0 & -(P_{12}^TQ_1 + P_{22}Q_2) & E_2^T \\ 0 & 0 & -\gamma_o I_p & 0 & 0 \\ -(P_{11}Q_1 + P_{12}Q_2)^T & -(P_{12}^TQ_1 + P_{22}Q_2)^T & 0 & -\gamma_o I_k & H_2^T \\ E_1 & E_2 & 0 & H_2 & -\gamma_o I_q \end{bmatrix} < 0$$

A necessary condition for the inequality above to hold is that

$$\begin{bmatrix} X_{11} & -(P_{11}Q_1 + P_{12}Q_2) & E_1^T \\ -(P_{11}Q_1 + P_{12}Q_2)^T & -\gamma_o I_k & H_2^T \\ E_1 & H_2 & -\gamma_o I_q \end{bmatrix} < 0 \tag{6.55}$$

Choosing $E_1 = -W_{sc}A_{21}$ and $H_2 = W_{sc}Q_2$ will yield the same inequality as (6.41).

The design method can now be summarised to be :

Minimise γ with respect to the variables $P_{11}, P_{12}, P_{22}, W_1$ and γ subject to inequalities (6.46), (6.41) and (6.37), where γ_o is an a-priori user-defined positive scalar.

Remark : Let γ_{min} be the minimum value of γ that satisfies (6.41), then, since (6.41) is a 'sub-block' of (6.46), $\gamma_{min} \leq \gamma_o$ always holds.

Standard LMI software, such as [39] can be used to synthesise numerically γ, P and W_1. Once P has been determined L^o (and hence L) can be determined from (6.10). The gain G_l can be determined from (6.47), G_n from (6.9), and P_o from (6.40).

For a given B_d, D_d, E and H, inequality (6.42) can be viewed as resulting from an $\mathcal{H}_\infty$ filtering problem (page 462 of Zhou *et al.* [130]), the idea being to minimise the effect of ξ on $\triangle_z$ (see Figure 6.1). However, in this chapter, E and H are regarded as design variables (which in particular depend on W_{sc} from (6.30)) and help determine a value for L from (6.10) which defines the optimal choice of sliding mode for fault reconstruction purposes. Once a sliding mode is established the choice of the linear gain G_l is technically not relevant since the linear output error injection term $G_l e_y$ disappears because $e_y \equiv 0$.

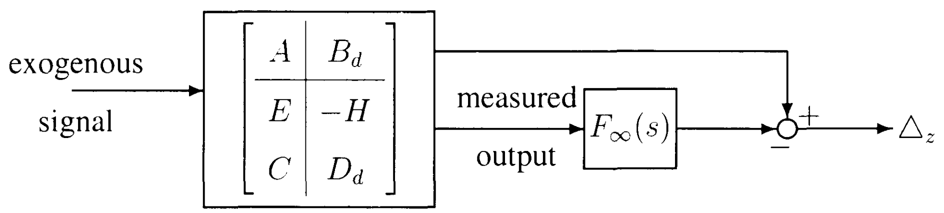

Figure 6.1: The $\mathcal{H}_\infty$ filtering problem (notation taken from [130])

Remark : In the robust fault reconstruction scheme that has been presented, the disturbance distribution matrix Q is essential to the design, otherwise there is no basis for the robustness optimisation. Therefore, in a real system, the nonlinearities (unmodelled dynamics, parametric uncertainty, external disturbances *etc.*) will need to be expressed as $Q\xi(t, x, u)$. It has been shown in Chapter 5 of [5] how this may be done. If the nonlinearities can be expressed as $Q\xi(t, x, u)$, then the robust fault reconstruction design can be implemented.

6.5 Robust reconstruction of sensor faults

In this section, the actuator fault reconstruction method in §6.3 will be modified to enable robust sensor fault reconstruction in the presence of uncertainty. The work in this section builds on the sensor fault reconstruction work in Chapter 5. In §6.2, a prerequisite for the analysis was that there are more outputs than faults. Hence, only the methods in §5.4 (which assume that some sensors are not potentially faulty) can be used in this section.

A system subject to sensor faults and disturbance can be modelled as

$$\dot{x}(t) = Ax(t) + Bu(t) + Q\xi(t, x, u) \qquad (6.56)$$

$$y(t) = Cx(t) + Ff_o(t) \qquad (6.57)$$

where $f_o \in \mathcal{R}^h$ is the vector of sensor faults, and $F \in \mathcal{R}^{p\times h}$ where $rank(F) = h$ and $h \leq p$.

6.5.1 Secondary observer method

Without a loss of generality, assume that the parameters A, Q and C are in the canonical coordinates of (6.8). Then applying the coordinate transformation T_L in (6.17), and assuming that sliding motion has been attained, the error system will satisfy

$$\begin{aligned} \dot{e}_1(t) &= \mathcal{A}_{11}e_1(t) + \mathcal{A}_{12}Ff_o(t) - \mathcal{Q}_1\xi(t,x,u) \qquad (6.58) \\ F\dot{f}_o(t) &= \mathcal{A}_{21}e_1(t) + \mathcal{A}_{22}Ff_o(t) - \mathcal{Q}_2\xi(t,x,u) + P_o^{-1}\nu_{eq} \qquad (6.59) \end{aligned}$$

Filter $P_o^{-1}\nu_{eq}$ to obtain

$$\dot{z}_1(t) = -A_{f,1}z_1(t) - A_{f,1}\mathcal{A}_{21}e_1(t) - A_{f,1}\mathcal{A}_{22}Ff_o(t) + A_{f,1}F\dot{f}_o(t) + A_{f,1}\mathcal{Q}_2\xi(t,x,u) \qquad (6.60)$$

Repeating the analysis in §5.4.1, the following augmented state-space system of order $n+p$ can be obtained

$$\begin{aligned} \begin{bmatrix} \dot{e}_1(t) \\ \dot{w}(t) \\ \dot{z}_2(t) \end{bmatrix} &= \underbrace{\begin{bmatrix} \mathcal{A}_{11} & 0 & 0 \\ -A_{f,1}\mathcal{A}_{21} & -A_{f,1} & 0 \\ 0 & A_{f,2} & -A_{f,2} \end{bmatrix}}_{A_a} \begin{bmatrix} e_1(t) \\ w(t) \\ z_2(t) \end{bmatrix} \\ &+ \underbrace{\begin{bmatrix} \mathcal{A}_{12}F \\ -A_{f,1}^2F - A_{f,1}\mathcal{A}_{22}F \\ A_{f,2}A_{f,1}F \end{bmatrix}}_{M_a} f_o(t) + \underbrace{\begin{bmatrix} -\mathcal{Q}_1 \\ A_{f,1}\mathcal{Q}_2 \\ 0 \end{bmatrix}}_{Q_a} \xi(t,x,u) \qquad (6.61) \end{aligned}$$

where the output equation is

$$z_2(t) = \underbrace{\begin{bmatrix} 0 & 0 & I_p \end{bmatrix}}_{C_a} \begin{bmatrix} e_1(t) \\ w(t) \\ z_2(t) \end{bmatrix} \qquad (6.62)$$

Equations (6.61) - (6.62) are now in the form of (6.1) - (6.2). Hence the design method in §6.4 can be used to design a sliding mode observer for the augmented system described by (6.61) - (6.62) to robustly reconstruct $f_o(t)$ despite the disturbance $\xi(t,x,u)$.

6.5.2 Single observer method

Consider the system described by (6.56) - (6.57). Repeating the procedure in §5.4.3, the following augmented state-space system of order $n + p$ can be obtained

$$\begin{bmatrix} \dot{x}(t) \\ \dot{z}_3(t) \end{bmatrix} = \underbrace{\begin{bmatrix} A & 0 \\ A_{f,3}C & -A_{f,3} \end{bmatrix}}_{A_b} \begin{bmatrix} x(t) \\ z_3(t) \end{bmatrix} + \underbrace{\begin{bmatrix} B \\ 0 \end{bmatrix}}_{B_b} u(t) + \underbrace{\begin{bmatrix} 0 \\ A_{f,3}F \end{bmatrix}}_{M_b} f_o(t) + \underbrace{\begin{bmatrix} Q \\ 0 \end{bmatrix}}_{Q_b} \xi(t,x,u) \quad (6.63)$$

$$z_3(t) = \underbrace{\begin{bmatrix} 0 & I_p \end{bmatrix}}_{C_b} \begin{bmatrix} x(t) \\ z_3(t) \end{bmatrix} \quad (6.64)$$

and hence a sliding mode observer can be designed for the augmented system (6.63) - (6.64) to robustly reconstruct the sensor fault $f_o(t)$.

Remark : The robust sensor fault reconstruction methods in §6.5.1 and this section have almost identical existence conditions, with some subtle differences, which have been discussed in §5.4.3

6.6 Example 1: VTOL aircraft model

The robust fault reconstruction scheme in this chapter will now be demonstrated with a 'Vertical Take-Off and Landing' (VTOL) aircraft model taken from [96, 120]. Its states, outputs and inputs respectively are

$$x = \begin{bmatrix} \text{horizontal velocity (knots)} \\ \text{vertical velocity (knots)} \\ \text{pitch rate (deg/s)} \\ \text{pitch angle (deg)} \end{bmatrix}$$

$$y = \begin{bmatrix} \text{horizontal velocity (knots)} \\ \text{vertical velocity (knots)} \\ \text{pitch angle (deg)} \end{bmatrix}$$

$$u = \begin{bmatrix} \text{collective pitch control} \\ \text{longitudal cyclic pitch control} \end{bmatrix}$$

The system is modelled as

$$\dot{x}(t) = (A + \triangle A)x(t) + (B + \triangle B)u(t) + Mf_i(t) \quad (6.65)$$

$$y(t) = Cx(t) + Ff_o(t) \quad (6.66)$$

where

$$A = \begin{bmatrix} -9.9477 & -0.7476 & 0.2632 & 5.0337 \\ 52.1659 & 2.7452 & 5.5532 & -24.4221 \\ 26.0922 & 2.6361 & -4.1975 & -19.2774 \\ 0 & 0 & 1.0000 & 0 \end{bmatrix}, \quad B = \begin{bmatrix} 0.4422 & 0.1761 \\ 3.5446 & -7.5922 \\ -5.5200 & 4.4900 \\ 0 & 0 \end{bmatrix}$$

$$C = \begin{bmatrix} 1 & 0 & 0 & 0 \\ 0 & 1 & 0 & 0 \\ 0 & 0 & 0 & 1 \end{bmatrix} \quad M = \begin{bmatrix} 0.4422 \\ 3.5446 \\ -5.5200 \\ 0 \end{bmatrix} \quad F = \begin{bmatrix} 0 \\ 0 \\ 1 \end{bmatrix}$$

The uncertain matrices are

$$\triangle A = \begin{bmatrix} 0 & 0 & 0 & 0 \\ 0 & 0 & 0 & 0 \\ 0 & \triangle a_{32} & 0 & \triangle a_{34} \\ 0 & 0 & 0 & 0 \end{bmatrix}, \quad \triangle B = \begin{bmatrix} 0 & 0 \\ \triangle b_{21} & 0 \\ 0 & 0 \\ 0 & 0 \end{bmatrix}$$

Hence in the notation of (6.1) - (6.2) and (6.56) - (6.57),

$$Q = \begin{bmatrix} 0 & 0 \\ 0 & 1 \\ 1 & 0 \\ 0 & 0 \end{bmatrix}, \quad \xi = \begin{bmatrix} \begin{bmatrix} 0 & \triangle a_{32} & 0 & \triangle a_{34} \end{bmatrix} x \\ \begin{bmatrix} \triangle b_{21} & 0 \end{bmatrix} u \end{bmatrix}$$

where $\triangle a_{32} = 0.5, \triangle a_{34} = 2, \triangle b_{21} = 2$ [96].

6.6.1 Robust reconstruction of actuator faults

The sliding mode observer was designed using the method presented in §6.4. The design parameters were chosen as $D_1 = I_3$ (from (6.44)) and $\gamma_o = 1$ (from (6.46)). The optimisation routine [39] yielded a value of $\gamma = 8.1968 \times 10^{-4}$. The associated gains for the sliding mode observer are

$$G_l = G_n = \begin{bmatrix} 0.1914 & 2.0408 & 0.5413 \\ 2.0408 & 46.4792 & 9.2975 \\ 4.5304 & 98.5651 & 20.3670 \\ 0.5413 & 9.2975 & 2.0644 \end{bmatrix}$$

and the matrix W_{sc} from (6.30) associated with the scaling of ν_{eq}, is given by

$$W_{sc} = \begin{bmatrix} -0.5952 & -2.2440 & -0.2799 \end{bmatrix}$$

The Lyapunov matrix from (6.9) is given as

$$P_o = \begin{bmatrix} 65.4422 & 5.6396 & -42.5575 \\ 5.6396 & 0.7031 & -4.6451 \\ -42.5575 & -4.6451 & 32.5628 \end{bmatrix}$$

The scalar function ρ from (6.6) was chosen to be 100, and the scalar δ from (6.29) was chosen to be 1×10^{-5}.

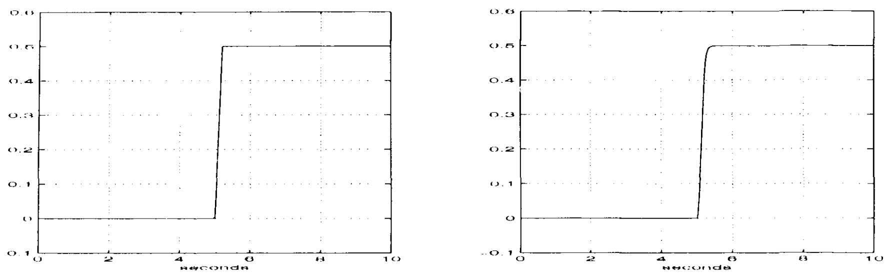

Figure 6.2: *The left subfigure is a fault on the first actuator, the right subfigure is the reconstruction.*

Figure 6.2 shows the sliding mode observer faithfully reconstructing the actuator fault, rejecting the effect of the uncertainty. This is to be expected, due to the small value of γ obtained.

6.6.2 Robust reconstruction of sensor faults (secondary observer method)

The sliding mode observer given in §6.6.1 has been used as the 'primary observer' in this example. The secondary observer has been designed based on $A_{f,2}$ and $A_{f,3}$ being chosen to be $2I_3$ and $15I_3$ respectively, and using the approach described in §6.4. Specifying $D_{1,a} = I_3$ and $\gamma_{o,a} = 1$ (where the subscripts 'a' indicate the parameters are for the augmented secondary observer), the optimisation routine yielded a value of 3.5312×10^{-4} for γ_a (again the subscript 'a' is used to differentiate the primary and secondary observer). The associated gain matrices for the augmented observer are :

$$G_{l,a} = G_{n,a} = \begin{bmatrix} 5.7585 & 12.7028 & 20.3629 \\ 1.6626 & 5.3059 & 5.7225 \\ 11.9811 & 277.0349 & 41.8259 \\ 5.8418 & 18.8459 & 20.1989 \\ 1.3324 & 3.5287 & 4.6261 \\ 3.5287 & 101.3107 & 12.4429 \\ 4.6261 & 12.4429 & 16.1556 \end{bmatrix}$$

The optimal choice of weighting matrix for the equivalent output error injection

$$W_{sc,a} = \begin{bmatrix} 0.1203 & 0.0000 & -0.0333 \end{bmatrix}$$

and the Lyapunov matrix associated with the switched unit vector component is

$$P_{o,a} = \begin{bmatrix} 129.4650 & 0.0483 & -37.1091 \\ 0.0483 & 0.0109 & -0.0223 \\ -37.1091 & -0.0223 & 10.7051 \end{bmatrix}$$

In the following simulations, $\rho_a = 240$ and $\delta_a = 5 \times 10^{-6}$.

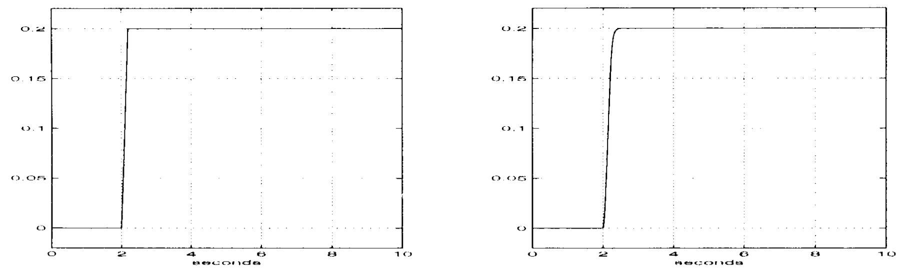

Figure 6.3: *The left subfigure is a fault on the third sensor, the right subfigure is the reconstruction of the fault.*

Figure 6.3 shows the secondary observer faithfully reconstructing the sensor fault, rejecting the effect of the uncertainty. Again, due to the small value of γ_a, this is to be expected.

6.6.3 Robust reconstruction of sensor faults (single observer method)

The following parameters were chosen for the design of the observer associated with the method described in §6.5.2. The filter matrix from (6.63) was chosen as $A_{f,3} = 20I_3$ and then the observer design method proposed in §6.4 was adopted for the triple (A_b, M_b, C_b) from

(6.63) - (6.64). The tuning parameter for the linear component of the observer, $D_{1,b}$ from (6.44), was chosen as I_3 and $\gamma_{o,b}$ was chosen to be unity (where the subscripts 'b' indicate the parameters are for the observer associated with sensor fault reconstruction). The optimisation routine yielded a value of $\gamma_b = 4.6735 \times 10^{-4}$. The associated gain matrices for the augmented observer are :

$$G_{l,b} = G_{n,b} = \begin{bmatrix} 3.9403 & 0.9843 & 8.4998 \\ 8.2558 & 216.5491 & 36.1942 \\ 28.8487 & 84.1515 & 68.8265 \\ 9.1354 & 14.5926 & 20.7617 \\ 3.4190 & 2.4941 & 7.5158 \\ 2.4941 & 106.6584 & 14.4692 \\ 7.5158 & 14.4692 & 17.5985 \end{bmatrix}$$

The optimal choice of weighting matrix for the equivalent control

$$W_{sc,b} = \begin{bmatrix} 0.1931 & 0.0002 & -0.0500 \end{bmatrix}$$

and the Lyapunov matrix associated with the switched unit vector component is

$$P_{o,b} = \begin{bmatrix} 15.1803 & 0.5904 & -6.9684 \\ 0.5904 & 0.0335 & -0.2797 \\ -6.9684 & -0.2797 & 3.2628 \end{bmatrix}$$

For this simulation, $\rho_b = 100$ and $\delta_b = 1 \times 10^{-5}$.

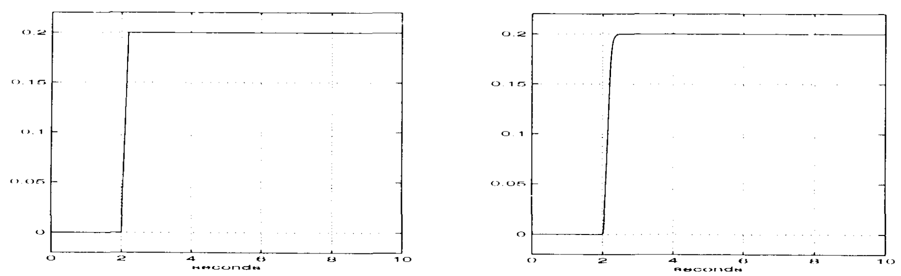

Figure 6.4: *The left subfigure is a fault on the third sensor, the right subfigure is the reconstruction of the fault.*

Figure 6.4 shows the observer faithfully reconstructing the sensor fault, rejecting the effect of the uncertainty.

6.7 Example 2: Gantry crane model

The methodology proposed in this chapter will now be demonstrated by means of a nonlinear model of a gantry crane with a hanging load, taken from [38].

The (nonlinear) equations of motion that govern the crane are :

$$(I + ml^2)\ddot{\theta} + c\dot{\theta} + mgl\,\sin\theta + ml\ddot{x}\,\cos\theta \;=\; 0 \tag{6.67}$$

$$(m_t + m)\ddot{x} + b\dot{x} + ml\ddot{\theta}\,\cos\theta - ml\dot{\theta}^2\,\sin\theta \;=\; u \tag{6.68}$$

The variable x represents the displacement of the truck in metres; θ represents the angular displacement of the load from the (downward) vertical in radians. The parameters are given as $m_t = 3.2kg, m = 0.535kg, b = 6.2kg/s, c = 0.009kg\; m^2, I = 0.062kg\; m^2, g = 9.81m/s^2$ and $l = 0.35m$.

Equations (6.67) and (6.68) can be re-arranged to be

$$\ddot{x} \;=\; \frac{mln}{MX}(\dot{\theta}^2 + \frac{mgl\,\cos\theta}{I_o})\theta - \frac{b}{MX}\dot{x} + \frac{mlc\,\cos\theta}{MXI_o}\dot{\theta} + \frac{1}{MX}u \tag{6.69}$$

$$\begin{aligned}\ddot{\theta} \;=\; & -\frac{mln}{I_o}(g + \frac{ml\,\cos\theta}{MX}(\dot{\theta}^2 + \frac{mgl\,\cos\theta}{I_o}))\theta - \frac{c}{I_o}(1 + \frac{(ml\,\cos\theta)^2}{MXI_o})\dot{\theta} \\ & + \frac{mlb\,\cos\theta}{MXI_o}\dot{x} - \frac{ml\,\cos\theta}{MXI_o}u\end{aligned} \tag{6.70}$$

where $M = m_t + m, I_o = I + ml^2, n = (\sin\theta)/\theta$ and $X = 1 - \frac{(ml\,\cos\theta)^2}{MI_o}$

For small displacements of θ, the following approximations can be made

$$\dot{\theta} = 0, \cos\theta = 1, n = 1, X = X_o$$

where $X_o = 1 - \frac{(ml)^2}{MI_o}$

Using these approximations, classifying all nonlinearities as disturbances, and then defining the state vector as $\begin{bmatrix}\theta & \dot{\theta} & x & \dot{x}\end{bmatrix}^T$, a state-space representation in the form of (6.1) - (6.2) can be obtained where :

$$A = \begin{bmatrix} 0 & 1 & 0 & 0 \\ -\frac{mlg}{I_o} - \frac{(ml)^3 g}{MX_o I_o^2} & -\frac{c}{I_o} - \frac{(ml)^2 c}{MX_o I_o^2} & 0 & \frac{mlb}{MX_o I_o} \\ 0 & 0 & 0 & 1 \\ \frac{(ml)^2 g}{MX_o I_o} & \frac{mlc}{MX_o I_o} & 0 & -\frac{b}{MX_o} \end{bmatrix} \tag{6.71}$$

$$B = \begin{bmatrix} 0 \\ -\frac{ml}{MX_o I_o} \\ 0 \\ \frac{1}{MX_o} \end{bmatrix} \qquad Q = \begin{bmatrix} 0 & 0 \\ \frac{1}{I_o} & 0 \\ 0 & 0 \\ 0 & \frac{1}{M} \end{bmatrix} \tag{6.72}$$

where ξ represents the lumped residual nonlinearities resulting from the linearisation.

Here it is assumed that the second sensor is not faulty. Substituting the physical parameters into (6.71) - (6.72) the following state-space matrices can be obtained (from the notation in (6.1) and (6.57))

$$A = \begin{bmatrix} 0 & 1.0000 & 0 & 0 \\ -15.5660 & -0.0731 & 0 & 2.6340 \\ 0 & 0 & 0 & 1.0000 \\ 0.8138 & 0.0038 & 0 & -1.7977 \end{bmatrix}, \quad M = B = \begin{bmatrix} 0 \\ -0.4248 \\ 0 \\ 0.2899 \end{bmatrix}$$

$$C = \begin{bmatrix} 1 & 0 & 0 & 0 \\ 0 & 0 & 1 & 0 \\ 0 & 0 & 0 & 1 \end{bmatrix}, \quad Q = \begin{bmatrix} 0 & 0 \\ 7.5033 & 0 \\ 0 & 0 \\ 0 & 0.2677 \end{bmatrix}, \quad F = \begin{bmatrix} 1 & 0 \\ 0 & 0 \\ 0 & 1 \end{bmatrix}$$

For the simulations which follow a simple phase advance controller was designed based on the measurements of θ and x to control the position of the crane x and minimise the oscillations in θ. The control signal u in transfer function form is

$$u(s) = \frac{485(s+1)}{s+50}\theta(s) + \frac{120(s+1)}{s+10}(r(s) - x(s))$$

where r is the reference signal for x.

6.7.1 Robust reconstruction of actuator faults

Specifying $D_1 = I_3$ and $\gamma_o = 1$, the synthesis procedure yielded $\gamma = 0.9239$ as well as the following gain matrices

$$G_l = G_n = \begin{bmatrix} 3.1488 & -0.0966 & 0.4582 \\ 3.8182 & -0.8507 & 0.0290 \\ -0.0966 & 0.6383 & -0.0109 \\ 0.4582 & -0.0109 & 0.4236 \end{bmatrix}$$

$$P_o = \begin{bmatrix} 0.3785 & 0.0503 & -0.4082 \\ 0.0503 & 1.5739 & -0.0141 \\ -0.4082 & -0.0141 & 2.8019 \end{bmatrix}, \quad W_{sc} = \begin{bmatrix} 0.0210 & 0 & -3.4489 \end{bmatrix}$$

For this simulation $\rho = 50$ and $\delta = 10^{-4}$.

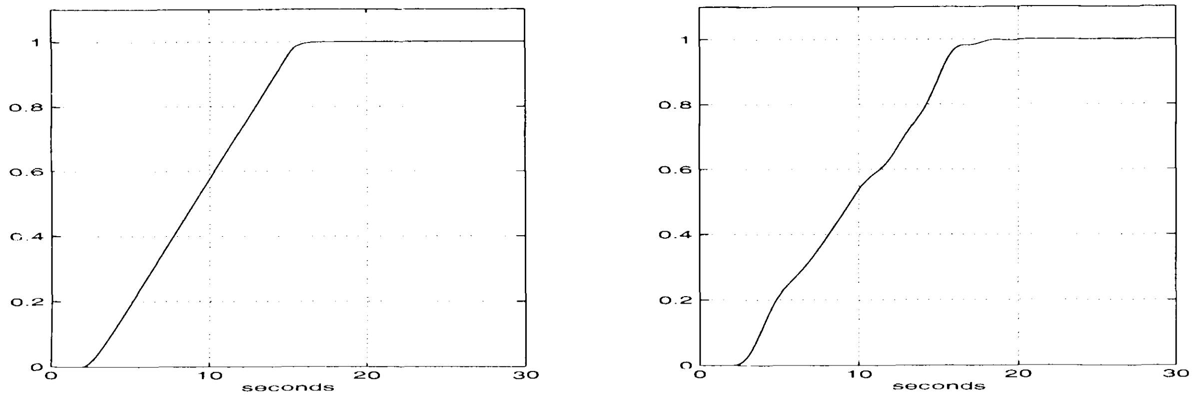

Figure 6.5: *The left subfigure is the demanded reference for the position of the crane, the right subfigure is its response.*

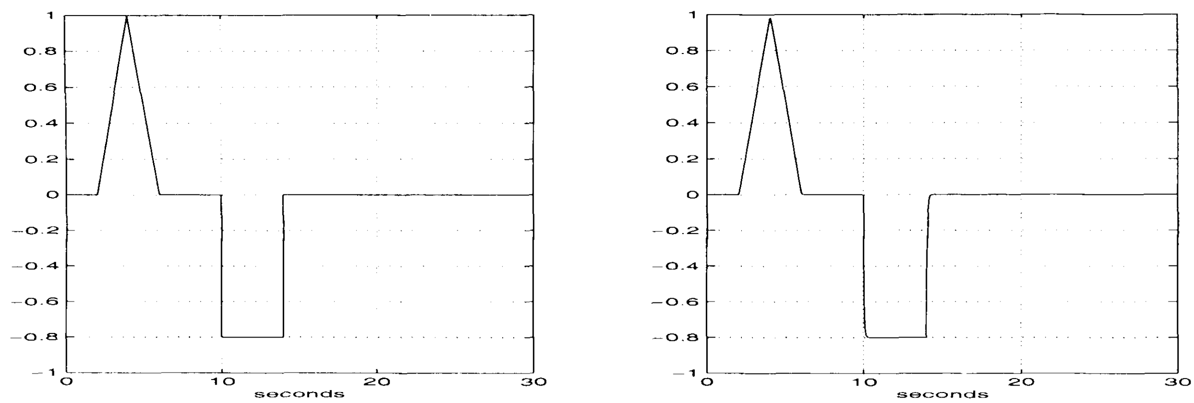

Figure 6.6: *The left subfigure is the fault that is applied to the actuator, the right subfigure is its reconstruction.*

Figure 6.5 shows the reference demand for the position of the crane (in metres) and also its response subject to the demand and also the actuator fault.

Figure 6.6 shows the fault applied to the actuator, as well as its reconstruction, which is visually almost identical to the fault. This is because of the small value of γ that was obtained.

6.7.2 Robust reconstruction of sensor faults

Specifying $A_f = 20I_3$, $D_{1,b} = 10I_3$ and $\gamma_{o,b} = 10$ and constructing the augmented state space matrices from (6.63) - (6.64), the synthesis procedure yields $\gamma_b = 9.2269$. In this example, it can be verified that (A_b, M_b, C_b) does not possess invariant zeros. Hence the fact that A from (6.71) has an eigenvalue at the origin does not present any difficulties. The following gain matrices were obtained from the synthesis procedure

$$G_{l,b} = \begin{bmatrix} -0.5782 & 0.3884 & -0.1354 \\ 15.0036 & -10.0781 & 3.5129 \\ -50.5093 & 33.9277 & -11.8261 \\ -0.7765 & 0.5216 & -0.1818 \\ 98.0001 & -50.4685 & 26.7489 \\ -50.4685 & 33.9003 & -11.8166 \\ 26.7489 & -11.8166 & 10.9589 \end{bmatrix}$$

$$G_{n,b} = \begin{bmatrix} -5.7817 & 3.8837 & -1.3537 \\ 150.0361 & -100.7812 & 35.1292 \\ -505.0927 & 339.2772 & -118.2615 \\ -7.7653 & 5.2161 & -1.8182 \\ 980.0009 & -504.6847 & 267.4886 \\ -504.6847 & 339.0031 & -118.1660 \\ 267.4886 & -118.1660 & 109.5885 \end{bmatrix}$$

$$P_{o,b} = \begin{bmatrix} 0.0094 & 0.0096 & -0.0126 \\ 0.0096 & 0.0146 & -0.0078 \\ -0.0126 & -0.0078 & 0.0315 \end{bmatrix}, \quad W_{sc,b} = \begin{bmatrix} 1.3645 & 0 & -0.0500 \\ 1.0001 & -0.0500 & 0 \end{bmatrix}$$

In the simulation that follows, $\rho_b = 50$ and $\delta_b = 5 \times 10^{-5}$.

Figure 6.7 shows the response of the crane's position to the demand as well as faults in sensors 1 and 3. Figure 6.8 shows the fault in sensor 1 and its reconstruction, and Figure 6.9 shows the fault in sensor 3 and its reconstruction. Because of the relatively high value of γ_b that was obtained, there is some corruption in the reconstruction (due to the oscillations in the crane) especially in Figure 6.8. However, the fundamental shape of the reconstruction still resembles the fault.

6.8 Conclusion

This chapter has presented a method for designing an Edwards - Spurgeon observer for robust actuator and sensor fault reconstruction purposes.

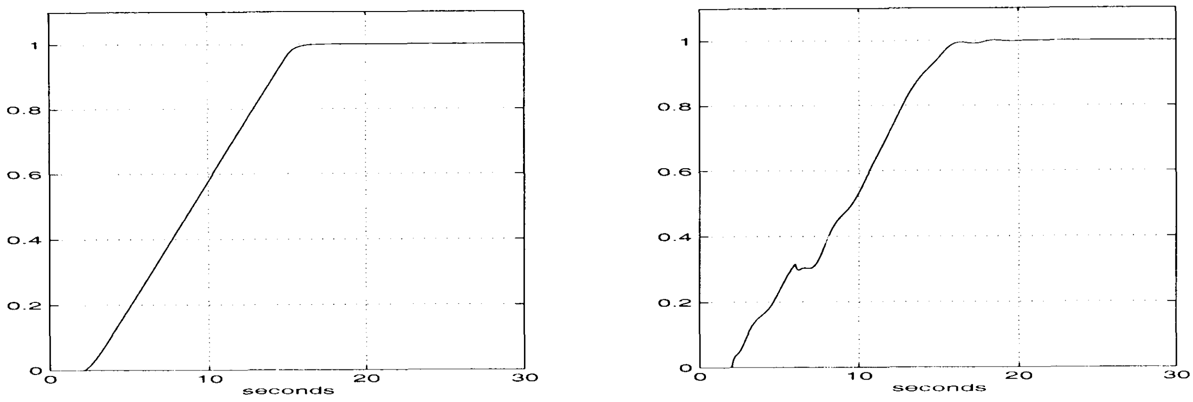

Figure 6.7: *The left subfigure is the demanded reference for the position of the crane, the right subfigure is its response.*

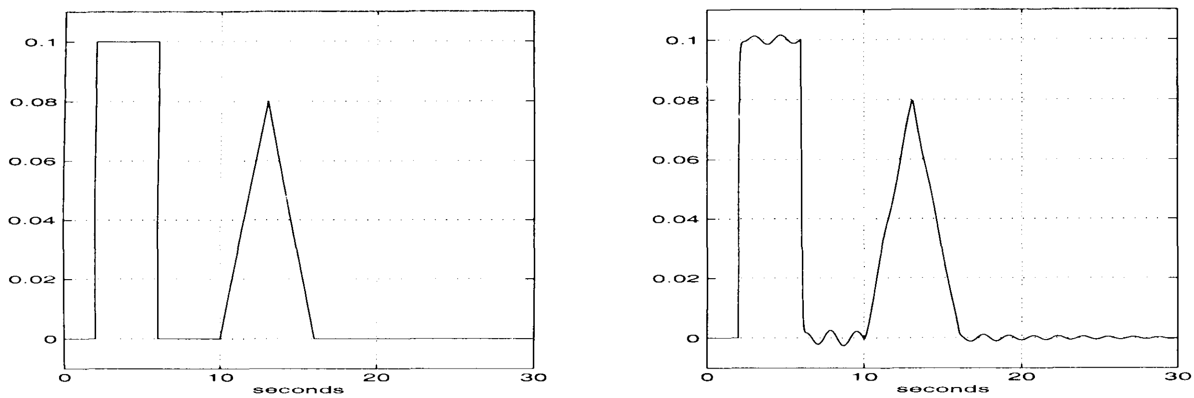

Figure 6.8: *The left subfigure shows the fault on the oscillation angle θ sensor (sensor 1). The right subfigure shows its reconstruction.*

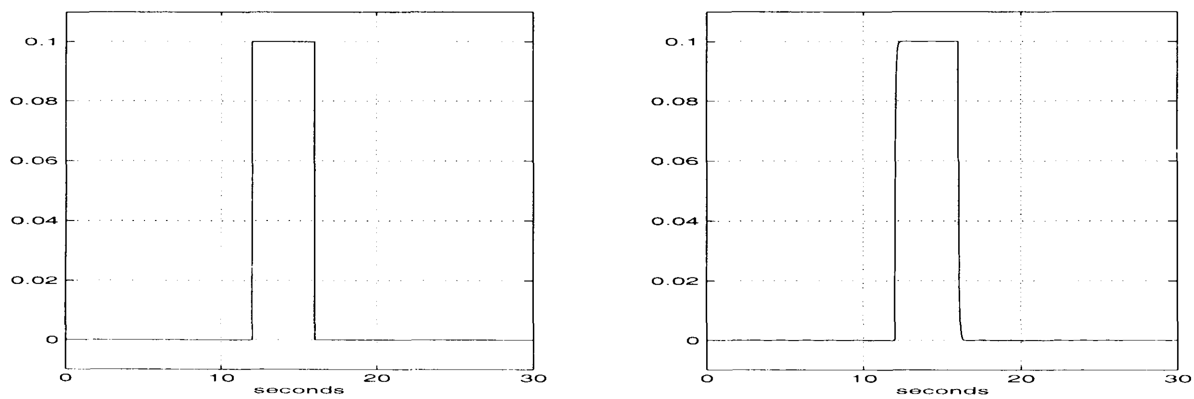

Figure 6.9: *The left subfigure shows the fault on the crane velocity $\dot{x}$ sensor (sensor 3). The right subfigure shows its reconstruction.*

This method was initially developed for the case of actuator faults. During sliding motion, the equivalent output error injection was scaled to reconstruct the fault. The method used LMIs to design the sliding motion and the scaling of the equivalent output error injection to minimise the upper bound of the $\mathcal{L}_2$ gain from the uncertainty/disturbance to the fault reconstruction.

The method also introduced a convenient way to design the gains of the sliding mode observer. The method was extended to the case of sensor faults by appropriate filtering of certain signals to obtain fictitious systems that treat the sensor faults as actuator faults.

The methods proposed in this chapter were demonstrated with two examples; a VTOL aircraft model and a nonlinear model of a gantry crane. The methods provided good fault reconstruction despite the presence of uncertainty/disturbances.

Chapter 7

A case study: Spey aero-engine

7.1 Introduction

An aero-engine is a very nonlinear and complicated system where reliability is required to be very high. There are many sensors in an aero-engine, to help monitor its condition, and to warn the pilot of any unwanted phenomenon, such as icing or fire. These sensors work in very harsh environments, and are considered the least reliable components of the engine [76, 78]. Therefore, in an aero-engine, efficient FDI for the sensors is of very high importance.

Much has been done in the area of robust sensor FDI for aero-engines using various schemes from the literature. Dassanyake *et al.* [18] used an unknown input observer scheme, while Patton & Chen used eigenstructure assignment methods [84, 83] and also parity space approaches [86]. However, the methods described above all evaluated the performance of the FDI scheme on linear models of an aero-engine. FDI schemes have also been demonstrated on real aero-engine systems. Merrill *et al.* [79, 77] considered a linear observer, using the statistical properties of the system and also a threshold to determine the occurrence of a fault. Kelly [58] devised an FDI scheme that processed both the actual output and the model output; if both processed signals did not have a similar 'shape', then a fault was deemed to have occurred. Merrington *et al.* [80] compared nonfaulty data with suspected faulty data obtained from actual flights, and the difference was processed. If the processed difference exceeds a threshold, then a fault was deemed to have occurred.

This chapter demonstrates the robust fault reconstruction method in Chapter 6 applied to a nonlinear Simulink model of an aero-engine, provided by QinetiQ [1], which is the largest science and technology research organisation in Europe.

[1]QinetiQ Ltd., Ively Road, Farnborough, Hampshire GU14 0LX, UK

7.2 Aero-engine description

The aero-engine under consideration is the Rolls-Royce Spey Mk 202. Although this engine is of a comparatively old design, it has two spools, variable inlet guide vanes and variable nozzle geometry that are typical of more modern engines. The engine consists of a low pressure (LP) compressor, a high pressure (HP) compressor, a combustion chamber and an exhaust passage. Air is taken into the engine; compressed through the LP compressor, and then part is compressed by the HP compressor, the remainder entering a bypass duct. The air delivered by the HP compressor enters a combustion chamber where fuel is burned, causing a large rise in temperature. The combustion gases are partially expanded during their passage through the HP and LP turbines, providing the mechanical energy needed to drive the compressors. On leaving the LP turbine, the combustion gases mix with the air that has travelled through the bypass duct and the mixture expands down to atmospheric pressure through the nozzle, providing the propulsive force for the engine.

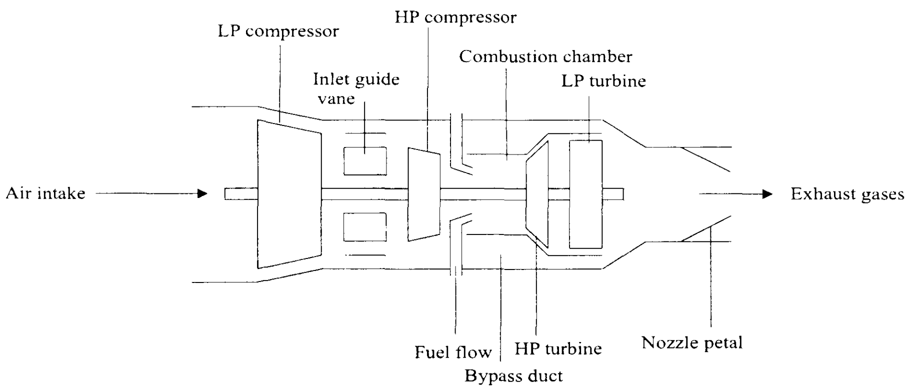

Figure 7.1: *A schematic representation of the engine. The reheat mechanism has been omitted for simplicity.*

The engine model, developed by QinetiQ, has 5 control inputs and 10 measured outputs. Respectively they are

$$u = \left[\begin{array}{c|l} wfe & \text{main engine fuel flow } (kg/s) \\ rf & \text{reheat flow rate } (kg/s) \\ sinth & \text{sine of the nozzle petal angle} \\ igv & \text{HP compressor guide vane angle } (degrees) \\ bov & \text{HP compressor handling bleed valve position } (\%) \end{array}\right]$$

$$y = \left[\begin{array}{c|l} nl & \text{corrected LP spool speed } (\%) \\ nh & \text{corrected HP spool speed } (\%) \\ t2c & \text{HP compressor inlet temperature } (K) \\ dp2b & \text{Bypass duct inlet differential pressure } (kPa) \\ t2b & \text{Bypass duct inlet total temperature } (K) \\ p3 & \text{HP compressor exit total pressure } (kPa) \\ t3 & \text{HP compressor exit temperature } (K) \\ t6 & \text{core exit mean temperature } (K) \\ dp3 & \text{HP compressor exit differential pressure } (kPa) \\ ps4 & \text{HPT stage 2 static pressure } (kPa) \end{array}\right.$$

The model also possesses a number of 'environmental inputs' such as the altitude and flight Mach number. For simplicity these were set to constant values corresponding to sea-level static conditions on a standard day. The second output *(nh)* is the controlled output and hence is used to generate the control signal. A simplified control scheme, designed to operate in the limited range of $88\% < nh < 93\%$, was provided by QinetiQ.

7.3 Identification of a model

A system identification approach was used to obtain a linearised model of the open loop aero-engine. The model was identified about the steady state operating condition of $nh = 90\%$. For the identification, only three of the control inputs were used - the first *(wfe)* , third *(sinth)* and fourth *(igv)* inputs. The other two were maintained at zero: it was assumed that there was no afterburning and so the second input *(rf)* was made zero. In this region of operation $(nh = 90\%)$, the fifth input (bov) is zero. Prior to linearisation the model was scaled at the inputs and outputs as shown in Figure 7.2.

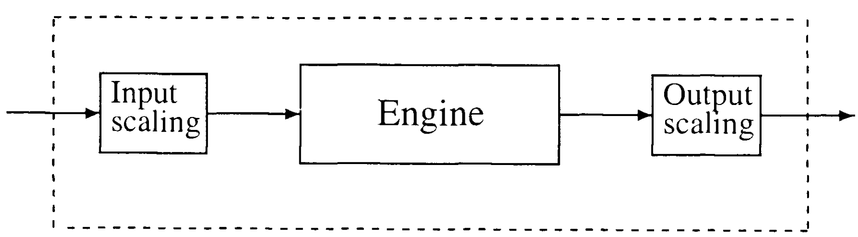

Figure 7.2: The scalings of the aeroengine

The scalings were obtained by varying the high pressure spool speed reference signal nh_{ref} from 88% to 93% under closed loop control, and examining the response of the other outputs. The scalings were chosen so that the variation of each scaled output, from the nominal operating point of, $nh = 90\%$ was of the same order. The scalings are given in Table 7.1.

Variable	**Scaling**
Input 1 *(wfe)*	$\frac{1}{100}$
Input 2 *(sinth)*	$\frac{1}{100}$
Input 3 *(igv)*	$\frac{1}{10}$
Output 1 *(nl)*	$\frac{1}{8}$
Output 2 *(nh)*	$\frac{1}{3}$
Output 3 *(t2c)*	$\frac{1}{15}$
Output 4 *(dp2b)*	$\frac{1}{4}$
Output 5 *(t2b)*	$\frac{1}{15}$
Output 6 *(p3)*	$\frac{1}{300}$
Output 7 *(t3)*	$\frac{1}{40}$
Output 8 *(t6)*	$\frac{1}{60}$
Output 9 *(dp3)*	$\frac{1}{12}$
Output 10 *(ps4)*	$\frac{1}{110}$

Table 7.1: The input-output scalings

For identification, a vector of *pseudo random binary sequence* (PRBS) signals was injected into the scaled system about an operating condition of $nh = 90\%$. Subspace methods were used to analyse the 'de-trended' input-output data [66]. A 15-th order model was used to fit the input-output data. To test the validity of the identified model, another vector of PRBS signals was injected into the nonlinear system and the outputs were compared with the outputs of the identified model. These can be seen in Figure 7.3, which shows that the identified model is a good representation of the aero-engine.

The identified model is open loop stable and has open loop poles at

$$\{-323.9521 \pm 191.7358i, -26.7392 \pm 64.3658i, -53.7300 \pm 19.0605i, -10.7185,$$
$$-29.9153, -6.7876 \pm 19.0686i, -2.0371, -5.3541, -3.5745, -33.7476 \pm 14.2665i\}$$

The state space matrices that describe the scaled identified model are available in the file in the disk attached to this thesis in *aero/modelparam.mat*.

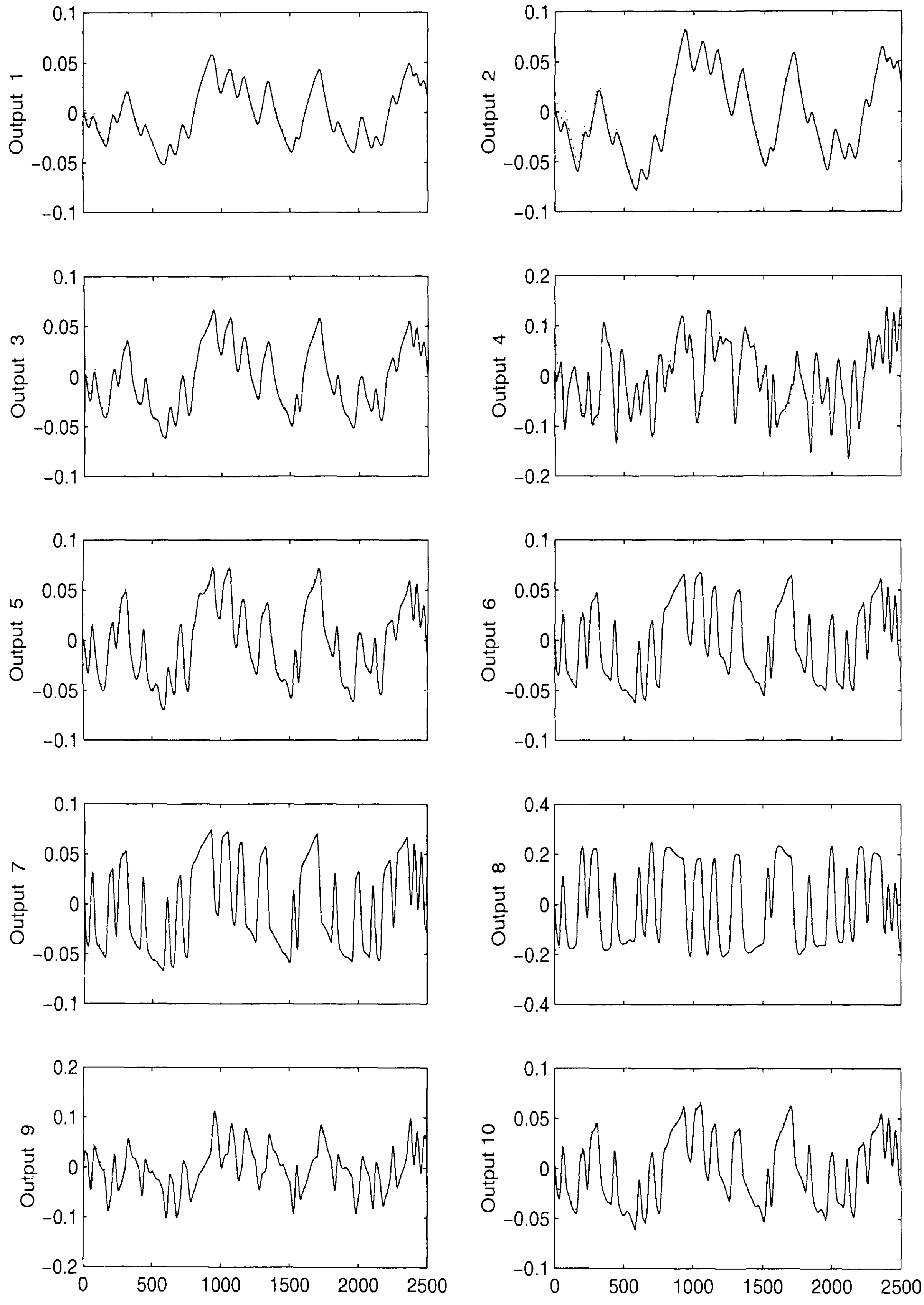

Figure 7.3: *The dotted line is the output of the actual system, and the solid line is the output of the identified model. Notice that the the dotted and solid lines mainly overlap each other.*

7.3.1 Obtaining a disturbance distribution matrix

In the robust fault reconstruction scheme in Chapter 6, a distribution matrix for the uncertainty in the system needs to be obtained.

As the second sensor (corrected high pressure spool speed (nh)) is the controlled output and is used to generate the control signal, a fault in that sensor will cause the controller to react, moving the system from its equilibrium point. This may in turn expose mismatches between the nonlinear and linear models. However, this will not be the case for the occurrence of faults in the other sensors, as they are not used to generate the control signal.

The corrected high pressure spool speed reference was set to be 90%. A ramp fault of slope 0.08 and height 0.8 was applied to the second sensor of the nonlinear model in the closed-loop. The resulting control signal and ramp fault was injected into the linear model. The difference between these outputs will be denoted as $d(t, x, u)$. The schematic diagram of this is shown in Figure 7.4.

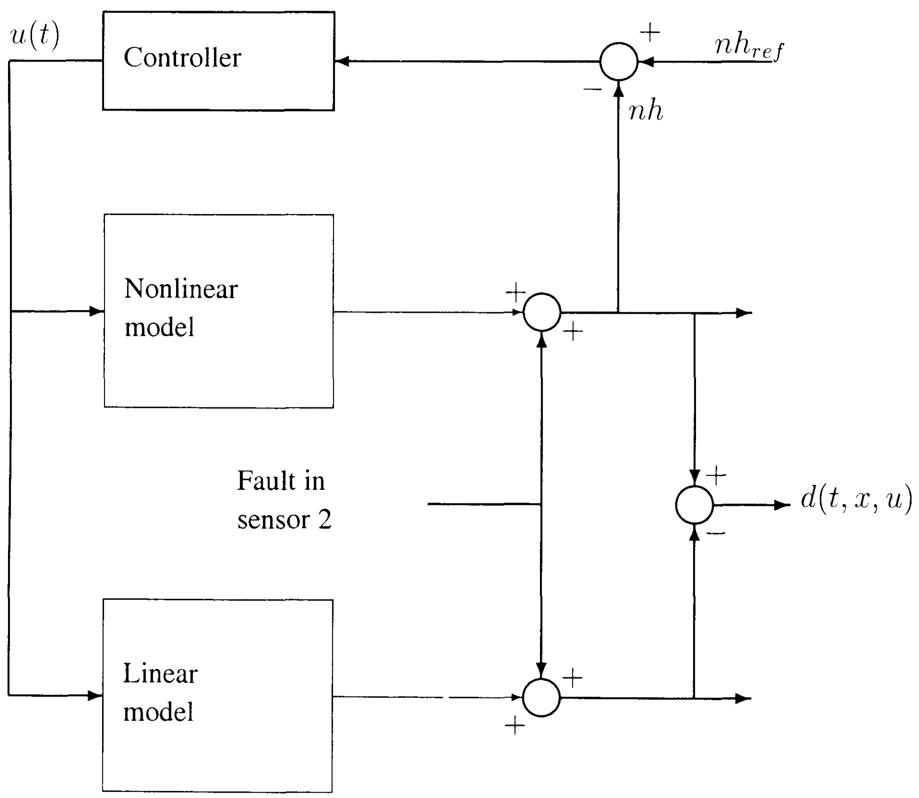

Figure 7.4: Schematic for obtaining $d(t, x, u)$

The components of $d(t, x, u)$ in each sensor channel are shown in Figure 7.5.

As in [91], the objective is now to approximate

$$d(t, x, u) = R\xi(t, x, u) \tag{7.1}$$

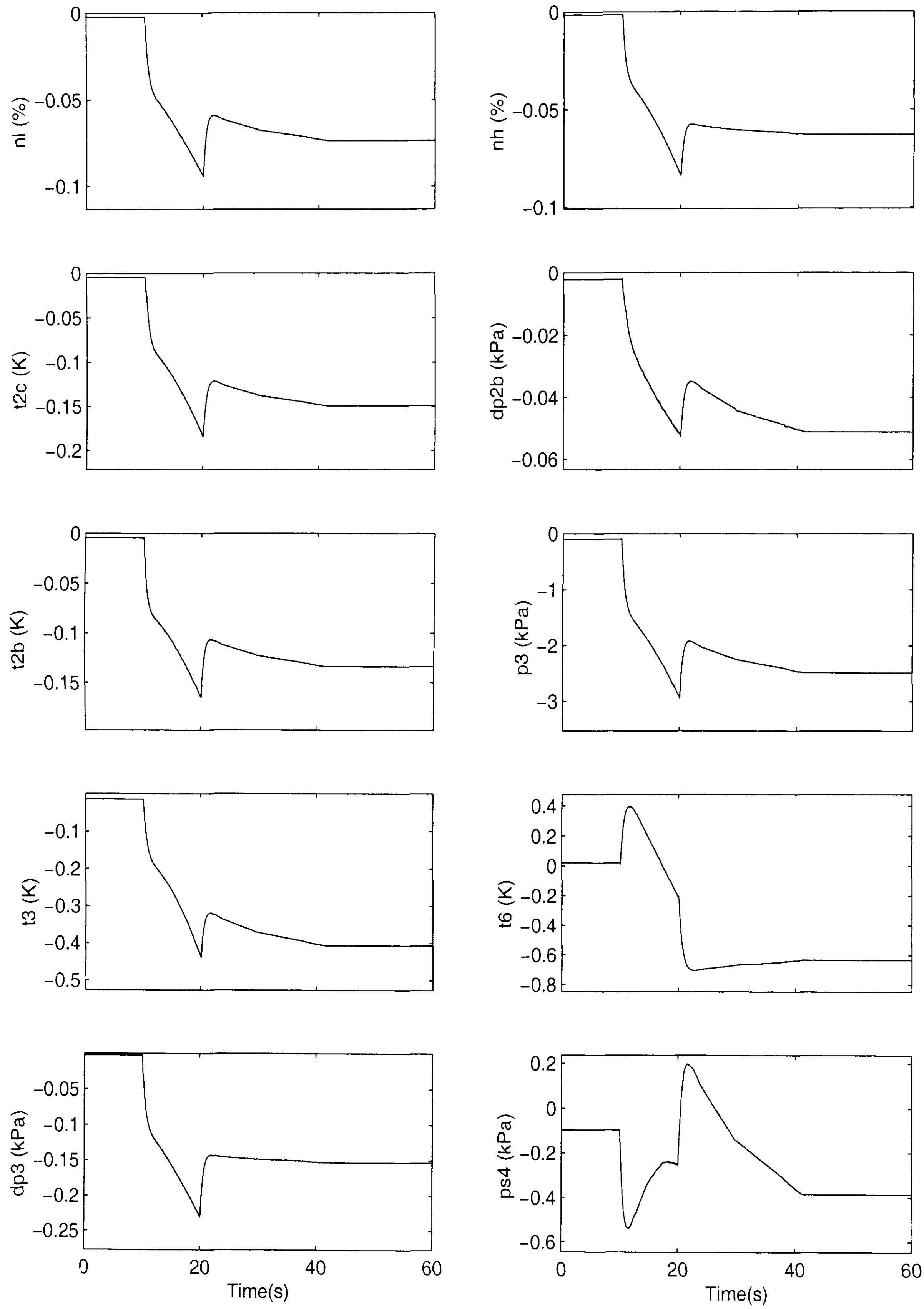

Figure 7.5: *The true values of the signal $d(t, x, u)$.*

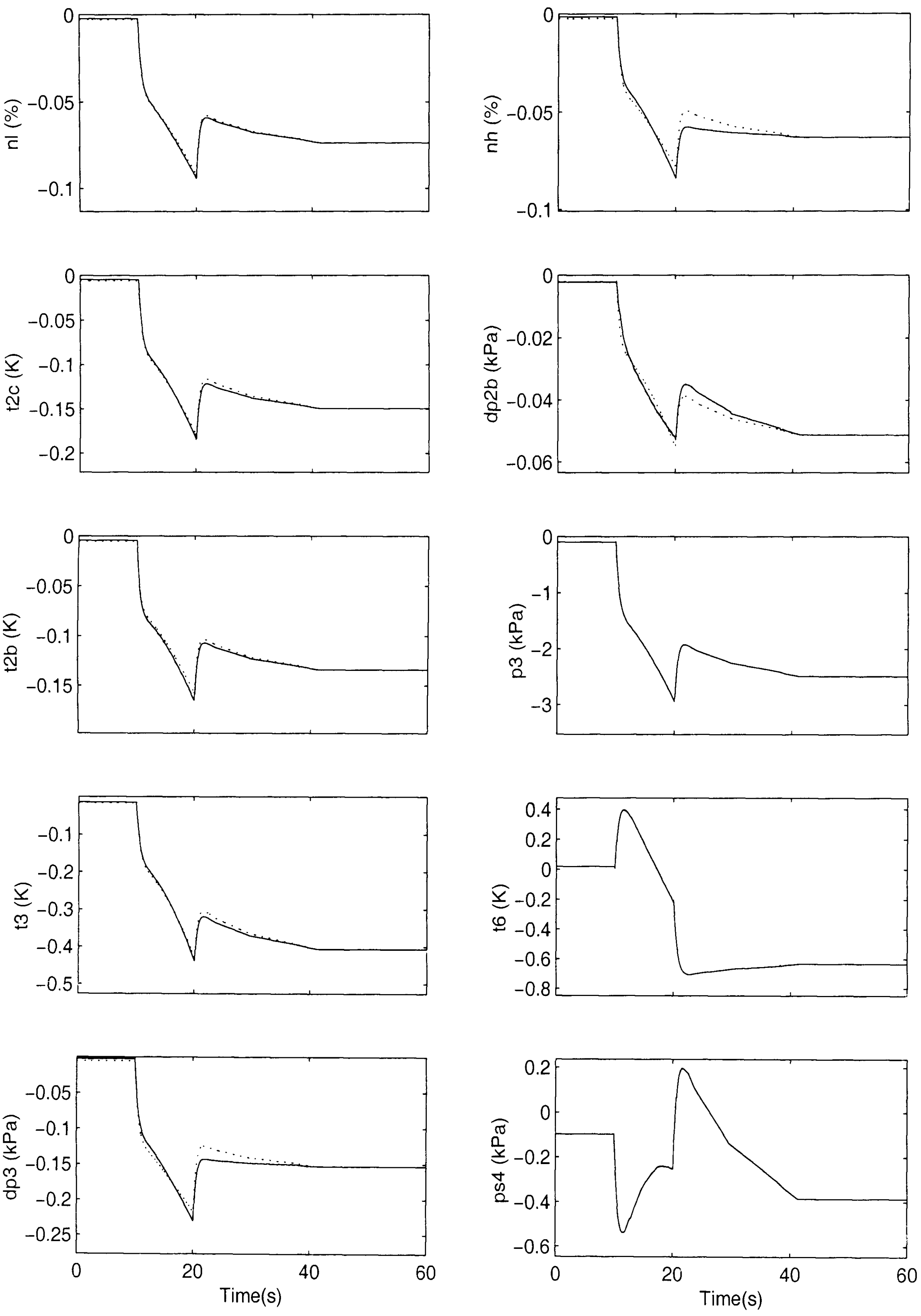

Figure 7.6: *Comparison of* $\hat{d}(t, x, u)$ *(dotted line) with* $d(t, x, u)$ *(solid line).*

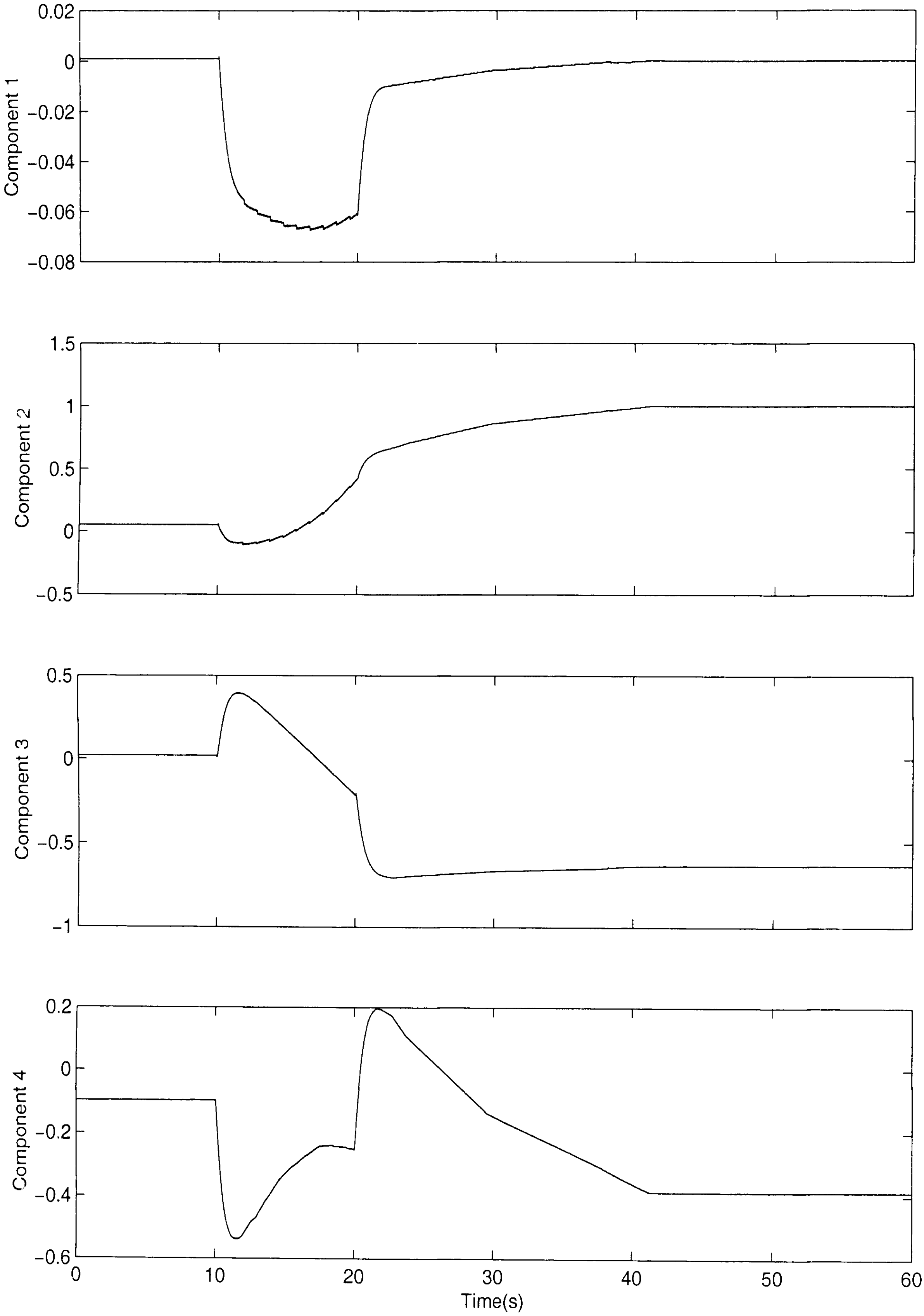

Figure 7.7: *The components of* $\xi(t, x, u)$.

where $\xi(t, x, u) \in \mathcal{R}^k$ and $k < p = 10$ (the number of outputs). In other words, the purpose is to decompose the components of $d(t, x, u)$ into fewer distinct components of $\xi(t, x, u)$.

From Figure 7.5, it can be seen that all components of $d(t, x, u)$ except for components 8 and 10 have the same fundamental shape. Hence, components 8 and 10 are taken to be two distinct signals of $\xi(t, x, u)$. The remaining components of $d(t, x, u)$ can be decomposed into the transient part (up to 20 seconds) and steady-state part (after 20 seconds). All the steady-state components are taken to be a scaled version of each other, and make up a third distinct component of $\xi(t, x, u)$. The transient parts, components 1, 2, 3, 4, 5, 6, 7 and 9 of $d(t, x, u)$ are of similar enough shape, to be considered scalings of each other. This results in another distinct component of $\xi(t, x, u)$.

Therefore, the ten components of $d(t, x, u)$ have been re-expressed as a linear combination of *four* distinct components of $\xi(t, x, u)$ as in (7.1) where

$$R = \begin{bmatrix} 1.0000 & -0.0737 & 0 & 0 \\ 0.8500 & -0.0630 & 0 & 0 \\ 1.9000 & -0.1496 & 0 & 0 \\ 0.5500 & -0.0512 & 0 & 0 \\ 1.6500 & -0.1340 & 0 & 0 \\ 31.0000 & -2.4899 & 0 & 0 \\ 4.2000 & -0.4062 & 0 & 0 \\ 0 & 0 & 1.0000 & 0 \\ 2.5000 & -0.1529 & 0 & 0 \\ 0 & 0 & 0 & 1.0000 \end{bmatrix} \tag{7.2}$$

The first column of R represents the transients of components 1, 2, 3, 4, 5, 6, 7 and 9, while the second column represents their respective steady state components. The last two columns represent components 8 and 10 of $d(t, x, u)$.

Obtaining the matrix R can also be performed using the 'principle of components', which has been demonstrated in [5].

7.3.2 Verifying the validity of the disturbance distribution approximation

The validity of the choice of the disturbance distribution matrix (7.2) can be verified using 'Least Squares' ideas. From the expression (7.1), the solution for $\xi(t, x, u)$ that minimises

$\|d - R\xi\|_2$ is given by

$$\xi(t, x, u) = (R^T R)^{-1} R^T d(t, x, u) \tag{7.3}$$

The signal $\xi(t, x, u)$ is available because $d(t, x, u)$ is measurable. The components of the resulting vector $\xi(t, x, u)$ are shown in Figure 7.7. Define $\hat{d}(t, x, u) = R\xi(t, x, u)$ as an estimate for $d(t, x, u)$, and hence

$$\hat{d}(t, x, u) = R(R^T R)^{-1} R^T d(t, x, u) \tag{7.4}$$

The comparison between $\hat{d}(t, x, u)$ and $d(t, x, u)$ can be used to check the validity of the choice of R. The results are shown in Figure 7.6, which shows that the choice of R is a good one. Figure 7.7 shows the components of $\xi(t, x, u)$ obtained from (7.3).

7.4 Robust sensor fault reconstruction

The aero-engine, subject to sensor faults and mismatches (due to a fault in sensor 2) can be modelled as

$$\dot{x}(t) = Ax(t) + Bu(t) \tag{7.5}$$

$$y(t) = Cx(t) + Du(t) + Ff_o(t) + R\xi(t, x, u) \tag{7.6}$$

where $A \in \mathcal{R}^{n\times n}, B \in \mathcal{R}^{n\times m}, C \in \mathcal{R}^{p\times n}, D \in \mathcal{R}^{p\times m}, F \in \mathcal{R}^{p\times h}$ and $R \in \mathcal{R}^{p\times k}$. The vectors $x(t)$ are the states, $y(t)$ are the measured outputs, $u(t)$ are the inputs, and $f_o(t)$ are the sensor faults. It is assumed that $rank\ (F) = h$ and $h < p$. The implication of this is that some of the sensors are assumed to be not potentially faulty. In the case of the identified model, $n = 15, m = 3, p = 10$ and $k = 4$. The number of faulty sensors h is left as a variable at this point.

The single observer method for robust sensor fault reconstruction in §6.5.2 will be used. Define a new state $z_3(t)$, a filtered version of $y(t)$, as

$$\dot{z}_3(t) = -A_{f,3}z_3(t) + A_{f,3}Cx(t) + A_{f,3}Du(t) + A_{f,3}Ff_o(t) + A_{f,3}R\xi(t, x, u) \tag{7.7}$$

where $-A_{f,3}$ is a stable filter matrix.

Combining (7.5) and (7.7) yields the following augmented state space system of order $n + p$

$$\begin{bmatrix} \dot{x}(t) \\ \dot{z}_3(t) \end{bmatrix} = \underbrace{\begin{bmatrix} A & 0 \\ A_{f,3}C & -A_{f,3} \end{bmatrix}}_{A_b} \begin{bmatrix} x(t) \\ z_3(t) \end{bmatrix} + \underbrace{\begin{bmatrix} B \\ A_{f,3}D \end{bmatrix}}_{B_b} u(t) + \underbrace{\begin{bmatrix} 0 \\ A_{f,3}F \end{bmatrix}}_{M_b} f_o(t) + \underbrace{\begin{bmatrix} 0 \\ A_{f,3}R \end{bmatrix}}_{Q_b} \xi(t, x, u) \tag{7.8}$$

$$z_3(t) = \underbrace{\begin{bmatrix} 0 & I_p \end{bmatrix}}_{C_b} \begin{bmatrix} x(t) \\ z_3(t) \end{bmatrix} \tag{7.9}$$

which has the same structure as equations (6.63) - (6.64) in §6.5.2. Since the system is open loop stable, the design method in §6.4 can be used to reconstruct the sensor fault $f_o(t)$ and yet be robust to the uncertainty/disturbance $\xi(t, x, u)$.

7.4.1 Validating the disturbance distribution matrix by actual implementation

The validity of the disturbance distribution matrix R obtained in (7.2) will now be tested by actually implementing it on a robust fault reconstruction scheme.

Firstly, it has been assumed that only sensors 1 - 5 are potentially faulty. Therefore the fault distribution matrix F from (7.6)

$$F = \begin{bmatrix} 1 & 0 & 0 & 0 & 0 \\ 0 & 1 & 0 & 0 & 0 \\ 0 & 0 & 1 & 0 & 0 \\ 0 & 0 & 0 & 1 & 0 \\ 0 & 0 & 0 & 0 & 1 \\ 0 & 0 & 0 & 0 & 0 \\ 0 & 0 & 0 & 0 & 0 \\ 0 & 0 & 0 & 0 & 0 \\ 0 & 0 & 0 & 0 & 0 \\ 0 & 0 & 0 & 0 & 0 \end{bmatrix}$$

The observer for the system (7.8) - (7.9) has been designed using the design method in §6.4. The design parameters D_1 from (6.44) and γ_o from (6.46) were specified to be $10I_{10}$ and unity respectively, while the filter matrix $A_{f,3}$ from (7.6) was specified to be $10I_{10}$. The design procedure gives $\gamma = 5.1979 \times 10^{-4}$. The observer gains are given in *aero/checkdist.mat*.

Figures 7.8, 7.9, 7.10 and 7.11 respectively show the response of the reconstruction signals to faults in sensors 1, 3, 4 and 5. As expected, since those sensors are not used in the controller, their faults do not generate a significant mismatch between the linear and nonlinear models, and hence their reconstructions are perfect.

Figures 7.12, 7.13 and 7.14 show the response of the fault reconstructions for a fault in sensor 2, at amplitudes of 0.2, 0.5 and 0.8 respectively. It can be seen from those figures that the reconstruction of the fault in sensor 2 is an almost perfect replica, and the coupling between the

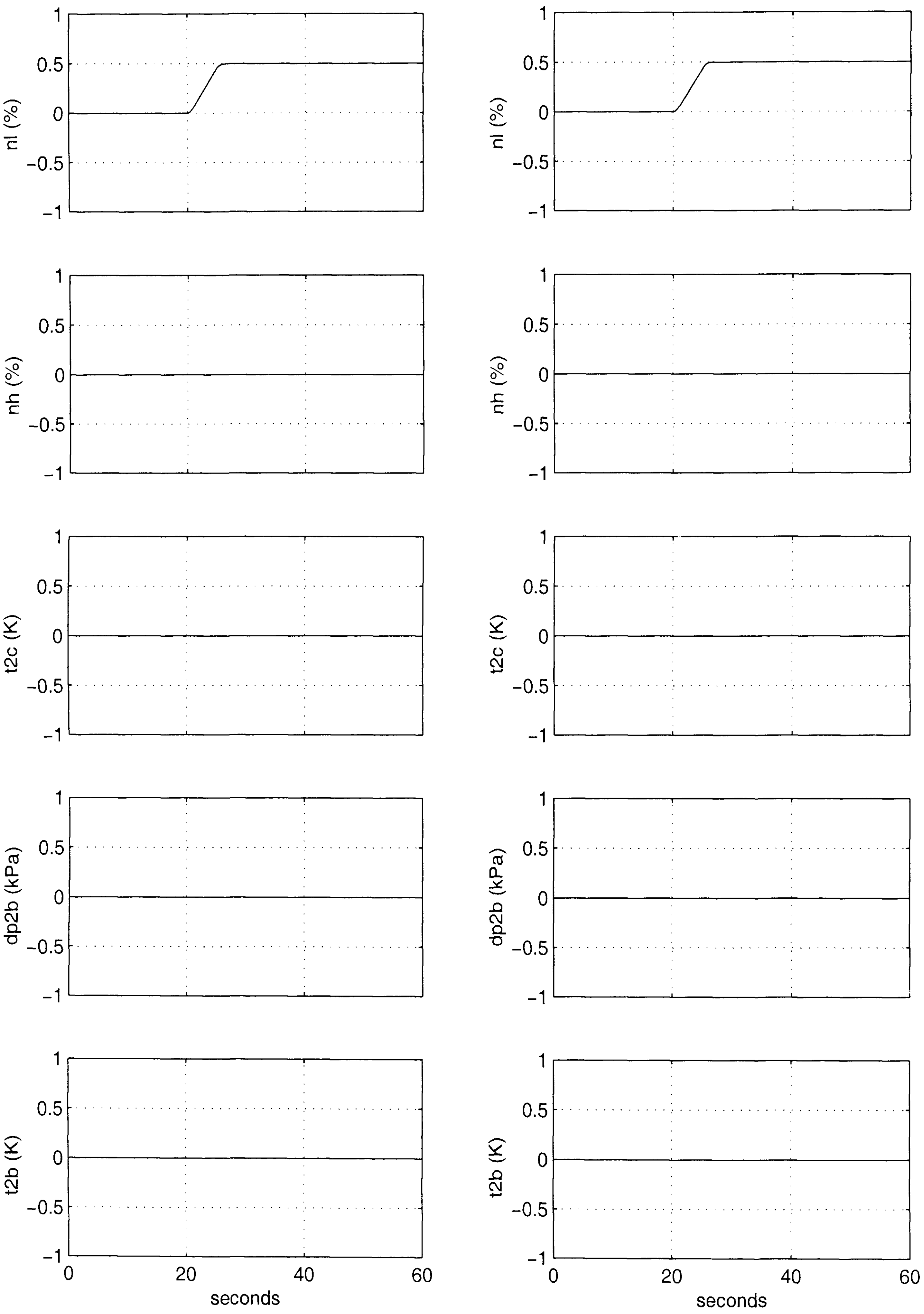

Figure 7.8: *Effect of a fault in sensor 1. The left subfigures are the faults, the right subfigures are their corresponding reconstructions.*

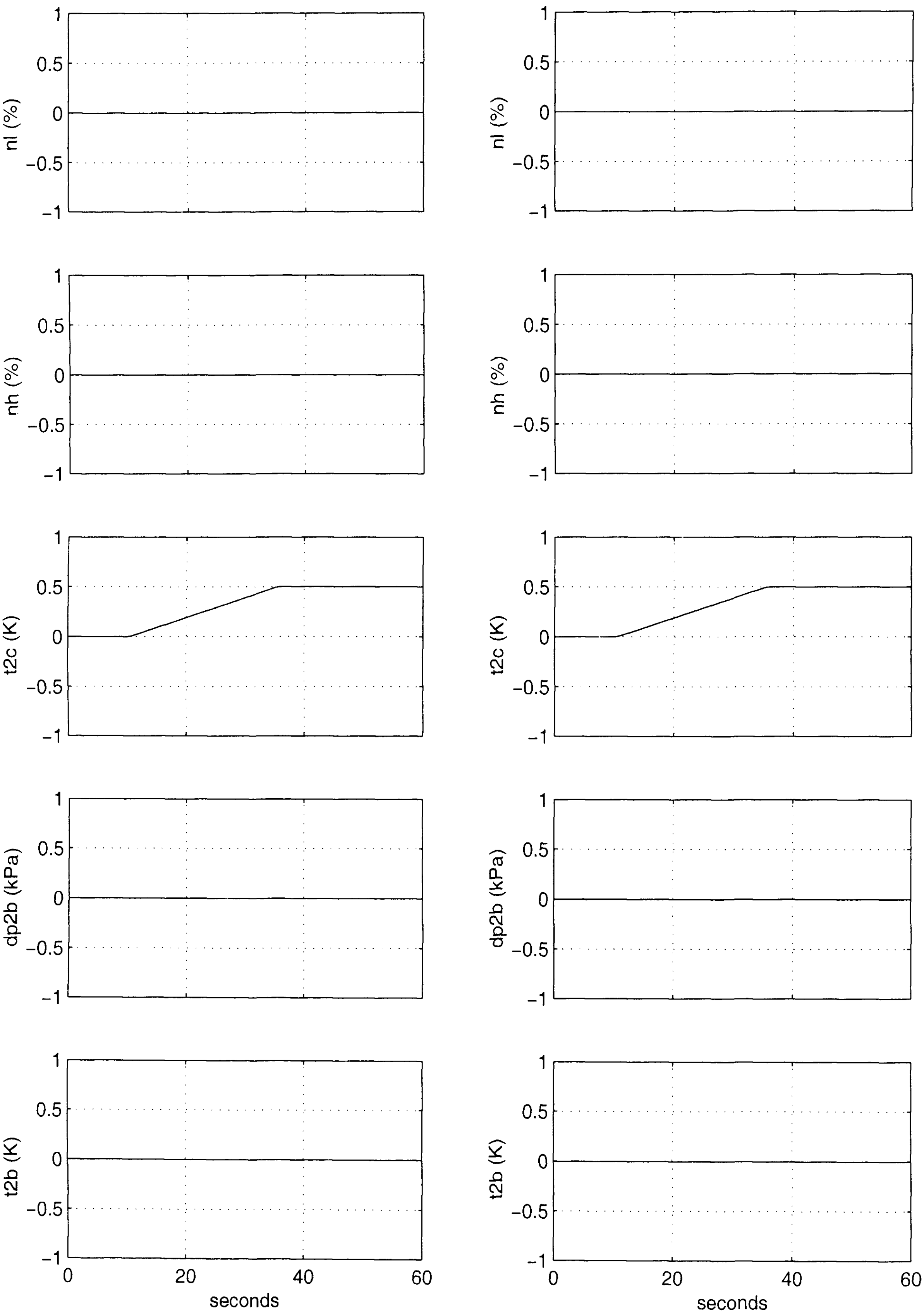

Figure 7.9: *Effect of a fault in sensor 3. The left subfigures are the faults, the right subfigures are their corresponding reconstructions.*

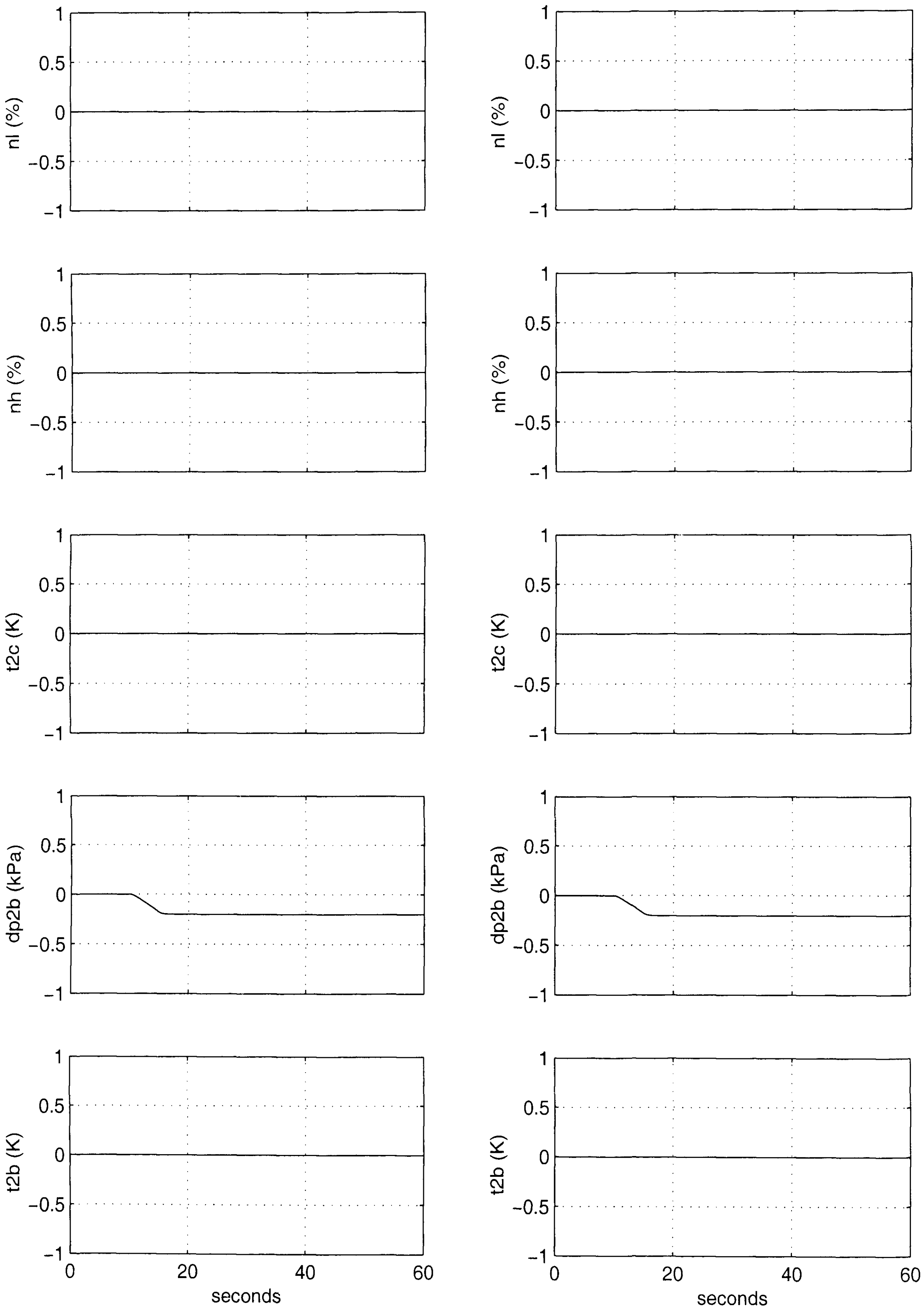

Figure 7.10: *Effect of a fault in sensor 4. The left subfigures are the faults, the right subfigures are their corresponding reconstructions.*

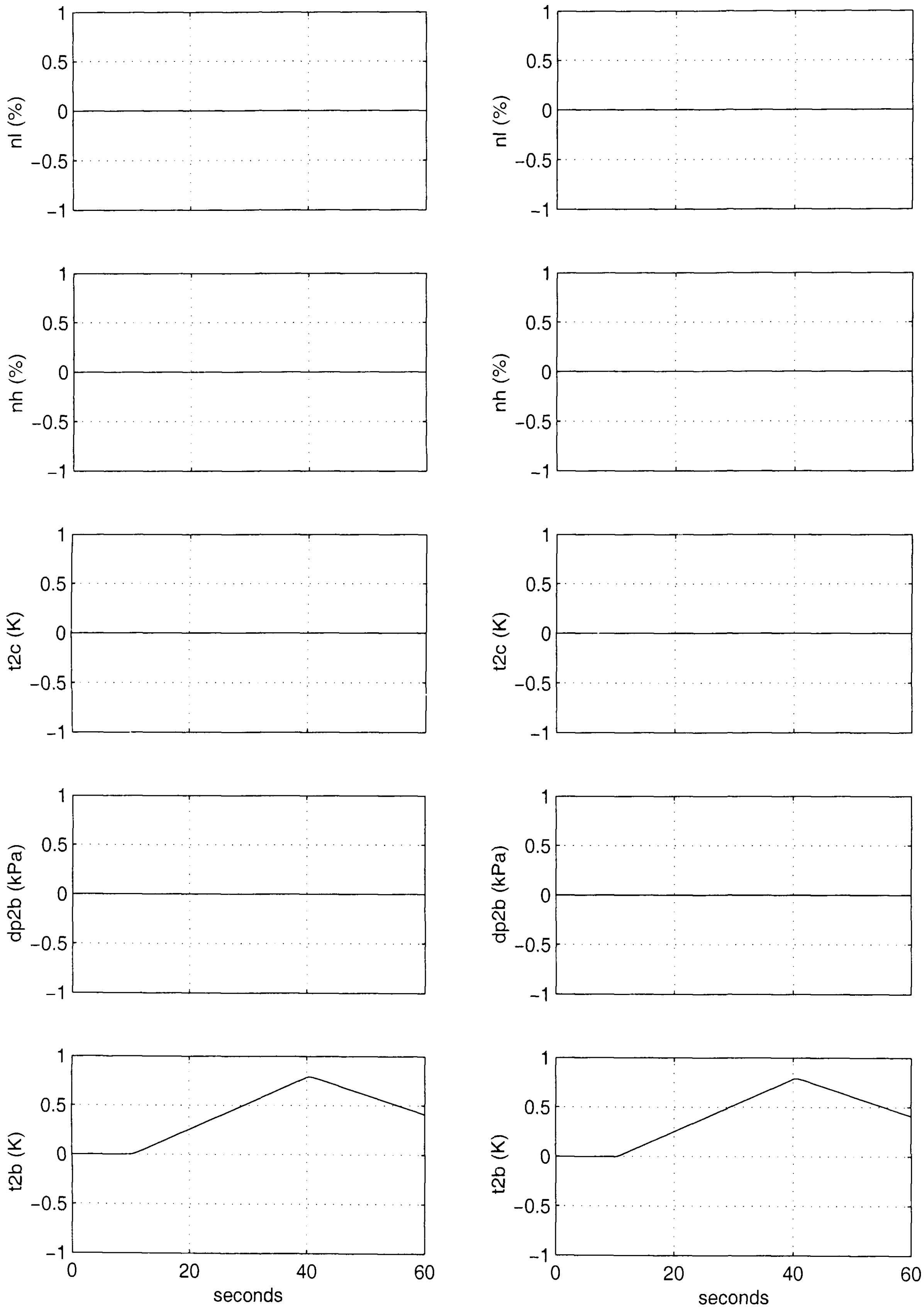

Figure 7.11: *Effect of a fault in sensor 5. The left subfigures are the faults, the right subfigures are their corresponding reconstructions.*

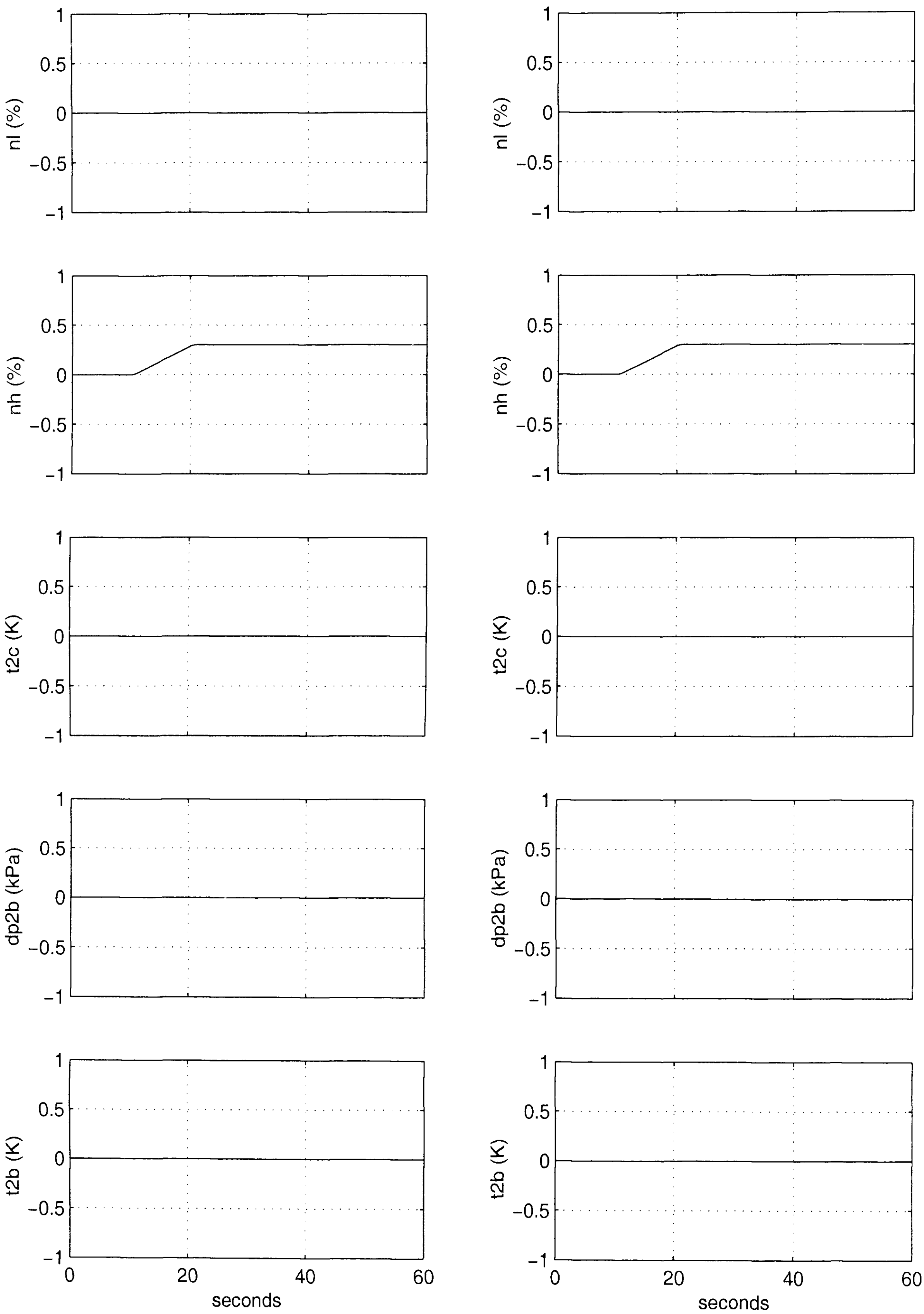

Figure 7.12: *Effect of a fault in sensor 2, of height 0.3. The left subfigures are the faults, the right subfigures are their corresponding reconstructions.*

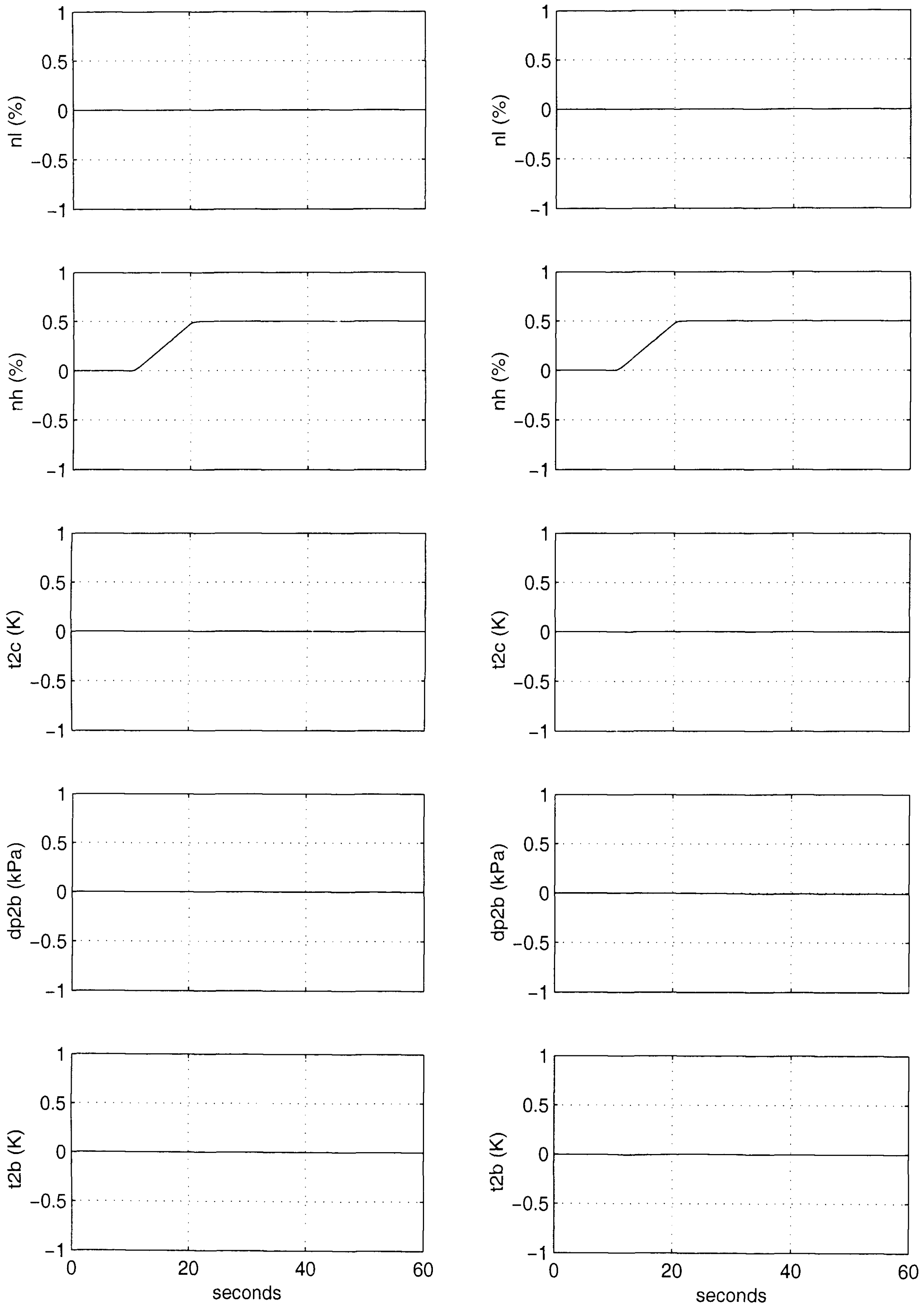

Figure 7.13: *Effect of a fault in sensor 2, of height 0.5. The left subfigures are the faults, the right subfigures are their corresponding reconstructions.*

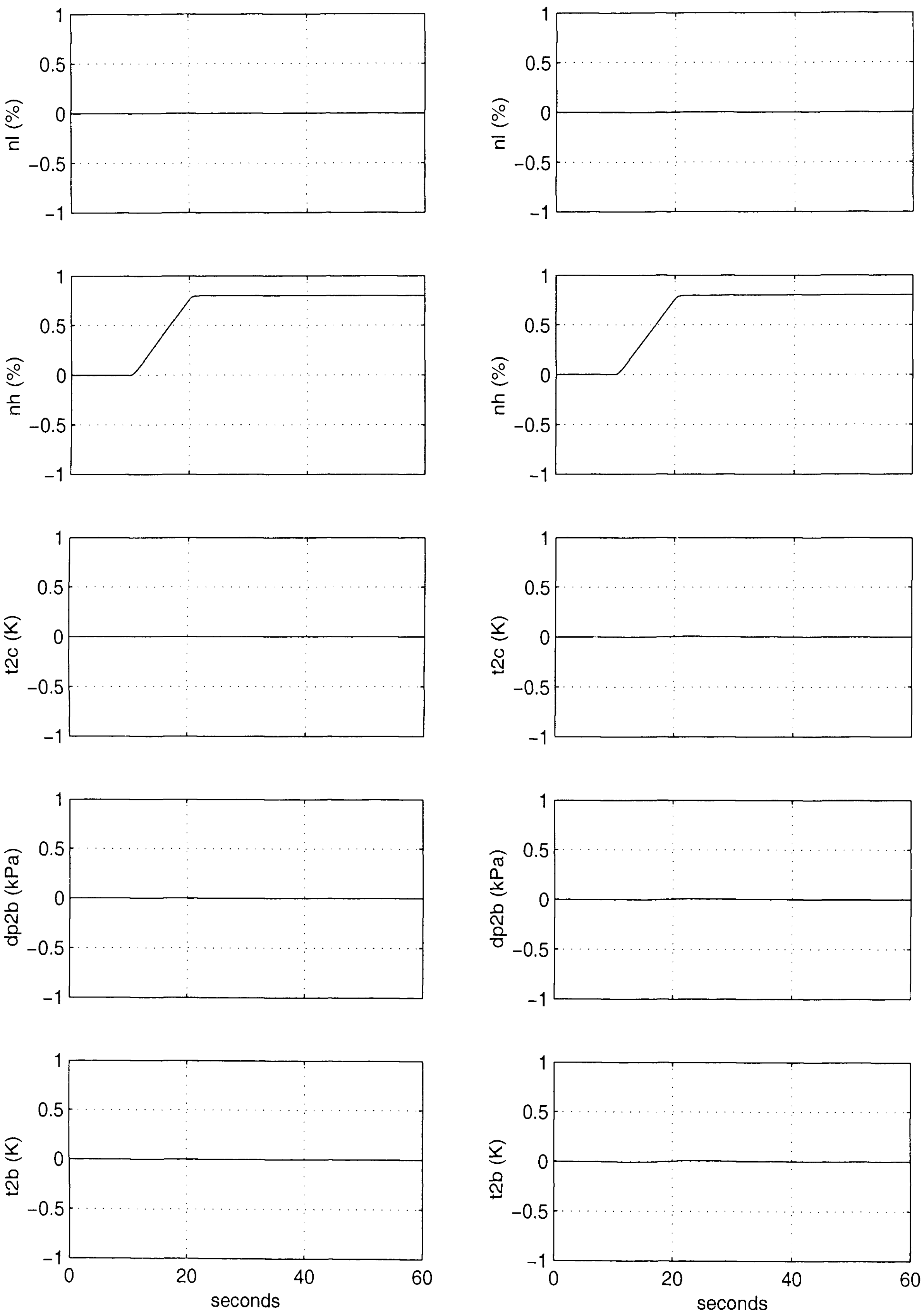

Figure 7.14: *Effect of a fault in sensor 2, of height 0.8. The left subfigures are the faults, the right subfigures are their corresponding reconstructions.*

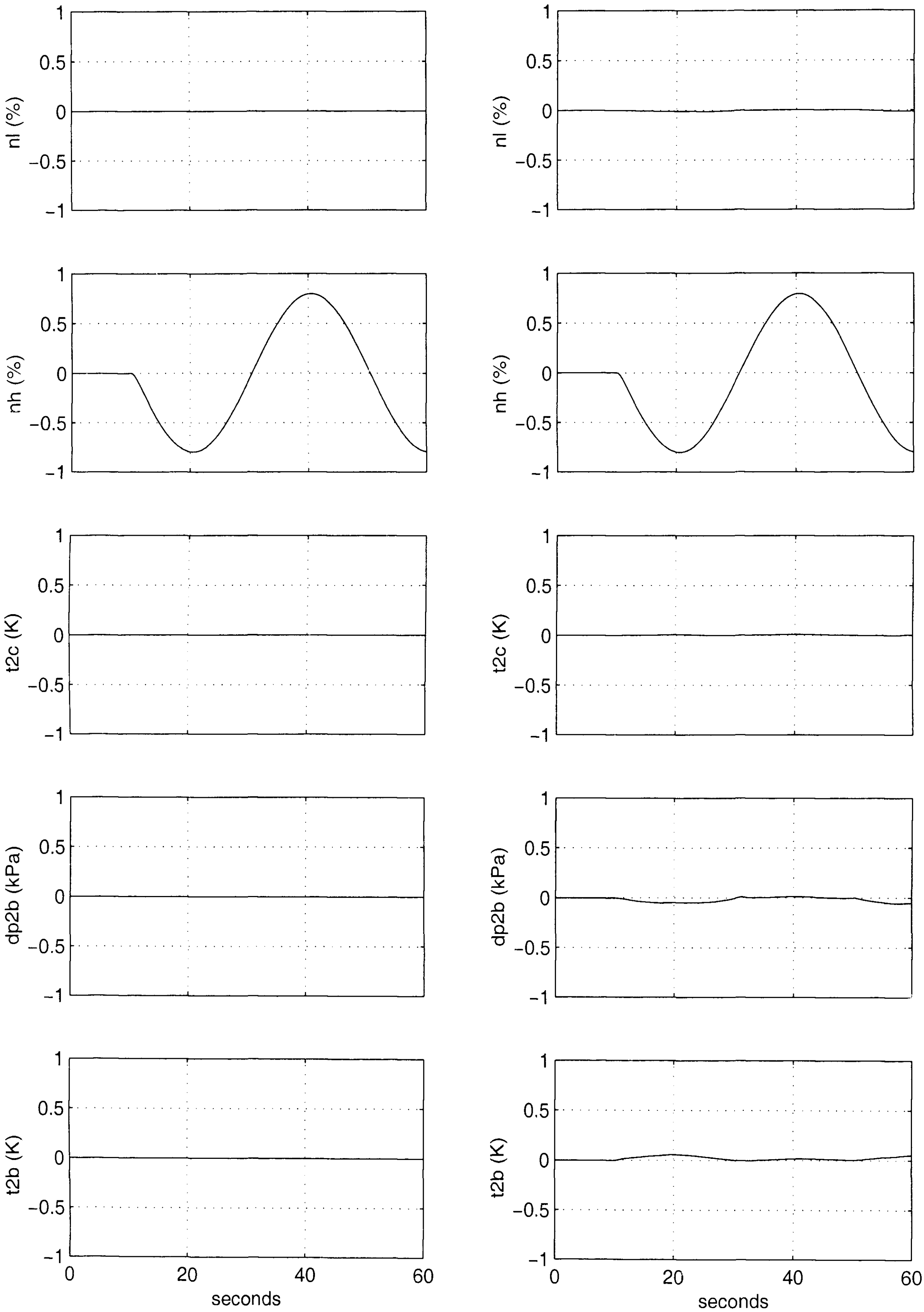

Figure 7.15: *Effect of a sine wave fault in sensor 2. The left subfigures are the faults, the right subfigures are their corresponding reconstructions.*

other channels is very small. This is not surprising, and is due to the small value of γ obtained. However, comparing Figure 7.12 with Figure 7.14, it is obvious that the larger the magnitude of the fault, the quality of the reconstruction reduces slightly. This is because of a greater magnitude of mismatch between the linear and nonlinear models. Figure 7.15 shows the fault reconstructions for a sine wave fault in sensor 2. It can be seen that the reconstruction captures the fault well. Even though the coupling between reconstruction channels (in particular channels 4 and 5) are bigger, they are still relatively small. This shows that the approximation for the disturbance distribution matrix R in (7.2) is a suitable one, and can be used also for the case of sinusoidal waves even though it was obtained using a ramp signal.

7.5 Robust sensor fault reconstruction assuming that no more than one sensor is faulty at any given time

In this section, a robust sensor fault reconstruction scheme will be presented, where *all sensors are assumed to be fault prone*, but *only one sensor is assumed to be faulty at any given time*; this is the key assumption.

For this case, two sliding mode observers were designed.

Observer A : This has been designed using the design method in Chapter 6, assuming that only sensor 2 is subject to faults. Therefore in this case the sensor fault distribution matrix

$$F = \begin{bmatrix} 0 & 1 & 0 & 0 & 0 & 0 & 0 & 0 & 0 & 0 \end{bmatrix}^T$$

The filter matrix was chosen to be $A_{f,3} = 10\ I_{10}$. The design parameters from (6.42) and (6.44) were chosen to be $D_1 = 10I_{10}, \gamma_o = 0.1$. The design method in §6.4 yielded a value of $\gamma = 9.2089 \times 10^{-4}$, which is the upper bound on the $\mathcal{L}_2$ gain from the disturbance to the fault reconstruction. This observer should therefore be able to reconstruct a fault in sensor 2 without any significant corruption, and will produce only one reconstruction signal (the fault in sensor 2).

Observer B : This has been designed using the LQG-like method in §4.4 assuming that sensor

2 is completely reliable. Therefore in this case

$$F = \begin{bmatrix} 1 & 0 & 0 & 0 & 0 & 0 & 0 & 0 & 0 \\ 0 & 0 & 0 & 0 & 0 & 0 & 0 & 0 & 0 \\ 0 & 1 & 0 & 0 & 0 & 0 & 0 & 0 & 0 \\ 0 & 0 & 1 & 0 & 0 & 0 & 0 & 0 & 0 \\ 0 & 0 & 0 & 1 & 0 & 0 & 0 & 0 & 0 \\ 0 & 0 & 0 & 0 & 1 & 0 & 0 & 0 & 0 \\ 0 & 0 & 0 & 0 & 0 & 1 & 0 & 0 & 0 \\ 0 & 0 & 0 & 0 & 0 & 0 & 1 & 0 & 0 \\ 0 & 0 & 0 & 0 & 0 & 0 & 0 & 1 & 0 \\ 0 & 0 & 0 & 0 & 0 & 0 & 0 & 0 & 1 \end{bmatrix}$$

The rationale for using the design method in §4.4 is because the assumption for this observer (that sensor 2 is not faulty) implies that there should be no mismatches present when all sensors except sensor 2 are faulty. Therefore the issue of robustness does not arise and the matrix R does not need to be incorporated into the design. The filter matrix was chosen to be $A_{f,3} = 10\ I_{10}$ and observer weighting matrices from inequality (4.39) in §4.4 were chosen to be $W_b = 0.1\ I_{25}$ and $V_b = I_{10}$. This observer will produce nine reconstruction signals, which are for faults in all sensors except sensor 2. The gains for both the observers are available in *aero/1fault.mat*.

The fault reconstruction logic is as follows: if a fault occurs on sensor 2, Observer A will reconstruct the fault almost perfectly, but Observer B will generate non-zero reconstructions of no particular signature, because the assumption which Observer B was based on (that sensor 2 is perfect) had been violated. It is then easy to say that the fault is from sensor 2, and the reconstruction from Observer A is the valid one based on the assumption that only one sensor can be faulty at any given time. If a fault occurs on any other sensor, then Observer B will reconstruct the fault properly (leaving the eight other reconstruction signals at zero). Observer A will have a nonzero reconstruction, but it is easy to discriminate that this is not a fault on sensor 2, because only 1 reconstruction signal from Observer B is nonzero in accordance with the assumption of only one faulty sensor at a time.

Figures 7.16 - 7.25 show the reconstructions by both observers when faults were injected into sensors 1 - 10. The dotted line is the actual fault, and the solid lines are the reconstructions. The reconstruction for a fault in sensor 2 was taken from Observer A, whereas the reconstruction for faults in the other sensors were taken from Observer B. It can be seen that when a fault

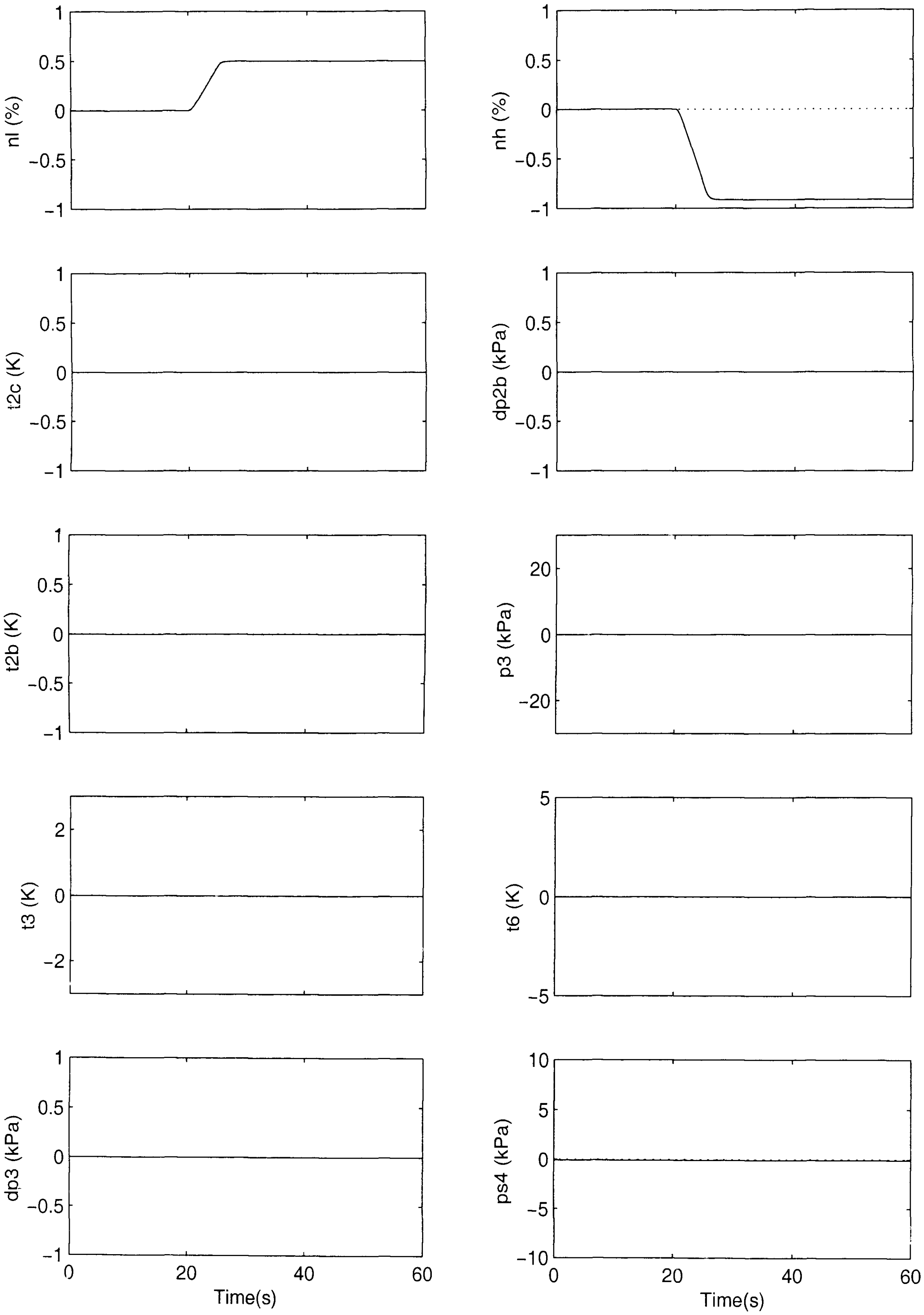

Figure 7.16: *The effect of a fault on sensor 1. The dotted line is the actual fault, whereas the solid lines are the reconstruction by the observers.*

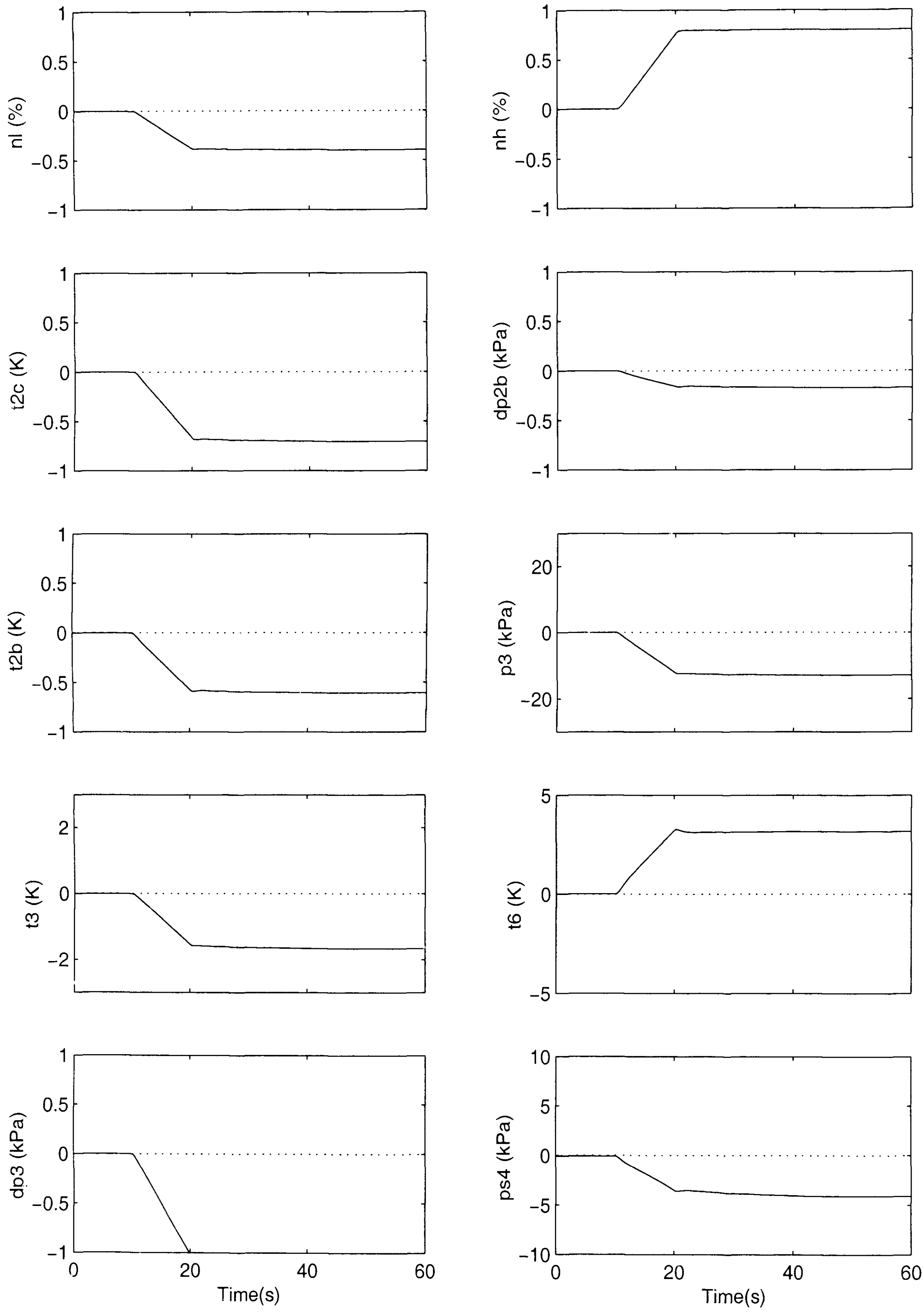

Figure 7.17: *The effect of a fault on sensor 2. The dotted line is the actual fault, whereas the solid lines are the reconstruction by the observers.*

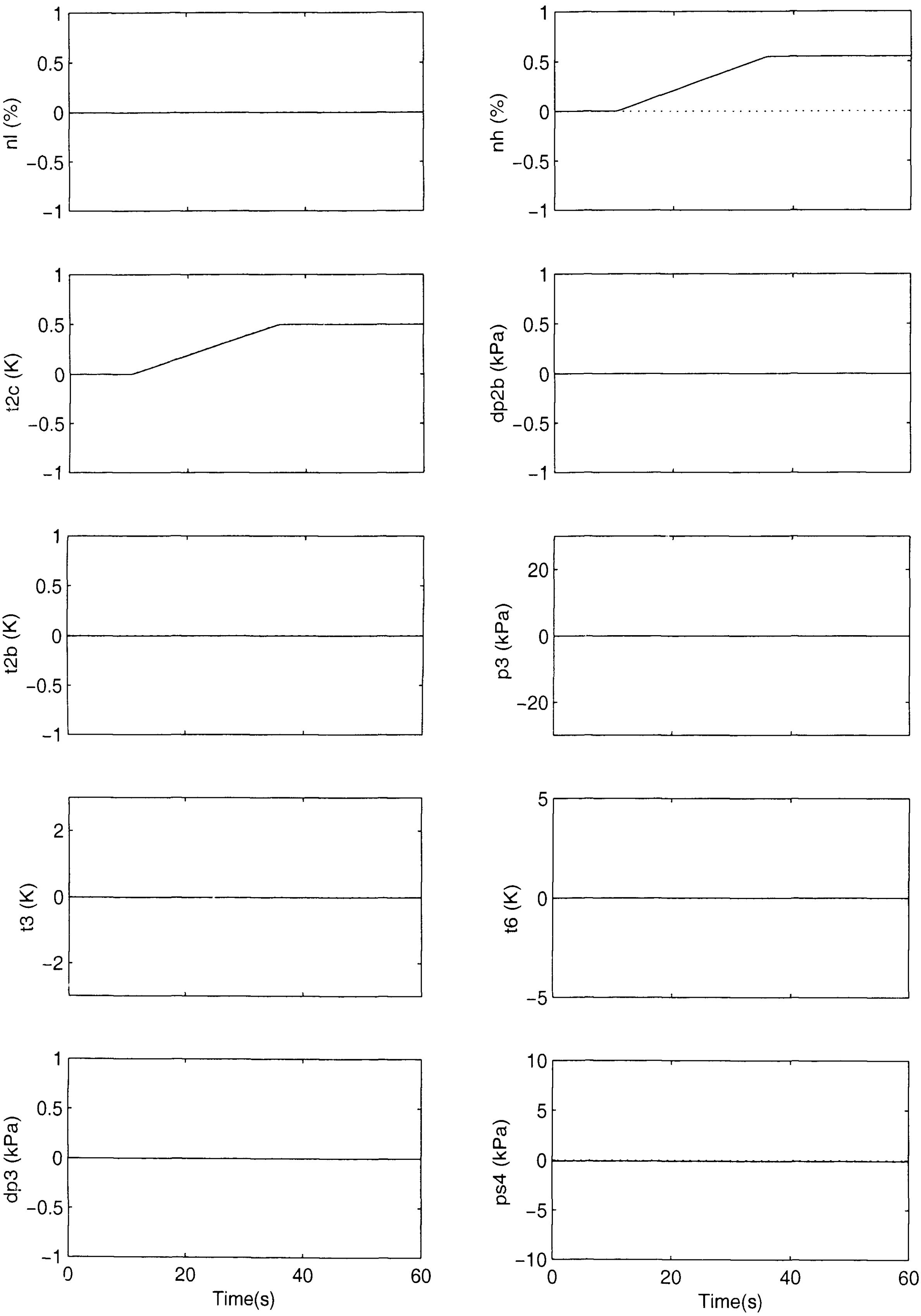

Figure 7.18: *The effect of a fault on sensor 3. The dotted line is the actual fault, whereas the solid lines are the reconstruction by the observers.*

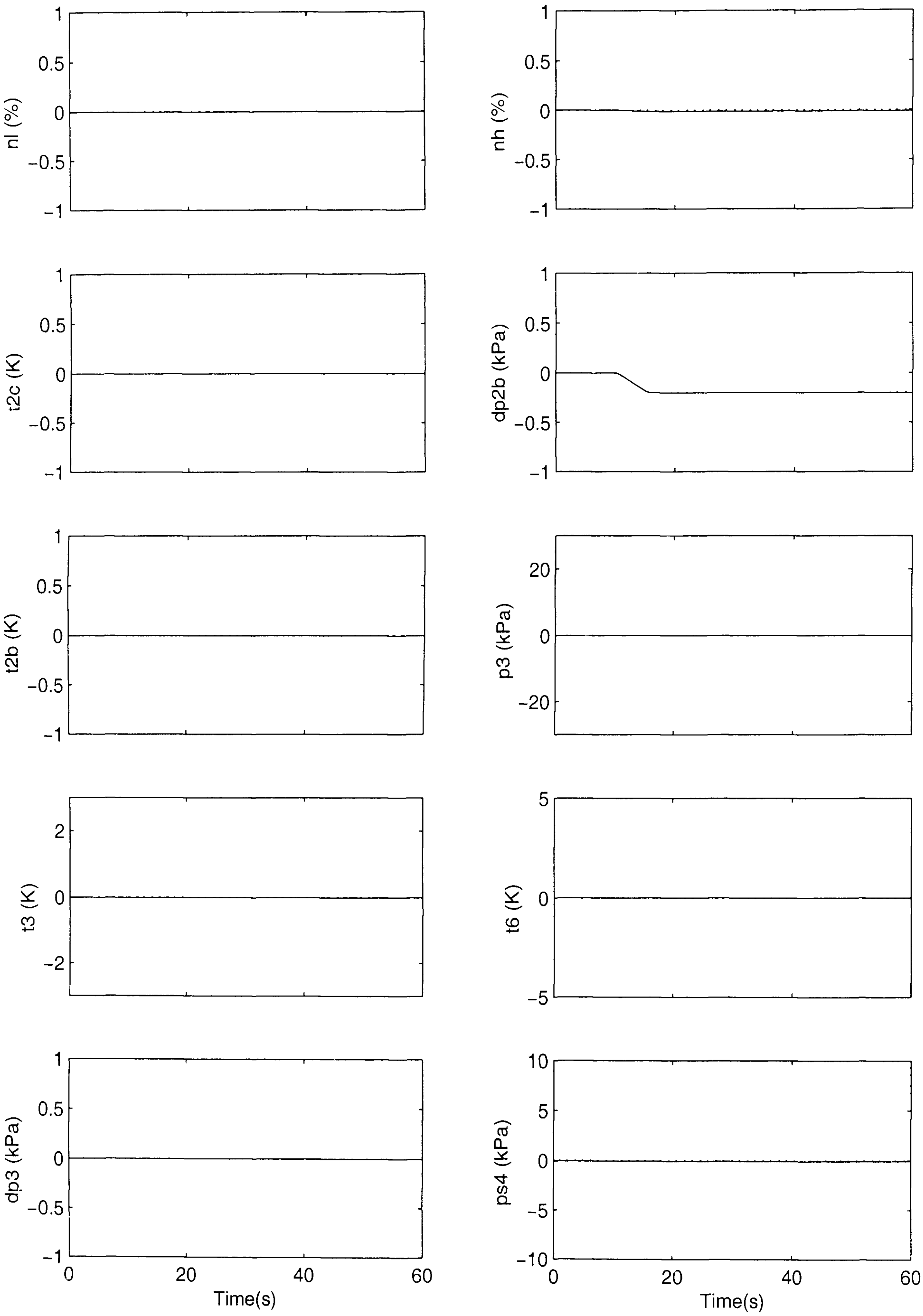

Figure 7.19: *The effect of a fault on sensor 4. The dotted line is the actual fault, whereas the solid lines are the reconstruction by the observers.*

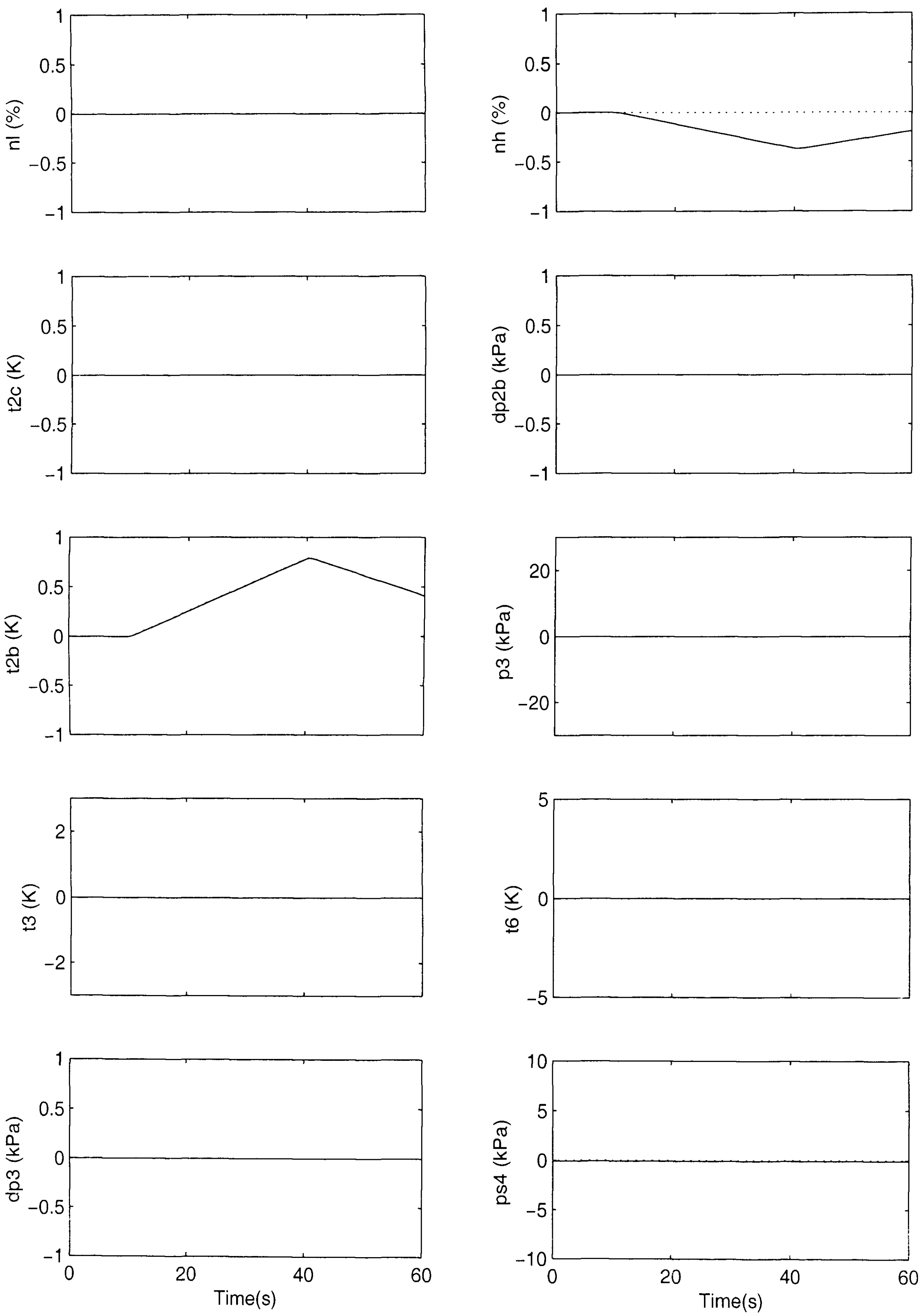

Figure 7.20: *The effect of a fault on sensor 5. The dotted line is the actual fault, whereas the solid lines are the reconstruction by the observers.*

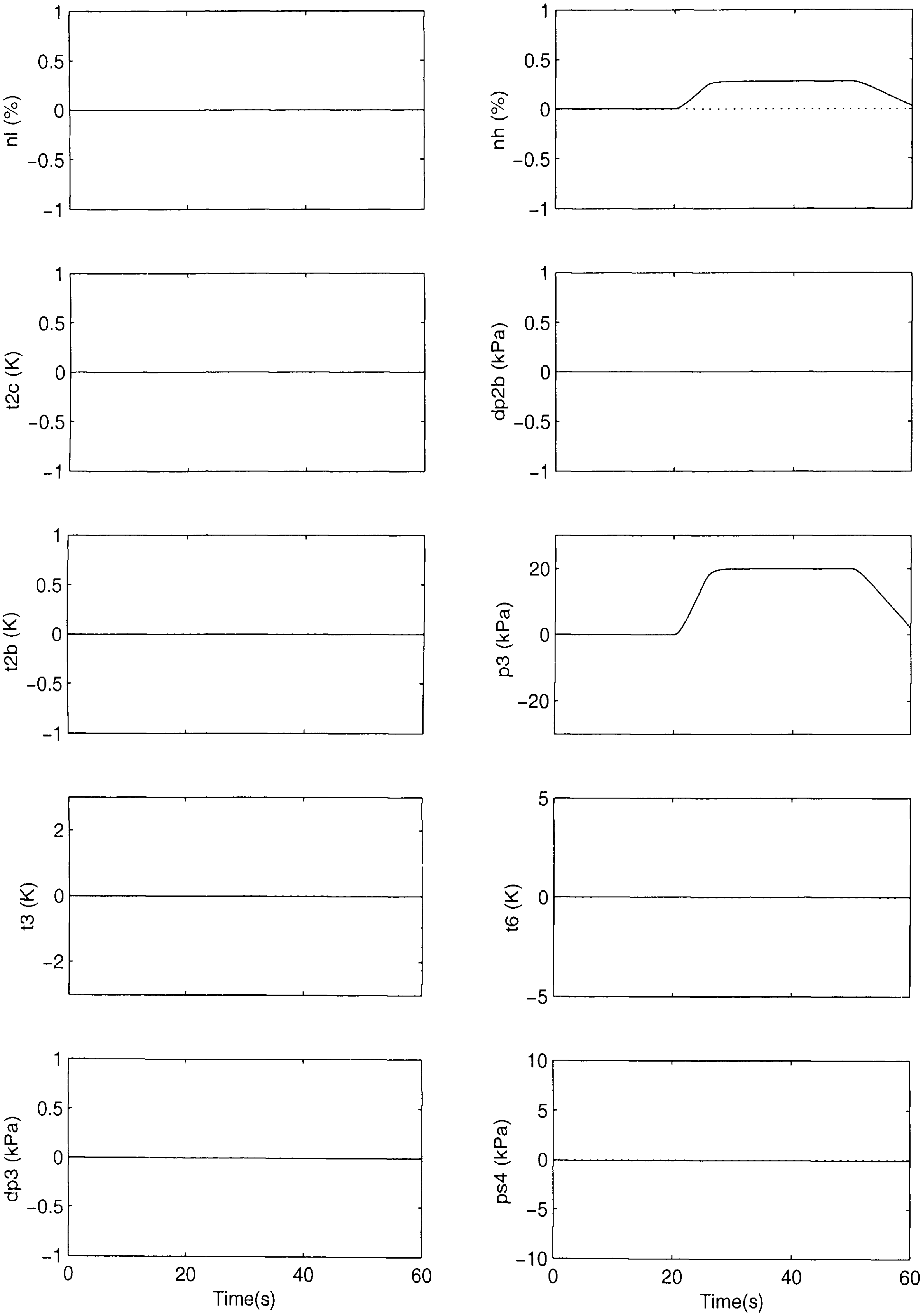

Figure 7.21: *The effect of a fault on sensor 6. The dotted line is the actual fault, whereas the solid lines are the reconstruction by the observers.*

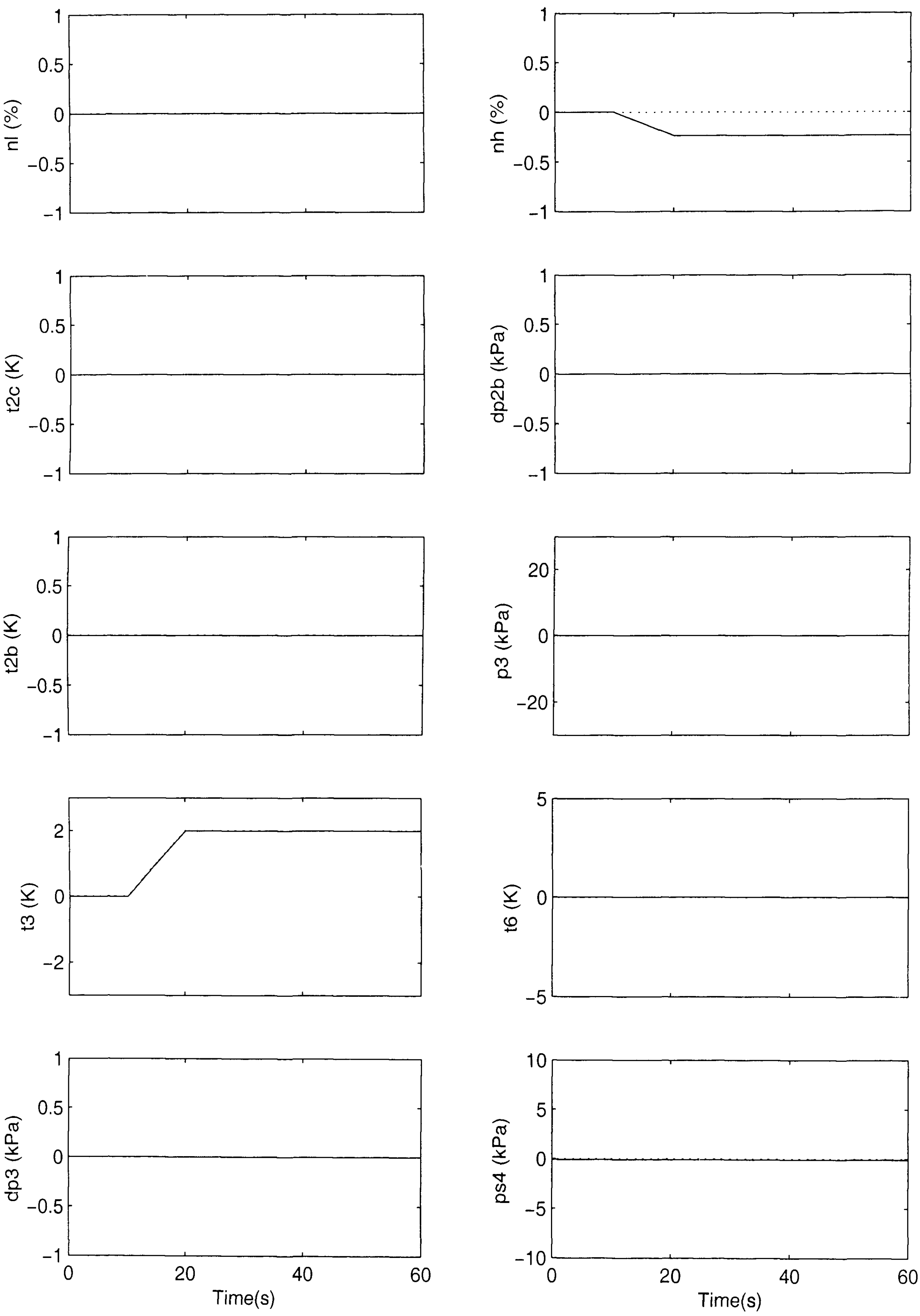

Figure 7.22: *The effect of a fault on sensor 7. The dotted line is the actual fault, whereas the solid lines are the reconstruction by the observers.*

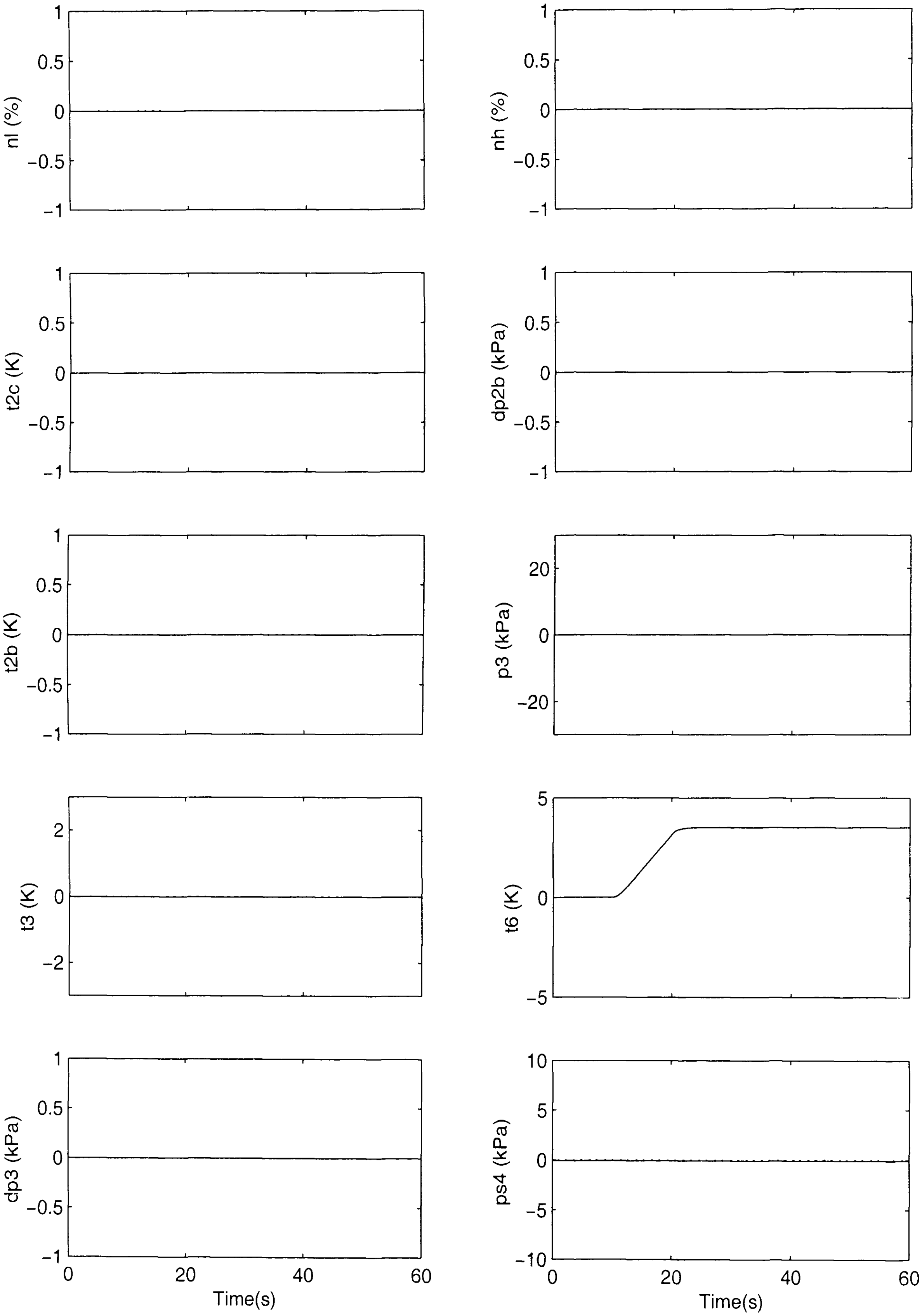

Figure 7.23: *The effect of a fault on sensor 8. The dotted line is the actual fault, whereas the solid lines are the reconstruction by the observers.*

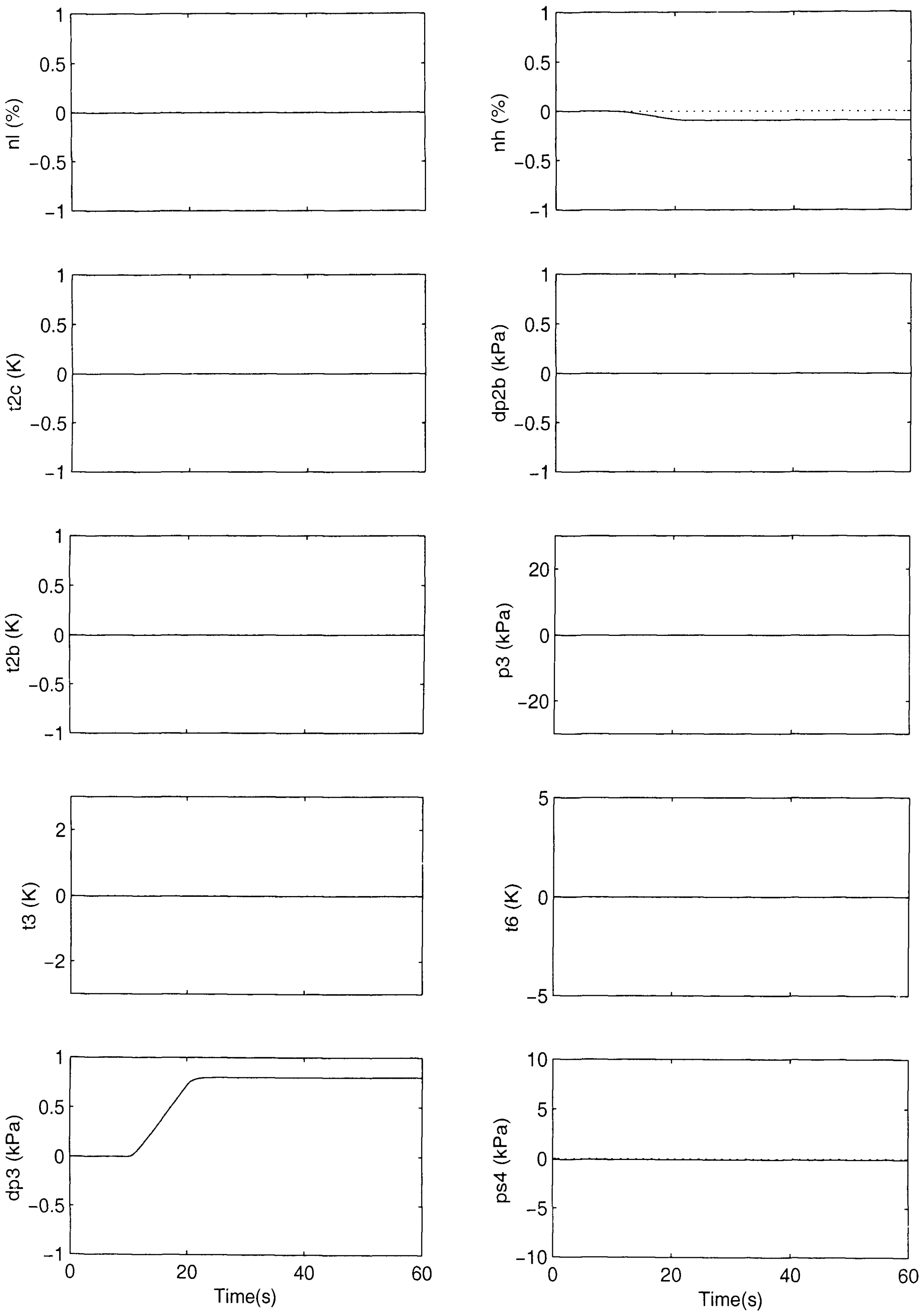

Figure 7.24: *The effect of a fault on sensor 9. The dotted line is the actual fault, whereas the solid lines are the reconstruction by the observers.*

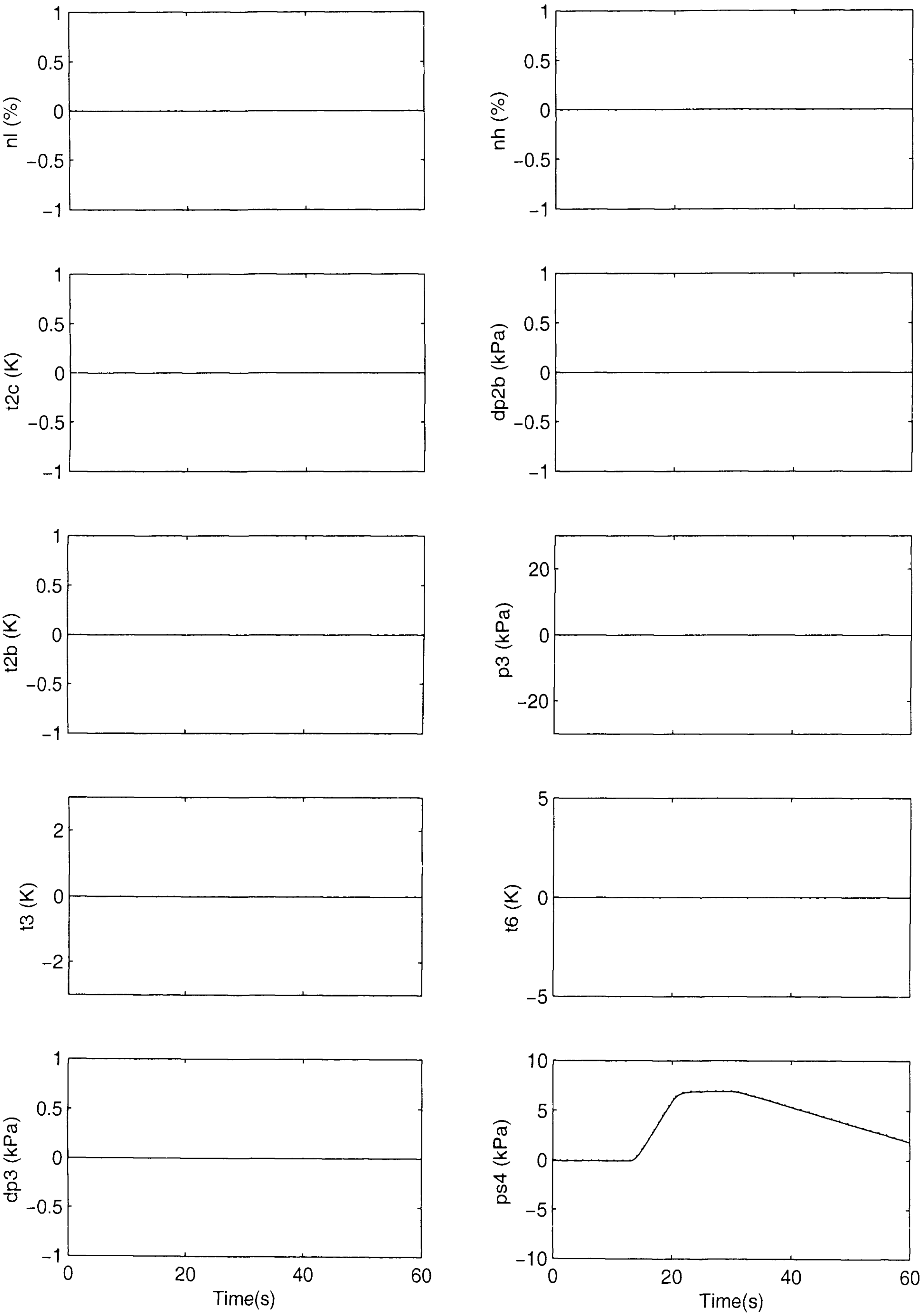

Figure 7.25: *The effect of a fault on sensor 10. The dotted line is the actual fault, whereas the solid lines are the reconstruction by the observers.*

occurs in sensor 2, Observer A reconstructs the fault perfectly, while Observer B produces nonzero reconstructions of no specific signature. When a fault occurs in any other sensor, Observer B reconstructs the fault perfectly (leaving the other reconstructions zero), and Observer A produces a nonzero reconstruction.

7.6 Conclusion

This chapter has presented an application of the robust sensor fault reconstruction scheme from Chapter 6 to a nonlinear model of an aero-engine.

Firstly, system identification was used to obtain a linear approximation of the engine. Then, an uncertainty distribution matrix to capture the linear/nonlinear model mismatch due to a fault in sensor 2 was derived. The approximation was verified to be a good one.

Finally, by using the identified model as well as the uncertainty distribution matrix, a sensor fault reconstruction scheme was designed, based on the assumption that only one sensor can be faulty at any given time. For this purpose, two observers were designed, each assuming certain sensors were faulty and the rest were perfect. Using an appropriate logic sequence, successful reconstruction and discrimination of the sensor faults was attained.

Acknowledgement

The author wishes to thank QinetiQ Ltd. for supplying the simulation model of the Spey engine and for advice in connection with this work. Any views expressed are those of the author and do not necessarily represent those of QinetiQ Ltd.

Chapter 8

Conclusion and future work

This chapter presents the conclusion and summarises the main contributions of this thesis, as well as some suggestions for further work.

8.1 Conclusions

In Chapter 4, a new design method for the Edwards - Spurgeon observer [23] was presented. In their previous design method, which was summarised at the end of Chapter 3, the sliding motion (parameterised by the matrix L^o) and linear gain (the matrix G_l of specific structure) were designed separately. This does not fully utilise all the freedom available in both design parameters. In the new method in this thesis, they were both designed together in one step, hence exploiting all possible degrees of freedom. The observer was designed using a Riccati inequality resembling one associated with a sub-optimal LQG observer. As in standard LQG theory, two weighting matrices influence the solution. In implementing this design method, it was found that the reduced order sliding motion also had a sub-optimal LQG interpretation. Furthermore, it is possible to impose additional inequalities to force the poles of the sliding motion to lie in certain convex regions of the complex plane. Finally, a modification to the design method was presented, incorporating additional inequalities to force the eigenvalues of the linear part of the observer to lie in certain regions of the complex plane. All the design methods can be posed as convex optimisation problems, implemented using LMIs and solved using standard software.

In Chapter 5 improvements to the sensor fault reconstruction methods of Edwards *et al.* [27, 26] have been presented. In the work of Edwards *et al.* [27, 26], actuator faults are very efficiently reconstructed using sliding mode observers. However, in their sensor fault reconstruction method, the dynamics of the fault and sliding motion were both neglected and only the steady-state components of the sensor fault could be replicated. Hence, the sensor fault reconstructions were corrupted by the dynamics of both the fault and the sliding motion. The improvements presented in this thesis are based on the actuator fault reconstruction method by Edwards *et al.* [27, 26]. By filtering certain signals, 'fictitious systems' that treat the sensor faults as 'actuator faults' can be obtained. The actuator fault reconstruction method by Edwards *et al.* [27, 26] can then be applied to the fictitious systems to efficiently reconstruct the sensor fault. Three methods were presented; the first one is able to reconstruct the sensor faults perfectly, under the condition that the original system must be open loop stable. The second method can also reconstruct the sensor fault perfectly and needs only certain (maybe none) of the modes of the open loop system to be stable. However, in this approach only certain sensors are allowed to be potentially faulty (and thus in general a bank of observers may need to be designed). The third method allows for all sensors to be potentially faulty and only needs the original system matrix to be full rank, with the compromise that the dynamics of the sensor fault are neglected in the analysis. This results in the reconstruction of the fault being corrupted by its dynamics. However, this is still an improvement on the method by Edwards *et al.* [27, 26] as its reconstruction is not corrupted by the dynamics of the sliding motion, and its corruption by the fault dynamics are not as severe.

In Chapter 6, this thesis has presented a new method for designing sliding mode observers to robustly reconstruct faults despite the presence of system uncertainty. In previous fault reconstruction work using the Edwards - Spurgeon observer [27, 26], there was no direct consideration of robustness built into the design. The method in Chapter 6 uses LMIs to design the observer gains as well as a scaling of the equivalent output error injection (that generates the fault reconstruction) so that the upper bound of the $\mathcal{L}_2$ gain from the uncertainty to the fault reconstruction is minimised. The problem was initially formulated for the case of actuator faults. Then the method was extended to the case of sensor faults by using the approach in Chapter 5 i.e. - filtering certain signals to generate 'fictitious systems' that treat the sensor faults as 'actuator faults'. In this design method, knowledge about the distribution matrix for the uncertainty in the system is required.

A robust sensor fault reconstruction case study is described in Chapter 7. The case study is based on a nonlinear model of a Spey aero-engine. System identification was used to obtain a linear model of the engine. It was found that a fault in the second sensor causes mismatches between the nonlinear and identified models. To apply the design method in Chapter 6, a representation of the mismatch due to a fault in the second sensor was obtained and it was found to be a good representation. A robust sensor fault reconstruction scheme was then presented, based on the assumption that only one sensor is potentially faulty at any given time. This was implemented using two sliding mode observers in parallel with the engine, each observer designed assuming that different sensors could be potentially faulty. Based on the reconstructions obtained from both observers, a logic sequence was used to identify the faulty sensor.

8.2 Future work

Throughout this thesis, the reconstruction schemes work on the assumption that the fault is known to be either an actuator or sensor fault. Without any a-priori knowledge or assumption, in practice it will be difficult to differentiate an actuator fault from an incipient sensor fault (step sensor faults are relatively straightforward to distinguish from actuator faults since the sliding motion is broken). A possible avenue to solve this would be to design two observers; the first for sensor fault reconstruction, robust to actuator faults (treating the actuator faults as uncertainty), and the second observer designed just for actuator fault reconstruction. A logic sequence could then be used to determine whether the fault is from the actuator or the sensor. Another possibility is to filter the output, to obtain a system whose 'actuator fault' vector comprises the original system's actuator and sensor faults. This is better than the previously suggested method, as both actuator and sensor faults could occur simultaneously and all faults could be reconstructed and distinctively identified.

In Chapter 6, the value of the nonlinear gain scaling the switched term is required to be quite large for sliding motion to occur. The value given is very conservative. It would be therefore desirable to obtain a formulation in which the gain is not so conservatively large. A possible method would be to incorporate this gain as a variable when designing the other gain matrices of the sliding mode observer.

In Chapter 7, the sensor fault reconstruction was presented for the aero-engine in which only one sensor was assumed to be faulty at any given time. This is somewhat restrictive. Sensor fault reconstruction schemes for more than one faulty sensor at a time can be developed. The concept of the logic sequence method in Chapter 7 can still be used. However, it will be more challenging and difficult, as there are many more fault scenarios to deal with when the number of faulty sensors is allowed to increase.

Furthermore in Chapter 7 sensor fault reconstruction was performed at a steady-state operating condition of $nh = 90\%$. It is desirable to be able to perform the fault reconstruction at different operating conditions. A suggested method would be to obtain steady-state input-output data for the engine at different operating conditions, then manually compensate the system when the engine changes operating condition using a look-up table.

Only sensor fault reconstruction was performed in Chapter 7. Even though this is very widely performed in the literature, it would be useful to develop a robust actuator fault reconstruction scheme. This however, will be much more difficult and challenging than sensor fault reconstruction, because in the case of sensor faults, only a fault in sensor 2 exposes significant mismatches between the linear and nonlinear models. In the case of actuator faults, a fault in any of the three actuators could cause mismatches. Therefore the mismatch representation will need to take into consideration all three sources of mismatch.

Appendix A

Linear Matrix Inequalities

A.1 Introduction

Linear Matrix Inequalities (LMIs) [3] have been used extensively in this thesis to design sliding mode observers. Many problems in system and control theory (for example LQR and $\mathcal{H}_\infty$) can be reduced to a few standard problems involving LMIs.

An LMI has the form

$$F(x) = F_0 + \sum_{i=1}^{m} x_i F_i > 0 \tag{A.1}$$

where $x \in \mathcal{R}^m$ is a vector whose scalar elements are the so-called LMI variable(s) and the *symmetric matrices* F_i, $i = 0, ..., m$ are given quantities. The inequality sign in (A.1) implies that $F(x)$ is positive definite.

A.1.1 LMI problems

From a theoretical viewpoint LMI problems can be split into

a. Feasibility problems: find a value for the LMI variable vector x that satisfies the LMI system

$$\mathcal{A}(x) < \mathcal{B}(x)$$

where $\mathcal{A}(x)$ and $\mathcal{B}(x)$ are affine functions in x (such as those in (A.1)). The corresponding solver in the Matlab LMI toolbox [39] is called $feasp$.

b. Minimisation of a linear objective problem: minimise $f(x)$, where $f(x)$ is an affine function in x that satisfies

$$\mathcal{A}(x) < \mathcal{B}(x)$$

The corresponding solver is called $mincx$.

c. Generalised eigenvalue problem: minimise the scalar λ subject to

$$\mathcal{A}(x) < \mathcal{B}(x)$$

$$0 < \mathcal{D}(x)$$

$$\mathcal{C}(x) < \lambda\mathcal{D}(x)$$

where $\mathcal{C}(x)$ and $\mathcal{D}(x)$ are affine functions in x. The corresponding solver is called $gevp$.

A.2 The Schur complement

In the application of LMIs to many control theory problems, the Schur complement [3] is used very extensively. It is used to transform nonconvex LMIs into convex ones, widely increasing the scope of problems that can be solved. Examples of these will be given in the following sections.

Given the decomposition of a symmetric matrix S as

$$S = \begin{bmatrix} S_{11} & S_{12} \\ S_{12}^T & S_{22} \end{bmatrix} < 0 \tag{A.2}$$

From the Schur complement [3], the following statements are equivalent:

$$S < 0 \tag{A.3}$$

$$S_{11} < 0,\ S_{22} - S_{12}^T S_{11}^{-1} S_{12} < 0 \tag{A.4}$$

$$S_{22} < 0,\ S_{11} - S_{12} S_{22}^{-1} S_{12}^T < 0 \tag{A.5}$$

Suppose S_{11}, S_{12}, S_{22} are LMI variables. Then the expressions in (A.4) and (A.5) which are not affine can be recasted as an affine inequality in (A.2).

A.3 Basic LMI formulation

As an example of a feasibility problem, consider the issue of Lyapunov stability. The matrix A is stable if and only if there exists a symmetric positive definite matrix P that satisfies

$$PA + A^T P < 0 \tag{A.6}$$

For a given matrix A this problem can be posed as an LMI feasibility problem :
find a symmetric matrix P that satisfies the LMI system

$$\begin{aligned} PA + A^T P &< 0 && \text{(A.7)} \\ P &> 0 && \text{(A.8)} \end{aligned}$$

Inequalities (A.7) and (A.8) are affine in the variable P and hence this is a convex problem and can be solved in its present form. If there exists a symmetric matrix P that satisfies (A.7) and (A.8), then the problem is feasible. Powerful and effecient algorithms such as [39] have been proposed to solve such problems.

A.4 Making an LMI convex by a change of variables

Some LMI problems require a transformation of variables. A very common control problem is that of finding a stabilising state feedback gain. Consider the system

$$\dot{x}(t) = Ax(t) + Bu(t) \tag{A.9}$$

and the state feedback control law

$$u(t) = Kx(t) \tag{A.10}$$

The closed loop system is

$$\dot{x}(t) = (A + BK)x(t) \tag{A.11}$$

and therefore the problem is one of finding K so that $A + BK$ is stable. The associated LMI problem is :
find a matrix K and a symmetric matrix P that satisfies the LMI system in P and K

$$\begin{aligned} P(A + BK) + (A + BK)^T P &< 0 && \text{(A.12)} \\ P &> 0 && \text{(A.13)} \end{aligned}$$

This problem is not convex in that (A.12) is not affine in the variables P and K. Defining $Q = P^{-1}$ and pre and post-multiplying the LMI (A.12) by Q, the LMIs (A.12) and (A.13) become LMIs in Q and K

$$\begin{aligned} (A + BK)Q + Q(A + BK)^T &< 0 && \text{(A.14)} \\ Q &> 0 && \text{(A.15)} \end{aligned}$$

However, the LMI (A.14) when expanded becomes

$$AQ + AQ^T + BKQ + QK^TB^T < 0 \tag{A.16}$$

Defining $Y = KQ$, the LMI (A.14) and (A.15) become LMIs in Y and Q

$$\begin{aligned} AQ + QA^T + BY + Y^TB^T &< 0 \quad \text{(A.17)} \\ Q &> 0 \quad \text{(A.18)} \end{aligned}$$

which are affine in Q and Y. The LMI solver will return the values of Y and Q. Then P and K can be calculated by

$$P = Q^{-1} \quad K = YQ^{-1} \tag{A.19}$$

A.5 LMI problems using the Schur complement

Given a system triple (A, B, C). Consider the following LQR problem [116]:
minimise $trace(P^{-1})$ subject to the following LMIs in P

$$\begin{aligned} PA + A^TP - C^TV^{-1}C + PWP &< 0 \quad \text{(A.20)} \\ P &> 0 \quad \text{(A.21)} \end{aligned}$$

where $W > 0$ and $V > 0$ are given symmetric positive definite matrices. Inequality (A.20) is not affine in P. However, by using the Schur complement, (A.20) is equivalent to

$$\begin{bmatrix} PA + A^TP - C^TV^{-1}C & P \\ P & -W^{-1} \end{bmatrix} < 0 \tag{A.22}$$

This inequality is now affine in the variable P. However, the quantity $trace(P^{-1})$ is not affine in P. This can be overcome by introducing a dummy matrix variable X, and imposing the following constraint

$$\begin{bmatrix} -P & I \\ I & -X \end{bmatrix} < 0 \tag{A.23}$$

Using the Schur complement, (A.23) is equivalent to $X > P^{-1}$, and hence X acts as an upper bound on P^{-1}. Therefore the nonconvex LMI problem originally posed can be transformed into a convex LMI problem:
minimise $trace(X)$ with respect to the variables X and P subject to inequalities (A.22) and (A.23).

A.6 Using LMIs for pole-placement

In §A.4, it was argued how a stabilising state feedback gain could be synthesised using LMIs. More sophisticated pole placement problems can be solved in which the eigenvalues of the closed-loop system are forced to lie in specific convex regions of the complex plane. If s represents a coordinate in the complex plane, and s^* represents its complex conjugate, then the following inequalities describe particular convex regions of the complex plane [11, 39].

Specifically

- a conic sector symmetric about the horizontal axis, centred at the origin, with an inner angle θ can be expressed as

$$\begin{bmatrix} (s+s^*)\sin\theta & (s-s^*)\cos\theta \\ (-s+s^*)\cos\theta & (s+s^*)\sin\theta \end{bmatrix} < 0 \tag{A.24}$$

- a circle of radius r and centre $(q, 0)$ can be written

$$\begin{bmatrix} -r & s-q \\ s^*-q & -r \end{bmatrix} < 0 \tag{A.25}$$

- a vertical strip $a < Re(s) < b$ is described by

$$\begin{bmatrix} s+s^*-2b & 0 \\ 0 & -(s+s^*)+2a \end{bmatrix} < 0 \tag{A.26}$$

If $A_o = A + BK$ from (A.11), and P is the Lyapunov matrix, then from [11], there is a relationship $(P, PA_o, A_o^T P) \leftrightarrow (1, s, s^*)$, and hence the following inequalities will force $\lambda(A_o)$ to lie in the regions as described from (A.24) - (A.26):

- the cone

$$\begin{bmatrix} (PA_o + A_o^T P)\sin\theta & (PA_o - A_o^T P)\cos\theta \\ (-PA_o + A_o^T P)\cos\theta & (PA_o + A_o^T P)\sin\theta \end{bmatrix} < 0 \tag{A.27}$$

- the circle

$$\begin{bmatrix} -rP & PA_o - qP \\ A_o^T P - qP & -rP \end{bmatrix} < 0 \tag{A.28}$$

- the vertical strip

$$\begin{bmatrix} PA_o + A_o^T P - 2bP & 0 \\ 0 & -(PA_o + A_o^T P) + 2aP \end{bmatrix} < 0 \tag{A.29}$$

Generally, the LMIs (A.27) - (A.29) are not affine in the variables involved, and require the change of variables as described in §A.4.

Appendix B

Mathematical notions

B.1 Mathematical Notation

$\mathcal{R}^{n\times m}$	the set of real matrices with n rows and m columns
$sgn(.)$	the signum function
$\|u\|$	the absolute value of the scalar u
$det(A)$	the determinant of the square matrix A
$\lambda(A)$	the eigenvalues of the square matrix A
$\lambda_{max}(A)$	the greatest eigenvalue of the square matrix A
$\lambda_{min}(A)$	the least eigenvalue of the square matrix A
A^{-1}	the inverse of the square matrix A
A^T	the transpose of the matrix A
I_n	$n \times n$ identity matrix
$A > 0$	implies that the square matrix A is symmetric positive definite
$A > B$	implies that the square matrix $(A - B)$ is positive definite
$\|\|.\|\|$	the Euclidean norm for vectors and the spectral norm for matrices
$\dot{y}$	the derivative of y with respect to time
$\ddot{y}$	the second derivative of y with respect to time
s^*	the complex conjugate of the complex number s

B.2 Quadratic stability

This section will explain the concept of *quadratic stability*.

Consider the nonlinear system

$$\dot{x} = f(x, t) \tag{B.1}$$

and the quadratic Lyapunov function

$$\mathcal{V} = x^T P x \tag{B.2}$$

where P is a positive definite matrix. Taking the derivative of $\mathcal{V}$ yields

$$\begin{aligned} \dot{\mathcal{V}} &= \dot{x}^T P x + x^T P \dot{x} \\ &= f^T P x + x^T P f \end{aligned} \tag{B.3}$$

$\mathcal{V}$ is a measure of the magnitude of the vector x, and is always positive for all $x \neq 0$ because P is positive definite. If a P can be found so that $f^T P x + x^T P f < 0$ for all x then the derivative $\dot{\mathcal{V}}$ is always negative. This shows that the magnitude of the vector x is always decreasing, hence as $t \to \infty, x \to 0$.

This type of stability is termed quadratic stability because a quadratic function is used to prove stability. However, this method is not explicit, as the measure of $\dot{\mathcal{V}}$ is not known, but all that is sought is $\dot{\mathcal{V}} < 0$ [25].

B.3 Matrix rank and determinant

If $det(A) \neq 0$ then the matrix A is said to be full rank.

For a matrix $A \in \mathcal{R}^{n \times m}$, $rank(A) \leq min\{n, m\}$

An important inequality relating to matrix rank [25] is

$$rank(AB) \leq min\{rank(A), rank(B)\}$$

Appendix C

Guide to attached disk

C.1 Secondary observer method for aircraft example in §5.3.4

Path and file name - *ch5/aircraft/secondaryobs.mat*. The link between the notation used in the thesis and the variables in Matlab is given in Table C.1.

Parameter	**Symbol**	**In disk**
Linear gain of primary observer	G_l	Gl
Nonlinear gain of primary observer	G_n	Gn
Matrix that scales nonlinear gain of primary observer	P_o	Po
Linear gain of secondary observer	$G_{l,a}$	Gla
Nonlinear gain of secondary observer	$G_{n,a}$	Gna
Matrix that scales nonlinear gain of secondary observer	$P_{o,a}$	Poa

Table C.1: Description for file *ch5/aircraft/secondaryobs.mat*

C.2 Single observer method for aircraft example in §5.3.4

Path and file name - *ch5/aircraft/singleobs.mat*. The link between the notation used in the thesis and the variables in Matlab is given in Table C.2.

Parameter	**Symbol**	**In disk**
Linear gain of augmented observer	$G_{l,b}$	Glb
Nonlinear gain of augmented observer	$G_{n,b}$	Gnb
Matrix that scales nonlinear gain of augmented observer	$P_{o,b}$	Pob

Table C.2: Description for file *ch5/aircraft/singleobs.mat*

C.3 Secondary observer method for helicopter example in §5.4.4

Path and file name - *ch5/helicopter/secondaryobs.mat*. The link between the notation used in the thesis and the variables in Matlab is given in Table C.3.

Parameter	**Symbol**	**In disk**
Linear gain of primary observer	G_l	Gl
Nonlinear gain of primary observer	G_n	Gn
Matrix that scales nonlinear gain of primary observer	P_o	Po
Linear gain of secondary observer	$G_{l,a}$	Gla
Nonlinear gain of secondary observer	$G_{n,a}$	Gna
Matrix that scales nonlinear gain of secondary observer	$P_{o,a}$	Poa
Scaling matrix to obtain fault reconstruction	$(\mathcal{M}_{2,a}^T\mathcal{M}_{2,a})^{-1}\mathcal{M}_{2,a}^T$	Mcal2a

Table C.3: Description for file *ch5/helicopter/secondaryobs.mat*

C.4 Single observer method for helicopter example in §5.4.4

Path and file name - *ch5/helicopter/singleobs.mat*. The link between the notation used in the thesis and the variables in Matlab is given in Table C.4.

Parameter	**Symbol**	**In disk**
Linear gain of augmented observer	$G_{l,b}$	Glb
Nonlinear gain of augmented observer	$G_{n,b}$	Gnb
Matrix that scales nonlinear gain of augmented observer	$P_{o,b}$	Pob
Scaling matrix to obtain fault reconstruction	$(\mathcal{M}_{2,b}^T\mathcal{M}_{2,b})^{-1}\mathcal{M}_{2,b}^T$	Mcal2b

Table C.4: Description for file *ch5/helicopter/singleobs.mat*

C.5 Helicopter example in §5.5.4

Path and file name - *ch5/helicopter/lastmeth.mat*. The link between the notation used in the thesis and the variables in Matlab is given in Table C.5.

Parameter	**Symbol**	**In disk**
Linear gain of primary observer	G_l	Gl
Nonlinear gain of primary observer	G_n	Gn
Matrix that scales nonlinear gain of primary observer	P_o	Po
Linear gain of secondary observer	$G_{l,c}$	Glc
Nonlinear gain of secondary observer	$G_{n,c}$	Gnc
Matrix that scales nonlinear gain of secondary observer	$P_{o,c}$	Poc
Scaling matrix to obtain fault reconstruction	$\mathcal{A}_{22}$	Acal22

Table C.5: Description for file *ch5/helicopter/lastmeth.mat*

C.6 Parameters of aero-engine in §7.3

Path and file name - *aero/modelparam.mat*. The link between the notation used in the thesis and the variables in Matlab is given in Table C.6.

Parameter	**Symbol**	**In disk**
Open loop state space system matrix	A	A
Input distribution matrix	B	B
Output distribution matrix	C	C
Direct feedthrough from input to output matrix	D	D

Table C.6: Description for file *aero/modelparam.mat*

C.7 Parameters of observer in §7.4.1

Path and file name - *aero/checkdist.mat*. The link between the notation used in the thesis and the variables in Matlab is given in Table C.7.

Parameter	**Symbol**	**In disk**
Linear gain of observer	$G_{l,b}$	Glb
Nonlinear gain of observer	$G_{n,b}$	Gnb
Matrix that scales nonlinear gain	$P_{o,b}$	Pob
Scaling matrix to obtain fault reconstruction	$W_{sc,b}$	Wscb

Table C.7: Description for file *aero/checkdist.mat*

C.8 Parameters of observers in §7.5

Path and file name - *aero/1fault.mat*. The link between the notation used in the thesis and the variables in Matlab is given in Table C.8.

Parameter	**Symbol**	**In disk**
Linear gain for Observer A	$G_{l,b,1}$	Glb1
Nonlinear gain for Observer A	$G_{n,b,1}$	Gnb1
Matrix that scales nonlinear gain for Observer A	$P_{o,b,1}$	Pob1
Scaling matrix to obtain fault reconstruction (Observer A)	$W_{sc,b}$	Wscb
Linear gain for Observer B	$G_{l,b,2}$	Glb2
Nonlinear gain for Observer B	$G_{n,b,2}$	Gnb2
Matrix that scales nonlinear gain for Observer B	$P_{o,b,2}$	Pob2
Scaling matrix to obtain fault reconstruction (Observer B)	$(\mathcal{M}_{2,b}^T\mathcal{M}_{2,b})^{-1}\mathcal{M}_{2,b}^T$	Mcal2b

Table C.8: Description for file *aero/1fault.mat*

References

[1] T. Ahmed-Ali and F. Lamnabhi-Lagarrigue. Sliding observer-controller design for uncertain triangular nonlinear systems. *IEEE Transactions on Automatic Control*, 4:1244–1249, 1999.

[2] R.V. Beard. *Failure accommodation in linear systems through self-reorganisation, Ph.D. thesis.* M.I.T., Cambridge, MA, 1971.

[3] S.P. Boyd, L. El-Ghaoui, E. Feron, and V. Balakrishnan. *Linear Matrix Inequalities in Systems and Control Theory.* SIAM: Philadelphia, 1994.

[4] S.K. Chang, P.L. Hsu, and K.L. Lin. A parametric transfer matrix approach to fault-idenfication filter design and threshold selection. *International Journal of Systems Science*, 26:741–754, 1995.

[5] J. Chen and R.J. Patton. *Robust model-based fault diagnosis for dynamic systems.* Kluwer Academic Publishers, 1999.

[6] J. Chen, R.J. Patton, and H.Z. Zhang. Design of unknown input observers and robust fault detection filters. *International Journal of Control*, 63:85–105, 1996.

[7] J. Chen and H. Zhang. Robust detection of faulty actuators via unknown input observers. *International Journal of Systems Science*, 22:1829–1839, 1991.

[8] M.S. Chen. Uncertainty estimator. *Proceedings of the American Control Conference*, pages 2020–2024, 1990.

[9] R.H. Chen and J.L. Speyer. Optimal stochastic multiple-fault detection filter. *Proceedings of the IEEE Conference on Decision and Control, Phoenix, Arizona*, pages 4965–4970, 1999.

[10] X. Chen and T. Fukuda. Vss theory-based disturbance estimation scheme for mimo systems and its application. *International Journal of Control*, 69:733–752, 1998.

[11] M. Chilali and P. Gahinet. $\mathcal{H}_\infty$ design with pole placement constraints: an LMI approach. *IEEE Transactions on Automatic Control*, 41:358–367, 1996.

[12] E.Y. Chow and A. Willsky. Analytical redundancy and the design of robust failure detection systems. *IEEE Transactions on Automatic Control*, 29:603–614, 1984.

[13] C.K. Chui and G. Chen. *Kalman filtering with real-time applications.* Springer Verlag, 1998.

[14] R.N. Clark. Instrument fault detection. *IEEE Transactions on Aerospace and Electronic Systems*, 14:456–465, 1978.

[15] R.N. Clark. A simplified instrument failure detection scheme. *IEEE Transactions on Aerospace and Electronic Systems*, 14:558–563, 1978.

[16] R.N. Clark, D.C. Fosth, and V.M. Walton. Detection instrument malfunctions in control systems. *IEEE Transactions on Aerospace and Electronic Systems*, 11:465–473, 1975.

[17] R. Da and C.F. Lin. A new failure-detection approach and its application to GPS autonomous integrity monitoring. *IEEE Transactions on Aerospace and Electronic Systems*, 31:499–506, 1995.

[18] S.K. Dassanayake, G.J. Balas, and J. Bokor. Using unknown input observers to detect and isolate sensor faults in a turbofan engine. *Proceedings of the AIAA/IEEE Digital Avionics Systems Conference*, pages E51–E57, 2000.

[19] J.C. Deckert, M.N. Desai, J.J. Deyst, and A.S. Willsky. F-8 DFBW sensor failure identification using analytic redundancy. *IEEE Transactions on Automatic Control*, 22:795–803, 1977.

[20] X. Ding, L. Guo, and T. Jeinsch. A characterization of parity space and its application to robust fault detection. *IEEE Transactions on Automatic Control*, 44:337–343, 1999.

[21] X.C. Ding and P.M. Frank. Fault detection via factorization approach. *Systems and Control Letters*, 14:431–436, 1990.

[22] R.K. Douglas and J.L. Speyer. Robust fault detection filter design. *Proceedings of the American Control Conference, Seattle, Washington*, pages 91–96, 1995.

[23] C. Edwards and S.K. Spurgeon. On the development of discontinuous observers. *International Journal of Control*, 59:1211–1229, 1994.

[24] C. Edwards and S.K. Spurgeon. Sliding mode stabilization of uncertain systems using only output information. *International Journal of Control*, 62:1129–1144, 1995.

[25] C. Edwards and S.K. Spurgeon. *Sliding Mode Control: Theory and Applications*. Taylor & Francis, 1998.

[26] C. Edwards and S.K. Spurgeon. A sliding mode observer based FDI scheme for the ship benchmark. *European Journal of Control*, 6:341–356, 2000.

[27] C. Edwards, S.K. Spurgeon, and R.J. Patton. Sliding mode observers for fault detection and isolation. *Automatica*, 36:541–553, 2000.

[28] P. Eide and P. Maybeck. An MMAE failure detection system for the F-16. *IEEE Transactions on Aerospace and Electronic Systems*, 32:1125–1135, 1996.

[29] A. Emami-Naeni, M.M. Akhter, and S.M. Rock. Effect of model uncertainty on failure detection: the threshold selector. *IEEE Transactions on Automatic Control*, 33:1106–1115, 1988.

[30] F.W. Fairman, S.S. Mahil, and L. Luk. Disturbance decoupled observer design via singular value decomposition. *IEEE Transactions on Automatic Control*, 29:84–86, 1984.

[31] Y.E. Faitakis and J.C. Kantor. Residual generation and fault detection for discrete-time systems using an l_∞ technique. *International Journal of Control*, 64:155–174, 1996.

[32] A.F. Filippov. Differential equations with discontinuous right hand sides. *Americal athematical Society Translations*, 42:199–231, 1964.

[33] F. Floret-Pontet and F. Lamnabhi-Lagarrigue. *State and parameter identification for nonlinear uncertain systems using variable structure theory, in pages 84 - 103 of* 4th Nonlinear Control Network Workshop, Sheffield. Springer-Verlag, 2001.

[34] P.M. Frank. Fault diagnosis in dynamic systems using analytical and knowledge based redundancy - a survey and some new results. *Automatica*, 26:459–474, 1990.

[35] P.M. Frank. Enhancement of robustness in observer-based fault detection. *International Journal of Control*, 59:955–981, 1994.

[36] P.M. Frank. Analytical and qualitative model-based fault diagnosis - a survey and some new results. *European Journal of Control*, 2:6–28, 1996.

[37] P.M. Frank and X. Ding. Survey of robust residual generation and evaluation methods in observer-based fault detection systems. *Journal of Process Control*, 7:403–424, 1997.

[38] G.F. Franklin, J.D. Powell, and A. Enami-Naeni. *Feedback control of dynamic systems*. Addison-Wesley, 1994.

[39] P. Gahinet, A. Nemirovski, A.J. Laub, and M. Chilali. *LMI Control Toolbox, Users Guide*. The MathWorks, Inc., 1995.

[40] E.G. Gai, M.B. Adams, and B.K. Walker. Determination of failure thresholds in hybrid navigation. *IEEE Transactions on Aerospace and Electronic Systems*, 12:744–755, 1976.

[41] E.G. Gai, M.B. Adams, B.K. Walker, and T. Smestad. Determination of failure thresholds in hybrid navigation. *IEEE Transactions on Aerospace and Electronic Systems*, 14:969–967, 1978.

[42] W. Ge and C.Z. Fang. Detection of faulty components via robust observation. *International Journal of Control*, 47:581–599, 1988.

[43] W. Ge and C.Z. Fang. Extended robust observation approach for failure isolation. *International Journal of Control*, 49:1537–1553, 1989.

[44] J.J. Gertler and M.W. Kunwer. Optimal residual decoupling for robust fault diagnosis. *International Journal of Control*, 61:395–421, 1995.

[45] J.J. Gertler and R. Monajemy. Generating directional residuals with dynamic parity relations. *Automatica*, 31:627–635, 1995.

[46] J.J. Gertler and D. Singer. A new structural framework for parity equation-based failure detection and isolation. *Automatica*, 26:381–388, 1990.

[47] S. Gutman and E. Jury. A general theory for matrix root-clustering in subregions of the complex plane. *IEEE Transactions on Automatic Control*, 26:853–863, 1981.

[48] F. Hamelin and D. Sauter. Robust fault detection in uncertain dynamic systems. *Automatica*, 36:1747–1754, 2000.

[49] I. Haskara and U. Ozguner. Estimation based discrete-time sliding control of uncertain nonlinear systems in discrete strict feedback form. *Proceedings of the IEEE Conference on Decision and Control, Sydney*, pages 2599–2604, 2000.

[50] I. Haskara, U. Ozguner, and V. Utkin. On sliding mode observers via equivalent control approach. *International Journal of Control*, 71:1051–1067, 1998.

[51] B.S. Heck, S.V. Yallapragada, and M.K.H. Fan. Numerical methods to design the reaching phase of output feedback variable structure control. *Automatica*, 31:275–279, 1995.

[52] F.J.J. Hermans and M.B. Zarrop. Sliding mode observers for robust sensor monitoring. *Proceedings of the 13th IFAC World Congress*, pages 211–216, 1996.

[53] M. Hou and P.C. Muller. Design of observers for linear systems with unknown inputs. *IEEE Transactions on Automatic Control*, 37:871–875, 1992.

[54] M. Hou and R.J. Patton. An LMI approach to $\mathcal{H}_-/\mathcal{H}_\infty$ fault detection observers. *Proceedings of the UKACC International Conference on Control*, pages 305–310, 1996.

[55] B. Jiang, J.L. Wang, and Y.C. Soh. Robust fault diagnosis for a class of bilinear systems with uncertainty. *Proceedings of the IEEE Conference on Decision and Control, Phoenix, Arizona.*, pages 4499–4504, 1999.

[56] H.L. Jones. *Failure detection in linear systems, Ph.D. thesis.* M.I.T., Cambridge, MA, 1973.

[57] J.Y. Keller, L. Summerer, M. Boutayeb, and M. Darouach. Generalized likelihood ratio approach for fault detection in linear dynamic stochastic systems with unknown inputs. *International Journal of Systems Science*, 27:1231–1241, 1996.

[58] R.W. Kelly. Application of analytical redundancy to the detection of sensor faults on a turbofan engine. *Proceedings of the International Gas Turbine and Aeroengine Congress and Exhibition*, pages 96–GT–3, 1996.

[59] S. Kilsgaard, M.L. Rank, H.H. Niemann, and J. Stoustrup. Simultaneous design of controller and fault detector. *Proceedings of the IEEE Conference on Decision and Control, Kobe, Japan*, pages 628–629, 1996.

[60] M. Kinnaert. Design of redundancy relations for failure detection and isolation by constrained optimization. *International Journal of Control*, 63:609–622, 1996.

[61] M. Kinnaert and Y. Peng. Residual generator for sensor and actuator fault detection and isolation: a frequency domain approach. *International Journal of Control*, 61:1423–1435, 1995.

[62] A.J. Koshkouei and A.S.I. Zinober. Sliding mode controller-observer design for multivariable linear systems with unmatched uncertainty. *Kybernetika*, 36:95–115, 2000.

[63] P. Kudva, N. Viswanadham, and A. Ramakrishna. Observers for linear systems with unknown inputs. *IEEE Transactions on Automatic Control*, 25:113–115, 1980.

[64] J.E. Kurek. The state vector reconstruction for linear systems with unknown inputs. *IEEE Transactions on Automatic Control*, 28:1120–1122, 1983.

[65] B. Liu and J. Si. Fault isolation filter design for linear time-invariant systems. *IEEE Transactions on Automatic Control*, 42:704–707, 1997.

[66] L. Ljung. *System Identification Toolbox: For Use with Matlab*. The MathWorks, Inc., 1995.

[67] X.C. Lou, A.S. Willsky, and G.C. Verghese. Optimally robust redundancy relations for failure detection in uncertain systems. *Automatica*, 22:333–344, 1986.

[68] D.G. Luenberger. An introduction to observers. *IEEE Transactions on Automatic Control*, 16:596–602, 1971.

[69] J.M. Maciejowski. *Multivariable Feedback Design*. Addison-Wesley, 1989.

[70] G. Marro, D. Prattichizzo, and E. Zattoni. A unified algorithmic setting for signal-decoupling compensators and unknown-input observers. *Proceedings of the IEEE Conference on Decision and Control, Sydney*, pages 4512–4517, 2000.

[71] M.A. Massoumnia. A geometric approach to the synthesis of failure detection filters. *IEEE Transactions on Automatic Control*, 31:839–846, 1986.

[72] M.A. Massoumnia, G.C. Verghese, and A.S. Willsky. Failure detection and identification. *IEEE Transactions on Automatic Control*, 34:316–321, 1989.

[73] G.L. Mealy and W. Tang. Application of multiple model estimation to a recursive terrain height correlation system. *IEEE Transactions on Automatic Control*, 28:323–331, 1983.

[74] R.K. Mehra and J. Peschon. An innovations approach to fault detection and diagnosis in dynamic systems. *Automatica*, 7:637–640, 1971.

[75] T.E. Menke and P.S. Maybeck. Sensor/actuator failure-detetion in the vista F-16 by mutiple model adaptive estimation. *IEEE Transactions on Aerospace and Electronic Systems*, 31:1218–1229, 1995.

[76] W.C. Merrill. Sensor failure detection for jet engines using analytical redundancy. *Journal of Guidance, Control and Dynamics*, 8:673–682, 1985.

[77] W.C. Merrill, J.C. DeLaat, and M Abdelwahab. Turbofan engine demonstration of sensor failure detection. *Journal of Guidance, Control and Dynamics*, 14:337–349, 1991.

[78] W.C. Merrill, J.C. DeLaat, and W.M. Bruton. Advanced detection, isolation, and accommodation of sensor failures – real-time evaluation. *Journal of Guidance, Control and Dynamics*, 11:517–526, 1988.

[79] W.C. Merrill, J.C. DeLaat, S.M. Kroszkewicz, and M. Abdelwahab. Full-scale engine demonstration of an advanced sensor failure detection, isolation, and accommodation algorithm - preliminary results. *Proceedings of the AIAA Guidance, Navigation and Control Conference*, pages 183–191, 1987.

[80] G. Merrington, O.K. Kwon, G. Goodwin, and B. Carlsson. Fault detection and diagnosis in gas turbines. *Journal of Engineering for Gas Turbines and Power*, 113:276–282, 1991.

[81] H. Niemann and J. Stoustrup. Filter design for failure detection and isolation in the presence of modeling errors and disturbances. *Proceedings of the IEEE Conference on Decision and Control, Kobe, Japan*, pages 1155–1160, 1996.

[82] J. Park and G. Rizzoni. An eignestructure assignment algorithm for the design of fault detection filters. *IEEE Transactions on Automatic Control*, 39:1521–1524, 1994.

[83] R.J. Patton and J. Chen. The design of a robust fault diagnosis scheme for a jet engine sensor system. *Mathematical and Intelligent models in system simulation*, pages 489–495, 1991.

[84] R.J. Patton and J. Chen. Robust fault detection of jet engine sensor systems using eigenstructure assignment. *Journal of Guidance, Control and Dynamics*, 15:1491–1497, 1992.

[85] R.J. Patton and J. Chen. A survey of robustness problems in quantitative model-based fault diagnosis. *Applied Maths and Computer Science*, 3:339–416, 1993.

[86] R.J. Patton and J. Chen. Review of parity space approaches to fault diagnosis for aerospace systems. *Journal of Guidance, Control and Dynamics*, 17:278–285, 1994.

[87] R.J. Patton and J. Chen. On eigenstructure assignment for robust fault diagnosis. *International Journal of Robust and Nonlinear Control*, 10:1193–1208, 2000.

[88] R.J. Patton, P.M. Frank, and R.N. Clark. *Fault Diagnosis in Dynamic Systems: Theory and Application*. Prentice Hall, New York, 1989.

[89] R.J. Patton and M. Hou. $\mathcal{H}_\infty$ estimation and robust fault detection. *Proceedings of the European Control Conference, Brussels*, 1997.

[90] R.J. Patton, S.W. Willcox, and J.S. Winter. Parameter-insensitive technique for aircraft sensor fault analysis. *Journal of Guidance, Control and Dynamics*, 10:359–367, 1987.

[91] R.J. Patton, H.Y. Zhang, and J. Chen. Modelling of uncertainties for robust fault diagnosis. *Proceedings of the IEEE Conference on Decision and Control, Tucson, Arizona*, pages 921–926, 1992.

[92] Y. Peng, A. Youssouf, P. Arte, and M. Kinnaert. A complete procedure for residual generation and evaluation with application to a heat exchanger. *IEEE Transactions on Control Systems Technology*, 5:542–555, 1997.

[93] E.P. Ryan. Adaptive stabilization of a class of uncertain nonlinear sstems: a differential inclusions approach. *Systems and Control Letters*, 10:95–101, 1988.

[94] A. Saberi, A.A. Stoorvogel, and P. Sannuti. Inverse filtering and deconvolution. *International Journal of Robust and Nonlinear Control*, 11:131–156, 2001.

[95] M.A. Sadrnia, R.J. Patton, and J. Chen. Robust $\mathcal{H}_\infty/\mu$ fault diagnosis observer design. *Proceedings of the European Control Conference, Brussels*, 1997.

[96] M. Saif and Y. Guan. A new approach to robust fault detection and identification. *IEEE Transactions on Aerospace and Electronic Systems*, 29:685–695, 1993.

[97] D. Sauter and F. Hamelin. Frequency-domain optimization for robust fault detection and isolation in dynamic systems. *IEEE Transactions on Automatic Control*, 44:878–882, 1999.

[98] H. Sira-Ramirez and S.K. Spurgeon. On the robust design of sliding observers for linear systems. *Systems and Control Letters*, 23:9–14, 1994.

[99] S. Skogested and I. Postlethwaite. *Multivariable feedback control: analysis and design*. John Wiley & Sons, 1996.

[100] J.J.E. Slotine, J.K. Hendrick, and E.A. Misawa. On sliding observers for nonlinear systems. *Journal of Dynamic Systems, Measurement, and Control*, 109:245–252, 1987.

[101] M.P. Spathopoulos and I.D. Grobov. Input disturbance estimation in the bounded noise context. *International Journal of Control*, 71:505–516, 1998.

[102] R. Sreedhar, B. Fernandez, and G.Y. Masada. Robust fault detection in nonlinear systems using sliding mode observers. *Proceedings of the IEEE Conference on Control Applications*, pages 715–721, 1993.

[103] J. Stoustrup. Fault detection for nonlinear systems - a standard problem approach. *Proceedings of the IEEE Conference on Decision and Control, Tampa, Florida*, pages 96–101, 1998.

[104] C.P. Tan and C. Edwards. An LMI approach for designing sliding mode observers. *Proceedings of the IEEE Conference on Decision and Control, Sydney*, pages 2587–2592, 2000.

[105] C.P. Tan and C. Edwards. An LMI approach for designing sliding mode observers. *International Journal of Control*, 74:1559–1568, 2001.

[106] C.P. Tan and C. Edwards. Reconstruction of sensor faults using a sliding mode observer. *Proceedings of the Conference on Decision and Control, Orlando, Florida*, 2001.

[107] C.P. Tan and C. Edwards. *Sliding mode observers for robust reconstruction of actuator and sensor faults for a nonlinear system, in pages 323 - 333 of* 4th Nonlinear Control Network Workshop, Sheffield. Springer-Verlag, 2001.

[108] C.P. Tan and C. Edwards. A robust sensor fault reconstruction scheme using sliding mode observers applied to a nonlinear aero engine model. *To be published in the Proceedings of the American Control Conference, Anchorage, Alaska*, 2002.

[109] C.P. Tan and C. Edwards. Sliding mode observers for robust fault detection and reconstruction. *To be published in the Proceedings of the IFAC World Congress, Barcelona*, 2002.

[110] V.I. Utkin. *Sliding Modes in Control Optimization.* Springer-Verlag, Berlin, 1992.

[111] B.L. Walcott and S.H. Zak. State observation of nonlinear uncertain dynamical systems. *IEEE Transactions on Automatic Control*, 32:166–170, 1987.

[112] B.L. Walcott and S.H. Zak. Combined observer–controller synthesis for uncertain dynamical systems with applications. *IEEE Transactions on Systems, Man and Cybernetics*, 18:88–104, 1988.

[113] H. Wang and S. Daley. A fault detection method for unknown systems with unknown input and its application to hydraulic turbine monitoring. *International Journal of Control*, 57:247–260, 1993.

[114] K. Watanabe and D.M. Himmelblau. Instrument fault detection in systems with uncertainties. *International Journal of Systems Science*, 13:137–158, 1982.

[115] J.E. White and J.L. Speyer. Detection filter design: spectral theory and algorithms. *IEEE Transactions on Automatic Control*, 32:593–603, 1987.

[116] J.C. Willems. Least squares optimal control and the Algebraic Ricatti Equation. *IEEE Transactions on Automatic Control*, 16:621–634, 1971.

[117] A.S. Willsky. A survey of design methods for failure detection in dynamic systems. *Automatica*, 12:601–611, 1976.

[118] A.S. Willsky and H.L. Jones. A Generalized Likelihood Ratio approach to the detection and estimation of jumps in linear systems. *IEEE Transactions on Automatic Control*, 21:108–112, 1976.

[119] N.E. Wu and Y.Y. Wang. Robust failure-detection with parity check on filtered measurements. *IEEE Transactions on Aerospace and Electronic Systems*, 31:489–491, 1995.

[120] Y. Xiong and M. Saif. A novel design for robust fault diagnostic observer. *Proceedings of the 37th IEEE Conference on Decision and Control, Tampa, Florida*, pages 592–597, 1998.

[121] Y. Xiong and M. Saif. Sliding-mode observer for uncertain systems part i: linear systems case. *Proceedings of the IEEE Conference on Decision and Control, Sydney*, 2000.

[122] Y. Xiong and M. Saif. Robust and nonlinear fault diagnosis using sliding mode observers. *Proceedings of the IEEE Conference on Decision and Control, Orlando, Florida*, pages 567–572, 2001.

[123] J.X. Xu and H. Hashimoto. Parameter identification methodologies based on variable structure control. *International Journal of Control*, 57:1207–1220, 1993.

[124] F. Yang and R.W. Wilde. Observers for linear systems with unknown inputs. *IEEE Transactions on Automatic Control*, 33:677–681, 1988.

[125] H. Yang and M. Saif. Fault detection in a class of nonlinear systems via adaptive sliding observer. *Proceedings of the IEEE International Conference on Systems, Man and Cybernetics*, 3:2199–2204, 1995.

[126] H. Yang and M. Saif. State observation, failure detection and isolation (FDI) in bilinear systems. *International Journal of Control*, 67:901–920, 1997.

[127] E. Yaz and A. Azemi. Variable structure observer with a boundary-layer for correlated noise/disturbance models and disturbance minimization. *International Journal of Control*, 57:1191–1206, 1993.

[128] T.K. Yeu and S. Kawaji. Fault detection and isolation for descriptor systems using sliding mode observer. *Proceedings of the IEEE Conference on Decision and Control, Orlando, Florida*, pages 596–597, 2001.

[129] D. Yu and D.N. Shields. A bilinear fault detection observer. *Automatica*, 32:1597–1602, 1996.

[130] K. Zhou, J. Doyle, and K. Glover. *Robust and Optimal Control*. Englewood Cliffs, N.J. : Prentice Hall, 1995.